Development of glacial lakes in the Everest and Kangchenjunga regions, Nepal Himalaya

A

Thesis

Submitted to the Graduate School of Environmental Science,
Hokkaido University, Sapporo, Japan

in partial fulfillment of the Requirements for the Degree of

Doctor of Philosophy

By

Mohan Bahadur CHAND

Sapporo, Japan

March 2020

Abstract

The widespread loss of glacier mass in the Himalaya is the evidence of the recent climate change. Increased melt rates of the glaciers and changes in their morphology are leading to the formation and expansion of glacial lakes. Glacial lakes are usually formed on gently sloping debris-covered glaciers in remote and poorly inhabited regions, and are at different stages of development. Such lakes are dammed by fragile materials and may break and cause glacial lake outburst floods (GLOFs). This study examined the evolution and dynamics of glacial lakes at seasonal to decadal timescales using assessments of remotely sensed satellite imageries and field measurements.

Inventories of glaciers and glacial lakes were prepared for the Everest region, upper Dudh Koshi River basin using WorldView and GeoEye imageries of 2015 and 2016 of 2-m spatial resolution. The inventory revealed a total of 109 glaciers with a total surface area of 268.22 ± 1.46 km^2. Comparison among the sub-basins showed that the largest number of glaciers (n=27) was observed in the Khumbu Glacier basin, while the largest area of glaciers (86.22 ± 0.33 km^2) was found in the Ngozompa Glacier basin. The number of debris-covered glaciers was 25 with the surface area of 239.99 ± 1.07 km^2. Similarly, a high-resolution inventory of the glacial lakes discovered a total of 3,290 glacial lakes with a total surface area of 8.11 ± 0.45 km^2. The supraglacial lakes were found most frequently among all types of glacial lakes, and they accounted for 91% of the total number of glacial lakes. The inventory also suggested that the largest area of supraglacial lakes appeared on the surface of large debris-covered glaciers with gently sloping surface and larger mean width. The inventory of the glacial lakes for the Kangchenjunga region using Sentinel-2 imagery of 10-m spatial resolution revealed a total of 373 glacial lakes with a total surface area of 6.18 ± 0.75 km^2 in 2018, where unconnected glacial lakes (n=221) were most frequent.

The Landsat imagery interpretation for the long-term development of supraglacial lakes in the Everest region revealed the continuous increase in the area and the number of the lakes from 1989 to 2017, with minor fluctuations. Similarly, seasonal dynamics of supraglacial lakes using Sentinel-2 showed the smallest lake area during the winter season, while the area of these features was comparable during the pre-monsoon and post-monsoon seasons. Measurements of the supraglacial lakes from 1989 to 2017 revealed the highest persistence of the lakes at the terminus of the eight glaciers, i.e., Thyanbo,

Chhule, Melung, Bhote Koshi, Lumsamba, Ngozompa, Khumbu, and Nuptse glaciers, which are termed as spillway lakes. These spillway lakes are expanding at faster rates and the four of them, i.e., Ngozompa, Bhote Koshi, Khumbu, and Lumsamba glaciers suggested that a trajectory towards large lake development. Analyses of both DEM, generated from the UAV survey in 2018 and freely available DEM of year 2010 for the spillway lakes on the Ngozompa Glacier suggested the larger surface-lowering rate in the lake area than the downstream of the lake area, which is suitable condition for becoming a single large glacial lake on the glacier. On the other hand, the rest of the four supraglacial lakes (Thyanbo, Chhule, Melung, and Nuptse) did not show the clear trajectory because of their slower rates of expansion, which is possibly controlled by the geometry of the glaciers.

Analyses of CORONA, Landsat and Sentinel-2 images revealed the net increase in the surface area of glacial lakes by 230% in the Kangchenjunga region from 1964 to 2018. The increase in the lake area was largely contributed by glacier-fed lakes (68%), while the increase in the number of unconnected and non-glacier-fed lakes indicated the retreat of the glaciers in the study region. New proglacial lakes in the Kangchenjunga region were found expanding at faster rates after 2000, while proglacial lakes that were developed in the earlier period (1960 – 1980) were mostly at static state. Similarly, traces of five GLOFs were for the first time discovered based on the geomorphological evidence detected by CORONA and Landsat image analyses: they had occurred before the 1980s in the Kangchenjunga region.

This study demonstrated the efficiency of the use of different spatial resolution imageries to map the different sized lakes. It also revealed that WorldView imagery of 2-m resolution can be used to map the feature of size >500 m^2 with uncertainty <15% by applying semi-automatic methods. However, it can map the lake as small as the size of 20 m^2 by improving the results with manual correction. This can be suitable for accuracy assessment of the results from coarse resolution imageries. Similarly, Sentinel-2 of 10-m and Landsat of 30-m spatial resolution determine the surface of the lakes that have size >0.02 km^2 and >0.1 km^2, respectively, under an uncertainty threshold of 15%.

Formation of new lakes and rapid expansion of already developed lakes may increase the possibility of occurrence of GLOFs. Therefore, continuous monitoring of the glacial lakes is required to understand their physical setting, hazard parameters, and associated risk, which can help to minimize the risk for the people living in the downstream region.

Acknowledgements

I am hugely grateful to my supervisor, Prof. Teiji Watanabe, Faculty of Environmental Earth Science, Hokkaido University for giving the best supervision I could ever have hoped for. Continued support in my idea, regular encouragement, and his huge range of expertise allowed this work to run smoothly. He provided me with wise advice whenever we met for discussions and paved the way for the successful completion of my Ph.D. studies. I will always be indebted to him for his constant supervision.

My deepest gratitude goes to Prof. Takayuki Shiraiwa, Institute of Low Temperature Science, Hokkaido University, for his constructive suggestions, instruction, and comments throughout the study. I would also give sincere thanks to Prof. Yuichi Hayakawa, Faculty of Environmental Earth Science, Hokkaido University, for providing field survey equipment and providing insightful suggestions and comments in my study. He suggested and guided me about a GPS survey for the UAV survey. I am indebted to Prof. Shin Sugiyama, Institute of Low Temperature Science, Hokkaido University for help in improving the thesis and making possible to complete the work within time.

I am hugely grateful to Prof. Masami Kaneko, College of Agriculture, Food and Environment Science, Department of Environmental and Symbiotic Science, Rakuno Gakuen University for providing high-resolution satellite images, which enabled me to prepare highest resolution inventory of the glaciers and glacial lakes in the Everest region, Nepal. It was a great opportunity to learn several remote sensing and GIS skills while training at Rakuno Gakuen University, supported by JICA and GLP Japan Nodal Office. Prof. Kaneko provided insightful comments and suggestions in my research work.

Gratitude also goes to Prof. Ram Avtar, Faculty of Environmental Earth Science, Hokkaido University for providing constructive suggestions on techniques of remote sensing application, which helped me to improve the methodological framework of the study. I would also like to express sincere thanks to Profs. Ralf Greve, Tatsufumi Okino, Masaaki Kurasaki, Hokkaido University, who provided critical comments and suggestions during GEM seminars.

I am grateful to Dr. Dhananjaya Regmi, Himalayan Research Centre, for providing continuous support from the beginning until the completion of the study. I am indebted to him and his team for enabling fieldwork with research and UAV permit acquisition and logistical support during the field expedition in the Everest region. I am thankful to

Prof. Rijan Bhakta Kayastha, Kathmandu University and Prof. Sudeep Thakuri, Tribhuvan University, Nepal for playing supportive roles during the Ph.D. work.

I am hugely grateful to the National Geographic Society for granting early career research grant and Nitobe Advance Program Research Grant, Frontier Foundation, Hokkaido University, which enabled me to conduct fieldwork in the remote mountains of the Nepal Himalaya. My research work was greatly facilitated by the DigitalGlobe Foundation, which provided very high spatial resolution (up to 0.5 m) WorldView and GeoEye satellite imageries. This enabled me to prepare a highly accurate inventory of glacial lakes and glaciers in the Everest region and to validate the coarse-resolution results. I am also thankful to Hexagon Geospatial, which provided the free license to ERDAS IMAGINE to process the satellite images.

I also want to express my sincere thanks to Yusuke Kobayashi, Cui Song for their great help in UAV and GPS survey in the Everest region. I am thankful to Takuro Ogura and Amrit Thapa for providing technical support in UAV image processing and help in the R programming language, respectively. I am indebted to Bhabana Thapa for playing a supporting role in my study.

I want to thank Kaori Kuribayashi Shigetomi and Teruyuki Tsuji for providing great support during the Nitobe Advanced Program course. I am thankful to Hiroshi Yazaki and Junko Abe who helped me and my family to live comfortably in Japan.

I heartily thank my parents and family, who always support my decision, and enabled me to reach this stage; otherwise, it could hard to go for Ph.D. Finally, I am hugely grateful to my wife Prazita and heartily thank her for allowing me to become dedicated in research during the most difficult period for her with the birth of our son, Mokshit. I am thankful to my son, Mokshit, who made me more active than before.

Table of contents

List of figures

List of tables

1. Introduction

1.1 Background

Glaciers are the perennial source of freshwater and play an important role in the Earth's climate and ecosystem. Glaciers are changing rapidly almost worldwide along with the increased temperature in recent decades (IPCC, 2013), and glaciers in many regions will very likely to suffer further ice loss, even if climate remains stable (Zemp et al., 2015). The consequences of loss of glacier mass are widespread and of global significance (Farinotti et al., 2019), which affect the global trends in freshwater availability (Kaser et al., 2010; Rodell et al., 2018) and contribute in sea-level rise (Parkes and Marzeion, 2018; Zemp et al., 2019).

The High Mountain of Asia (HMA) which comprises the Himalayas, Hindu-Kush, Karakoram, Pamir Alai, Kunlun Shan, and Tian Shan mountains have the highest concentration of glaciers globally (Pritchard, 2017; Bolch et al., 2019). Rivers originating from this region are among the most meltwater-dependent river systems on the earth (Lutz et al., 2014; Azam et al., 2018), and approximately 800 million people depend in part on meltwater from these mountains (Pritchard, 2017; Maurer et al., 2019). The spatial pattern of snow and ice melt plays key roles in providing water for downstream irrigation, hydropower generation, and general consumption.

Glaciers around the world are retreating and losing their mass (Zemp et al., 2015), and HMA glaciers are also not exception (Bolch et al., 2012; Lamsal et al., 2017; Sherpa et al., 2017; Acharya et al., 2018; Azam et al., 2018; Maurer et al., 2019). Glaciers of the HMA region show the very negative mass balance of up to -0.62 ± m w.e. yr^{-1} (Brun et al., 2017). The rate of average loss in glacier mass in the HMA region is doubled during 2000 and 2016 compared to 1975 and 2000, which is consistent with atmospheric warming and associated energy fluxes (Maurer et al., 2019). The glaciers of the Karakoram and Kunlun Shan ranges are exceptionally in equilibrium or even gaining mass, where mass balance is in sharp contrast with the rest of the HMA (Azam et al., 2018; Bonekamp et al., 2019; Maurer et al., 2019). These variations including seasonality in glacier mass balance are driven by contrasting meteorological conditions. The central and eastern Himalayas are dominated by Indian Summer Monsoon and the western region by westerly circulation (Yi and Sun, 2014). Besides the climatic factor, glacier mass heterogeneity across the HMA has been also attributed to morphometric factors which

comprise the debris cover (Pratap et al., 2015; Vincent et al., 2016); glacier surface velocity (Bolch et al., 2011a; Gardelle et al., 2013); glacier elevation (Liu et al., 2016); and presence of glacial lakes (Basnett et al., 2013; King et al., 2017). The role of runoff from glacierized basins has received increasing attention as climate change is expected to have widespread consequences on snow and glacier runoff across the region (Immerzeel et al., 2010). The increase in runoff at least until 2050 has been projected for river basins of HMA which is primarily caused by the increased ice melt and precipitation in the upper catchment area of the basins (Lutz et al., 2014).

1.2 Debris-covered glaciers

A glacier that has a continuous cover of supraglacial debris across its full width in part of the ablation zone (Figure 1.1) is defined as a debris-covered glacier (Kirkbride, 2011; Mayr and Hagg, 2019). They exist in all the major mountain regions of the world especially in the Himalaya, Karakoram, Alaska, New Zealand and parts of the Andes (Scherler et al., 2018). Debris is typically sourced from surrounding valley walls, which comes down with rockfall and avalanche (Scherler et al., 2011), lateral moraines of the glaciers, and also englacial transport during glacier movement. About 13–36% of the Himalayan region's glacierized area exhibits debris cover (Irvine-Fynn et al., 2017), which shows very slow movement rates at their tongues (Bolch et al., 2008a; Quincey et al., 2009). Heavily debris-covered glaciers with stagnant low gradient terminus regions typically have stable front and not losing their mass (Scherler et al., 2011). The debris-cover glaciers have heterogeneous surfaces with debris thickness that ranging from a few centimeters to meters, and these possess different thermal properties (Chand and Kayastha, 2018), and ice melt decreases as debris thickness increases (Chand et al., 2015). Debris thickness varies widely over short spatial scales (Nicholson et al., 2018), and it tends to increase towards the glacier margins and terminus due to concentration by decelerating ice velocity and increasing background melt-out rate (Kirkbride, 2000; Rounce et al., 2018).

The surface-lowering of the debris-covered glacier associated with ice cliffs and supraglacial lakes are found to be significantly reduce debris thickness (Rounce et al., 2018). The thermal properties of the debris play an important role in the heat conduction from the surface to debris-ice interface, which attenuates the diurnal melt signal due to the time taken for energy to be conducted (Nicholson and Benn, 2013; Fyffe et al., 2014; Chand and Kayastha, 2018). Spatial distribution of supraglacial debris influences the

structure and seasonal evolution of the glacial drainage system (Fyffe et al., 2019). Setting of the debris-covered glaciers favors the formation and expansion of glacial lakes, whose hydrological buffering role remain unconstrained (Irvine-Fynn et al., 2017).

Bajracharya et al. (2014) estimated the area of debris-covered glaciers when they prepared a glacier inventory of Nepal by using Landsat image from 2009 to 2011, which accounted about 11.4% of the total glacier area. The fraction of debris-covered glacier area varies from zero in the Indrawati sub-basin to 28.1% in the Dudh Koshi sub-basin. The total number of debris-covered glaciers in Nepal are 256 covering an area of 445.7 km^2 with an average slope of 14°.

1.3 Glacial lakes

The downwasting of debris-covered glaciers has long been associated with the formation of large and small lakes typically at their terminus and surface (Figure 1.2). The lateral and terminal moraines of the debris-covered glaciers are left standing tens of meters above the glacier surface once downwasting continued and become potential for the formation of glacial lakes. These features affect drainage of meltwater from the glacier surface and facilitate the ponding of meltwater (Kirkbride, 1993) by collapsing roofs of englacial conduits and coalescence of small lakes (Gardelle et al., 2011). Glacial lakes are common features on the surfaces and terminus of relatively slow-moving, debris-covered glaciers (Röhl, 2008) in comparison with clean glaciers. Glacial lakes form where the inclination of the glacier surface is <2° (Reynolds, 2000), and glacier velocity <10 m a^{-1} (Quincey et al., 2007). The rate of ice melt has been found largest at thinner debris (Chand et al., 2015), which helps to develop glacial lakes on the debris-covered glacier with thinner debris in comparison to thick debris.

The increased storage of meltwater from glaciers and snow in the form of supraglacial and proglacial lakes is also an indication of volumetric loss of glacier ice and snow (Nie et al., 2013; Shea et al., 2015). The formed glacial lakes later enhance and accelerate glacier recession through undercutting and calving action of water, and expand rapidly if the outlet channel remains at the same level. In the beginning, small lakes develop near the terminus of the glacier, and enlarges by coalescing together (Figure 1.2) and finally develop into large glacial lake.

Several studies have been conducted in the Himalayan region with a focus on development of glacial lakes (Yamada, 1998; Bajracharya and Mool, 2009; Fujita et al., 2009; Watanabe et al., 2009; Gardelle et al., 2011; ICIMOD, 2011; Thompson et al.,

2012; Nie et al., 2013, 2017; Zhang et al., 2015; Shrestha et al., 2017; Khadka et al., 2019). These glacial lakes are found to be increasing in size and number of glacial lakes in the region. The number and area of the glacial lakes have been increased by about 9% and 14%, respectively between 1990 and 2015 (Nie et al., 2017). Glacier-fed lakes are expanding faster than the non-glacier-fed lakes (Zhang et al., 2015) with significant expansion in the southern slopes of the central Himalaya (Nie et al., 2017).

Glacial lakes are classified differently according to their position with glacier proximity, morphological features, moraines, and outwash plains (ICIMOD, 2011; Raj and Kumar, 2016), and source of water (Song and Sheng, 2016; Qiao and Zhu, 2019) (Figure 1.3). Glacial lakes positioned differently from the proximity of the glacier with different shape, size, and dammed by either ice or debris materials. ICIMOD (2011) classified glacial lakes of the Nepal Himalaya into moraine-dammed lakes, ice dammed lakes (supra-glacial lakes), glacier erosion lakes, and other glacial lakes. Moraine-dammed lake is a water body between moraine ridge and glacier due to the obstruction of moraine ridge and divided into end moraine-dammed (Figure 1.3a), lateral moraine-dammed (Figure 1.3b), and other moraine-dammed lake (Figure 1.3c) (Yao et al., 2018). The moraine is usually composed of debris materials and may be ice-cored or ice-free within it. End moraine-dammed lake is formed when glacier retreats and meltwater is accumulated in the depression between end moraine ridge and terminus of the glacier, while lateral moraine-dammed lake is formed when water accumulated beside the lateral moraine crest. The other moraine-dammed lake is moraine thaw lake, which is formed due to freeze-thaw process of dead ice and is close to end and lateral moraines. Similarly, cirque lakes (Figure 1.3d) develop at the depression caused by glacial erosion on the hanging valley. Glacial lakes are also classified according to the source of water for the lakes, i.e., glacier-fed lakes (Figure 1.3a) and non-glacier-fed lakes (Figure 1.3e) reported in previous studies (Song and Sheng, 2016; Khadka et al., 2018; Qiao and Zhu, 2019). Glacier-fed lakes have a glacier at their catchment, which may either connected or unconnected with the glacier, while non-glacier-fed lakes do not possess the glacier at their catchment and fed by snowmelt and rainwater (Figure 1.4). Supraglacial lakes (Figure 1.4a) and proglacial lakes (Figure 1.4b) are examples of glacier-fed lakes, which are directly connected with a glacier. Lakes that formed at the terminus of the glaciers, moraine-dammed and connected with the glaciers are termed as proglacial lakes. Recently, these lakes started to become disconnected with glaciers with continuous retreating of the glaciers. Spillway lakes at the terminuses of glaciers are dammed by the ice and cannot

be considered as proglacial lakes. Unconnected glacier-fed lakes have a glacier in their proximity but not directly connected with the glacier and receive meltwater from the glacier (Figure 1.4c), while unconnected non-glacier-fed lakes might fed by a glacier in the past; however glaciers were disappeared with time (Figure 1.4d).

1.3.1 Supraglacial lakes

Supraglacial lakes are known for meltwater storage (Watson et al., 2016), which progressively buffering the runoff regimes of the glacier-originated river in increased projections of debris cover (Irvine-Fynn et al., 2017). These features form at the surface of the glacier (Figure 1.4a) and about 77% of supraglacial lake area is found to be associated with an adjacent ice cliff in the Everest region (Watson et al., 2017), which accelerate the glacier recession. The water bodies play an important role in the ablation of debris-covered glaciers (Reynolds, 2000; Benn et al., 2012) through absorbing atmospheric energy (Sakai et al., 2000; Miles et al., 2017a). The majority of absorbed atmospheric energy leaves the lake system through englacial conduits (Sakai et al., 2000; Miles et al., 2016; Watson et al., 2016), and hydraulic connection of lake to englacial water level exerts a key control on whether the lake contributes to longer-term terminus disintegration (Röhl, 2008). This process enlarges the englacial conduits which can collapse the roof of the conduits, leading to the formation of ice cliffs and new lakes (Sakai et al., 2000; Miles et al., 2017b; Watson et al., 2018a). However, the majority of lakes occupy closed basins with no perennial connection to the englacial system and can undergo rapid growth until they find the connection (Benn et al., 2001). Supraglacial lakes are highly recurrent and persistent with high interannual variability (Miles et al., 2017b), but small lakes have the potential to expand rapidly (Sakai et al., 2009).

Previous studies on supraglacial lakes have shown that the lake areas change from year-to-year (Gardelle et al., 2011; Qiao et al., 2015; Watson et al., 2016; Miles et al., 2017b), which may be due to the downwasting of glaciers (Gardelle et al., 2013; Shea et al., 2015; Sherpa et al., 2017; Acharya et al., 2018). These features also show the substantial seasonal variations in response to draining and freeze-thaw activities in different seasons (Miles et al., 2017b), and seasonal differences in the ice melt (Chand et al., 2015). The condition of lake formation according to the glacier's characteristics, including slope and surface velocity has also been demonstrated (Reynolds, 2000; Quincey et al., 2007; Sakai and Fujita, 2010; Miles et al., 2017b).

1.3.2 Glacial lakes of the Nepal Himalaya

The increased storage of glacial meltwater in the Himalayan region have been a focus of interest in recent years (Gardelle et al., 2011; Sawagaki et al., 2012; Nie et al., 2013, 2017; Somos-Valenzuela et al., 2014a; Lamsal et al., 2016; Watanabe et al., 2016; Shrestha et al., 2017; Khadka et al., 2018), as several glacial lakes are leading to potentially dangerous for GLOFs. Several GLOFs have caused significant damage to lower stream of the glacial lakes in the past periods in the Nepal Himalaya (Mool et al., 2001; ICIMOD, 2011; Higaki and Sato, 2012; Veh et al., 2018), and frequency of the GLOF is increasing in the recent period. In Nepal, 12 GLOFs were reported to have occurred between 1964 and 2011 (Harrison et al., 2018). However, Nepal have experienced more than 24 GLOFs including the GLOFs originated in China and caused effect in Nepal (ICIMOD, 2011). Recently, GLOF events documented on the Lhotse Glacier in 2016 (Rounce et al., 2016a), Khangri Nup Glacier in 2017 (Miles et al., 2018), in upper Barun Valley in 2017 (Byers et al., 2019) indicated the frequent occurrence of GLOFs in the latest period. GLOFs have occurred in Nepal more than every three years since the 1960s (Yamada and Sharma, 1993). These statistics indicate the increased frequency of GLOFs resulted from rapid expansion of glacial lakes and increased in their number. Nepal is the country with the greatest national-level economic consequences (Carrivick and Tweed, 2016) and potential impacts of the GLOFs likely to increase in the future with increase in number of glacial lakes.

ICIMOD (2011) prepared a glacial lake inventory of Nepal using Landsat images from 2005/06 except for small area of the Mahakali basin for which images from 2000 and 2001 had been used. The inventory identified a total of 1,466 glacial lakes covering the total area of 64.78 km^2 and mean area of 0.044 km^2 applying area threshold of >1,000 m^2. The glacial lakes were classified as moraine-dammed (66.6%), ice-dammed or supraglacial (7.3%) and glacier erosion lakes (25.1%). The largest number (346) of the lakes is found in the Humla Karnali subbasin; however, largest area (13.2 km^2) covered by the lakes is observed in the Dudh Koshi subbasin. The study also identified 21 potentially dangerous lakes by evaluating 49 lakes with size >0.02 km^2 based on size, expansion rate, water level, dam condition, glacier characteristics, physical conditions of surroundings and intermittent activity of supraglacial lakes.

Similarly, Rounce et al. (2017) identified 131 glacial lakes in the Nepal Himalaya that are greater than 0.1 km^2 and classified 11 lakes as very high risk and 31 as high risk

based on mass entering the lake, the moraine stability and lake expansion. They also classified six lakes as supraglacial lakes, 64 as unconnected glacier-fed lakes, 37 proglacial lakes and 24 non-glacier-fed lakes.

Khadka et al. (2018) revealed 1,541 glacial lakes with the total glacial lake area of 80.95 ± 15.25 km^2 using the area threshold of ≥3,600 m^2 using the Landsat images of 2017. They identified 1,064 (64.69 km^2) lakes as glacial-fed lakes, and the remaining 477 (16.26 km^2) as non-glacier-fed lakes. They further classified the lakes into supraglacial lakes, proglacial lakes and unconnected glacier-fed lakes. Maximum lake area was recorded in the Koshi River basin among the four major river basins in Nepal, which was largely contributed by the proglacial lakes (Figure 1.5). The number of supraglacial lakes were also the largest in the Koshi River basin. They also presented the decadal expansion of glacial lakes for the whole Nepal, where glacial lake area expanded at rates of 1.63 % yr^{-1} between 1977 and 1987, 0.67 % yr^{-1} between 1987 and 1997, 0.77% yr^{-1} between 1997 and 2017, and 0.91 % yr^{-1} between 2007 and 2017.

1.4 Remote sensing of glacial lakes

High mountain glacial lakes are difficult to access due to their remoteness, expensiveness and rugged topography. Therefore, field-based study that focuses on the development of glacial lakes is limited. The use of multi-temporal satellite imagery is a common technique for monitoring large glacial lakes (Watanabe et al., 1994, 2009; Gardelle et al., 2011; Somos-Valenzuela et al., 2014b; Zhang et al., 2015; Lamsal et al., 2016) and widely applied in the HMA region. Large glacier lakes can be delineated using remote sensing techniques by applying manual methods (Wang et al., 2015; Zhang et al., 2015) and automatic mapping in combination with manual editing methods (Gardelle et al., 2011; Watson et al., 2016; Miles et al., 2017b; Nie et al., 2017). The accurate classification of glacial lakes is required to reveal spatiotemporal variation in lake area. Automatic mapping of the glacial lakes include object based image analysis (OBIA) and segmentation (Qiao et al., 2015; Watson et al., 2016); and index based classification, i.e., Normalized Difference Water Index (*NDWI*) (Huggel et al., 2002; Gardelle et al., 2011; Miles et al., 2017b) techniques. The band ratio approach is widely used method and *NDWI* initially used the near infra-red and green band (McFEETERS, 1996) to delineate open water features and enhance their presence in remotely-sensed multispectral imageries. Similarly, blue band was also used instead of green band (Huggel et al., 2002). Clear and green water bodies reflect more green light than red light, while brown water bodies

reflect more red light than green light and thus believed to be and act differently in mapping inland water bodies with different colours (Yan et al., 2017). Later, the *NDWI* was replaced by the modified normalized difference water index (*MNDWI*) to suppress noise from built-up land (Xu, 2006).

Additionally, Normalized Difference Moisture Index (NDMI), Water Ratio Index (WRI), Normalized Difference Vegetation Index (*NDVI*), and Automatic Water Extraction Index (AWEI) were also proposed for the extraction of surface water from satellite images (Rokni et al., 2014). However, *NDWI* is most popular and found superior to other indexes and have been used for spatiotemporal changes of the water bodies (Ji et al., 2009; Rokni et al., 2014). Recent study has optimized the *NDWI* and proposed an optimized *NDWI* by using the reference dataset of supraglacial lakes in the Everest region (Watson et al., 2018b). Water can be distinguished from surrounding snow and ice or debris cover and misclassification arising from topographic shadows can be reduced by using shadow and slope mask (Miles et al., 2017b). The possibility of misclassification and omission of lakes increases significantly with moderate resolution of the dataset (Watson et al., 2016) and manual editing is recommended to increase the accuracy of the mapping (Mergili et al., 2013; Shukla et al., 2018).

1.5 Motivation and research objectives

Several glacial lakes are developing and increasing in their size with the downwasting of debris-covered glaciers. Several of these lakes are becoming potentially hazardous in high mountain regions of the Himalayas. Several GLOFs have been occurring more than every three years after the 1960s (Yamada and Sharma, 1993). The Everest region in the Nepal Himalaya is one of the hotspots of glacial lakes (Salerno et al., 2012; Rounce et al., 2016b; Watson et al., 2016). Several previous studies were conducted in the Nepal Himalaya focusing on the development of glacial lakes (e.g., Watanabe et al., 2009; Fujita et al., 2009; Byers et al., 2013; Lamsal et al., 2016). Past study also focused on hazard assessments (e.g., Quincey et al., 2007; Bolch et al., 2008b; Watanabe et al., 2009; Aggarwal et al., 2016; Rounce et al., 2016b), and involvement of community in glacial lake research (e.g., Singh et al., 2016; Watanabe et al., 2016). Most of these studies demonstrated the development of glacial lakes usually on a decadal basis (Bajracharya and Mool, 2009; Shrestha et al., 2017; Khadka et al., 2018), and were regionally aggregated (Gardelle et al., 2011). Furthermore, these studies were glacier or lake specific (Benn et al., 2000, 2001; Bolch et al., 2008b; Thompson et al., 2012) or used

one time satellite imagery (Salerno et al., 2012). Study to understand the spatial, seasonal and interannual patterns of the supraglacial lakes using Landsat images of 30-m resolution for five glaciers in the Langtang Valley (Miles et al., 2017b) has been carried out, but no study is found in the eastern region of Nepal.

Furthermore, there is almost no research being conducted on the spatial, seasonal variations and long-term development of the supraglacial lakes on an annual basis, despite their importance in studies on the impact of recent climate change (Richardson and Reynolds, 2000; Salerno et al., 2012) that comprises all the debris-covered glaciers of the Everest region. Similarly, detailed studies on development of glacial lakes for the Kangchenjunga region are not documented unlike the Everest region. Several GLOFs are reported near the Everest region and only one event has been reported from the Kangchenjunga region. It is important to understand the historical GLOFs events, which improve the knowledge of the past GLOFs in the Kangchenjunga region.

Study of glacial lakes are also important in understanding the evolution of small lakes into large glacial lakes in the future. Efforts for documenting the development of the supraglacial lakes and their variations were made for the Everest region (Watson et al., 2016) by using satellite imageries of 0.5- to 2-m resolution. However, their study incorporated only eight glaciers and used historical imageries only from 2000 to 2015. Therefore, this study examined all the debris-covered glaciers of the Everest region to understand the evolution of supraglacial lakes, their persistence, and their trajectory towards large glacier lakes.

Therefore, this study aims: i) to prepare the high-resolution inventory (2 m) of the glaciers and glacial lakes for the Everest region; ii) to understand the spatial, annual, and seasonal variations of supraglacial lakes from 1989 – 2018 for the Everest region; and iii) to study the decadal development of glacial lakes between 1964 and 2018 and tracing the historial GLOFs in the Kangchenjunga region. Based on these analyses, I would like to discuss the uncertainty in mapping of glacial lakes, future trajectory of glacial lakes, past and future GLOFs and their consequences in the eastern Nepal Himalaya. The ultimate goal of this study is to prepare the highly accurate inventory of the glacial lakes using the very high-resolution satellite images and understanding their trajectory.

1.6 Thesis structure

The structure of the thesis has been designed to understand the development of glacial lakes in the Everest and Kangchenjunga regions, eastern Himalaya. Chapter 2

provides a detailed description of the data and methods used to achieve the aims of the research. Chapter 3 focused on the high-resolution inventory for the debris-covered glaciers and glacial lakes in the Everest region. The correlation between the area of the supraglacial lakes and characteristics of the glaciers is presented in this chapter. Chapter 4 investigated the dynamics of the supraglacial lakes in the study areas in terms of their spatial, seasonal and annual variation between 1989 and 2018. This chapter also explains a future trajectory of the spillway lakes and major finding of the unmanned aerial vehicle (UAV) survey at the spillway lakes of the Ngozompa Glacier. Chapter 5 examines the development of glacial lakes during 1964 and 2018 using Corona, Landsat and Sentinel-2 imageries in the Kangchenjunga region. It also explains the footprint of past GLOFs in this region, which has not been documented before. Chapter 6 discusses the major findings of the research in the Everest and Kangchenjunga regions and synthesizes the results of the previous investigations to provide a comprehensive overview of development of supraglacial lakes in the Everest region and all glacial lakes in the Kangchenjunga region. Some relevant suggestions for monitoring glacial lakes and future direction for the research are included at the end of this chapter. Finally, conclusions of this research are presented in Chapter 7, which includes uniqueness, major outcomes and future direction of the research.

Figure 1.1 Ngozompa Glacier, a typical debris-covered glacier of the Nepal Himalaya showing an outlet channel from the spillway lakes (Photo was taken during the fieldwork on 10 December 2018).

Figure 1.2 Complex of spillway lakes at the terminus of the Ngozompa Glacier showing several supraglacial lakes and enclosed ice cliffs (Photo was taken during fieldwork on 10 December 2018).

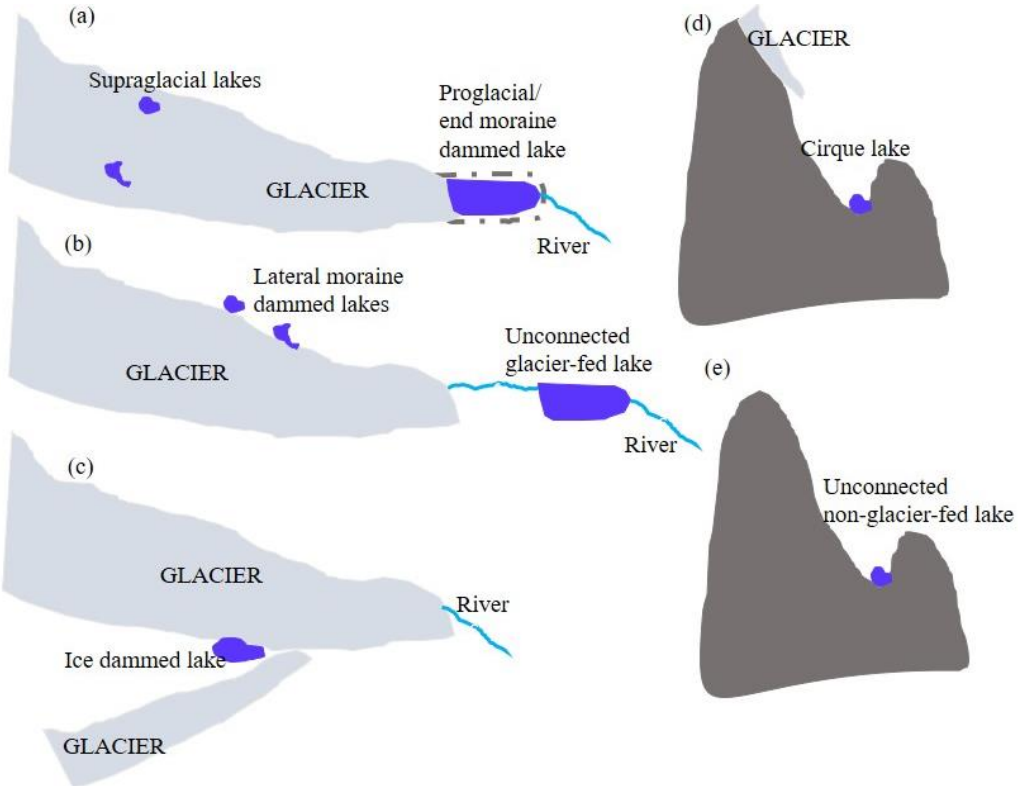

Figure 1.3 Schematic diagrams of the types of glacial lakes: (a) supraglacial and proglacial/end moraine-dammed lakes; (b) unconnected glacier-fed lake and lateral moraine-dammed lakes; (c) ice-dammed lake; (d) cirque lake with glacier at upstream; and (e) and unconnected non-glacier-fed lake.

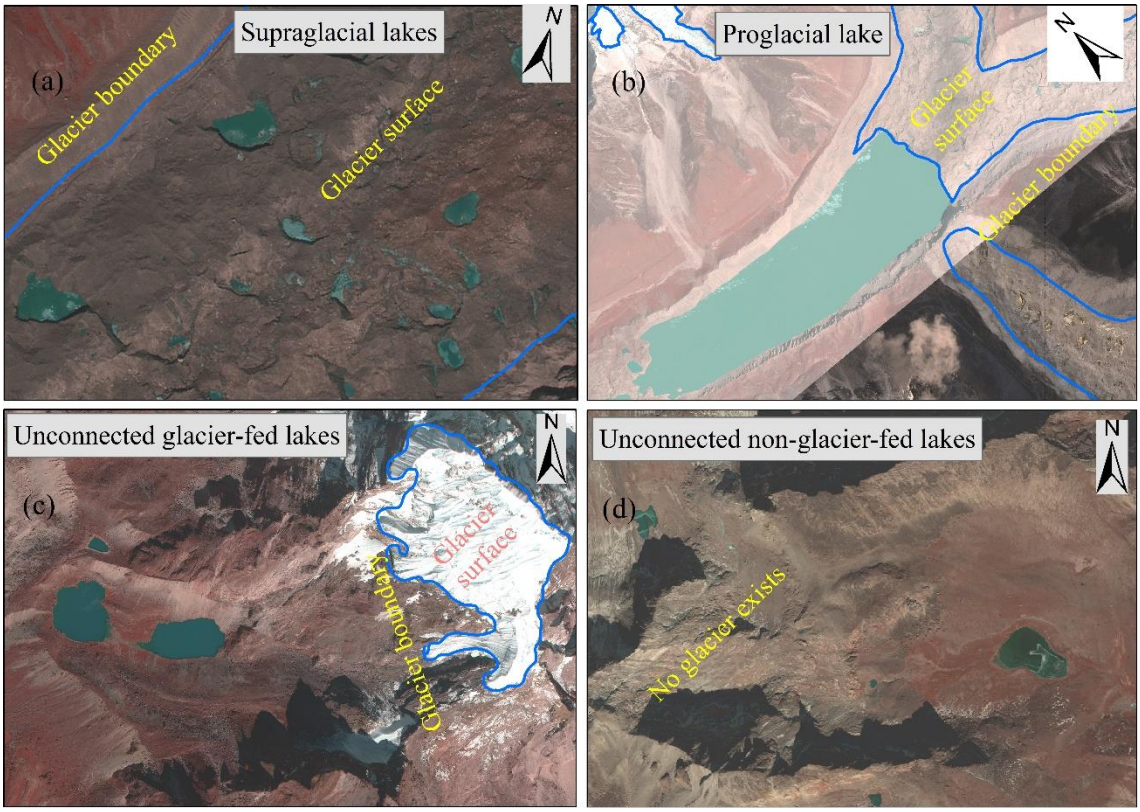

Figure 1.4 Examples of different types of glacial lakes: (a) supraglacial lake at the surface of glacier; (b) proglacial lake at the terminus of the glacier; (c) unconnected glacier-fed lakes; and (d) unconnected non-glacier-fed lakes. (Base images: WorldView of 2-m spatial resolution)

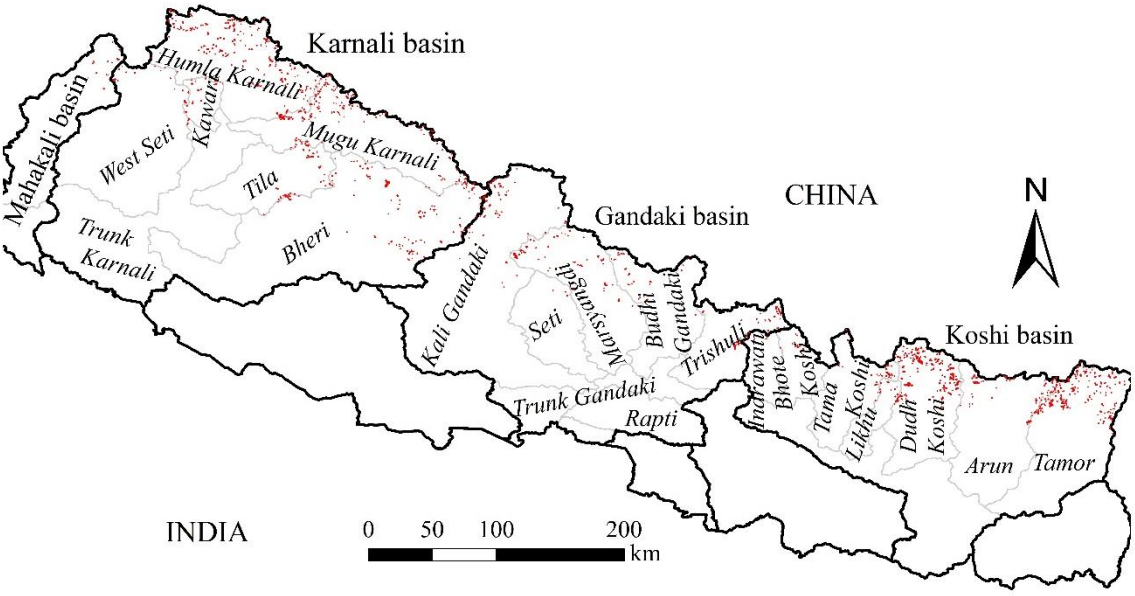

Figure 1.5 Distribution of glacial lakes in Nepal (Khadka et al., 2018).

2. Methodology and study areas

2.1 Definitions and terminology

Glacial lake is a body of water formed by the action of a glacier. Lakes in the Nepal Himalayas also known locally as *Tsho, Taal, Pokhari, Kunda,* and *Daha.* Glacial lakes in the high mountain Himalayas can be divided in to glacier-fed and non-glacier-fed lakes according to the source of water. The lake from where river is originated is termed as spillway lake and spillway lake associated with supraglacial lakes is termed as complex spillway lake in study.

Glacial Lake Outburst Floods (GLOF) also known as *Aluviones*, *Débâcles*, Glacial outwash floods, *Gletscherlauf* (German), *Jökulhlaup* (Icelandic), Megafloods, and superfloods (Quaternary large-scaled glacier floods) and refer to sudden and in some cases cyclic release of meltwater from a glacier-dammed or moraine dammed lake, which can result in a catastrophic flood (Richardson and Reynolds, 2000; Iturrizaga, 2011). The mechanism of GLOF is the rupture of an internal water pocket, the progressive enlargement of internal drainage channels and catastrophic glacier buoyancy (Richardson and Reynolds, 2000) and triggered by avalanche, rockfall, seismic activities, slope, moraine stability and others. Glacial lake outburst produces flow of water that may be an order of magnitude greater than average rainfall-derived peak.

2.2 Datasets and methodology

This study has used remote sensing data to assess the evolution, variation, and to prepare the high-resolution inventory of the glacial lakes from the 1960s to 2018. Remote sensing data used in this study are from multiple platforms and sensors with medium- to high-resolution. These were Landsat (30-m resolution), Sentinel-2 (10-m resolution); Corona KH-4a (2.7-7.6 m), WorldView-2, WorldView-3 and GeoEye-1 (2-m and 0.5-m resolution), Advance Spaceborne Thermal Emission and Reflection Radiometer (ASTER) (30 m), Advanced Land Observing Satellite- Phased Array type L-band Synthetic Aperture Radar (ALOS- PALSAR) (12.5 m), High Mountain Asia DEM (8 m), and (UAV) photographs. The dataset used for each chapter and methods applied for each objective of the study are described in the respective chapters.

2.3 Study area

The mountain ranges in the Hindu-Kush Himalaya (HKH) are the highest on the Earth and form natural barriers in the landscape, and moving air masses in the atmosphere are lifted when passing the mountain range (Lutz, 2016). The HKH encompasses an area of about 4.2×10^6 km^2 (Bajracharya et al., 2015), extending about 3,500 km from Afghanistan in the west to Myanmar in the east. Monitoring the Himalayan glaciers continues to be a practical challenge and the response of Himalayan glaciers to climate is documented less extensively. Therefore, this thesis focused on high-elevation catchments in the Nepal Himalaya, which are extensively covered by the glaciers. Nepal lies in the eastern region of the HKH (Figure 2.1), characterized by the high relief and steep slopes. Two sites, i.e., Everest region and Kangchenjunga regions were chosen to understand the dynamics of the glacial lakes. The Everest and Kangchenjunga regions are located in northeastern part of Nepal and part of the central Himalaya (Figure 2.2) and described in detail in the following sections.

Nepal lies on the south edge of the elevated Tibetan Plateau, and alluvial plains of the Ganga delimit this mountain range from the south (Figure 2.1). About 80% of the country's land is occupied by mountains (Dhital, 2015a). Its altitude ranges from 64 m to 8,848 m within an aerial distance of about 150 km and divided in to five major tectonic zones, i.e., Gangetic plain, sub-Himalayan (Siwalik) zone, lesser Himalayan zone, higher Himalayan zone, and Tibetan-Tethys Himalayan zone (Dahal, 2006). Physiographically, the territory of Nepal is divided into eight physiographic regions: 1) Terai (southern most plain area); 2) Siwalik range with dun valleys (Chure hills); 3) Mahabharat range; 4) Midlands (low land between Mahabharat and High mountains); 5) Fore Himalaya (foot of Great Himalayan range); 6) Great Himalaya (Highest mountains range); 7) inner Himalayan valleys (valleys surrounded by the Great Himalayan and Tibetan Marginal ranges); and 8) Tibetan marginal ranges (North most boundary of the Inner Himalaya) (Figure 2.3) (Dhital, 2015b).

Nepal encompasses four major river systems, i.e., Mahakali and Karnali in the west, Gandaki or Narayani in the center and the Koshi in the east, which are the major tributaries in the Ganges River basin (WECS, 2011). Depending on the origin and discharge, the rivers of Nepal can be classified into three types. The major rivers are originated from the Himalaya and their discharge is largely contributed from snow and ice melt. These rivers are perennial source of water for irrigation and hydropower

development. The second type of rivers are originated from the Midlands and has wide seasonal fluctuations, and the third type of rivers are originated from the Siwalik Range and have very little flow during the dry season.

The climate of the Nepal Himalaya is dominated by the monsoon season, with its spatial meteorological variability through relief, illumination, and wind channelization by rugged topography. Mean annual precipitation in Nepal varies from less than 150 mm in upper Mustang to above 5,000 mm in Lumle of Kaski District, Gandaki province with mean annual precipitation of 1,858 mm (Figure 2.4) (DHM, 2015). Nepal receives about 80% of the total annual precipitation in summer (June – September) (Shrestha, 2000; DHM, 2015). The effect of monsoon is more in the eastern half of the country than the western half. Winter season (December – February) is influenced by the westerly disturbances. However, it brings only 3.5% of the total annual precipitation in the form of snow in higher altitude (DHM, 2015). The winter precipitation is large in the Far-western province and low in southern parts of central and eastern regions. Glaciers of this region are of summer-accumulation type, and accumulation and ablation mainly occur simultaneously (Ageta and Higuchi, 1984) during the summer season. Melting and runoff of snow and ice occur, especially in the pre-monsoon season (March – April) when maximum temperatures are the highest (DHM, 2015). In Nepal, temperature is the lowest during the winter (December – January) and increases as spring advances and monsoon rain checks the increase of temperature. Mean annual maximum temperature is more than 30°C in the southern plains of the country, while it is below 0°C in the high altitudes (Figure 2.5).

2.3.1 Everest region: upper Dudh Koshi basin

2.3.1.1 Physiographic setting

The Everest region is located in the Khumbu Pasanglhamu rural municipality of the Solukhumbu District, in upper part of the Dudh Koshi River (DKR) basin (Figure 2.6), which is one of the most glacierized regions of the Nepal Himalaya. The whole DKR basin encompasses the 287 glaciers covering an area of 391.1 km^2 (Bajracharya et al., 2014), 9.62% of the total basin area. The glaciers in this region are characterized by the presence of debris in their lower reaches. The debris area covers approximately 28% (110 km^2) of the total glacier area in the DKR basin (Bajracharya et al., 2014). Solukhumbu district is known for highest mountain in the world (Mt. Everest), and several other

mountains, i.e., Lhotse, Choyu, Gyanchung Kang, Thamserku, Pumori, Nuptse, Island peak (Imja Tse), Baruntse, and Ama Dablam have elevation above 6,000 m. DKR is one of the seven major tributaries of the Koshi River. The Everest region including the highest peaks Mt. Everest, Lhotse and Choyu is located in the transition zone between the metamorphic sequence of the High Himalaya and the overlying sedimentary series of the Tibetan (or Tethys) Himalaya (Ferrara et al., 1983). Typical landform of the Everest region comprises the high-elevated mountains with rivers in deep gorges (Figure 2.7).

The Everest region is also a part of the Sagarmatha National Park (SNP), a World Heritage site that is the highest mountainous area in the world. The SNP covers the northern part of the DKR basin, which was established in 1976, and encompasses an area of 1,148 km^2 (DNPWC, 2019a). In this study, the boundary of the Everest region is delineated based on the confluence of the Bhote Koshi River and the Dudh Koshi River, and elevations of the region ranges from 2,880 m a.s.l. at confluence point to 8,848 m a.s.l. at the peak of Mt. Everest. The area of the Everest region is 1,131 km^2, and about 65% of the total area of the Everest region has an elevation higher than 5,000 m. The largest area (52%) of the region lies in the elevation between 5,000 and 6,000 m and followed by the elevation between 4,000 and 5,000 m (32%). The Everest region is bordering with the Tibet Autonomous region of China in North, Makalu Barun National Park in East, Gaurishankar Conservation Area in West and lower part of the Solukhumbu District in South. The major settlements in the Everest region include Namche Bazar, Khumjung, Khunde, Thame, Phortse, Pheriche, Dingboche, Dole, and Machhermo.

2.3.1.2 Rivers and catchments

Upper DKR basin in the Everest region encompasses three major sub-catchments based on three glacier-fed rivers, i.e., Bhote Koshi in the western side, Dudh Koshi in the middle and Imja Khola in the eastern side. Imja Khola comprises two main tributaries: Khumbu Khola from the Khumbu Glacier and Imja Khola from the Imja Glacier, which merge at ~1.3 km down from Pheriche and Dingboche villages and continue as Imja Khola. Imja Khola merges with the Dudh Koshi River that originated from the Ngozompa Glacier, while Bhote Koshi merges with the Dudh Koshi River about 1.7 km below Namche Bazar. The detail of the sub-basins of the Everest region is explained in the section 3.4.1.

2.3.1.3 Flora and fauna

SNP has six vegetation zones: 1) upper temperate (2,500 3,000 m); 2) lower subalpine (>3,000 m) with forest of blue pine (*Pinus wallichiana*), east Himalayan fir (*Abies spectabilis*) and dropping juniper (*Juniperus recurva*); 3) upper subalpine (>3,600 m) with birch rhododendron forest (*Rhododendron campanulatum* and *Rhododendron campylocarpum*), *Betula utilis*; 4) lower alpine (3,800 – 4,000 m) with scrub of *Juniperus* species, *Rhododendron anthopogon* and *Rhododendron lepidotum*; 5) upper alpine (>4,500 m) with grassland and dwarf shrubs; and 6) nival zone with cushion plants (>5,000) (SNP, 2019). Forest occupy less than 10% of the total area of the park and its buffer zone and mostly found in the lower valley gorges below 3,500 m (DNPWC, 2016).

The main mammals in the park are snow leopard, Himalayan musk deer, Himalayan black bear, red panda, Himalayan tahr and wolf, while the park has eight species of reptiles, seven species of amphibians, 30 species of butterflies (DNPWC, 2016) and 194 species of birds (Basnet, 2004 cited in DNPWC, 2016). Out of 33 mammals found in SNP, 13 species are protected by CITES (Bhuju et al., 2007).

2.3.1.4 Climate

The influence of monsoon is relatively higher in eastern Nepal as Monsoon enters from the eastern region, while the Everest region is characterized by a semi-arid climate (Tartari et al., 1998), probably due to obscured by the series of hills and mountains as altitude increases. The mean annual temperature and total precipitation at the Pyramid station (5,050 m) from 1994 – 2013 was observed to be -2.45°C, and 446 mm, respectively (Figure 2.8) (Salerno et al., 2015, 2016). The mean minimum temperature (-12°C) was found in January and February, while minimum temperature (-22°C) has been recorded in January. Similarly, July is the warmest month but air temperature can drop below freezing even in the warmest months (27% in June) and on average, night freezing does not occur on less than a quarter of days during the year (Tartari et al., 1998). In total, 90% of the precipitation falls between June and September, during which probability of snow is only 4% but reaches 20% at the annual level (Salerno et al., 2016).

2.3.1.5 Land use and land cover

The land use and land cover map of the SNP and Buffer Zone (SNPBZ) revealed that largest portion of the area is dominated by the bare rock and soil, which contributed

58% (817.9 km^2) of the total area of the SNPBZ in 2011 (Garrard et al., 2016). Garrard et al. (2016) plotted the 15% of area as shrub land and similar area as permanent ice. They also classified the area into forest, agriculture, grazing, settlements and lake, all of which contributed only 12% of the total area. The continuing use of firewood has caused to the thinning of forests in part of the national park and to the depletion of shrub juniper in the alpine region (Stevens, 2003).

2.3.2 Kangchenjunga region: upper Tamor River basin

2.3.2.1 Physiographic setting

The Kangchenjunga region (upper Tamor River (UTR) basin) lies in the Phaktanglung rural municipality of Taplejung District in the upper Tamor basin, also a tributary of the Koshi basin (Figure 2.9). The whole Tamor basin consists of 262 glaciers covering an area of 385.9 km^2, 6.4% of the total basin area, and debris area covered approximately 18% (73 km^2) of the total glacier area in the Tamor basin (Bajracharya et al., 2014). The Kangchenjunga region is also a part of the Kangchenjunga Conservation Area (KCA), covering an area of 2,035 km^2 (DNPWC, 2019b). In this study UTR basin is delineated based on the confluence point of the Tamor, Ghunsa, and Shinbuwa rivers near Lelep Village. Typical landscape within the KCA includes forest, rivers, glaciers, glacial lakes, high mountains, bare lands (Figure 2.10). The elevation of UTR basin is ranges from 1,472 m a.s.l. at the confluence point to 8,586 m a.s.l. at the peak of the Mt. Kangchenjunga. The area of the UTR basin is 1,783 km^2. The Kangchenjunga region is also bordering with the Tibet Autonomous region of China in the North, Sikkim of India in the East, Sankhuwasabha district and lower part of the Taplejung District. About 46% of the total area of the Kangchenjunga region has an elevation higher than 5,000 m a.s.l. This region consists of 253 glaciers covering an area of 383.7 km^2, more than 96% of the total glacier area within the whole Tamor basin. The Nangama glacial lake in this basin experienced a GLOF in 1980, which caused severe damage to the downstream region.

2.3.2.2 Rivers and catchments

The name of the Tamor River is assumed to be based on the Tamor Khola that originated near the Tiptal Bhanjyan bordering with the Tibet and upstream of the Olanchungola Village. The UTR basin comprises three main river: 1) Tamor Khola, 2) Ghunsa Khola, and 3) Simbuwa Khola. These three rivers merge near the Lelep Village

to form a larger Tamor River. In this study, the UTR basin was divided into five sub-basins based on the major tributaries in the basin (details in section 5.4.1).

2.3.2.3 Flora and fauna

Kangchenjunga Conservation Area was established in 1997, being named after Mt. Kangchenjunga (8,586 m), second highest mountain in Nepal and the third highest in the world (DNPWC, 2019b). This area is a key link in the chain of transboundary protected areas in the vast landscape, maintaining contiguity between the Quomoloangma Nature Reserve in China and Kanchendzonga Biosphere Reserve in India (Bhandari et al., 2018). This conservation area comprises nine bioclimatic zones from lower sub-tropical (1,000-1,500 m) to nival zone (>5,000 m), where more than 15 mammals, 280 bird, 300 species of flora including 77 vascular plants are reported (Bhuju et al., 2007). Snow leopard, musk deer and red panda are considered as symbolic of KCA and blue sheep is assumed as a great attraction for trekkers (Watanabe, 2006).

2.3.2.4 Climate

No meteorological measurements area available near the KCA above 2,000 m of elevation. Temperature and precipitation data for Taplejung and Lungthung stations were collected from the Department of Hydrology and Meteorology (DHM), while mean temperature at an elevation of 4,765 m was extracted from ERA5 reanalysis dataset. The mean annual temperature at Taplejung station (1,732 m) from 2000 – 2008 and total precipitation at Lungthung station (1,780 m) in 2008 were observed to be 16.6 °C and 2,220 mm, respectively. The highest mean maximum temperature was observed in the June, July and August, while the lowest temperature was observed in January (Figure 2.11). The reanalysis data showed the positive mean monthly temperature (>0°C) during the monsoon period (June – September), while negative during the rest of the period. In total, 82% of the precipitation falls between June and September. Erratic pattern of annual precipitation has been observed between 1948 and 2014 that ranges from 1,408.9 mm in the year 2009 and 2,505 mm in the year 2003 at the Taplejung station (Bhatta et al., 2018), where mean annual precipitation was found 1,978.8 mm (Kattel and Yao, 2013), less than that of the Lungthung station. However, precipitation between June and November in 2001 was only 299.2 m on the Kangchenjunga Glacier (4,648 m) and 425.4 mm on the mid-slope at an altitude of 5,235 m (Watanabe, 2006), which is far less than the

precipitation observed at lower altitudes. The major settlements in the Kangchnejunga region include Lelep, Olanchungola, Ghunsa, Tapethok, and Yamphudin.

2.3.2.5 Land use and land cover

Land use and land cover of the KCA comprises 31% of the area covered by the ice/glaciers and snow in 2000 (Kellenberger et al., 2006). Similarly, they classified the 24% of total area as forest, 20% as alpine grassland/meadows, 9% as rocks and bare land. However, the area covered by the rocks together with ice/rivers was about 65% (Amatya et al., 1995 cited in Gurung, 2006). The percentage of area cover by the water bodies and cultivated land was about 2% of total area of the KCA. The area of the ice/glaciers and snow is found decreased by about 61 km^2 between 1989 and 2000 (Kellenberger et al., 2006). Similarly, forest land also shown to have decreased by 36% in Lelep, Sekhathum-Amjilesa, Syajunma and Ramsympati part of the region (Gautam and Watanabe, 2004).

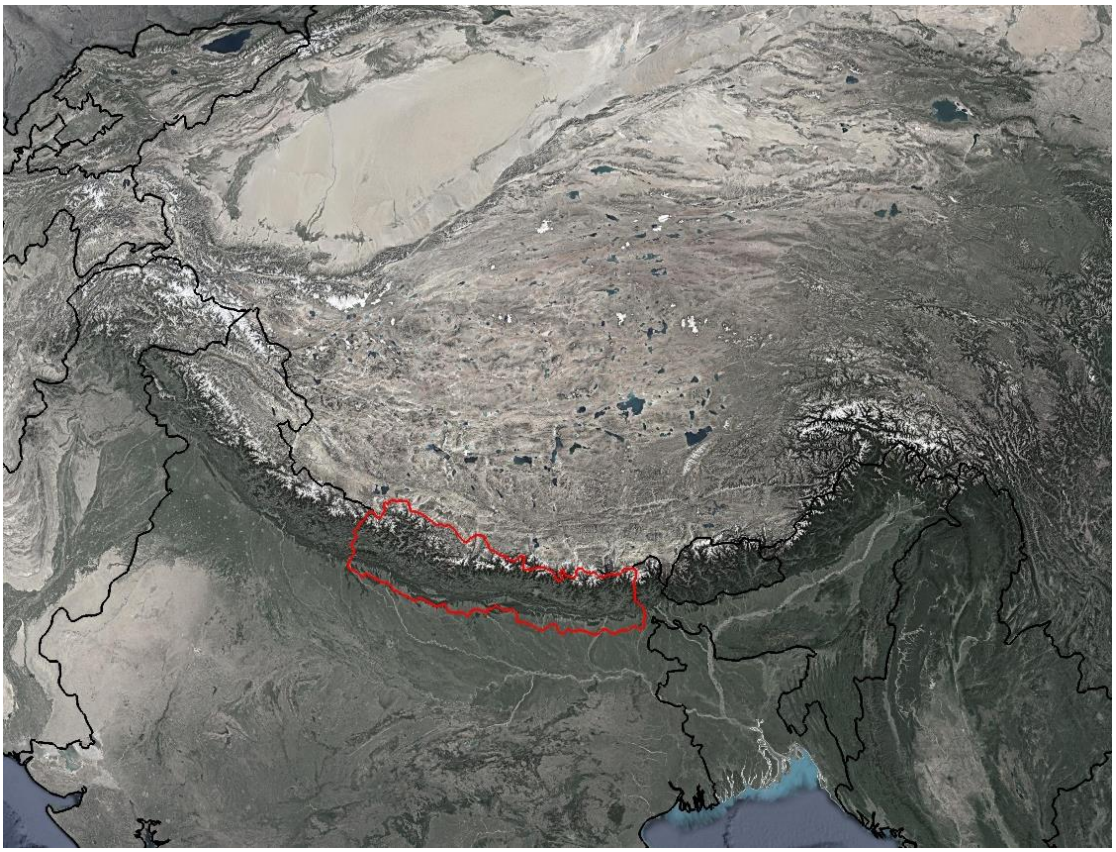

Figure 2.1 Location of the Nepal Himalaya.

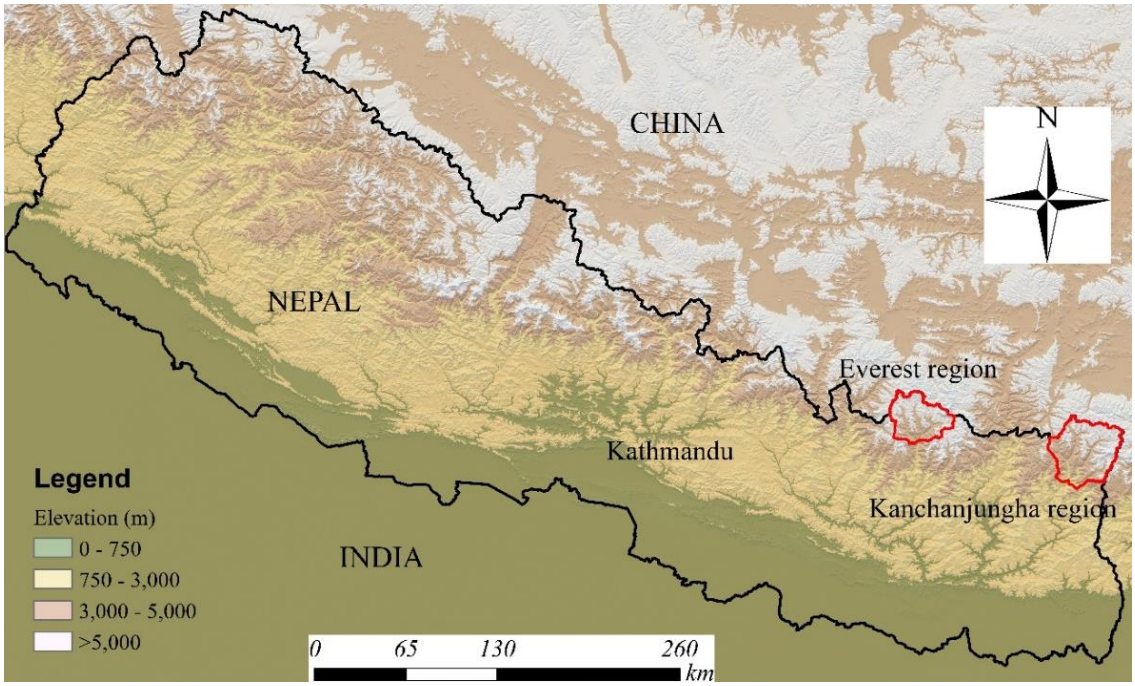

Figure 2.2 Location of the Everest and Kangchenjunga regions within the Nepal Himalaya.

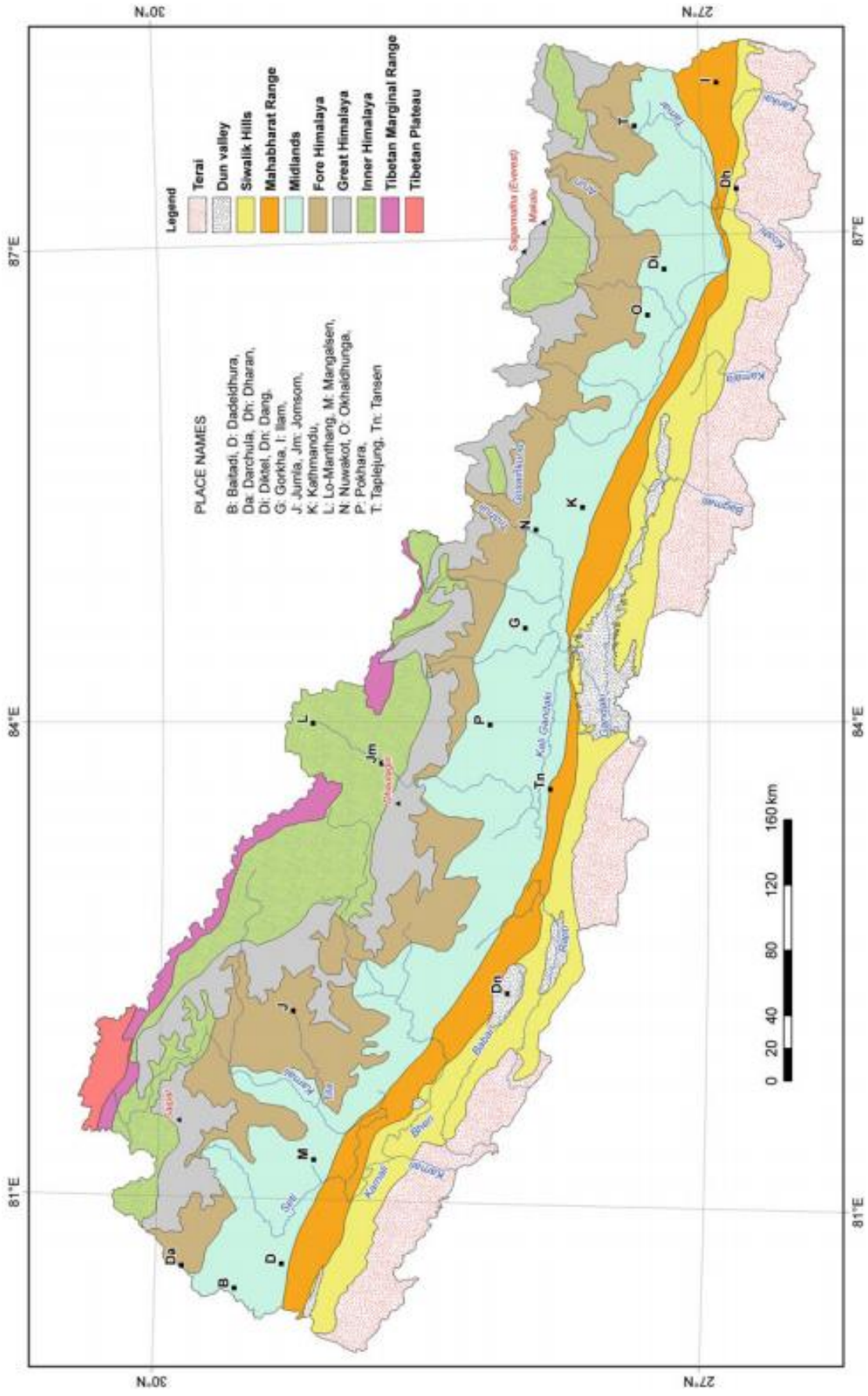

Figure 2.3 Physiographic divisions of Nepal (Dhital, 2015b).

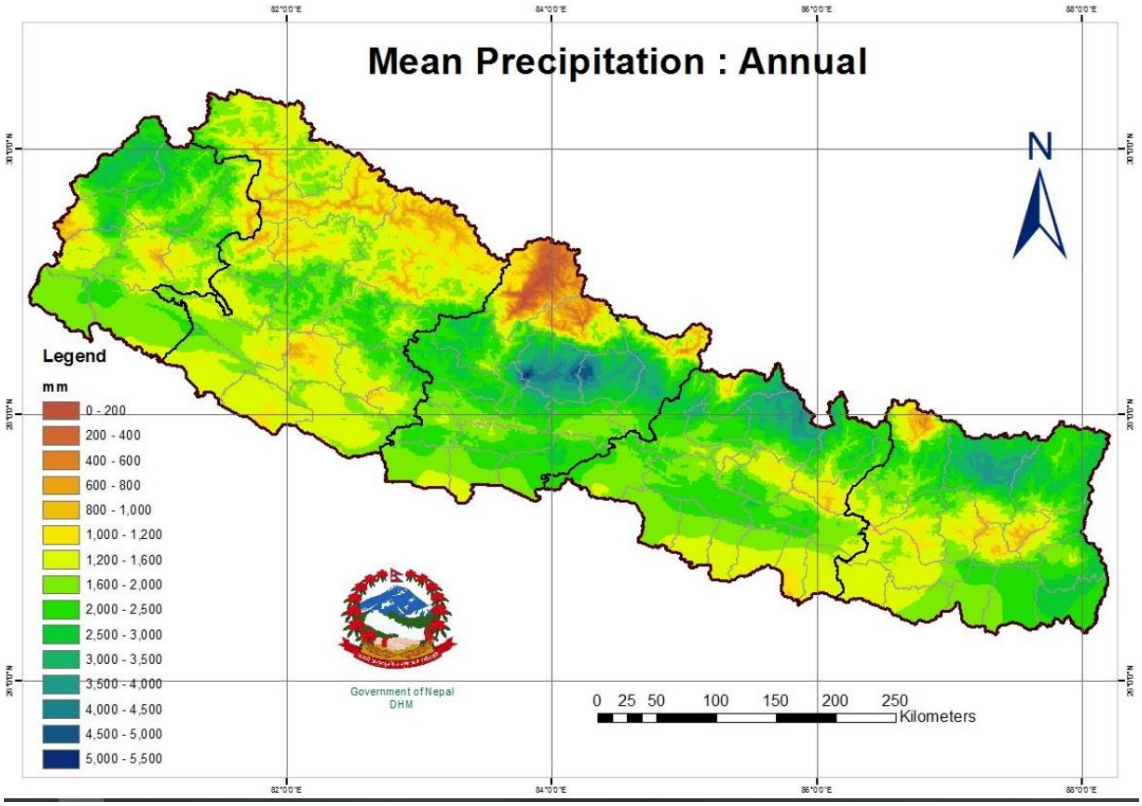

Figure 2.4 Mean annual precipitation variation over Nepal (reference period 1971 – 2014) (DHM, 2015).

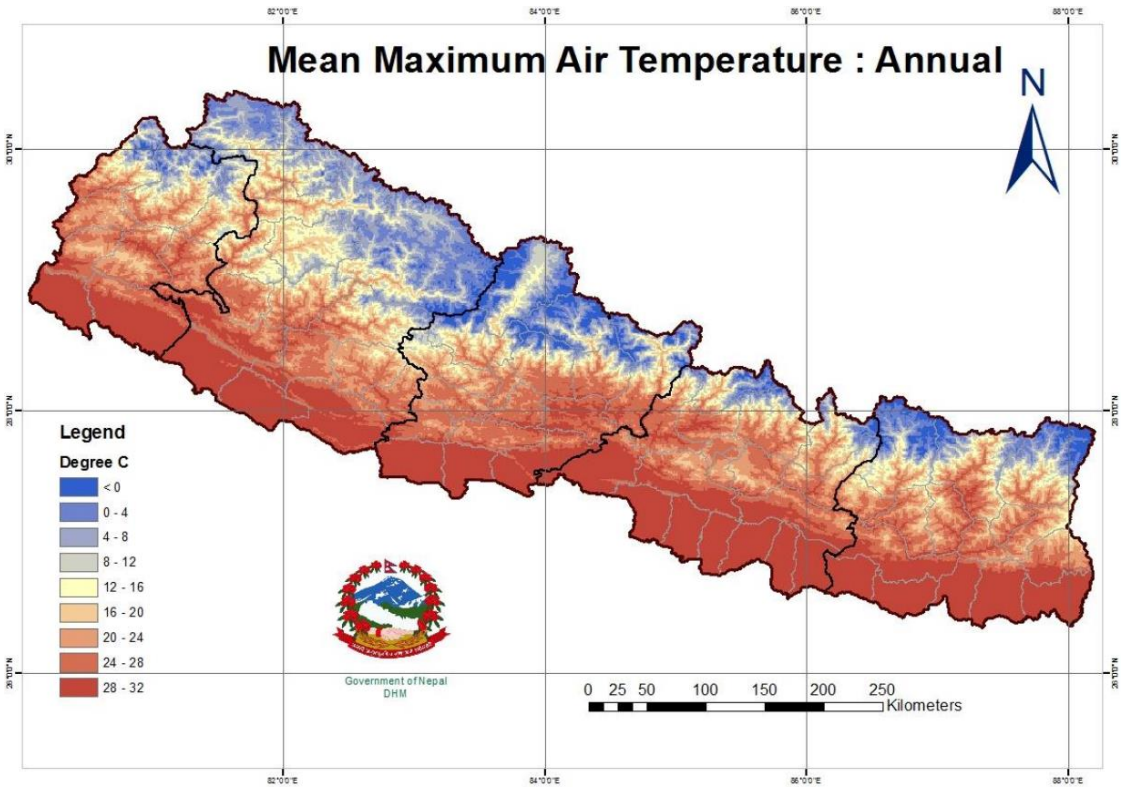

Figure 2.5 Mean annual maximum air temperature over Nepal (reference period 1971 – 2014) (DHM, 2015).

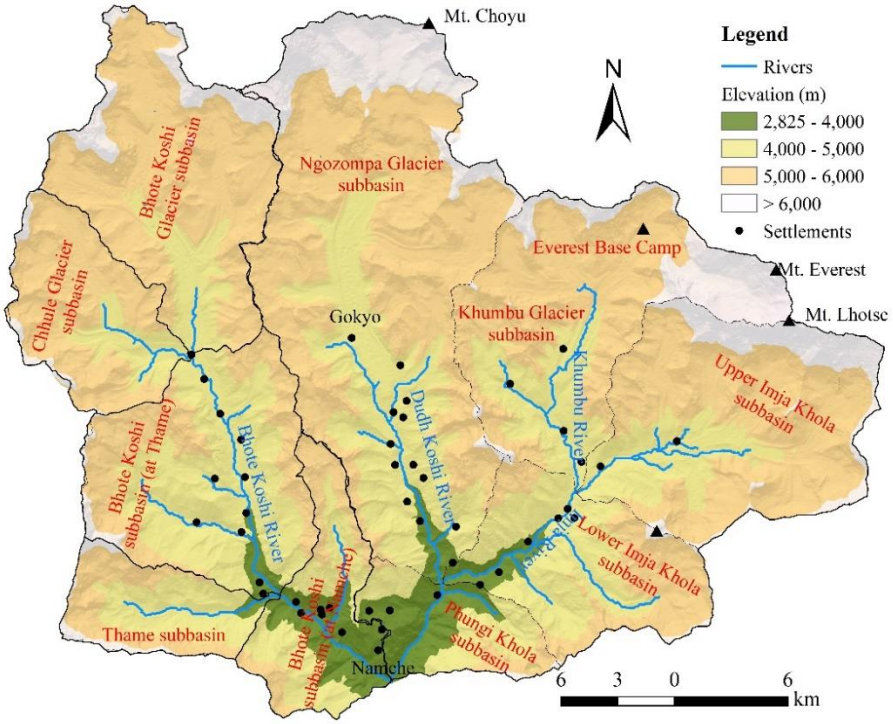

Figure 2.6 Upper Dudh Koshi basin showing its sub-basins, river network, elevation distribution and location of settlements.

Figure 2.7 Typical landforms in the Everest region: (a) Nuptse debris-covered Glacier; (b) Gokyo Lake in Gokyo Valley; (c) Gorge of Bhote Koshi River; (d) Glacier eroded U-shape Valley near Machhermo Village; and (e) Mt. Amadablam and surrounding landscape (Photographs were taken during field trip in December 2018).

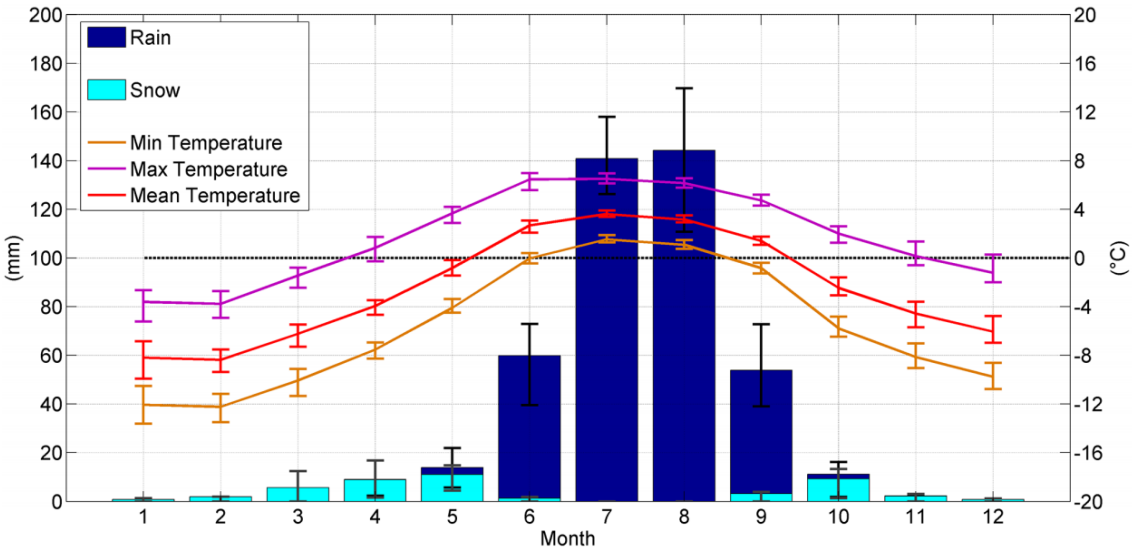

Figure 2.8 Mean monthly precipitation subdivided into snowfall and rainfall, and minimum, maximum, and mean temperature at 5,050 m (reference period 1994 – 2013). The bars represent the standard deviation (Salerno et al., 2015).

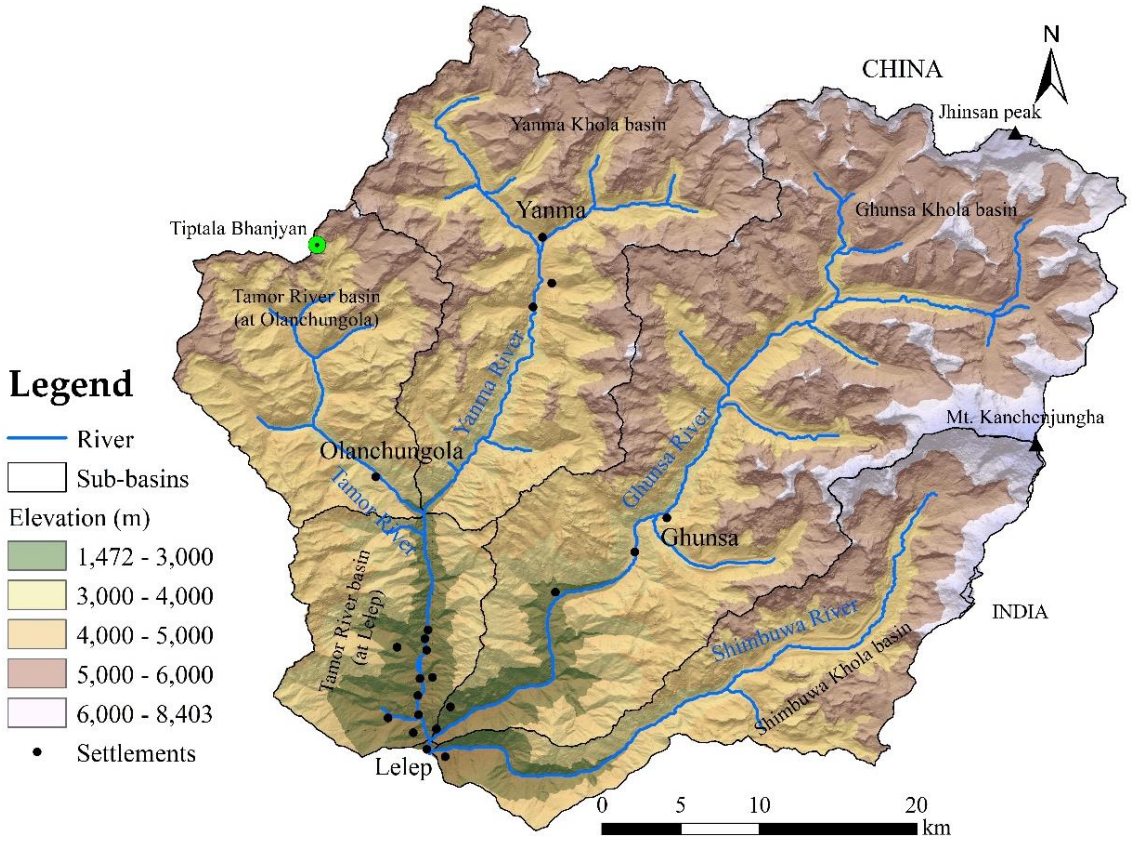

Figure 2.9 Digital Elevation Model (DEM) of the Kangchenjunga region showing rivers, sub-basins, and major settlements.

Figure 2.10 Field photographs from the Kangchenjunga region showing landscape of the region (Photographs in first row were taken in 2010 and photographs in second row were taken from Carsten Nebel, 2017).

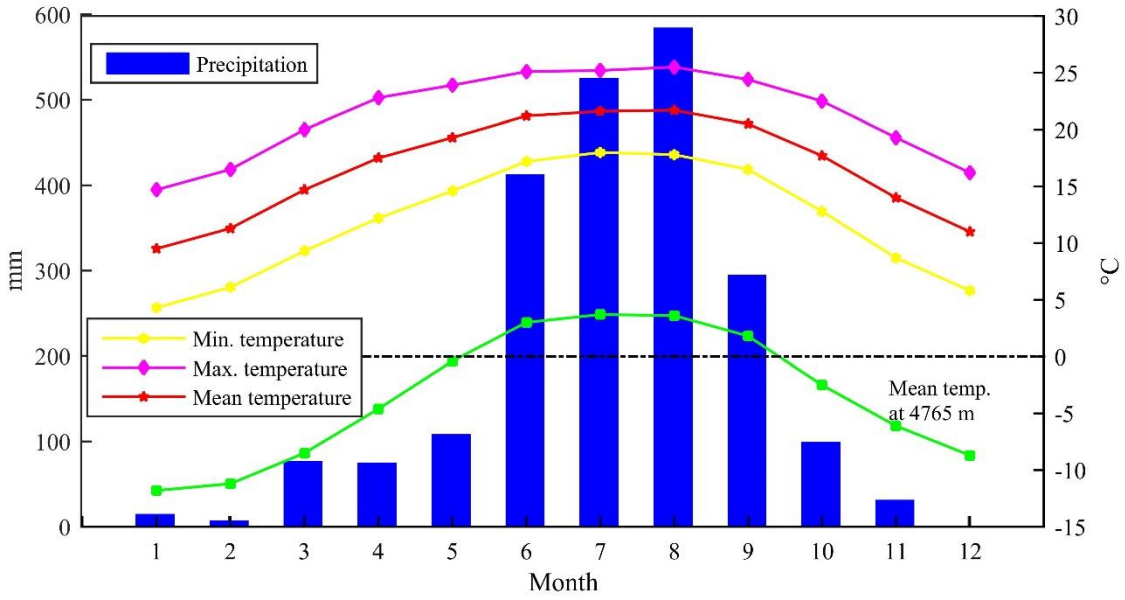

Figure 2.11 Mean monthly cumulated precipitation of the year 2008 at the Lungthung station (1,780 m), and mean monthly minimum, maximum, and mean temperature at the Taplejung station at an elevation of 1,732 m (reference period 2000 – 2008). The green line plot represent the mean monthly temperature at an elevation of 4,765 m near Lhonak obtained from the ERA2 reanalysis data (reference period 1979 – 2018).

3. High-resolution inventory of the glaciers and glacial lakes in the Everest region

3.1 Introduction

The rate of mass loss of the glaciers is higher in the Himalayan region compared with the global mean of glacier mass balance, and wastage of glaciers in this region is spatially heterogeneous (Fujita and Nuimura, 2011). Bolch et al. (2011b, 2012), however, indicated that Himalayan glaciers are losing mass at significant rate but not higher than the global average. The area of the glaciers had been observed to be lost by more than 20% from the 1980s to 2010 in the Hidden Valley, Nepal Himalaya and had retreated by 30-60 m in terminus elevation over 20 years between 1974 and 1994 (Fujita et al., 1997). Pratap et al. (2015) estimated the melt rate of debris-covered and clean type glaciers and found higher melt rate at clean-type glaciers. The melt rate is retarded where debris thickness increases (Östrem, 1959; Chand et al., 2015). However, debris-covered glaciers have also lost significant mass despite the presence of thick debris (Bolch et al., 2008a; Kääb et al., 2012; Basnett et al., 2013). The altitudinal heterogeneity of the mass balance of the glaciers was also observed in the Langtang Valley, Nepal during 1989 and 1991 due to difference in amount of precipitation at different altitudes (Shiraiwa et al., 1992). Consistent loss of ice observed across 2,000-km transect of the Himalaya and doubling of the average loss rate have been observed during 2000 and 2016 compared to 1975 and 2000 (Maurer et al., 2019). Mass wastage in the Himalaya resulted in increasing debris cover (Bolch et al., 2008a; Azam et al., 2018) and the elevation of the debris-covered glaciers is changing (Lamsal et al., 2011), which depend on their scale, slope and the existence of glacial lakes (Nuimura et al., 2012). The loss of glacier mass in the Himalayas leads to dramatic changes in total runoff, affect the irrigation and hydropower, and alter hazards (Bolch et al., 2012).

King et al. (2017) estimated the more negative mass balance of the glaciers that border on a lake compared to land terminating glaciers. Similarly, Watanabe et al. (1995) also observed a very high melt rate (5.0 m y^{-1}) where the ice surface was submerged by lake water and ice-cored moraines can become extremely unstable due to undercutting action of lake water (Watanabe et al., 1994). Glacier recession driven by climate change produces glacial lakes and some of which are hazardous (Richardson and Reynolds, 2000; Haritashya et al., 2018), and the number and area of the glacial lakes is increasing in

recent decades (Gardelle et al., 2011; Nie et al., 2013). Gardelle et al. (2011) reported the increase in area by 20% between 1990 and 2009 in the extended Everest region, Nepal. A recent study by Khadka et al. (2018) revealed an increase in the number of glacial lakes by more than 150% and increase in area by about 45% from 1977 to 2017 in the Nepal Himalaya.

A continuous retreat of the glaciers and increase in the area and number of glacial lakes lead to the changes in water storage and formation of potentially hazardous glacial lakes. Therefore, it is important to monitor glaciers and glacial lakes to understand their status with higher accuracy. The aim of this chapter is to prepare high-resolution inventory of the glaciers and glacial lakes for the Everest region, Nepal by using 2-m spatial resolution images of WorldView and GeoEye for the years 2015 and 2016 (Figure 3.1).

3.2 Glaciers and glacial lakes of the Everest region

The glaciers of the Everest region are characterized by presence of debris at their tongues and extremely variable surface topography (Figure 3.2). Bajracharya et al. (2014) prepared a glacier inventory for Nepal, in which they presented 132 glaciers covering an area of 262 km^2 in the Everest region, which is 23% of the total area of the region and 67% of the total glacier area in the DKR basin in 2010. Similarly, Randolph Glacier Inventory Version 6.0 mapped the 149 glaciers with the surface area of 246.14 km^2 (RGI, 2017). Inventory of glaciers for HMA revealed the 230 glaciers (288.66 km^2) in the Everest region (Sakai, 2019). Sakai (2019) used the satellite images from 1992 to 1999, where the smallest glacier was 0.01 km^2. The Ngozompa Glacier of size 78.7 km^2 is the largest glacier of Nepal, which is located in this region (Bajracharya et al., 2014). These studies used the Landsat images of 30-m spatial resolution, and inventory utilized the images before 2010. The discrepancies in area and number of the glaciers between different inventories are probably due to the use of different year's satellite images and different area thresholds. Therefore, it is necessary to update and prepare the latest inventory of the glaciers for this highly glacierized region with higher accuracy.

Salerno et al. (2012) prepared inventory of the glacial lakes using Advanced Visible and Near Infrared Radiometer type 2 (AVNIR-2) satellite image from 2008 and of 10-m spatial resolution and mapped 624 (7.43 km^2) glacial lakes in the Everest region. Of these lakes, unconnected glacial lakes were 170 (4.28 km^2), proglacial lakes 17 (1.76 km^2) and supraglacial lakes 437 (1.39 km^2). Similarly, Shrestha et al. (2017) mapped the

480 glacial lakes covering an area of 16.9 km^2 using 30-m Landsat images within the whole Dudh Koshi basin in the year 2010. They classified the glacial lakes into bedrock-dammed (37), ice-dammed (219), moraine-dammed (82), and other (1). Khadka et al. (2018) classified the glacial lakes into glacier-fed lakes and non-glacier-fed lakes. Further, they classified the glacier-fed lakes into supraglacial lakes and proglacial lakes with ice-connected and unconnected. They identified 234 glacial lakes that cover an area of 16.82 km^2 in the whole Dudh Koshi basin in the year 2017. The Nare Drangka and Dig Tsho glacial lakes (Figure 3.3) experienced GLOF in 1977 and 1985, respectively in the Everest region.

3.3 Datasets and methodology

3.3.1 Dataset

3.3.1.1 WorldView and GeoEye images

High-resolution WorldView and GeoEye images from 2015 and 2016 were obtained from the DigitalGlobe Foundation and were used to prepare the inventory of glaciers and glacial lakes. This study employed the 2-m (multispectral) and 0.5-m (panchromatic) spatial resolution Basic 1B (Level 1) and Standard 2A (Level 2) imagery products of WorldView-2, WorldView-3 and GeoEye-1 images, which were originally taken at much higher spatial resolution (Table 2.1). The WorldView-2 and 3 comprise eight multispectral bands, and the GeoEye-1 sensor has four bands with slight difference in wavelength (Table 2.2). WorldView-3 has additional eight SWIR bands and 12 CAVIS bands. Level 1 images are radiometrically and sensor corrected but not projected to a plane using a map projection or datum. Level 2 products are projected to plane using the map projection. Level 1 products have different ground sampling distance (GSD), while Level 2 products have uniform GSD and corrected for topographic relief using coarse DEM (Terrain corrected). The 2-m resolution images were not available for the south-western region of the study region, so Sentinel-2 image of 10-m resolution from 30 October 2016 was used for this part.

3.3.1.2 Digital Elevation Model (DEM)

The HMA 8-meter DEMs derived from along-track optical imagery, version 1 for the period from 2015 to 2016 from the Earth Data website (Shean, 2017) were used for

an analysis of glacier characteristics. These DEMs were generated from very-high-resolution (VHR) stereoscopic imagery from DigitalGlobe satellites. Gaps were filled that existed in each of the individual DEM tiles using the focal statistics tool in ArcMap and the filled tiles were mosaicked to cover the entire glacier area. However, these DEMs have significant data gaps in accumulation zones of the glaciers. So, Advanced Land Observing Satellite Phase Array type L-band Synthetic Aperture Radar (ALOS PALSAR) and the Shuttle Radar Topography Mission (SRTM) DEMs-based on data in 2011 and 2000, respectively were used for high elevation area.

3.3.2 Methodology

3.3.2.1 Preprocessing of WorldView and GeoEye

Level 1 products of WorldView and GeoEye are for customers with advanced images processing capabilities and suitable for advanced photogrammetric processing. Firstly, a rapid atmospheric correction tool available in ERDAS IMAGINE was applied to convert sensor raw Digital Number (DN) values to ground reflectance values. Rapid atmospheric correction uses information from companion metadata files (*.IMD) and normalized the top-of-atmosphere (TOA) reflectance to ground reflectance scaled by 10,000 (Hexagon Geospatial, 2019). Secondly, orthorectification of each used image was carried out in the ERDAS IMAGINE. The best horizontal geopositioning accuracies can be attained by using third order 3D rational functions with vendor's Rational Polynomial Coefficients (RPCs) (Aguilar et al., 2013). Therefore, Level 1 images were orthorectifed using RPCs and the 30-m SRTM DEM. The RPCs are type of sensor model, which is a mathematical transform that defines the physical relationship between image coordinates and ground coordinates. Sensor models are different for each sensor and the accuracy depends on the accuracy of the original sensor model and the quality of the imagery. Orthorectification process orthorectifies an image containing a RPC sensor model and geometrically corrects the data to remove distortions that occur during image capture. In this study, orthorectification was carried out without Ground Control Points (GCPs), which is sufficiently accurate to map the features of single time. However, horizontal distortion obtained by this method is greater than sub pixel range and not suitable for change detection with sub pixel accuracy. In this study, these images were only used to make high-resolution inventory of the glacial lakes and glaciers for one time.

3.3.2.2 Preprocessing of Sentinel-2 images

The ESA sen2cor plugin, which is available on the Sentinel Application Platform (SNAP), was used to conduct atmospheric and terrain corrections of the Level 1C images, and to produce an atmospherically corrected Level 2A Bottom of Atmosphere (BOA) reflectance product. In this study, only 10-m resolution bands, being blue, green, red, and infrared bands were used.

3.3.3 Methods

3.3.3.1 Glacier inventory and characteristics

Automatic and semi-automatic methods have been applied for detection of water bodies in several studies, however, mapping results might not be accurate or misclassified (He et al., 2019). Therefore, glaciers within the Everest region were manually digitized and mapped accordingly. The boundaries of the glaciers in 2-m spatial resolution were clearly visible and were delineated with high accuracy. In case of clean-type glaciers, boundaries were delineated by including the all-white pixels and half of the mixed pixels with other colors in False Color Composite (FCC). The Normalized Difference Snow Index (SNOW) (details in section 3.3.3.2) supported this approach. In case of debris part, glacial structures, i.e., deposits, lateral moraines, successive end moraines, ice cliffs near the terminus, location of outlet channel and other structures were identified and delineated accordingly. All the glaciers were assigned the GLIMS ID: a nomenclature of the glaciers by the Global Land Ice Measurements from Space (GLIMS), based on longitudes and latitudes of the glaciers (Paul et al., 2009).

Mean elevations of the glaciers were estimated from ALOS PALSAR DEM using spatial analyst tool and zonal statistics feature available in ArcGIS, which estimate the mean value by dividing the sum of all pixels by total number of pixels. Similarly, minimum and maximum elevations of all glaciers were also determined for each glacier. Slope and aspect of all the glaciers were also computed using the DEM to investigate the relationship with the supraglacial lake area.

In this study, 23 debris-covered glaciers were selected based on the potentiality of the formation of supraglacial lakes at the surface. Eight descriptive metrics for the selected debris-covered part of the glaciers were estimated and compared them with lake areas using Spearman's rank-order correlation (Miles et al., 2017b). Correlation

coefficient (r_s) ranging from a perfect negative correlation (-1) to a perfect positive correlation (+1), was estimated for each glacier to analyze the relationship between characteristics of the glaciers and lake area.

The total glacier area, debris-covered area and width of the glaciers were determined by using the outlines of the glaciers. HMA DEMs (8 m) were used to determine morphometric characteristics of the debris part of the glacier. HMA DEMs were of poor quality at higher elevations; therefore, ALOS PALSAR DEMs (12.5 m) were used to estimate the slope, aspect and elevation of the glaciers of total glacier surface. Average width of the glaciers were estimated based on 3–13 transects, depending on the sizes of the glaciers. The minimum and mean elevations of the debris-covered glaciers were computed based on the 8-m DEM, assuming that air temperature has a strong control on the surface mass balance of the glaciers. Similarly, the accumulation-area ratio (AAR) was calculated based on the equilibrium-line altitude (ELA) of 5,477 based on a previous study in the Everest region (King et al., 2017). The average height of the moraine from the glacier surface (DGM) was approximated based on the 3–13 transects to understand the cumulative downwasting of the glacier surface (Sakai and Fujita, 2010; Miles et al., 2017b). Similarly, mean slopes of the glaciers were estimated using a recent 8-m DEM, which has a strong control on lake formation and distribution (Quincey et al., 2007; Salerno et al., 2012; Miles et al., 2017b). The mean aspect of the debris-covered part of the glaciers was also computed; however, r_s was not estimated for this metric, which was used solely to understand the dominance of lakes on certain aspects of the glaciers.

3.3.3.2 Inventory of the glacial lakes

Automatic lake mapping methods for glacial lakes have been well discussed (Huggel et al., 2002; Watson et al., 2016; Miles et al., 2017b). However, the possibility of misclassification and omission of lakes increases significantly with moderate resolution of the dataset (Watson et al., 2016). Manual editing is recommended to increase the accuracy of the mapping (Mergili et al., 2013; Shukla et al., 2018), and therefore, to improve the results, post editing was adopted in this study after applying the water index and band ratios. Preprocessed scenes of each WorldView, GeoEye, and Sentinel images were utilized for mapping glacial lakes. Several combinations of bands for Normalized Difference Water Index (*NDWI*) have been proposed by several previous studies (Huggel et al., 2002; Xu, 2006; Gardelle et al., 2011; Miles et al., 2017b;). Modified *NDWI* (*MNDWI*) that uses the SWIR and green band is useful in built up or urbanized area to

minimize the noise (Xu, 2006). The bands used in *MNDWI* are similar to *NDSI* and it omits the lake area especially when lake is frozen. The *NDWI* proposed by Huggel et al. (2002) uses the blue band in combination with NIR band, which misclassify the water bodies as shadow area (Gardelle et al., 2011), especially in high mountain areas with significant shadow. Therefore, here *NDWI* by using NIR and green band (Eq. (3.1)) was used for each scene as used by previous studies (e.g., Huggel et al., 2002; Bolch et al., 2011a; Gardelle et al., 2011; Jha and Khare, 2017; Miles et al., 2017b) to delineate the boundaries of the supraglacial lakes.

$$NDWI = \frac{B_{Green} - B_{NIR}}{B_{Green} + B_{NIR}} \quad (3.1)$$

Band ratios (*BR1*) of green-to-near-infrared (Eq. (3.2)) were applied, which is useful for differentiating between moisture and non-moisture (Miles et al., 2017b).

$$BR1 = \frac{B_{Green}}{B_{NIR}} \quad (3.2)$$

The presence of shadow leads to misclassified lakes (Huggel et al., 2002) due to similar reflectance with water bodies. Therefore, the scene classification algorithm was used in sen2cor for Sentinel-2 images to remove the effect of the shadow. The above-mentioned metrics did not work efficiently for the images with snow cover and frozen lakes. Prior efforts to identify snow have used *NDSI* (Hall et al., 1995), which is similar to the *MNDWI* (Eq. (3.3)) (Xu, 2006), but cannot differentiate between the presence of snow and water bodies.

$$NDSI\ and\ MNDWI = \frac{B_{Green} - B_{SWIR}}{B_{Green} + B_{SWIR}} \quad (3.3)$$

The mask obtained from the conventional *NDSI* leads to the significant removal of lakes. Therefore, considering that snow had the highest reflectance in the mountains, this study proposed the new spectral metric (*BR*2) (Eq. (3.4)).

$$BR2 = \frac{B_{Blue} + B_{Green} + B_{Red}}{3} \quad (3.4)$$

Lakes are evident where the surface gradient of a glacier is less than 2° (Reynolds, 2000; Quincey et al., 2007; Miles et al., 2017b), while discrete and small isolated lakes are evident where slopes are between 2° and 10° (Reynolds, 2000). This suggests that a glacial lake can expand on a debris-covered glacier that has low inclination and little ice flux from upstream (Sakai, 2012). In this study, higher surface slope threshold of 30°

(Miles et al., 2017b) was applied to eliminate steep avalanche fans or icefall from the debris-covered area in which lakes can form.

This study initially tested several thresholds of *NDWI* that ranges from 0.0 to 0.50 with a step of 0.1 and checked the results from each threshold. The results obtained from threshold 0.3 was better than the other results, which was crosschecked with histogram of *NDWI*. Similar approach was applied to detect threshold for *BR2*, and threshold of 1.2 for *BR1* used by (Miles et al., 2017b) was adopted. Finally, lakes that met the slope threshold as well as *NDWI* > 0.3 or *BR*1 > 1.2 and *BR2* > 0.45 were delineated, following an approach similar to Gardelle et al. (2011) and Miles et al. (2017b). However, the threshold values can vary with time and may lead to overestimation or underestimation of water bodies. Therefore, all delineated lakes were checked for accuracy and edited manually to minimize the error due to variations in threshold values and reflectance among turbid and blue glacial lakes. During manual editing, the boundaries of lakes were edited by including all pure pixels of water body and about half of the pixels that surround the pure pixels. Different area thresholds have been used for glacial lake mapping, ranging from 3,000 m^2 to 0.1 km^2 (Gardelle et al., 2011; Zhang et al., 2011; Fujita et al., 2013; Rounce et al., 2016b; Shrestha et al., 2017). The possibility of an overestimation of a lake area can increase at smaller thresholds (4 pixels or less). Therefore, a threshold of 5 pixels (Jiang et al., 2018) was realistic for mapping glacial lakes which comprise an area of 500 m^2 and 20 m^2 for the Sentinel and WorldView and GeoEye images, respectively. Therefore, this study used a threshold of five pixels, and polygons smaller than these thresholds were removed. Glacial lakes were classified into three categories: supraglacial lakes, proglacial lakes and unconnected glacial lakes (Ageta et al., 2000; Wang et al., 2015; Nie et al., 2017).

3.4 Results

3.4.1 Glacier distribution

Inventory of glaciers was prepared for the Everest region in the upper DKR basin. The analysis of hydrographic network and major glaciers in the basin led to identification of the 10 sub-basins in the study region. The unnamed sub-basins were named based on the name of their largest associated glacier or the main tributary (Salerno et al., 2012). The identified 10 sub-basins are: Bhote Koshi River (at Namche) basin, Thame Khola and Bhote Koshi River (at Thame) basins, Chhule Glacier and Bhote Koshi Glacier

basins, Ngozompa Glacier basin, Khumbu Glacier basin, upper Imja Khola basin, lower Imja Khola basin, and Phungi Khola basin (Table 3.3). The Ngozompa Glacier basin was delineated at the confluence with the Imja Khola and is the largest (279.26 km^2) basin, while the Phungi Khola basin is the smallest (43.26 km^2) basin among 10 sub-basins within the upper DKR basin.

Glaciers within all the sub-basins were mapped and distribution of glaciers in each sub-basin is presented (Figures 3.4 - 3.9 and Table 3.3). Mapping of the glaciers in the Everest region delineated 109 glaciers covering an area of 268.22 ± 1.46 km^2 (Annex 1). The largest number (27) of the glaciers was observed in the Khumbu Glacier basin, while largest area (86.22 ± 0.33 km^2) of the glaciers was found in the Ngozompa Glacier basin. Only two glaciers were detected in the smallest Phungi Khola basin covering an area of 1.88 ± 0.02 km^2. The Ngozompa Glacier was the largest glacier in the upper DKR basin with an area of 80.15 ± 0.26 km^2. Glaciers in this study were divided into two types: a) clean type, and b) debris-covered type glaciers. The number of clean type glaciers and debris-covered glaciers were 84 and 25 covering an area of 28.23 ± 0.39 km^2 and 239.99 ± 1.07 km^2, respectively. Debris part of the debris-covered glaciers comprised an area of 103.45 km^2, accounted 39% of the total glacier area in the Everest region. The terminus of the Khangri Nup and Khangri Shar glaciers were merged together and considered a single glacier, the Khangri Nup Glacier. The Imja and Lhotse Shar glaciers were also merged together and considered a single glacier, the Imja Glacier. The Thyanbo Glacier in the Thame Khola basin has three tributary glaciers and mapped as a separate glacier, which was considered as one glacier for further analysis.

Therefore, a total of 23 of debris-covered glaciers in the upper DKR basin were considered for further study. The characteristics of the 23 glaciers were studied for the total glacier area and debris part of the glaciers. The clean part of the glaciers is usually in steep slope and has higher surface gradients compared to debris portion of the glaciers. The mean slope for the total area of the glaciers ranges from 13.68° (Taweche) to 26.44° (Imja Glacier) (Table 3.4). Glaciers were categorized into different size classes and found that only seven glaciers were larger than 10 km^2 and 82 glaciers were with size smaller than 1 km^2 (Figure 3.10). Glaciers with size larger than 1 km^2 were 27 out of which 21 were debris-covered glaciers. The glaciers were observed as high as of 8,000 m a.s.l.; however, the majority of the glaciers were below 6,500 m a.s.l. The mean elevation of the glaciers ranges from 4,868 m a.s.l. (Cholo) to 6,099 m a.s.l. (Khumbu), while none of the glacier had mean elevation below 4,500 m (Figure 3.11). The majority of the glaciers

were observed with minimum elevations above 4,500 m, and only two glaciers one in the Khumbu Glacier basin and other in the Thame Khola basin were observed to have elevation below 4,500 m. The larger glaciers dominantly oriented towards south, while small glaciers oriented towards east, south and west (Figure 3.12). The Ngozompa Glacier was the largest glacier, which was oriented at azimuth of 180°.

Debris-covered glaciers were relatively larger than the only clean-type glaciers occupy the 89.5% of the total glacier area in the upper DKR basin. The largest number (n=7) of the debris-covered glaciers was observed in the upper Imja Khola basin. The morphometric characteristics of the debris portions of the 23 glaciers studied for 2015/16 are presented in Table 3.6. They exhibited a wide range of geometric conditions. The smallest glacier was the Taweche Glacier (0.31 km^2) in which no accumulation zone was observed, while the largest was the Ngozompa Glacier, with debris-covered area of 25.99 ± 0.09 km^2. The proportion of debris-covered glaciers to the total glacier area ranges from 30% (Khumbu) to 100% (Taweche). The average glacier width was 465.8 m. The two extremes were the Khangri Nup Glacier, with the largest average width of 923 m, and the Thaynbo Glacier, with the smallest average width of 206 m. The mean DGM, that is, the elevation difference between the lowest elevation of the glacier and the dominant outermost lateral moraine peak elevation, was 63.2 m. The Thyanbo Glacier had the lowest mean DGM (15 m), and the Imja Glacier had the highest mean DGM (129 m). The minimum elevation of all glaciers (debris-covered area) exceeded 4,600 m a.s.l., with the exception of the Cholo and Thyanbo glaciers that extended below 4,500 m a.s.l. Only six glaciers had a mean elevation below 5,000 m a.s.l. Major debris part of the glaciers had an elevation ranges from 4,900 – 5,400 m a.s.l, and about 90% of the glacier area was below 5,400 m a.s.l. (Figure 3.13).

The mean slope of the debris part of the glaciers ranges from 6.8° (Lumsamba) to 20.3° (Tingbo), and 11 glaciers had mean surface gradients below 10°, which was much lower than the mean slope of the total glacier area. Only four glaciers (Ngozompa, Imja, Nareyargaip, and Khumbu glaciers) had an accumulation area greater than 50%, and the ablation portion was dominated by debris-cover part. The Cholo and Thyanbo glaciers were oriented towards the east, with mean average azimuth of 88.8°, while the rest of the glaciers were oriented towards the south (south, southwest, and southeast) with an average azimuth of 188.7°.

3.4.2 Glacial lake distribution

Mapping of the glacial lakes using an area threshold of 20 m^2 (5 pixels of 2-m images) had identified the 3,290 glacial lakes covering an area of 8.11 ± 0.45 km^2 in the Everest region and a mean size of 2,500 m^2 during the years 2015 and 2016. The distribution of glacial lakes in each sub-basin is presented in Figures 3.4-3.9. The Shapiro-Wilk distribution test at 95% confidence interval reveals that the distribution of lakes was not normal (Figure 3.14a) and skewed positively with a factor of 35.2. The probability distribution of lakes reveals that 95% (n = 2,949) of lakes have an area of <5,000 m^2, which contribute approximately 13% of the total surface area of lakes (Figure 3.14b). Only ~5% (n = 164) of the glacial lakes of sizes >5,000 m^2 contribute to ~87% of the total lake area. Glacial lakes were categorized into three types: 1) supraglacial lakes, 2) proglacial lakes, and 3) unconnected lakes. The lakes were classified into four size classes (<0.01 km^2, 0.01-0.02 km^2, 0.02-0.1 km^2, and >0.1 km^2) and distribution of lakes in each class is presented in Figure 3.15.

3.4.2.1 Supraglacial lakes

Supraglacial lakes that form at the surface of the debris-part of the glacier occur most frequently in the Everest region. The total number of the supraglacial lakes observed to be 3,009, which was 91% of the total number of lakes in the Everest region. The area covered by these lakes is about 2.04 ± 0.32 km^2 with mean size of 678.7 m^2 and median size of 80 m^2, accounted for about 25% of the total lake area. There were 2,984 (~99%) supraglacial lakes with size <0.01 km^2 in 2015 and 2016, with a total surface area of 1.17 km^2 (Figure 3.15), accounting the 57% of the total area of supraglacial lakes. Only 25 supraglacial lakes (>0.01 km^2) account about 43% (0.87 km^2) of the total supraglacial lake area. The largest number (n=925) of the supraglacial lakes was observed in the Ngozompa Glacier basin and followed by the Bhote Koshi Glacier basin (n=796), and the largest area (0.62 ± 0.10 km^2) was in the Ngozompa Glacier basin and followed by the Khumbu Glacier basin (0.57 ± 0.06 km^2). The Bhote Koshi basin at Thame and at Namche, and the Phungi Khola basins lack the debris-covered glaciers, and subsequently the supraglacial lakes. The three largest studied glaciers (Ngozompa, Bhote Koshi, and Khumbu) featured 60% of the total lake area among 23 glaciers, and the maximum number (896) and area (0.61 ± 0.1 km^2) of supraglacial lakes were observed on the

Ngozompa Glacier. The majority of the glaciers (n = 14) that have debris-covered areas <5 km^2 (Table 3.5) exhibited only 13% of the total lake area.

Significant variability in the surface area of supraglacial lakes was observed among the studied glaciers, ranging from 0.03% (Mingbo Glacier) to 3.89% (Khumbu Glacier) of the debris-covered area, while no supraglacial lakes were observed in the Thyanbo Glacier of the Thame Khola basin in 2015 and 2016. The rank-order correlation coefficient between lake area and different morphometric characteristics of the debris-covered glaciers was estimated and exhibited a very strong rank-order correlation with the total glacier area (r_s = 0.90) and debris area (r_s = 0.90), a strong correlation with the mean slope (r_s = -0.75), mean elevation (r_s = 0.72), and mean glacier width (r_s = 0.70), and a moderate correlation with the AAR (r_s = 0.61), which was statistically significant at 99% confidence level. However, no significant rank-order correlation was found for glacier minimum elevation (r_s = -0.11) and DGM (r_s = 0.21). These results suggested the largest lake area was evident on the larger glaciers. The altitudinal-area distribution of the lakes showed that supraglacial lakes could be found as high as ~5,560 m a.s.l., ~200 m lower than the upper extent of debris portion of the glacier (Figure 3.16a). About 87% of the lake area was observed on the glaciers with slopes <10°, of which 55% of the lake area was observed on slopes from 2–6°, 17% on slopes <2° and 15% on slopes from 6–10° (Figure 3.16b). Large number of supraglacial lakes were concentrated at lower reaches of the glaciers, below 5,200 m a.s.l. and the largest area (~20%) of the lake was observed between 5,100 and 5,200 m a.s.l. To understand the elevation wise distribution of the supraglacial lake area, largest glaciers (Ngozompa, Khumbu and Bhote Koshi) were divided into 100 m elevation difference zones (elevation bins).The largest area of the lakes was observed at first 100 m elevation bin in each glacier (Figure 3.17). The relationship between lake area and distance from the terminus was non-monotonic and displayed the regular variation. However, the lake area monotonically decreased after elevation of 5,200 m in each glacier. These variations can be attributed to the change in area, slope, aspect, and velocities of the glaciers.

Large glaciers, i.e., Ngozompa, Khumbu, and Bhote Koshi were characterized by the presence of large supraglacial lakes on their termini, termed spillway lake (Figure 3.18). In this study, the presence of lakes adjacent to spillway lake termed as a complex spillway lake. The area of complex spillway lakes on the Ngozompa, Khumbu, and Bhote Koshi glaciers was 0.25 km^2, 0.12 km^2, and 0.12 km^2, respectively. These spillway lakes accounted 41%, 28%, and 25% of the total area of the supraglacial lakes on the Ngozompa,

Khumbu, and Bhote Koshi glaciers, respectively. Besides the three largest glaciers, the Lumsamba, Melung, Chhule, Nuptse, and Thyanbo glaciers also exhibited the presence of either spillway lakes or several small sized lakes near their termini. The details on spillway lake development will be presented in Chapter 4.

Supraglacial lakes were dominated by the small-sized lakes, and the percentage of lake area that was smaller than one Landsat pixel (900 m^2) and five pixels (4,500 m^2) were significantly large and vary with glaciers (Figure 3.19). Seven larger glaciers (Ngozompa, Khumbu, Bhote Koshi, Melung, Chhule, Lumsamba, and Nuptse) in the study region revealed that lakes with size <900 m^2 accounted for 86% to 93% and 10% to 46% of the total number and surface area of the supraglacial lakes, respectively. Similarly, lakes <3,600 m^2 accounted for 95 to 99% of the total number of lakes and 35 to 83% of the total lake area. These statistics suggested the potential omissions of lakes with size less than 3,600 m^2 (four pixels of Landsat) when coarser resolution imagery was used for the supraglacial lake delineation. The Melung Glacier is a medium sized glacier in the study region, which had debris-covered part of 6.3 km^2 and supraglacial lake with size <3,600 m^2 accounting for 99% of the total number of lakes on the Melung Glacier, while only 1% of the lakes have size >3,600 m^2. Supraglacial lakes were most frequent in elevation between 5,000 and 5,500 m (Figure 3.20), while area of the supraglacial lakes plotted at the elevation between elevation of 4,500 and 5,000 m and at the elevation between 5,000 and 5,500 m was comparable.

3.4.2.2 Proglacial lakes

In this study, proglacial lakes of the Everest region mapped using high-resolution imageries for the year 2015/2016 in 10 sub-basins of the region (Figures 3.4-3.9) and were second most frequent typology in terms of area. Results of mapping revealed 16 proglacial lakes with a total area of 2.39 ± 0.3 km^2 (Table 3.6) with mean and median size of 0.15 km^2 and 0.046 km^2, respectively. The median size of the proglacial lakes was 33 and 575 times larger than the median size of the unconnected and supraglacial lakes, respectively. The Imja Lake was the largest lake with the area of 1.43 ± 0.01 km^2. Similarly, the Dig Tsho Lake also known as Langmoche Lake at the foot of the Langmoche Glacier was the second largest lake with the area of 0.40 ± 0.001 km^2. Glacial lake of an area of 0.11 km^2 observed at an elevation of 5,268 m in the Bhote Koshi basin (at Namche) was the third largest proglacial lake, which was connected with the unnamed glacier (GLIMS ID: G086676E27898N) and dammed by low elevated end moraine. Out

of 16 proglacial lakes, 14 were found with size >0.01 km^2, accounting about 99.6% of the total area of the proglacial lakes, while lakes with size >0.05 km^2 contributed about 89% of the total surface area of the proglacial lakes (Table 3.7). The largest number and area of the proglacial lakes was observed in the upper Imja Khola basin and accounted for 65% of the total proglacial lake area in the region. Proglacial lakes were not observed on the Bhote Koshi Glacier, Khumbu Glacier, lower Imja Khola, and Phungi Khola basins. The elevation of proglacial lakes range from 4,368 m (Dig Tsho Lake) to 5,304 m (lake connected with the G086582E27918N glacier) in the Bhote Koshi basin (at Thame) with mean elevation of 4,995 m.

3.4.2.3 Unconnected lakes

The inventory of glacial lakes plotted the 265 unconnected glacial lakes covering an area of 3.68 ± 0.1 km^2 (Table 3.6), contributed the largest area (45%) of the total glacial lake area in the Everest region. The distribution of the unconnected glacial lakes in each sub-basin within the upper DKR basin is presented in Figures 3.4 to 3.9. The mean area of the unconnected lakes was 0.014 km^2, smaller than mean size of the proglacial lakes and larger than the mean size of supraglacial lakes. The median surface area of unconnected lakes (1,400 m^2) was found 17 times higher than the median size of the supraglacial lakes. The size distribution of the unconnected glacial lakes showed that about 89% of the total surface area of unconnected lakes was contributed by the lake with size >0.01 km^2 (Figure 3.15 and Table 3.7). Unconnected lakes comprises either glacier-fed or non-glacier-fed and have a variety of landforms developed by erosional action of glaciers. These include a cirque lake, lateral moraine-dammed lake, debris-dammed lake and others. These glacial lakes were distributed in the whole upper DKR basin and the largest number (93) of lakes was detected in the Ngozompa Glacier basin that covers an area of 1.90 km^2, corresponding to 52% of unconnected lakes of the entire DKR basin in terms of area and 35% in terms of number. The Ngozompa Glacier presented the second and third largest lake among unconnected glacial lakes with surface area of 0.42 ± 0.7% km^2 and 0.39 ± 0.7% km^2, respectively. The upper Imja Khola basin also presented the large number of lakes (50) with the total surface area of 0.23 km^2 (19% of unconnected glacial lakes of the Everest region in terms of number). Similarly, the Khumbu Glacier basin also presented the second largest surface area (0.86 km^2) (23% of unconnected glacial lakes of the Everest region). Chola Cho (Lake) located in the Khumbu Glacier basin was the largest lake among unconnected glacial lakes and had surface area of 0.56

± 0.5% km^2. However, unconnected lakes were not detected in the Phungi Khola basin, smallest sub-basin of the upper DKR basin. The mean elevation of unconnected glacial lakes was ranges from 4,463 to 5,633 m, with mean elevation of 5,100 m with 5% standard deviation, which was approximately 29 m and 105 m higher than the mean elevation of supraglacial lakes and proglacial lakes, respectively (Figure 3.20).

3.5 Summary

3.5.1 Glaciers

Multispectral images of WorldView and GeoEye with 2-m resolution were utilized to prepare the high-resolution inventory of the glaciers in the upper DKR basin. The results presented the 109 glaciers (268.22 ± 1.46 km^2) in the basin with mean area of 2.46 ± 0.01 km^2 and median size of 0.33 km^2. The largest area (86.2 km^2) of glaciers was observed in the Ngozompa Glacier basin, which accounted approximately 32% of the total surface area of the glaciers in the basin. The Ngozompa Glacier was the largest glacier with the surface area of 80.15 ± 0.26 km^2, and alone contributed to 30% of the total area of the glaciers.

3.5.2. Supraglacial lakes

Supraglacial lakes were mapped in the 23 debris-covered glaciers using WorldView and GeoEye imageries and found most frequently presented lake in the Everest region. The inventory of the supraglacial lakes revealed the 3,009 lakes covering an area of 2.04 ± 0.32 km^2 and distributed spatially on debris-covered glaciers.

The debris-covered areas of the studied glaciers in 2015 and 2016 showed significant variability of lake area among glaciers, ranging from 0.03% (Mingbo Glacier) to 3.89% (Khumbu Glacier) of the debris-covered area. The area of the supraglacial lakes on each glacier was correlated with the glacier's characteristics and showed very strong rank order correlation with the total area of the glacier and debris-covered area (Miles et al., 2017b), and strong correlation with the slope and width of the glacier. This also suggested that larger lake cover for the larger glaciers, which generally had surface gradients of <10° (Reynolds, 2000). Approximately 6%, 45% and 69% of the glacier area had slopes of less than 2, 6, and 10°, respectively, suggesting that all the glaciers studied had the potential to form supraglacial lake.

The smallest percentage of lake area on the Mingbo Glacier was correlated with its smallest size and steepest mean slope (20.3°) of all the glaciers studied. Similarly, the largest lake area on the Khumbu Glacier was the result of a low mean gradient (7.6°) and stagnant tongue (Quincey et al., 2009). A series of several inter-connected supraglacial lakes at the terminus (0.12 km^2) and a large lake of the same size at a tributary of the glacier in 2017 contributed to the significant lake cover on the Khumbu Glacier. The largest area of lake (0.61 km^2) on the Ngozompa Glacier was also highly correlated with its largest area, low mean slope, large DGM (Sakai and Fujita, 2010; Miles et al., 2018), and glacier width, with southern aspect (Table 3.1). Similarly, the Bhote Koshi, Khangri Nup, and Lumsamba glaciers exhibited large surface area of supraglacial lakes, i.e., 1.6%, 3.1%, and 3% of the debris-covered area and comprised an area of 0.28, 0.23, and 0.16 km^2, respectively. The larger lake area on these glaciers can be explained by the large debris-covered area, low mean slope, southern aspect, and higher DGM and width of the glaciers (Table 3.5). The lake area was also strongly correlated with mean elevation of the glaciers, corresponding to large area of the glaciers at higher elevations (5,000 – 5,300 m a.s.l.) and less area of the glaciers at lower elevations (4,400 – 4,900 m a.s.l.).

3.5.3 Proglacial lakes

Proglacial lakes were the least frequent typology in the Everest region in terms of their number; however, these features with the surface area of 2.39 ± 0.03 km^2 accounted for 29% of the total glacial lake area. The Imja Lake, one of the most studied GLOF-risk lakes, was found with the surface area of 1.43 km^2. This was the largest glacial lake in the study area. Similarly, Dig Tsho Lake that caused GLOF event in 1985 was found the second largest lakes at the foot of the Langmoche Glacier with the surface area of 0.40 ± 0.7% km^2.

3.5.4 Unconnected lakes

Lakes without direct connections with glaciers were found most dominant in the study area in terms of area, with the surface area of 3.68 ± 0.1 km^2 and accounted for 45% of the total lake area. Unconnected glacial lakes were most frequently observed in the Ngozompa Glacier basin, largest sub-basin within the upper DKR basin, where the total surface area of unconnected lake was 1.90 km^2, corresponding to 52% of this types of lakes.

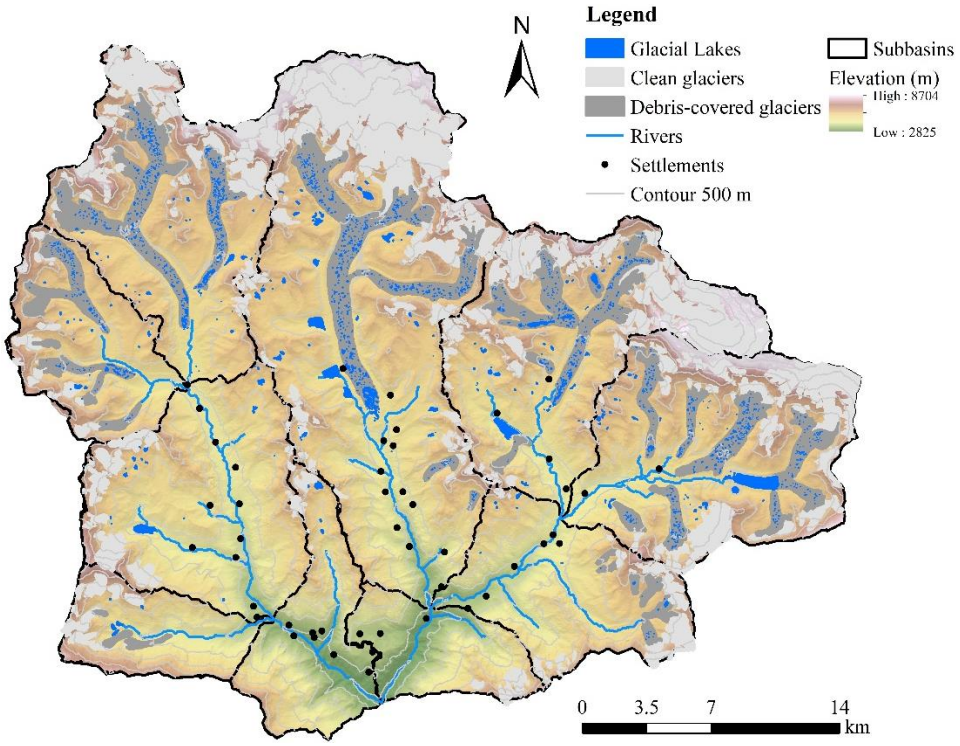

Figure 3.1 Digital Elevation Model (DEM) of the study area showing sub-basins, glaciers, glacial lakes, major rivers and major settlements. The glaciers and glacial lakes obtained from 2-m WorldView and GeoEye images. The background is ALOS PALSAR DEM.

Figure 3.2 The Ngozompa Glacier showing the presence of debris and heterogeneous surface at lower part of the glacier.

Figure 3.3 Dig Tsho Glacial Lake, which caused GLOF in 1985 (PC: Tomomi Yamada).

Table 3.1 List of WorldView and GeoEye basic level images used for inventory of glaciers and glacial lakes.

SN	Image Catalogue ID	Date	Satellite	Resolution (m)
1	103001004B849300	11/17/2015	WV-02	1.85
2	10300100553C3D00	04/16/2016	WV-02	1.85
3	1050010007140900	11/05/2016	GE01	1.65
4	104001002469AD00*	10/25/2016	WV-03	1.24 (0.31*)
5	1040010019841600	04/27/2016	WV-03	1.24
6	103001005E3EFF00*	10/29/2016	WV-02	1.85 (0.46*)
7	10300100531C0A00	04/3/2016	WV-02	1.85
8	103001005496C400	04/03/2016	WV-02	1.85
9	10300100553C3D00	04/03/2016	WV-03	1.24
10	104001001854B000	02/11/2016	WV-03	1.24
11	10300100553C3D00	04/03/2016	WV-02	1.85
12	S2A_OPER_MTD_SAFL1C_PDMC_20161030T121245_R076_V20161030T044922_20161030T044922	10/10/2016	Sentinel-2	10

*Image of 0.5 m resolution also used for accuracy assessment.

Table 3.2 Band designations for the WorldView-2, WorldView-3 and GeoEye-1 and their wavelengths.

SN	Band	Wavelength (nm)		
		GeoEye-1	WorldView-2	WorldView-3
1	Coastal		400-450	397-454
2	Blue	450-510	450-510	445-517
3	Green	520-580	510-580	507-586
4	Yellow		585-625	580-629
5	Red	655-690	630-690	626-696
6	Red Edge		705-745	698-749
7	Near Infrared 1	780-920	770-895	765-899
8	Near Infrared 2		86-1040	857-1039
	Panchromatic	450-800	450-800	450-800

Table 3.3 Distribution of the glaciers in sub-basins of the upper Dudh Koshi River basin.

Sub-basins	Area (km^2)	Glaciers	
		No.	Area (km^2)
Bhote Koshi River (at Namche)	60.49	5	1.36±0.013
Thame Khola	44.54	9	5.87±0.19
Bhote Koshi River (at Thame)	122.3	13	8.75±0.097
Chhule Glacier	70.72	5	14.77±0.08
Bhote Koshi Glacier	134.73	7	42.86±0.19
Ngozompa Glacier	279.26	20	86.22±0.33
Khumbu Glacier	144.54	27	48.57±0.23
Upper Imja Khola	146.46	9	47.16±0.22
Lower Imja Khola	84.68	12	10.78±0.08
Phungi Khola	43.26	2	1.88±0.015
SUM	1130.98	109	268.22±1.46

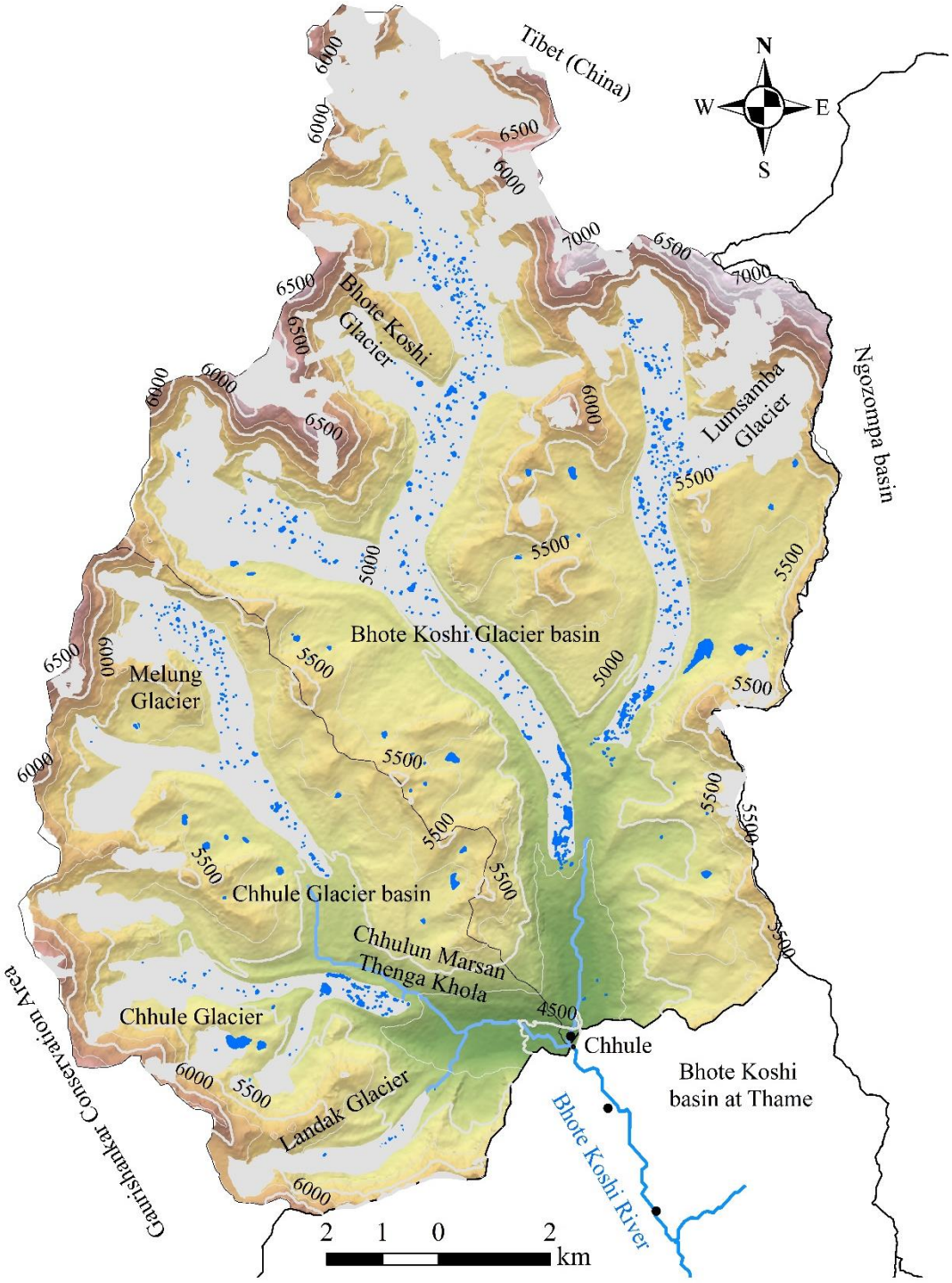

Figure 3.4 Map of the glaciers and glacial lakes of the Bhote Koshi Glacier and Chhule Glacier basins.

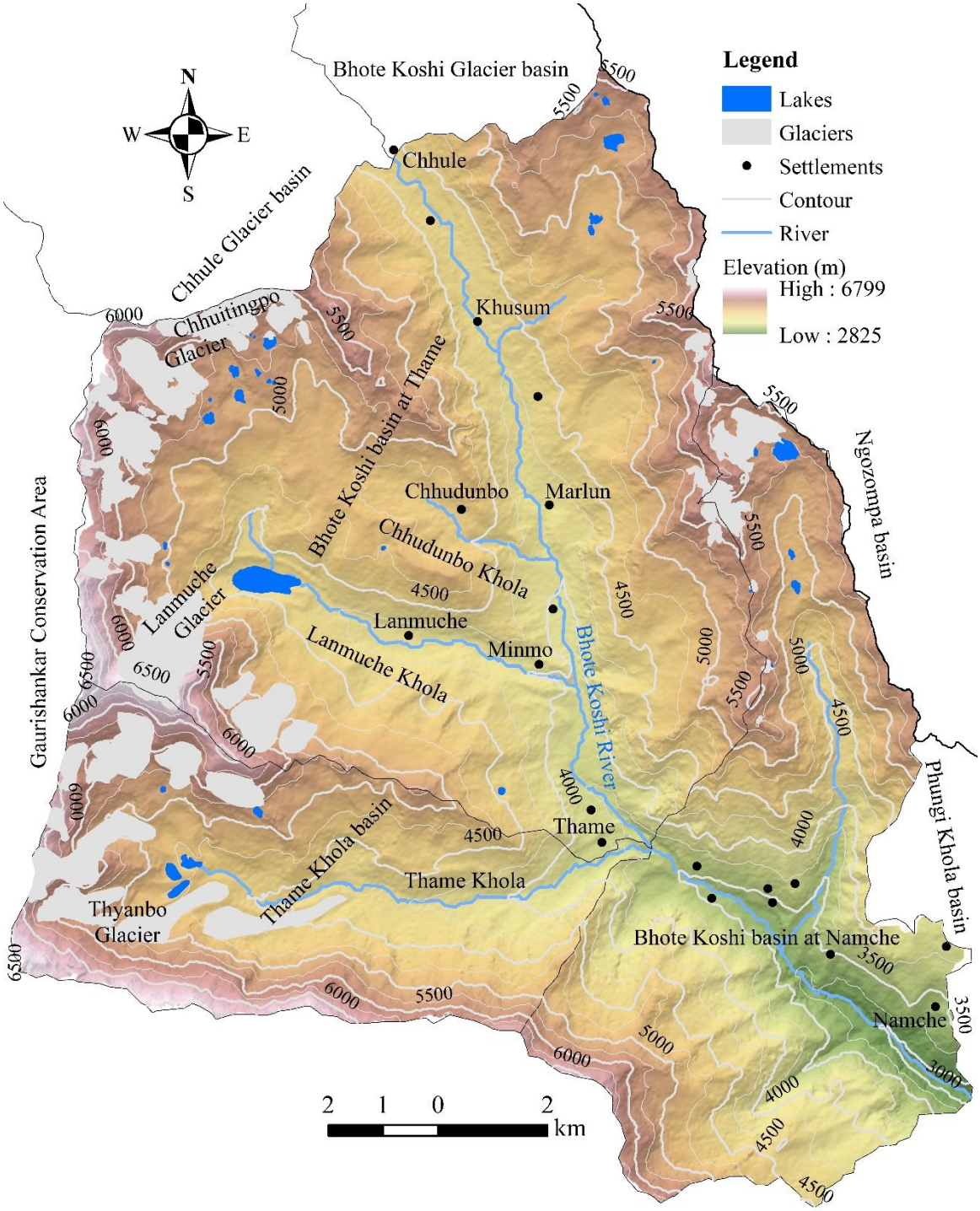

Figure 3.5 Map of the glaciers and glacial lakes of the Bhote Koshi and Thame Khola basins at Thame, and Bhote Koshi basin at Namche.

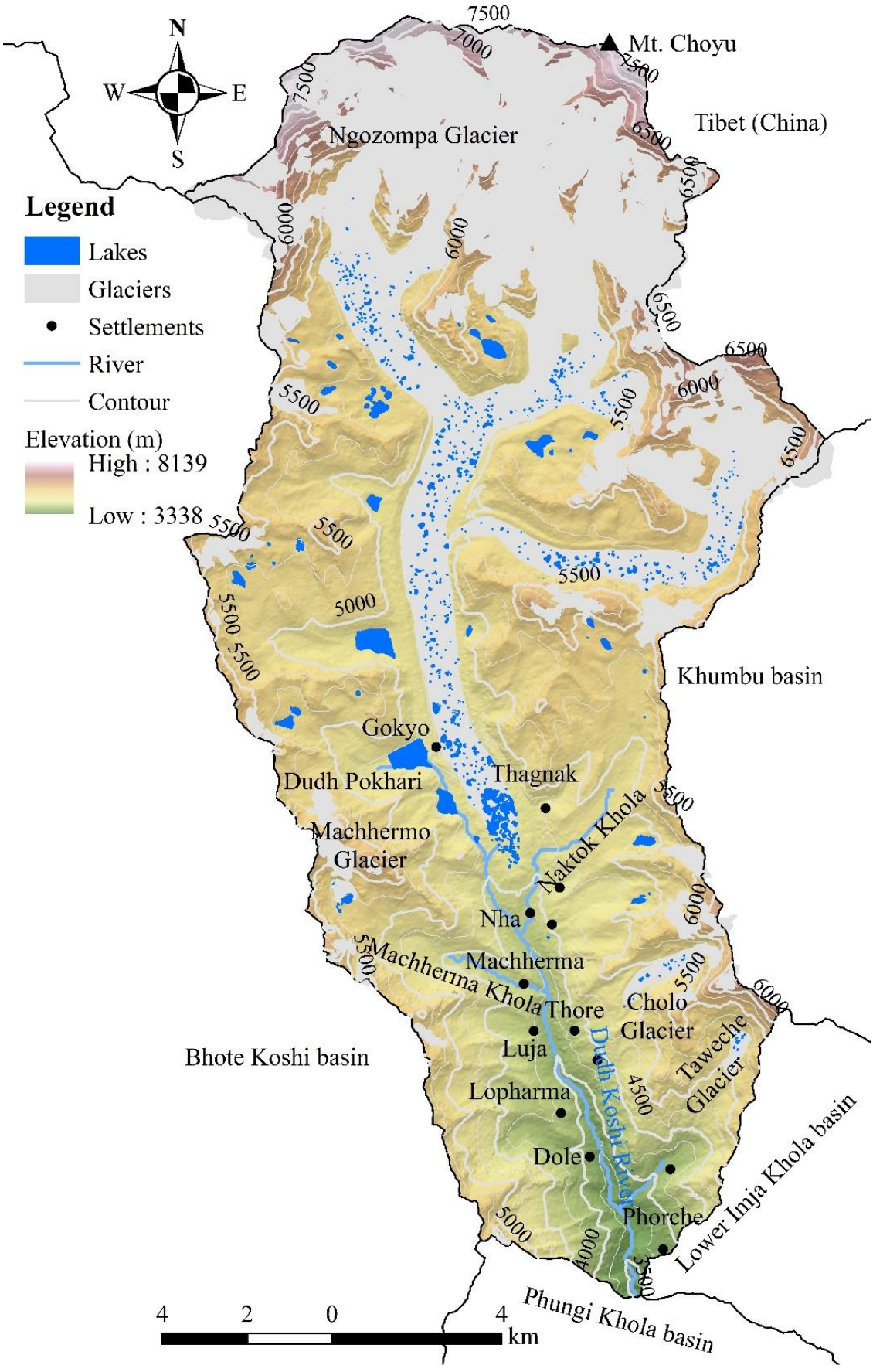

Figure 3.6 Map of the glaciers and glacial lakes of the Ngozompa Glacier basin.

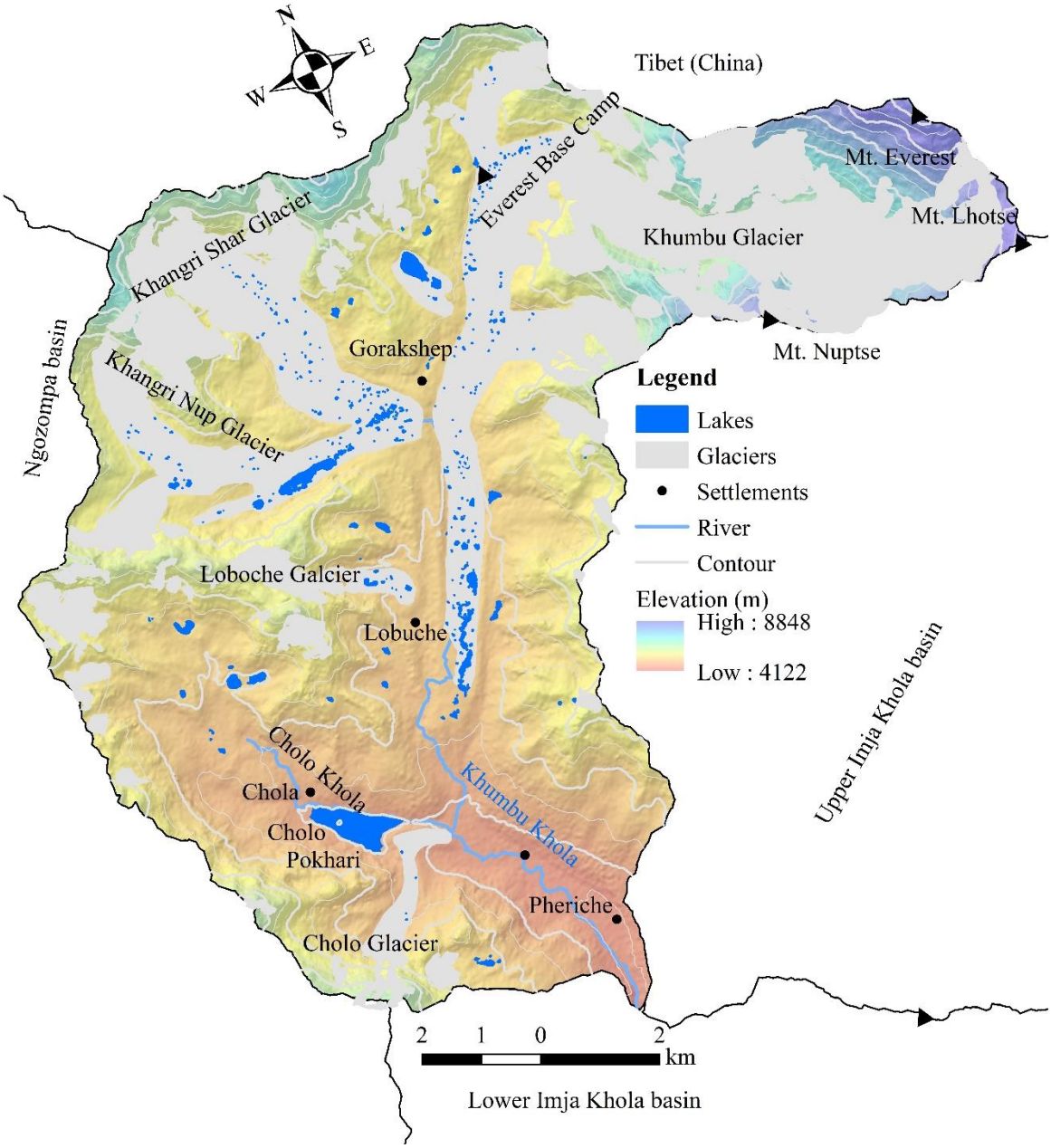

Figure 3.7 Map of the glaciers and glacial lakes of the Khumbu Glacier basin.

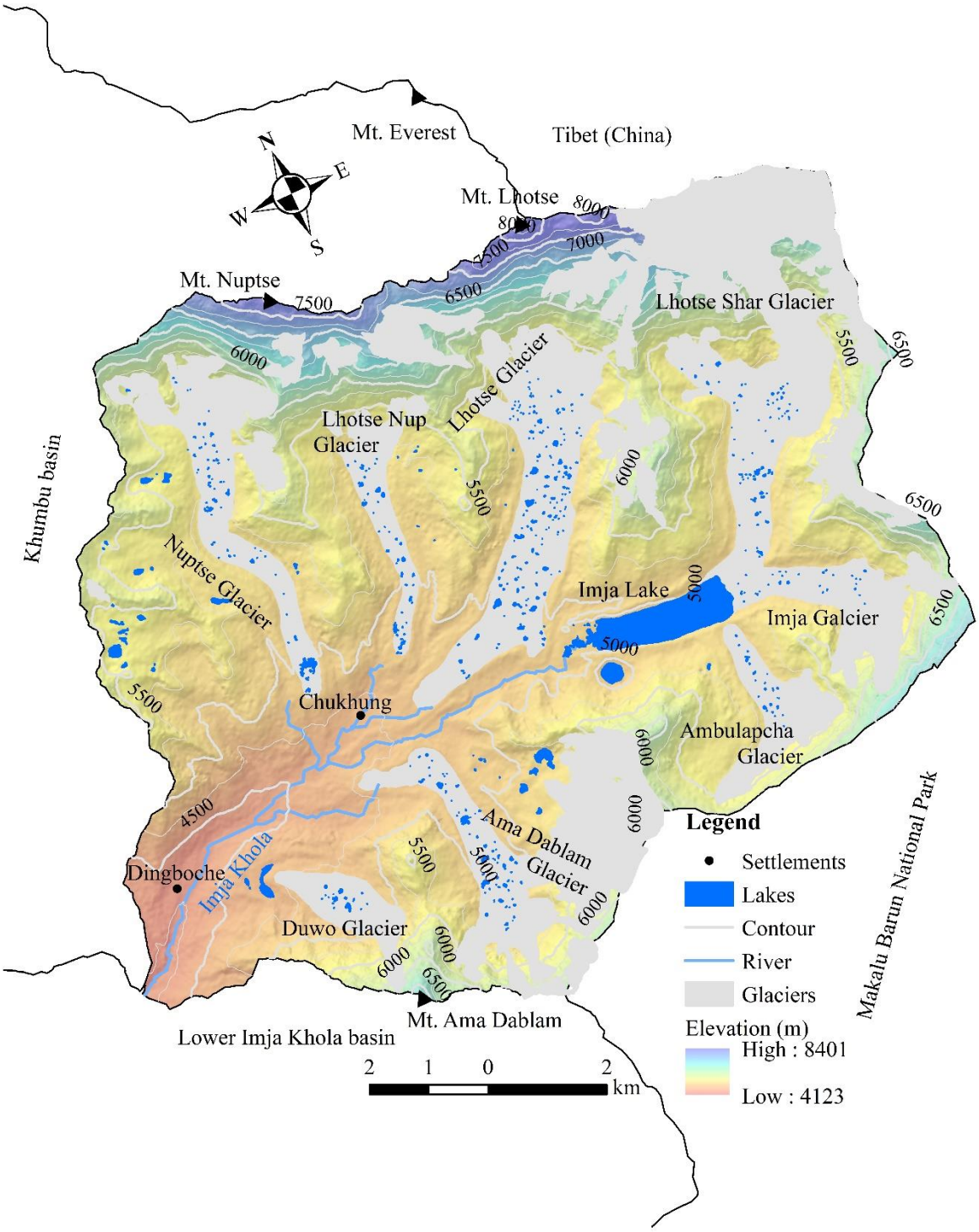

Figure 3.8 Map of the glaciers and glacial lakes of the upper Imja Khola basin.

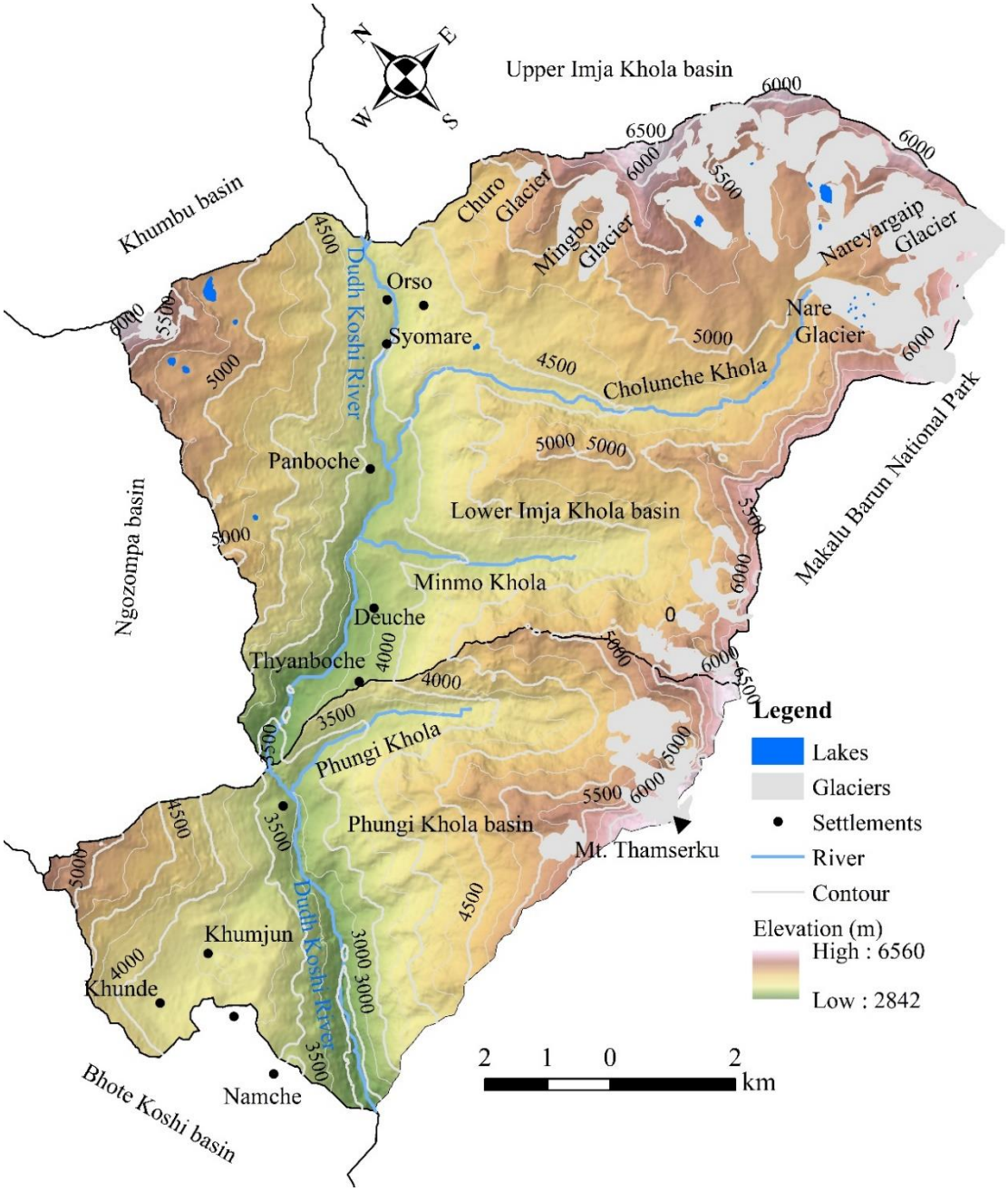

Figure 3.9 Map of the glaciers and glacial lakes of the lower Imja Khola and Phungi Khola basins.

Table 3.4 Characteristics of 23 debris-covered glaciers in the Everest region.

SN	Glacier Name	Area (km^2)	Mean slope (°)	Elevation (m)		
				Mean	Min	Max
1	Landak	1.61	17.12	5278.6	4896	5874
2	Chule	5	15.07	5154.3	4818	5974
3	Melung	7.15	14.03	5293.3	4960	6579
4	Bhote Koshi	30.76	16.82	5448.4	4758	6891
5	Lumsamba	10.89	17.97	5507.5	4931	6960
6	Ngozompa	80.15	19.04	5784.4	4684	8085
7	Cholotse	1.17	19.21	5218.4	4889	6281
8	Taweche	0.31	13.68	5034.3	4967	5150
9	Cholo	1.25	22.08	4868.5	4445	6301
10	Lobuche	1.35	17.21	5354.1	4960	5802
11	Khangri Nup	14.37	16.01	5431.1	5094	6378
12	Khumbu	27.17	24.83	6098.7	4909	8113
13	Nuptse	5.25	18.43	5470.4	4944	7177
14	Lhotse Nup	2.29	19.75	5329.7	4958	6826
15	Lhotse	10.54	21.60	5533.4	4848	7367
16	Imja	16.38	26.44	5903.4	5011	8093
17	Ambulapcha	2.17	20.67	5297.7	5055	5658
18	Ama Dablam	8.45	24.60	5354	4775	6192
19	Duwo	1.45	18.31	4903.2	4744	5602
20	Mingbo	0.89	25.07	5260.6	4894	5831
21	Nareyargaip	5.79	20.30	5497.5	5066	6001
22	Nare	1.59	20.71	5329.6	5021	5876
23	Thyanbo	3.65	20.38	5023.8	4373	6016
	TOTAL	239.99				

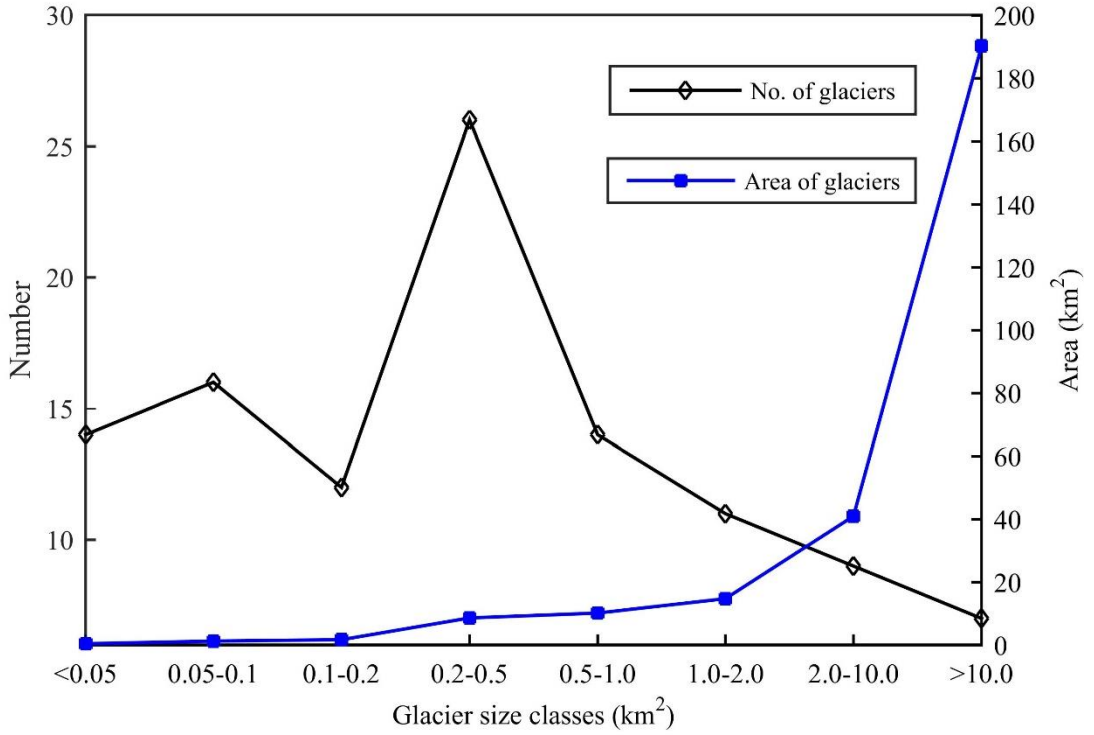

Figure 3.10 Distribution of the glaciers in the upper Dudh Koshi River basin in different size classes.

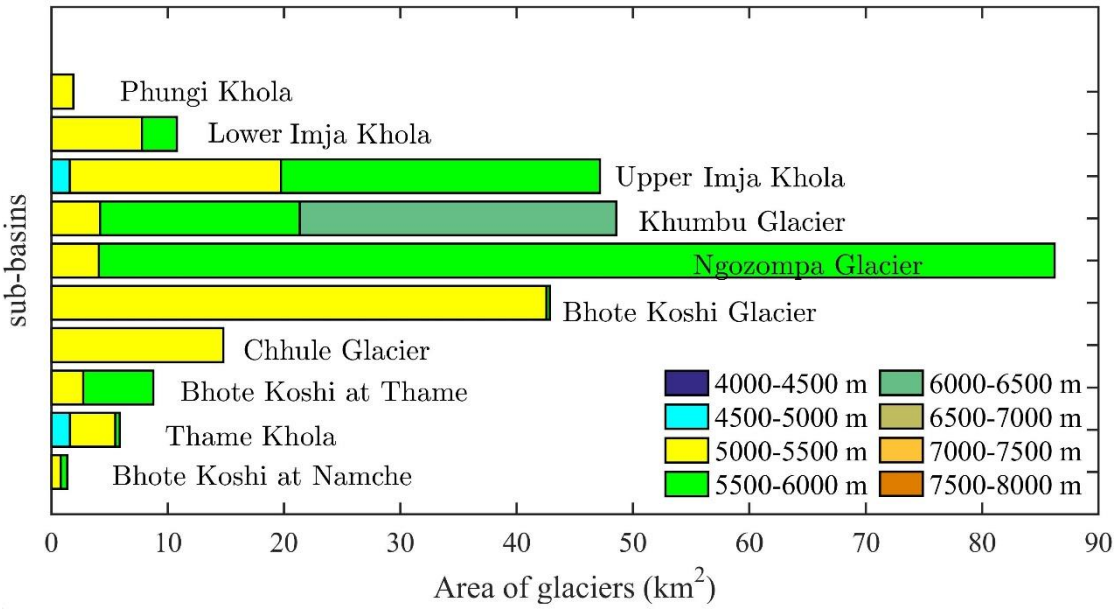

Figure 3.11 Mean elevations of the glaciers in ten sub-basins of the Everest region.

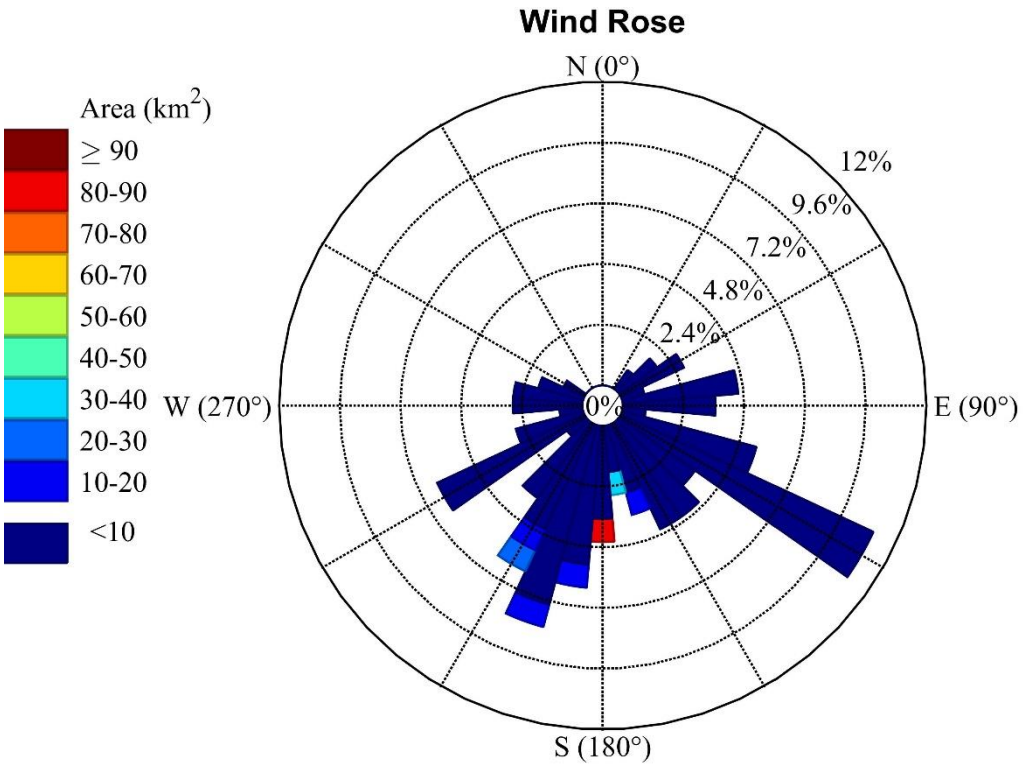

Figure 3.12 Distribution of aspects of the glaciers in the Everest region.

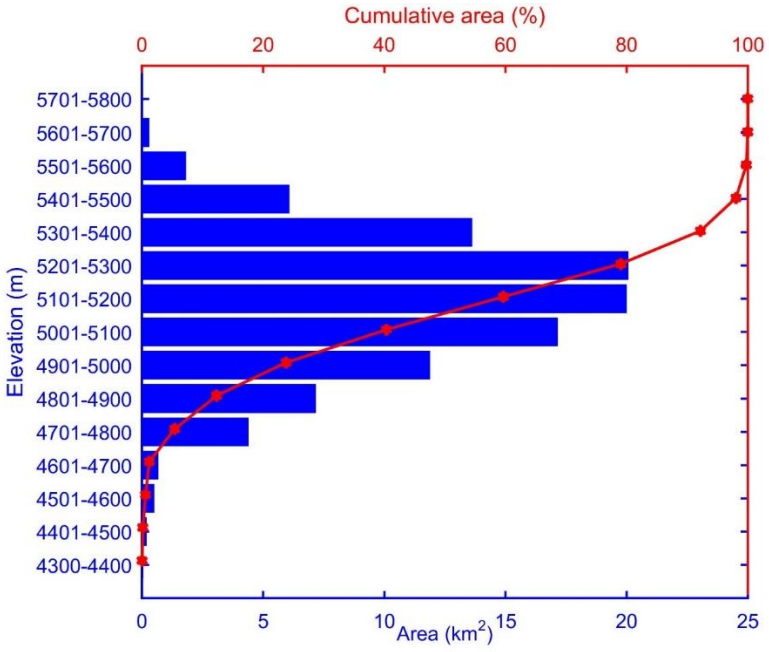

Figure 3.13 Distribution of the elevations of the debris-part of the glaciers.

Table 3.5 Morphometric characteristics of the 23 debris-covered glaciers in the Everest region and correlations with the supraglacial lake area.

	Glacier Name	Area (km^2)	Width (m)	DGM (m)	Elevation (m)		Slope (°)	AAR (%)	Aspect	Supraglacial lakes		
					Min.	Mean				No. of Lakes	Area (km^2)	Lake area (%)
1	Landak	0.97	312	41	4896	5281	11.9	30	SE	8	0.002	0.21
2	Chhule	3.35	408	22	4818	5157	10.5	14	SE	111	0.056	1.67
3	Melung	6.31	443	58	4960	5297	9.66	11	SE	135	0.044	0.69
4	Bhote Koshi	17.85	510	63	4758	5453	9.55	38	S	452	0.282	1.55
5	Lumsamba	5.13	463	61	4931	5511	6.81	45	S	312	0.157	2.98
6	Ngozompa	25.99	904	75	4684	5791	6.95	57	S	896	0.607	2.33
7	Cholotse	0.84	344	70	4889	5221	13.2	21	SW	18	0.007	0.81
8	Taweche	0.31	268	64	4967	5035	13.7	0	SW	11	0.005	1.62
9	Cholo	0.98	253	39	4445	4872	16.5	5	E	5	0.001	0.06
10	Lobuche	0.6	364	44	4960	5356	15.8	48	SE	10	0.019	3.24
11	Khangri Nup	7.41	923	98	5094	5434	9.57	38	SE	205	0.23	3.11
12	Khumbu	8.02	568	70	4909	6105	7.6	66	SW	220	0.323	3.89
13	Nuptse	3.29	419	49	4944	5475	9.24	44	S	84	0.04	1.22
14	Lhotse Nup	1.59	297	39	4958	5333	8.8	18	SW	74	0.024	1.53
15	Lhotse	5.86	740	42	4848	5538	7.1	33	SW	201	0.09	1.54
16	Imja	5.46	718	129	5011	5909	8.7	53	SW	125	0.028	0.52
17	Ambhulapcha	1.3	380	113	5055	5299	14.5	12	SW	27	0.008	0.65
18	Ama Dablam	2.37	441	63	4775	5357	8.8	37	S	81	0.049	2.06
19	Duwo	1.17	616	57	4744	4905	13.4	1	SW	16	0.015	1.3
20	Mingbo	0.5	235	26	4894	5262	20.3	19	SW	1	0.0001	0.03
21	Nareyargaip	2.1	375	107	5066	5499	15.5	61	S	7	0.046	2.17
22	Nare	0.67	526	108	5021	5331	12.5	24	S	10	0.001	0.17
23	Thyanbo	1.38	206	15	4373	5027	13.9	26	E			
	rs	0.9	0.7	0.21	-0.11	0.72	-0.75	0.61	Total	3009	2.04	

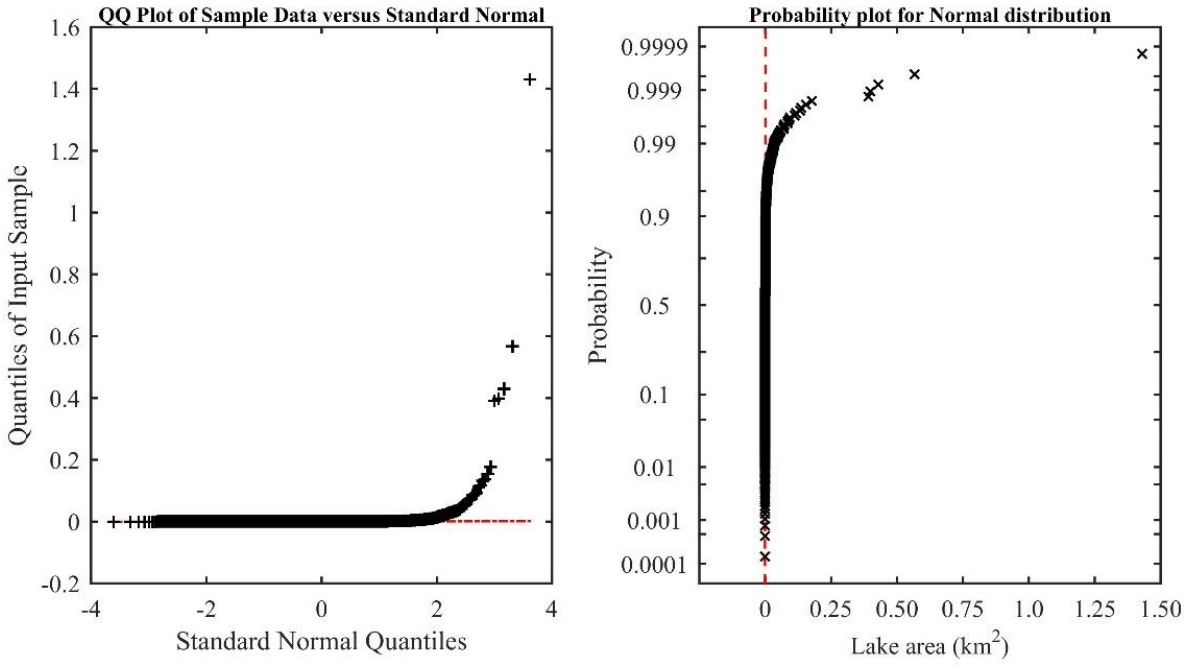

Figure 3.14 Distribution of glacial lakes in the Everest region using normal Q-Q plot on left side and normal probablity plot on the right side.

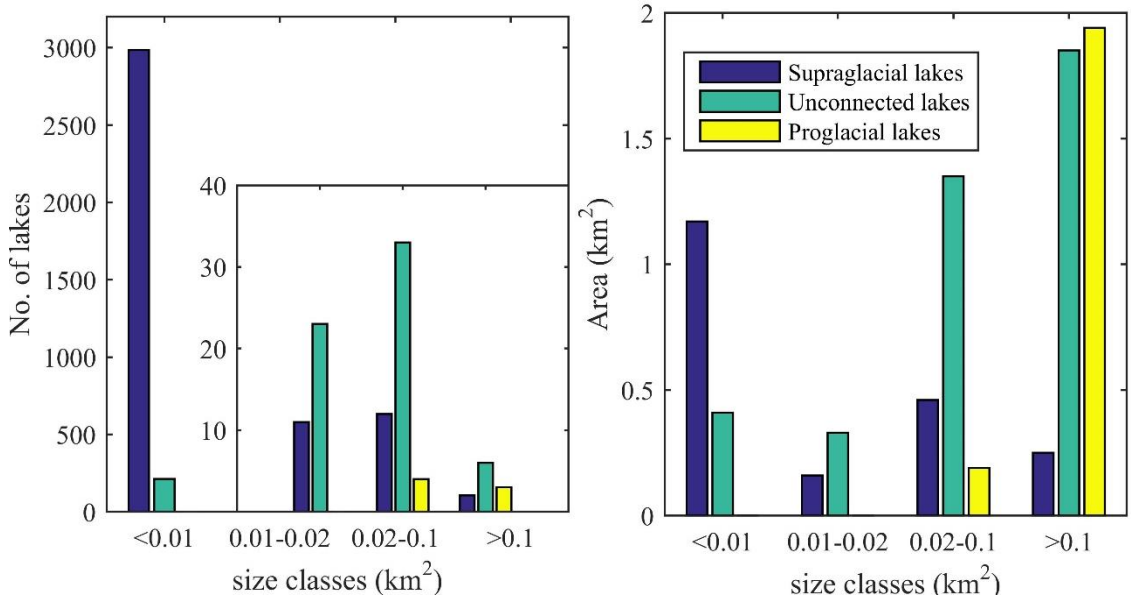

Figure 3.15 Distribution of glacial lakes in the upper Dudh Koshi basin according to their different size classes: number on the left isde and area on the right side.

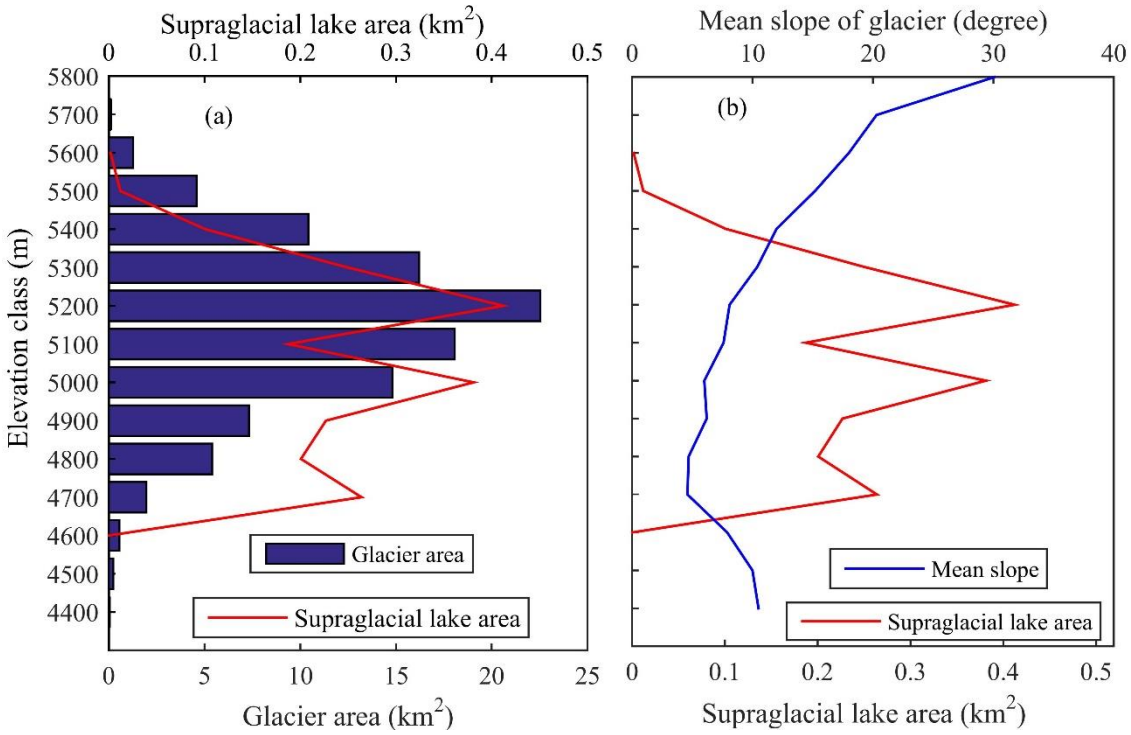

Figure 3.16 Relationship between supraglacial lake area and glacier characteristics with (a) elevation and (b) slope. The altitudinal area distribution of the debris portion of the glacier and area of all supraglacial lakes were mapped using 2-m resolution imagery in the Everest region. The elevation class values on the y-axis indicates the uppermost value.

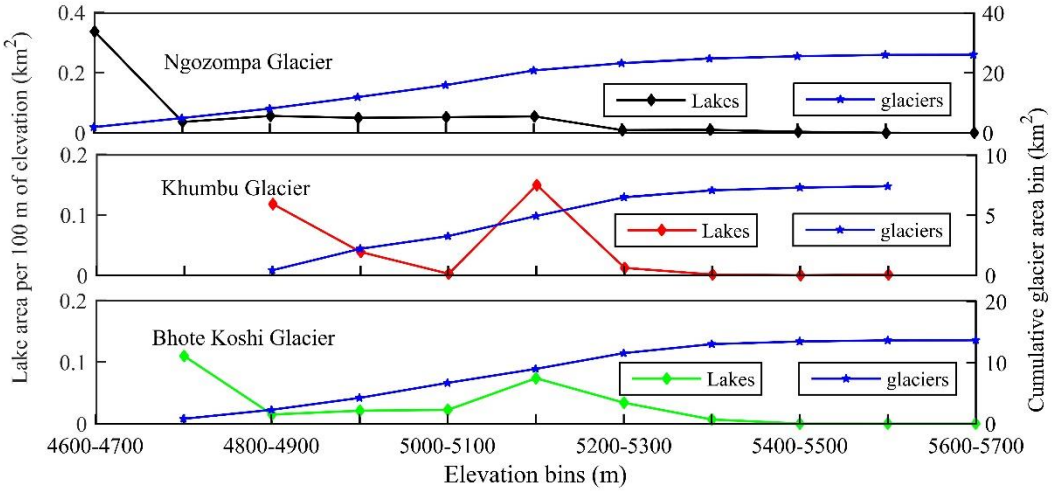

Figure 3.17 Supraglacial lake area per 100-m elevation bins for the three largest study glaciers with spillway lakes, i.e., Ngozompa Glacier, Khumbu Glacier, and Bhote Koshi Glacier.

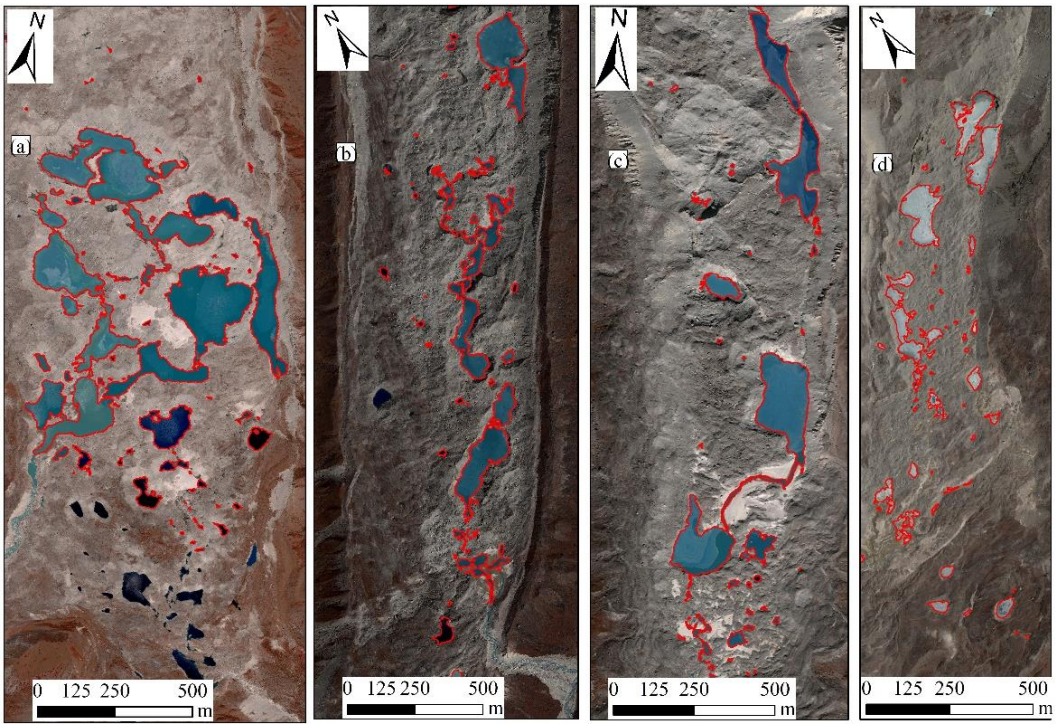

Figure 3.18 WorldView extent of spillway lakes and associated lakes at the terminuses of (a) Ngozompa Glacier from November 2016, (b) Khumbu Glacier from October 2016, (c) Bhote Koshi Glacier from November 2015, and (d) Lumsamba Glacier from April 2016.

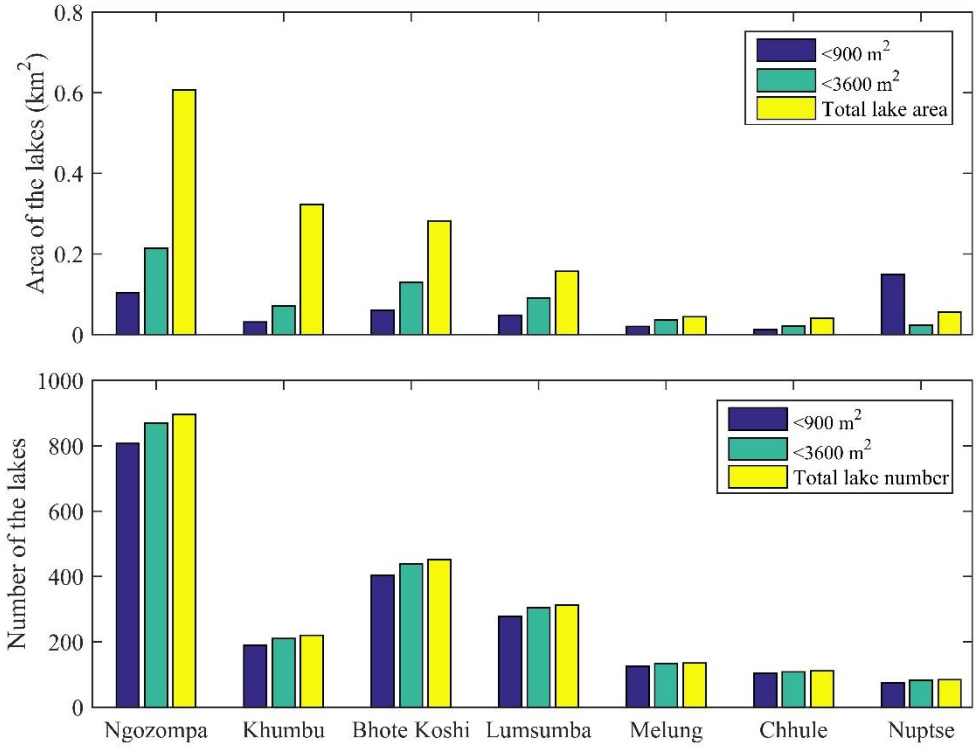

Figure 3.19 Proportion of lakes area (upper part) and lake frequency (lower part, falling below a 900 m^2/3,600 m^2 threshold for seven selected glaciers.

Table 3.6 Distribution of glacial lakes in the sub-basins of the upper Dudh Koshi River basin.

Sub-basins	All lakes		Supraglacial lakes		Proglacial lakes		Unconnected Lakes	
	No.	Area	No.	Area	No.	Area	No.	Area
Bhote Koshi River (at Namche)	5	0.15	0	0	1	0.11	4	0.04
Thame Khola	5	0.17	0	0	2	0.09	3	0.08
Bhote Koshi River (at Thame)	25	0.64	0	0	2	0.43	23	0.21
Chhule Glacier	269	0.25	254	0.1	1	0.06	14	0.09
Bhote Koshi Glacier	796	0.66	764	0.44	0	0	32	0.22
Ngozompa Glacier	1022	2.67	925	0.62	4	0.15	93	1.90
Khumbu Glacier	478	1.41	440	0.57	0	0	38	0.84
Upper Imja Khola	664	2.05	608	0.26	6	1.56	50	0.23
Lower Imja Khola	26	0.11	18	0.05	0	0	8	0.06
Phungi Khola	0	0	0	0	0	0	0	0
SUM	3290	8.11	3009	2.04	16	2.39	265	3.68

Area in km^2

Table 3.7 Distribution of glacial lakes in different size class.

Size class (km^2)	Supraglacial lakes		Proglacial lakes		Unconnected lakes		Sum	
	No.	Area	No.	Area	No.	Area	No.	Area
<0.0009	2715	0.41	0	0	115	0.04	2830	0.45
0.0009-0.005	234	0.5	1	0.005	61	0.14	296	0.64
0.005-0.01	35	0.26	1	0.01	34	0.23	70	0.49
0.01-0.05	21	0.46	8	0.25	42	0.90	71	1.62
>0.05	4	0.41	6	2.13	13	2.37	23	4.91
TOTAL	3009	2.04	16	2.39	265	3.68	3290	8.11

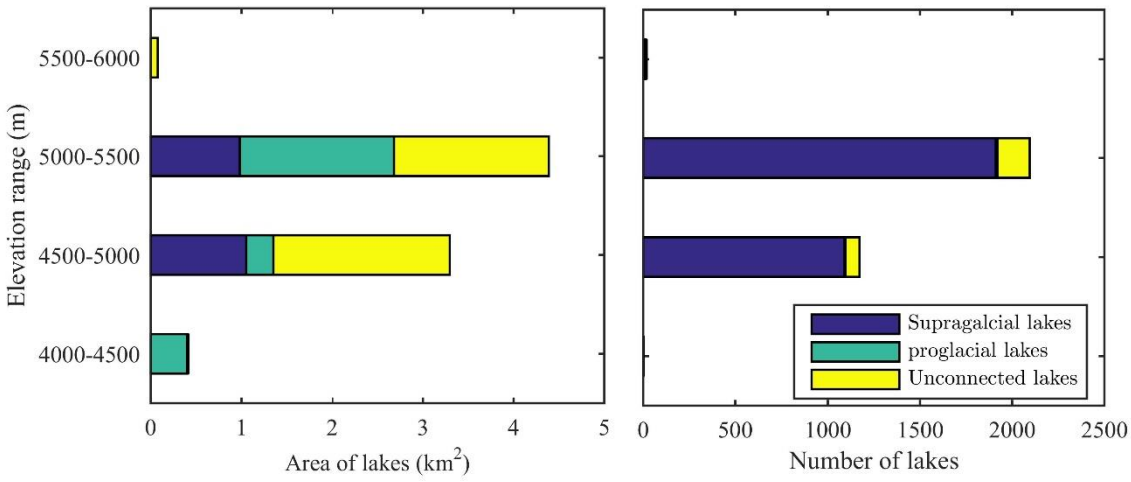

Figure 3.20 Distribution of area (left side) and number (right side) of three types of lakes according to their elevations.

4. Development of supraglacial lakes in the Everest region between 1989 and 2018

4.1 Introduction

4.1.1 Background

A negative glacier mass balance within the central and eastern Himalaya (Scherler et al., 2011; Bolch et al., 2012, 2019; Kääb et al., 2012;) is leading to development of several glacial lakes (Gardelle et al., 2011; Nie et al., 2013), corresponds with warming temperatures. Studies on proglacial lakes that formed at the terminus of the glaciers are well documented in the Himalayan region including GLOF risk (Watanabe et al., 2009; Rounce et al., 2017, 2016b;). Large valley glaciers of the Himalayan region are heavily covered by the debris in their lower extent and losing their mass in terms of surface-lowering rather than the up-valley retreat of a glacier (Scherler et al., 2011; Thakuri et al., 2014). Rockfalls and avalanches, medial moraines, and englacial debris bands are the most common sources of supraglacial debris (Schomacker and Benediktsson, 2018). Recent studies have shown that supraglacial lakes play a key role in the ablation of debris-covered glaciers and increasing interest among scientific communities to gain a better physical understanding of glaciers (Benn et al., 2012; Bolch et al., 2012; Watson et al., 2016, 2017; Miles et al., 2017b). Past studies also demonstrated that the supraglacial lake area changes from year to year (Gardelle et al., 2011; Watson et al., 2016; Miles et al., 2017b) and have different shape, size and colours (Figure 4.1). About 77% of supraglacial lake area is found associated with an adjacent ice cliff, and 49% of ice cliffs featured an adjacent supraglacial lake (Watson et al., 2017). Ice cliff plays a significant role in expansion of supraglacial lakes. Spillway lake on the Khumbu Glacier is developing a chain of connected lakes indicative of trajectory towards large a lake (Watson et al., 2016). This development is indicative of future proglacial lake, enhancing risk of GLOF.

Studies on a glacial lake in the Everest region are regionally aggregated (Gardelle et al., 2013; Nie et al., 2013), or glacier or lake specific (Bolch et al., 2008b; Watanabe et al., 2009; Lamsal et al., 2016). Additionally, studies are also documented covering only one point in time (Salerno et al., 2012). High-resolution mapping of the supraglacial lakes has been conducted in the Everest region (Watson et al., 2016), which covered multi-time points from 2000 to 2015, examined only eight glaciers in the southern part of the region.

Similarly, previous studies that cover the whole Everest region utilized the multispectral Landsat imagery on decadal basis to understand the growth of the glacial lakes including supraglacial lakes (Gardelle et al., 2011; Nie et al., 2013; Shrestha et al., 2017). However, studies focused on short- and long-term evolution of the supraglacial lakes and their spatial variation covering all debris-covered glaciers in the Everest region are not available. Therefore, this study aims to present the short- and long-term development of supraglacial lakes at the surface of the 23 debris-covered glaciers to address this shortcoming. The objectives of this chapter are to: (1) quantify short- and long-term variation in supraglacial lakes between 1989 and 2018; (2) understand the spatial evolution of supraglacial lakes among 23 debris-covered glaciers; and (3) understand the future trajectory of the spillway lakes in the region focusing on the Ngozompa Glacier.

4.1.2 Past studies in supraglacial lakes in the Everest region

Salerno et al. (2012) prepared an inventory of the supraglacial lakes including other types of glacial lakes covering the SNP, upper DKR basin. They used Advanced Visible and Near Infrared Radiometer type 2 (AVNIR-2) onboard ALOS images of 10-m resolution, revealed the 437 supraglacial lakes with the total surface of 1.39 km^2, and showed the lowest median size (1,000 m^2) among all types of glacial lakes present in the region. These features were found on 18 glaciers out of 29 studied glaciers in the region and the largest number (108) and area (0.50 km^2) of the supraglacial lakes were observed on the Ngozompa Glacier and the second largest number (100) and area (0.23 km^2) were observed on the Bhote Koshi Glacier.

Watson et al. (2016) studied the spatiotemporal variation of the supraglacial lakes from 2000 to 2015 using OBIA and manual digitizing approach. They mapped supraglacial lakes on eight glaciers in the southern part of the Everest region and found inter- and intra-annual area changes up to 17% to 52%, respectively. The spillway lakes found partially drained over the study period and dynamic over the study period. They demonstrated the heterogeneous spatial change in area of the lakes. The Khumbu Glacier gained the area and the Ngozompa Glacier exhibited a net loss in the lake area. They also displayed the least area in October in smaller glaciers and an increase thereafter with the largest lake area during the summer periods.

Thompson et al. (2012) used ASTER imagery and field survey to document growth of lake near terminus of the Ngozompa Glacier from 1984 to 2008. They revealed the

larger growth rate of 10% y^{-1} for the period 2001 – 2010 compared to before 2001. Annual growth rates varied from 5% y^{-1} to 15% y^{-1} for the period 2001 – 2010.

Shrestha et al. (2017) identified 218 supraglacial lakes in the whole DKR basin using Landsat imageries of 2010. They also presented the appearance and disappearance of the lakes over time. Similarly, Khadka et al. (2018) presented the dynamics of glacial lakes on a decadal basis from 1977 to 2017 in the Nepal Himalaya and revealed the dominant presence of supraglacial lakes in the Koshi River basin over the Gandaki and Karnali River basins. They presented the increase in the number of the glacial lakes largely contributed from the increase in the number of supraglacial lakes between 1997 and 2007. ICIMOD (2010) delineated 107 supraglacial lakes in their inventory using Landsat images of 2009 with the mean area of 9,000 m^2. They observed the coalescing of small lakes to form a large lake, and they also reported the GLOF event, which originated from a supraglacial lake (Chubung) on the surface of the Ripimoshar Glacier adjacent to Tsho Rolpa in 1991.

Nie et al. (2017) also revealed the dramatic spatial-temporal changes and rapid expansion between 1990 and 2015 in the Himalayan region including the Everest region. They were able to report 173 supraglacial lakes in 2015 through the Himalaya using the minimum area threshold of 8,100 m^2 but were unable to detect seasonal variations. Supraglacial lakes in the Himalaya are found to be increased by 11.35% from 1990 to 2010 (Nie et al., 2013). Wessels et al. (2002) demonstrated an application of ASTER images to detect and monitor supraglacial lakes on glaciers in the Everest region, and the results showed the varying turbidity of lakes, the largest lakes being bright blue (highly turbid) and small lakes found mostly dark blue (relatively clear water). They indicated the high rates of meltwater input from streams or erosion of ice cliffs was responsible for high levels of turbidity. They also revealed the episodic filling and drainage of the supraglacial lakes on glaciers of the Everest region. The summary of the past studies is provided in Table 4.1.

4.2 Dataset

Supraglacial lakes were mapped from 1989 to 2018 using freely available Landsat and Sentinel-2 images.

4.2.1 Landsat

Surface Reflectance Level-2 science products of the Landsat 5 Thematic Mapper (TM), Landsat 7 Enhanced Thematic Mapper (ETM+), and Landsat 8 Operational Land Imager (OLI) were used to study the long-term development of the supraglacial lakes. Landsat images are of 30-m resolution and Level-2 are available only after 1987 for the study. Images were downloaded from the USGS website for each year from 1987 to 2017. Unfortunately, no suitable scenes were available from the same month for each year due to the presence of significant cloud during the summer monsoon season and snow during the winter and pre-monsoon seasons. Seasonal changes in glaciers and glacial lakes are relatively minor from September to December (Jiang et al., 2018). Therefore, images that lie within the three- month's period of October to December (Figure 4.2) were selected for the whole period except for 1990, 2013, and 2014. Images from January for 1990 and September for 2013 and 2014 were used in this study. Most utilized scenes were without snow/cloud cover on the debris portions of the glaciers and were suitable for the identification of water bodies. However, no suitable scenes were available for 1987, 1988, 1991, 1997, 1999, 2006, 2007, 2011, and 2012 due to extensive snow/cloud cover and data gaps caused by a scan-line error. Two scenes were used for 2014, one from September and the other from November, to minimize the effect of clouds. In total, 23 scenes (Table 4.2) of path 140 and row 41 were used for the 22 different years for this study. Surface reflectance products are atmospherically corrected products using a radiative transfer model, which are the Second Simulation of Satellite Signal in the Solar Spectrum (6S) for Landsat 5 and 7, and an internal algorithm for Landsat 8. In these models, the effects of water vapor, aerosol, and ozone have been removed to obtain accurate surface reflectance. Landsat images were also radiometrically calibrated and orthorectified using GCPs and a Dgital Elevation Model (DEM).

4.2.2 Sentinel-2

Sentinel-2A and 2B images of 10-m resolution for the years between 2016 and 2018 were acquired from the European Space Agency's (ESA) Sentinel Scientific Data Hub, incorporating the post-monsoon (October), winter (December – January), and pre-monsoon (April – May) seasons (Figure 4.2). The Level-1c product is composed of 100 x 100 km^2 tiles (ortho-images in UTM/WGS84 projection). This product results from using a DEM to project the images in cartographic geometry and are resampled with a

constant GSD of 10, 20 and 60 m. Sentinel-2 have 13 spectral bands at different resolution: four bands at 10 m; six bands at 20 m; and three bands at 60 m with orbital swath width of 290 km. Two scenes of Sentinel-2 each with tile identification number of T45RVM and T45RVL and relative orbit number 76 were acquired to cover the entire study area for each period. Two images from same month of the pre-monsoon season of 2018 were acquired to minimize the error due to freezing of the lakes. A total of 14 Sentinel 2A and four Sentinel 2B images of the level 1C (Table 4.3) covering the entire study area were used to map the supraglacial lakes for the eight different seasons between 2016 and 2018.

The ESA sen2cor plugin, which is available on the SNAP was used for atmospheric and terrain corrections of the Level 1C images and to produce an atmospherically corrected Level 2A Bottom of Atmosphere (BOA) reflectance product. The Level 2A product is similar to that of the Landsat surface reflectance product. In this study, only 10-m resolution bands, being blue, green, red, and infrared bands were used. A mosaic of two scenes of the same period was created to incorporate the entire area.

4.3 Methods for long and short-term variation of supraglacial lakes

Semi-automatic method for mapping supraglacial lakes was applied. *NDWI* in combination with band ratios were applied to delineate the supraglacial lake boundaries, which was corrected manually by visual checking and editing. The details of methodology were provided in chapter 3 and processing workflow is presented in Figure 4.3.

Landsat 5, 7, and 8 were used for long-term variation and development of lakes and Sentinel-2A and 2B were used to study short-term variation of lakes. Landsat images were atmospherically corrected products and clipped to the boundary of the 23 glaciers, while Sentinel-2, level 1C products were atmospherically and topographically corrected before clipping to the glacier boundaries. *NDWI* (Eq. (3.1)) and band ratio (*BR1*) of green and near infrared (Eq. (3.2)) were applied to delineate the boundaries of the lakes. A threshold of 0.3, 1.2, and 0.45 were applied for *NDWI, BR1,* and *BR2*, respectively to delineate the boundary of the lakes. Quality assessment (QA) band available in the Landsat surface reflectance product and scene classification algorithm in sen2cor for Sentinel-2 images were used to remove the effect of the shadow. Similarly, spectral metric of blue, green and red bands (Eq. (3.4)) was applied to remove the effect of snow, and slope threshold of 30° was applied, considering that lake can develop in lower slope.

Finally, all delineated lakes were visually inspected and corrected manually. In this study, Landsat images of 30-m resolution were used for historical mapping, a threshold of 5,000 m^2 was used to classify the lake to reduce the overestimation of the lakes. The same threshold for 10-m Sentinel-2 images was used to make comparison with Landsat results. However, a threshold of 500 m^2 was also applied for seasonal analysis of the lakes. Finally, polygons smaller than these thresholds were removed, and further analysis was conducted.

4.4 Unmanned Aerial Vehicle (UAV) images

4.4.1 Post processing of GCPs

GCPs were collected before conducting a UAV survey using Emild Reach RS Global Navigation Satellite System (GNSS) (Figure 4.4). One receiver was mounted on a tripod to establish a temporary static base station at the right moraine of the glacier, and position was changed to cover the different part of the glacier. Another receiver was used as a rover to occupy target features for ~10 minutes for each measurements. Measurements were taken on the glacier, which were spatially distributed over survey area and mostly concentrated on left and right lateral moraines of the glacier (Figure 4.5). Overall, 20 GCPs were taken during the survey, however, only 13 points were utilized for the analysis of UAV photographs (Figure 4.6), because rest of the GCPs were outside of the survey area.

GNSS observations from each receivers were downloaded and were processed using RTKLIB (RTKPOST v.2.4.3) using precise GPS data. Initially, coordinates of the base receiver were processed using JIR2 station, Jiri, Dolakha, a GNSS network of UNAVCO (Jean-Philippe et al., 2015), which is located at distance of about 60 km from the Ngozompa Glacier. GNSS data from the same day of the observation were acquired from JIR2 station, and post processing in RTKLIB was carried out to achieve horizontal accuracy within 5 cm and vertical accuracy within 15 cm. Post processing of measurements from a rover was carried out based on the post-processed base coordinates.

4.4.2 UAV Surveys

To produce and evaluate the UAV-derived high-resolution topographic maps of the spillway lake at the terminus of the Ngozompa Glacier, UAV survey was carried out. Survey was conducted from December 8 to 12 in 2018, in which optical images were collected. A series of UAV flights were performed over the course of the morning to early

afternoon. Survey was not possible in the late afternoon due to strong wind. Mavic Pro by DJI with a 12-megapixel camera was automatically flown in most cases and also manually flown on 10-12 December 2018. The drone captured near-nadir imagery to ensure the overlap of ~70% and more. Each image captured from the drone was automatically georeferenced with 3D coordinates from UAV's Global Positioning System (GPS) and Global Navigation Satellite System (GLONASS) receiver. The flight was started from the right lateral moraine, near terminus of the glacier, and flight paths followed linear routes to the left moraine and back to the right moraine.

4.4.3 Orthomosaic and DEM processing

Agisoft Photoscan 1.4.0 was used to process the UAV photographs to produce orthomosaic and DEM. Following a SfM-MVS workflow (Ferreira et al., 2017; Mertes et al., 2017; Watson et al., 2019), is most frequently applied technique, which offers a user-friendly solution to SfM-MVS (Smith et al., 2016). SfM is a low-cost and effective tool for photogrammetry for geoscience application (Westoby et al., 2012). Images were first imported into Photoscan and the area that was not modeled was masked out. Masked area includes mountains beyond the glacier area and sides of the lateral moraines. A total of 1,130 images were aligned using the 3D coordinates of UAV and sparse point clouds generated contained the 916,412 tie points after filtering (Table 4.3). Points that appear distant or obviously erroneous due to angle of images were removed during filtering. GCPs were measured on large boulders and used to georeference points clouds imported to Photoscan. The position of each GCPs was identified and adjusted manually where necessary based on the field experience. Alignment of the images was repeated after adding GCPs. High-quality settings and moderate depth filtering were used in Photoscan to generate dense point clouds. The resulting dense point clouds were then edited, and points far beyond the area of interest were removed. The dense cloud contained 338,288,277 points in the whole area. Generation of DEM with the setting 'interpolated' enabled resulted the 10-cm DEM and orthoimage was produced using the DEM as the underlying surface with 5-cm resolution. Complex of the spillway lake was mapped manually using orthomosaic to prepare the latest and high-resolution map. Topographic map was created at 10-cm spatial resolution and generated DEM (Figure 4.7a) was used to understand the topography and geomorphology of the lake and surrounding environment. The generated DEM was compared with HMA DEM of 8-m spatial resolution of the year 2010 (Figure 4.7b).

HMA DEM for the year 2010 and UAV DEM for the year 2018 were utilized to obtain a deeper insight of the morphologies of the lakes and change in surrounding morphologies. The accuracy of produced topographic, orthomosaic, and DEM was less than one meter based on the GCPs and check points used during processing in the Photoscan.

4.5 Lake frequency

Frequency of the supraglacial lakes were estimated based on the occurrence of each individual lake in each study year, and score was normalized to percentage (Eq. (4.1)). Frequency map for the each glacier were prepared using statistical software R. Frequency map help to understand to distinct between the lakes that persist over time, those that drain, and those that drain and subsequently refill between time periods (Watson et al., 2016). Raster images of supraglacial lakes from each year from 1989 to 2017 (n=22) were utilized to prepare the frequency map of lakes to report their trend toward persistency, reoccurrence, and disappearance. Pixel of the image that was covered with water for one or more time was considered to represent the frequency of map (Watson et al., 2016; Miles et al., 2017b).

$$\text{Frequency} = \frac{No.\ of\ years\ of\ lake\ occurence}{Total\ no.of\ study\ years} \times 100 \quad (4.1)$$

4.6 Volume estimation of spillway lakes

Potential volume of the spillway lakes were estimated based on the mean depth and lake volume equation of Huggel et al. (2002), which were revised by Cook and Quincey (2015). These equations were used for estimating the volume of the supraglacial lake in the Nepal Himalayas (Watson et al., 2016). Cook and Quincey (2015) utilized the equations for the lakes, which predominately comprise large glacial lakes. In this thesis, volume for the spillway lakes was calculated, which comprised several small lakes associated with them. Hence, the uncertainty for smaller lakes is likely to be large; however, lacking the bathymetry data, empirical equations were used for first-order estimate of spillway lake water storage. The mean depth was estimated as:

$$D = 0.1217A^{0.4129} \quad (4.2)$$

where D is the mean depth (m) and A is the lake area (m^2) and the equation for volume (m^3) used was

$$V = 3 \times 10^{-7}A^{1.3315} \quad (4.3)$$

4.7 Results

4.7.1 Long-term evolution of the lakes

Long-term study of supraglacial lakes between 1989 and 2017 revealed a total number of 1,026 supraglacial lakes (>5,000 m^2) in the Everest region on the surfaces of 23 debris-covered glaciers. A large lake at the Khangri Nup Glacier excluded for an analysis because this was observed in only a few images due to the presence of shadow. Approximately 59% (n=594) of the supraglacial lakes were <0.01 km^2 in size, which accounts for only one-third of the total lake area over the period studied. Of the total lake area studied during the period, lakes with sizes of 0.01–0.02 km^2, and >0.02 km^2 have lake areas of 32% (n=294), and 35% (n=120), respectively.

The Shapiro-Wilk distribution test statistics at 95% confidence interval reveals that the distribution of lakes was not normal (Figure 4.8a) and skewed positively with a factor of 4.23. The probability distribution of lake area also reveals that ~90% (n=923) of lakes have an area <0.025 km^2, and approximately 96% (n=983) of the lakes have an area <0.05 km^2, which contributes approximately 60% and 73% of the total lake area between 1989 and 2017, respectively (Figures 4.8b and c). Only 4% (n=43) of the lakes comprised approximately 27% of the total lake coverage.

Overall increase in the number (Figures 4.9a) and area (Figure 4.9b) of supraglacial lakes was observed from 1989 to 2017, with minor fluctuations (Annex II-IV). The overall area of the lakes was increased from 0.38 ± 0.19 km^2 in 1989 to 1.32 ± 0.727 km^2 in 2017 (Figure 4.10a), representing an overall growth of 350%. The size of the lakes varies from 5,000 m^2 to 0.13 km^2, with a mean size of 0.015 ± 0.019 km^2 and mean size of the lakes remained mostly static (Figure 4.10b). The rate of increase was comparatively slower between 1980 and 2005 (0.01 $km^2 y^{-1}$) than between 2008 and 2017 (0.07 $km^2 y^{-1}$). In the 1989 imagery, 25 supraglacial lakes were identified, and this number increased to 85 (increased by 3.4 times) in 2017, with the largest number of lakes (88) in 2015. The number of lakes almost doubled between 1989 and 2002, slightly decreased between 2003 and 2005, and increased rapidly from 2009. The year-by-year variations in the number and total area for different dimensional classes of supraglacial lakes showed that the frequency of small-sized lakes (<0.01 km^2) was higher than the larger lakes (>0.02 km^2) in each studied year. However, the area covered by larger lakes contributes significantly more than the small lakes in the majority of years (Figures 4.9a and b). The largest

increase in the number of lakes was observed that have dimensional classes of <0.01 km^2 in the recent period. However, the largest increase in lake areas was observed in the dimensional class of >0.02 km^2. The increase in the lake area with size >0.02 km^2 ranges from 45 to 54% after 2008. Lakes were observed in 16 of the 23 studied glaciers in the region, whereas lakes ere not observed on the Cholo, Choloste, Landak, Nare, Tingbo, and Twaeche glaciers (<1 km^2). However, a significant area of the supraglacial lake was observed frequently from 1989 to 2017 on the smaller Lobuche Glacier (0.45 km^2).

4.7.2 Glacier-wise trends of lake cover

The glaciers studied here demonstrated the significant variability in lake cover over time. Of the 23 glaciers investigated in this study, supraglacial lakes were observed on nine glaciers in 1989 and 16 glaciers in 2014 and 2015. All glaciers except for the Loboche Glacier experienced either increase in the area of lakes or the appearance of new lakes. The increase of lake cover varies among the glaciers, and the largest increase in the number, from 8 to 27 and in area, from 0.06 ± 0.05 to 0.42 ± 0.24 km^2 was observed on the Ngozompa Glacier during the studied period of 28 years (Figure 4.10a). Similarly, the Bhote Koshi and Khumbu glaciers contributed significant increase in lake area. The Ngozompa, Bhote Koshi, and Khumbu glaciers exhibited a total lake area of 81% in 1989 and 67% in 2017. The Ngozompa Glacier alone contributed approximately 32% of the total lake area in 2017. The Nareyargaip and Lumsamba glaciers recorded the increased lake coverage by approximately 10 times than in 1989, although the actual increase in lake area was 0.05 km^2.

Substantial inter-annual variation in the lake area was observed due to draining of the lakes. The lake area on the Ngozompa Glacier increased by approximately 370% between 1990 and 1993 and then decreased until 1996. This variation in lake area was controlled by the formation and development of one large lake (0.1 km^2) at about 1.5 km from the current outlet of the glacier (Figure 4.11). It was almost completely drained (7,000 m^2) by 1994. Similarly, a large lake on the Bhote Koshi Glacier also lost its size significantly between 1990 and 1992 and contributed to a decrease in lake area on this glacier.

The Thyanbo, Chhule, Melung, Bhote Koshi, Lumsamba, Ngozompa, Khumbu, and Nuptse glaciers exhibited the presence of either spillway lakes or lakes near their terminuses. However, the area of the spillway lakes on the Ngozompa, Bhote Koshi, Khumbu, and Lumsamba glaciers increased significantly. Most of these lakes were larger

than the lakes in the upstream region and exhibited ~40% of the total lake area in 2017 and contributed in increasing in the total area of the lakes during the study period. The details of the spillway lakes are presented in section 4.7.3.

4.7.3 Change in spillway lake area

Spillway lakes and their surrounding lakes at the termini of the glaciers were studied in detail to understand their trajectory towards to a large glacial lake. The detail of eight glaciers, i.e., Thyanbo, Chhule, Melung, Bhote Koshi, Lumsamba, Ngozompa, Khumbu, and Nutpse, which exhibited the lakes near the terminus are described as follows.

4.7.3.1 Thyanbo Glacier

The Thyanbo Glacier encompasses the total area of 3.6 km^2 with 1.38 km^2 area of debris-covered part. This glacier had four tributary glaciers and separated with each other and three tributaries exhibited the debris portion at their lower stream. Spillway lake at the Thyanbo Glacier was observed only after 2010 (Figure 4.12). Small lake with size of 11,497 m^2 was detected in 2010 on the left tributary of the glacier. It started to expand and reached at the size of 35,202 m^2 in 2017. Similarly, lake at the terminus of the right tributary was observed only after 2016 and size of this lake increased from 6,147 m^2 to 29,299 m^2 in 2017. Draining from the lakes could not be observed and found persistent, and the lakes were continuously expanding during the observation period.

4.7.3.2 Chhule Glacier

A lake with size of 11,024 m^2 was observed in 1989, while another lake of size 9,296 m^2 was detected in 1990 towards upward stream from the first lake. The first lake was continuously observed after its formation, while the second lake displayed episodes of occurrence and disappearance until 2004 and showed limited expansion in size (Figure 4.12). Additional lake was identified in 2008 at the location of the second lake and disappeared again in 2009. The third lake between the first and second lake was detected in 2010 and could not be identified in the later period. The total area of the three lakes was 48,568 m^2 in 2010. The first lake also disappeared after 2010, while the lake at the location of second lake expanded continuously by coalescing of the small lakes. The size of this lake reached to 50,830 m^2 in 2017. Lakes on the Chhule Glacier exhibited dynamic activity with regular draining events during the observation period.

4.7.3.3 Melung Glacier

No lakes at the terminus of the Melung Glacier were observed in the earlier period of the observation. A lake of size 6,843 m^2 was identified in 1994 and showed episodes of appearance and disappearance till 2004. However, this lake persisted till 2008 and another lake with relatively larger size (14,273 m^2) towards upstream was also observed in this year. These lakes shown the occurrence and disappearance after 2008 and only a lake (12,301 m^2) close to the terminus of the glacier persisted till 2017 after 2010, and expansion of lakes was found limited (Figure 4.12).

4.7.3.4 Bhote Koshi Glacier

The Bhote Koshi Glacier was the second largest glacier in the Everest region, which had debris-covered area of 17.85 km^2. The Bhote Koshi river, a tributary of the DKR originated from the Bhote Koshi Glacier, positioned towards upstream of the villages Chhule, Chhulun Marsan, Hauche and Thokchambo. Complex of spillway lake on the Bhote Koshi Glacier was interconnected and its area was increased by 20 folds from 1989 to 2017 (Figure 4.12). A small lake of size 5,092 m^2 was observed in first year of observation and two additional lakes were appeared with the total area of 23,620 m^2 in 1992. Topographic map prepared by the Survey Department, Government of Nepal also revealed the lakes of similar size in 1992, which displayed four small lakes. Results of the Landsat analysis could not recognized lake near the terminus and the left lateral moraine of the glacier before 1992. A total area of the four lakes in 1993 was 26,989 m^2. The lake near the right moraine disappeared after 1993. The three lakes increased in their area and encompassed the total area of 36,963 m^2 in 1995. The lower lake close to the terminus probably lost its area during 1998 and 2000 and could not be mapped due to the threshold of 5,000 m^2 in 2000. Therefore, the total area of the lakes was decreased during this year. The size of the lakes remained similar until 2005, and increased rapidly after 2005 with the total size of 59,780 m^2 in 2008 and 67,338 m^2 in 2010. The number of lakes also increased to 5, where the largest lake was located close to the left moraine and close to the terminus. The size of lakes continued to expand in total after 2010 and reached at largest size in 2015 with the total area of 116,097 m^2, which was slightly decreased in 2017. Similar area (115,220 m^2) of complex spillway lake was observed using high-resolution WorldView image in 2015, which validated the Landsat results. Lower two lakes were found connected to each other with a surface channel in WorldView image of

2015. The rapid increase in the area of the spillway lake on this glacier showed the trajectory towards a single large glacial lake in the future. However, further study is needed about its physical setting, morphology including field investigations.

4.7.3.5 Lumsamba Glacier

The Lumsamba Glacier is located in the left side of the Bhote Koshi Glacier and showed the rapid expansion of the spillway lake. A lake at the terminus of the Lumsamba Glacier was observed from the beginning of the observation. The lake was with size of 6,025 m^2, and its area was increased rapidly between 1989 and 1995 (Figure 4.12), which gained the size of 59,179 m^2 in 1995. The number of lakes was three during this period, and two lakes disappeared and another lake was also lost its area between 1995 and 1996, which left only a size of 7,198 m^2. The significant expansion of the lake could not be observed from 1996 to 2010, except minor up and down in the area. The number and area of lakes near the terminus increased uninterruptedly from 2010 to 2016, and gained an area of 85,244 m^2 in 2016, which was later decreased to 50,384 m^2 in 2017. The lakes near the terminus of the glacier were dynamic and displayed the incidences of expansion and reoccurrence within the shorter period.

4.7.3.6 Ngozompa Glacier

Spillway lakes on the Ngozompa Glacier was found to be largest and expanding rapidly (Figure 4.12). Three lakes with the total area of 31,798 m^2 were identified in 1989, and gained an area of 43,242 m^2 in 1995, and 75,054 m^2 in 2000. Topographic map of the Everest region showed the four lakes in 1992. The number of lakes obtained from Landsat in the 1992 was the same as that on the topographic map. However, an elongated lake at the southern part of the terminus was mapped as two individual lakes, and one northern lake was not identified in the Landsat image. Expansion of the lake from 2000 and 2003 was limited, while it increased after 2003 and attained total area of 114,365 m^2 in 2005. Most rapid expansion of the lakes can be observed from 2005 to 2010, supplemented by the elongated lake close to the left lateral moraine. The total area of the eight lakes plotted was 231,170 m^2 in 2010, which was twice larger than the lake size in 2005. The Landsat results revealed the limited expansion of the lakes from 2010 with size of 228,272 m^2 in 2017, almost similar to the size in 2010. The largest area (248,439 m^2) was observed in 2014. The overall growth rate of ~30% y^{-1} for the period 1989 – 2010 was observed, while

this growth rate varied between the different periods. The WorldView mapping in 2016 plotted an area of 254,834 m^2, which was similar to the Landsat results. Marked increase in the area was observed after 2005, while remained at nearly steady state after 2010 until 2017. By 2014, the area was 7.8 times larger than that in 1989. The lake and associated lakes at the terminus of the Ngozompa Glacier have potential to become a single large proglacial lake (described in section 4.7.7).

4.7.3.7 Khumbu Glacier

Series of lakes were observed near terminus of the Khumbu Glacier, and WorldView results of 2016 revealed the second largest complex of spillway lakes after lake on the Ngozompa Glacier. Interconnected lakes presented the rapid expansion in their size after 2004 (Figure 4.12). A small lake of size 5,020 m^2 was detected at ~1.6 km upstream from the terminus of the glacier in 1989, which was not detected after 1989. A new lake of the similar size appeared in 1993 at ~400 m downward from the lake mapped in 1989, and an additional lake emerged at the terminal boundary of the glacier in 1995. Lakes at the terminus of the Khumbu Glacier appeared to be more dynamic and showed the incidences of appearance and disappearance. Growth of lakes between 1995 and 2005 was limited, while it presented rapid increase in the area between 2005 and 2008 with area of 37,225 m^2 in 2008. The lakes again displayed the decreased area in 2009 and increased after 2010. Five lakes with different size were distributed along the near straight line and positioned close to the left lateral moraine of the glacier in 2015. The area (91,938 m^2) of the lakes was the largest during the observation period. The northernmost lake and southernmost lake attained the largest size in 2017, and displayed the trend of merging of lakes. This result indicated that spillway lake on the Khumbu Glacier also has high potential to form a large glacial lake. Detailed field investigations are needed to understand the physical setting, potentiality of the large lake formation, and potential risks from the potential outburst.

4.7.3.8 Nuptse Glacier

The Nuptse Glacier is placed at upstream of the Chukhung Village in the Imja Khola basin, which showed the presence of a spillway lake at the terminus (Figure 4.12). A lake close to the right moraine was formed in 1994, which was disappeared after 1995. A new lake appeared nearby the left moraine of the glacier in 2000 and persisted until 2017,

which also indicated the increment in size. Similarly, another lake also appeared in 2014 and prolonged until 2017. The total area of the two lakes in 2017 was 20,271 m^2.

4.7.4 Change in spillway lakes volume

Volumetric estimates are required to assess the water storage dynamics at the surface of the glacier. In this study, a first-order estimate of the depth and volume of the spillway lakes was carried. The largest mean depth of the spillway lake was estimated for the Ngozompa, Bhote Koshi, Khumbu, Lumsamba, and Thaynbo glaciers, and found about 20 m, 15 m, 14 m, 13 m, and 12 m, respectively. The mean depth of lake for the Chhule, Melung, and Nuptse was less than 10 m. The volume of the lakes presented the continuous increase, where the area of the lakes was found to have increased (Figure 4.13). This can be clearly observed on the Ngozompa, Bhote Koshi, Khumbu, Lumsamba and Thyanbo glaciers, where the volume estimated was 4.09, 1.40, 0.95, 0.55, and 0.76 million m^3, respectively. The volume estimated using the area obtained from the WorldView imageries displayed the slightly higher water volume, corresponding to relatively larger area plotted using the high-resolution WorldView imageries.

4.7.5 Lake persistency

Lake persistency is described in terms of the frequency of the lakes. The lake persistency depends on the development of englacial connections. A lake develops and expands when drainage points of depression is blocked. Four glaciers namely; Ngozompa, Bhote Koshi, Khumbu, and Nareyargaip demonstrated the presence of lakes in each year of the observation with 100% frequency, while the Lumsamba and Chhule glaciers displayed about 95% occurrence of lakes (Figures 4.14 and 4.15). Most lakes at the glacier termini, especially on the Ngozompa, Khumbu, Bhote Koshi, and Lumsamba glaciers were persistent for long duration, and lake area was increased rapidly. One of the tributaries of the Khumbu Glacier had a very high persistent lake (100%) over 22 scenes and over the 28-year studied period, with very little expansion in size. However, lakes on the smaller glaciers with relatively steeper slope tend to be less persistent for the longer period. They featured different range of frequencies with high frequencies on the Lobuche Glacier, terminus of the Nuptse and Chhule glaciers. Lakes on the Imja, Lhotse, Khangri Nup and Ama Dablam glaciers also displayed the discrete area of high-persistency. Similarly, lakes were shorter-lived at the upper part of the each glacier in comparison to the downstream part. Supraglacial lakes were observed only on nine glaciers in 1989 and

new lakes emerged on additional seven glaciers in 2014 and 2015 with a few disappearances and reoccurrences of the lakes in the same period. The emergence, expansion and disappearance of lake suggested the increased hydrological connectivity in the glaciers.

Lake frequency maps for the periods 1989 – 1998, 1999 – 2008, and 2009 – 2017 were computed for the three selected glaciers to highlight the expansion, distribution and persistency between the different shorter periods (Figure 4.16). The lake frequency map for the three periods revealed the high persistent lakes in the later period (2009 – 2017) than the earlier periods. Individual lakes on each glacier can be easily identified as features with high and low frequency, which demonstrated the lake emergence, expansion and disappearance during the study period. Lakes at the terminuses of the glaciers demonstrated the continued expansion in their area, and no draining events within lakes were detected (NG1, BK1, BK3, KB1, and KB2, in Figure 4.16). Expansion of the existing lakes or emergence of new lakes was frequently observed for the later period. Lake at the tributary of the Khumbu Glacier was persisted in each period, however, no continued expansion was observed (KB3 in Figure 4.16). Part of the glaciers represented the persistent or repeated lake formation in the earlier period, which decayed slowly and showed a decrease in area and frequency for the middle period and later periods, and entire disappearance entirely in some cases (NG2, NG4 in Figure 4.16). Lake at the point NG2 was observed to have a large area in the earliest period, which was studied in detail to find out the drainage event (Figure 4.11). The lake emerged in 1990 with small area (3,939 m^2), and expanded during 1991 and 1993, and attained the size of 102,188 m^2, and drained before 1994 (7,263 m^2). Similarly, lakes became more active and persistent with the increased area during the middle period, which decreased in their area for the later period (NG3, BK2, and KB4 in Figure 4.16).

4.7.6 Seasonal lake cover

A total of 3,027 supraglacial lakes (>500 m^2) for the eight different seasons between January 2016 and May 2018 were mapped using Sentinel-2 images. The mean size of the lake was 4,600 ± 1,400 m^2. Supraglacial lake cover in the Everest region showed no clear trend among seasons; however, the smallest number and area of the lakes were observed in the winter season (Figure 4.17). Lake area in the pre- and post-monsoon seasons of 2016 were very similar at 1.7 ± 0.55 km^2; however, the largest number and area of the lakes were observed in the pre-monsoon season of 2018. Trend of supraglacial lake

among different glaciers varies specially for the pre- and post-monsoon seasons (Figure 4.18). The greatest variability was observed on the Ngozompa Glacier, which displayed the largest area in the pre-monsoon season of 2018 and the least area during the winter season of 2016.

4.7.7 UAV mapping

4.7.7.1 Topographic map of spillway lakes on the Ngozompa Glacier

Surface morphologies around the spillway lake and associated lakes on the Ngozompa Glacier was analyzed with topographic map (Figure 4.19a) and orthomosaic (Figure 4.19b) generated using the UAV photographs. Topographic map displayed the heterogeneous surface of the debris-covered glacier with several surpaglacial lakes. The main spillway lake was interconnected with lakes of different size, and had mean elevation of 4,666 m. The lateral moraines of the glacier were high-elevated area with an elevation up to 4,755 m, which had very steep slope. Elevations surrounding the complex of spillway lake were ranged from 4,670 to 4,680 m in 2010 and from 4,660 to 4,670 in 2018, indicating the surface-lowering of the glacier and lakes.

The difference between roughness of the lakes and their surrounding was clearly identifiable from the topographic and 3D model. Lake boundaries were delineated manually using the orthomosaic and topographic maps and assumed to be highly accurate. Overall, 126 lakes covering an area of 0.33 km^2 were mapped at the terminus of the glacier. A complex of the spillway lakes constitutes a single lake of 0.24 km^2 in size and the rest of the lakes comprised the area of 0.09 km^2. A complex of the spillway lakes enclosed with the ice cliffs and ridges of the debris-covered ice with localized depressions.

4.7.7.2 Changes in glacier and lake morphology

DEM of 2018 was resampled to 8 m, a spatial resolution of the HMA DEM of 2010 to produce an elevation change map (Figure 4.20). The elevation change map for the survey area was produced by subtracting the DEM of 2010 from 2018. Positive values in the map represent the increase in the elevations, and negative values indicate the decrease in the elevations. The values for elevation change was presented in seven classes to display the different intensity of change in elevations. Figure 4.20 clearly showed the substantial decrease in elevation of the glaciers and lakes area between 2010 and 2018. The classes with the most dominant surface-lowering were -5 to -10 m (39%), 0 to -5 m

(27%), -10 to -25 m (19%), while classes with very small surface-lowering were -15 to -20 m (6%) and -20 to -36 m (1%). The range of the surface-lowering from 0 to -15 m accounts for 85%. Extensive surface-lowering e.g. as large as -36 m within the nine years was close to the center of the largest lake. Increase in the elevations also observed close to the lateral moraines and also on the surface of the glacier, which indicates the deposition of debris materials from the moraines to fill the depression from the ridges. The range of increase in elevation from +5 to 0 m (7%) and +12 to +5 m (1%).

Cross-sectional profiles across the glacier and longitudinal profiles along the glacier surface (Figure 4.21) were evaluated to understand the fluctuations of the glacier surface between 2010 and 2018. The longitudinal profile (L-L′) revealed the surface-lowering along the glacier from the near end moraine to the upstream of the glacier. The maximum surface-lowering (~-36 m) occurred near the largest spillway lake. Lower stream of the glacier down to spillway lake also presented the significant surface-lowering (~-9 m in average) along the profile, while couple of points showed the increased elevation. Cross-sectional profile (A-A′) was below the main lake, and was assumed to be located in the dead-ice zone. This profile displayed the melting of the ice within nine years. Lower elevation at the beginning of the profiles indicated the lateral moraine transected by active outlet channel, while the end of profile also claimed the presence of the low-elevated left moraine. Lateral moraines of the height >75 m above the cross-sectional profile B-B′ indicated the surface-lowering of the glacier probably since the Little Ice Age. Profiles B–B′, C–C′, D–D′ revealed the lowering at the location, where lake was already developed in 2010. This indicated the presence of ice underneath of the water. Lowering of the glacier surface occurred spatially, and no clear trend toward upward was obtained. However, moderate lowering of the surface could be observed between the lower narrow part of the glacier and the largest spillway lake. Lowered elevation of up to ~-5 to -6 m within nine years was noticed near the outlet of the river, while change was much larger close to the lake area (as large as of -36 m). The maximum elevation difference between the lake level and top of the ridge surrounded by the lake was ~24 m, while the majority of the area was with less than 10 m higher than the lake level.

4.8 Summary

In this chapter, long and short-term development of supraglacial lakes was examined at the surface of the 23 debris-covered glaciers in the Everest region. All the lakes were mapped using the area threshold of 5,000 m^2 from 1989 to 2017. Continuous

increase in the number and area was observed with minor fluctuations in the study period. The total number of lakes in 1989 was 25, which increased to 85 in 2017. Similarly, the area of the lakes increased by 350% from 0.38 ± 0.19 km^2 in 1989 to 1.32 ± 0.73 km^2 in 2017. Supraglacial lakes were observed on nine glaciers in 1989, which increased to 16 glaciers in 2017. The number and area of the lakes also varied among the glaciers. The largest number and area were found on the Ngozompa Glacier, the largest glacier in the study region, which revealed 32% of the total supraglacial lake area in 2017. The three largest glaciers namely; Ngozompa, Bhote Koshi, and Khumbu glaciers exhibited a 67% of the total lake area in 2017. Reduction in area and number of lakes within the study period indicated the draining of the lakes. Seasonal fluctuations in area and number of the lakes obtained from a seasonal study also proved the existence of seasonal and inter-annual dynamics of the lakes in the study region.

A complex of lakes near the terminus of the glaciers were studied to understand their trajectory towards large glacial lakes, which were observed at eight glaciers, i.e., Thyanbo, Chhule, Melung, Bhote Koshi, Lumsamba, Ngozompa, Khumbu, and Nuptse glaciers. The Ngozompa, Khumbu, Bhote Koshi, Lumsamba, and Chhule glaciers comprised the spillway lakes with size >50,000 m^2 and volume ranges from 0.55×10^6 m^3 on the Lumsamba and Chhule glaciers to 4.1×10^6 m^3 on the Ngozompa Glacier. Similarly, results of the frequency maps of the supraglacial lake revealed the persistent lake near the termini of the glaciers rather than the lakes at the upstream of the glaciers.

The morphological study on the spillway lake of the Ngozompa Glacier showed the remarkable surface-lowering (up to ~-36 m) within and surrounding the lake area. It suggested the lowering the level and the melt of the ice underneath the lake. The surface-lowering was lower near the outlet of the river than the within and near lake area.

Figure 4.1 Examples of the sizes, shapes, and colours of the supraglacial lakes on the Ngozompa Glacier.

Table 4.1 Summary of remote sensing studies of supraglacial water storage excluding studies in Imja Lake in the Everest region (modified after Watson et al. 2016).

Reference	Data range	Coverage overlap with this study	Imagery (resolution)	Notes
(Iwata et al., 2000)	1978-1995	Khumbu Glacier	SPOT (not specified)	A sketch map made with SPOT imagery was compared to that of a field survey in 1978.
(Wessels et al., 2002)	2000	Ngozompa, Khumbu Glacier	ASTER (15 m)	Band ratios were used to delineate water bodies.
(Bolch et al., 2008b)	1962-2005	Khumbu, Lhotse and Imja glaciers	CORONA, Landsat, IKNOS, topographic maps, ASTER (2-79 m)	*NDWI* and/or manual delineation was used to classify water bodies.
(Gardelle et al., 2011)	1990-2009	All glaciers	Landsat (30 m)	A decision tree was used to classify lakes >3,600 m^2 incorporating the *NDWI*.
(Salerno et al., 2012)	2008	All glaciers	AVNIR-2 (10 m)	Water bodies were manually digitized.
(Thompson et al., 2012)	1984-2010	Ngozompa Glacier	Aerial photographs (<1 m), ASTER (15 m)	Expansion of spillway lake was conducted.
(Nie et al., 2013)	1990-2010	All glaciers	Landsat (30 m)	OBIA and *NDWI* based water detection.
(Zhang et al., 2015)	1990-2010	All glaciers	Landsat (30 m)	Lakes >2,700 m^2 were manually digitized.
(Watson et al., 2016)	2000-2015	Seven glaciers	WorldView, Google Earth	OBIA based delineation of water bodies.
(Shrestha et al., 2017)	1977-2010	All glaciers	Landsat (30 m)	Lakes >3,000 m^2 were mapped using *NDWI*.
(Khadka et al., 2018)	1977-2017	All glaciers	Landsat (30 m)	*NDWI* and manual correction to map the water bodies.

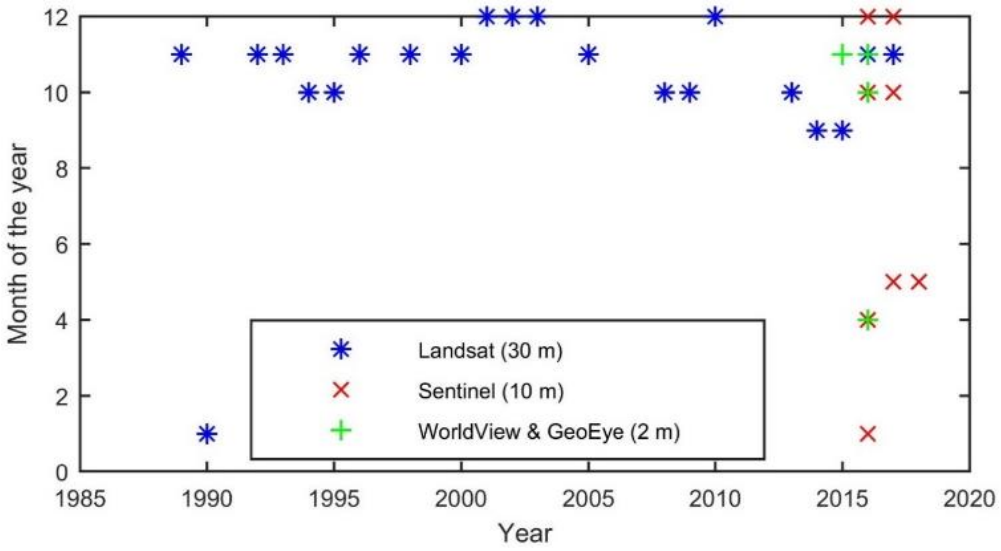

Figure 4.2 Temporal and seasonal distributions of scenes used in the study. Blue marks are for Landsat, red marks are for Sentinel-2, and green marks for WorldView and GeoEye scenes used for the high-resolution inventory of the glacial lakes.

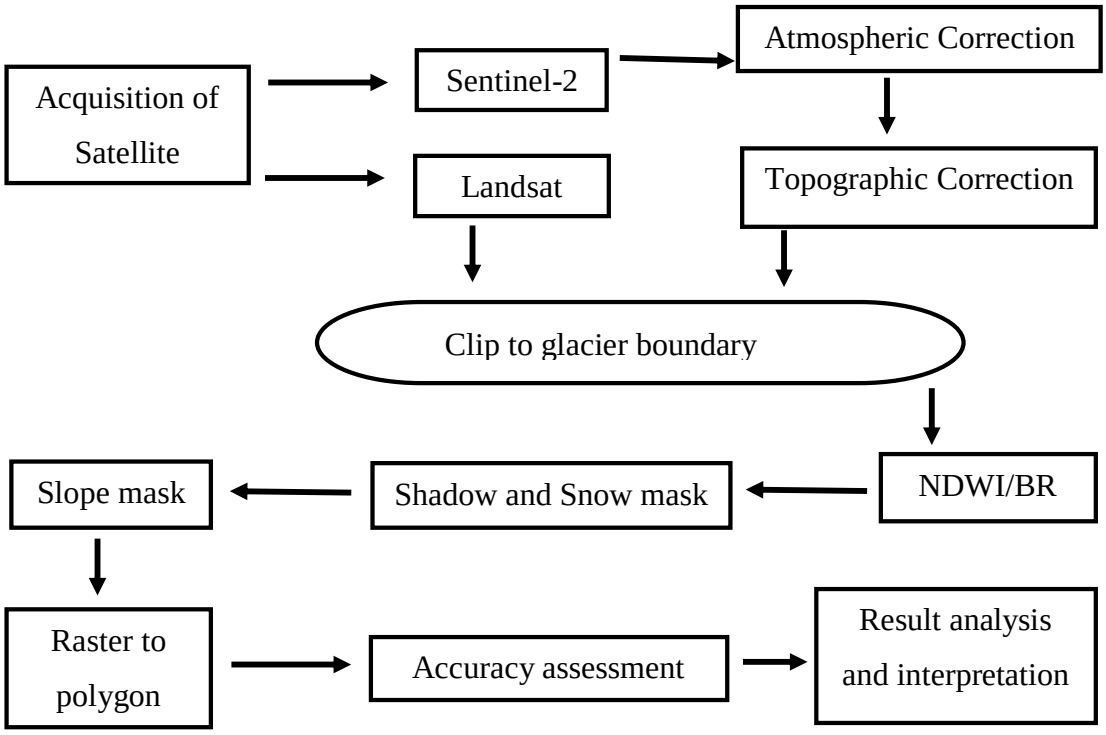

Figure 4.3 Processing workflow for the supraglacial lake classification.

Table 4.2 List of Landsat images used for long-term development of supraglacial lakes.

SN	Image	Date
1	LT05_L1TP_140041_19891109_20170201_01_T1	11/9/1989
2	LT05_L1TP_140041_19900112_20170201_01_T1	1/12/1990
3	LT05_L1TP_140041_19921101_20170121_01_T1	11/1/1992
4	LT05_L1TP_140041_19931120_20170116_01_T1	11/20/1993
5	LT05_L1TP_140041_19941022_20170111_01_T1	10/22/1994
6	LT05_L1TP_140041_19951009_20170106_01_T1	10/9/1995
7	LT05_L1TP_140041_19961128_20170101_01_T1	11/28/1996
8	LT05_L1TP_140041_19981102_20161220_01_T1	11/2/1998
9	LT05_L1TP_140041_20001107_20161213_01_T1	11/7/2000
10	LE07_L1TP_140041_20011220_20170201_01_T1	12/20/2001
11	LE07_L1TP_140041_20021223_20170128_01_T1	12/23/2002
12	LT05_L1TP_140041_20031218_20161203_01_T1	12/18/2003
13	LT05_L1TP_140041_20041204_20161129_01_T1	12/4/2004
14	LT05_L1TP_140041_20051105_20161123_01_T1	11/5/2005
15	LT05_L1TP_140041_20081012_20161029_01_T1	10/12/2008
16	LT05_L1TP_140041_20091015_20161019_01_T1	10/15/2009
17	LT05_L1TP_140041_20101205_20161011_01_T1	12/5/2010
18	LC08_L1TP_140041_20131010_20170429_01_T1	10/10/2013
19	LC08_L1TP_140041_20140927_20170419_01_T1	9/27/2014
20	LC08_L1TP_140041_20141114_20170417_01_T1	11/14/2014
21	LC08_L1TP_140041_20150930_20170403_01_T1	9/30/2015
22	LC08_L1TP_140041_20161103_20170318_01_T1	11/3/2016
23	LC08_L1TP_140041_20171021_20171106_01_T1	10/21/2017

Table 4.3 List of Sentinel-2 Images (Level 1c product).

SN	Image	Date
1	S2A_MSIL1C_20160114T045142_N0201_R076_T45RVM_20160114T045802	01/14/2016
2	S2A_MSIL1C_20160114T045142_N0201_R076_T45RVL_20160114T045802	01/14/2016
3	S2A_MSIL1C_20160413T044642_N0201_R076_T45RVM_20160413T045850	04/14/2016
4	S2A_MSIL1C_20160413T044642_N0201_R076_T45RVL_20160413T045850	04/14/2016
5	S2A_MSIL1C_20161030T044922_N0204_R076_T45RVM_20161030T045514	10/30/2016
6	S2A_MSIL1C_20161030T044922_N0204_R076_T45RVL_20161030T045514	10/30/2016
7	S2A_MSIL1C_20161209T045202_N0204_R076_T45RVM_20161209T04560	12/09/2016
8	S2A_MSIL1C_20161209T045202_N0204_R076_T45RVL_20161209T045602	12/09/2016
9	S2A_MSIL1C_20170508T044701_N0205_R076_T45RVM_20170508T045856	05/08/2017
10	S2A_MSIL1C_20170508T044701_N0205_R076_T45RVL_20170508T045856	05/08/2017
11	S2A_MSIL1C_20171015T044751_N0205_R076_T45RVM_20171015T045632	10/15/2017
12	S2A_MSIL1C_20171015T044751_N0205_R076_T45RVL_20171015T045632	10/15/2017
13	S2B_MSIL1C_20171209T045149_N0206_R076_T45RVM_20171209T082401	12/09/2017
14	S2B_MSIL1C_20171209T045149_N0206_R076_T45RVL_20171209T082401	12/09/2017
15	S2B_MSIL1C_20180508T044659_N0206_R076_T45RVM_20180508T083014	05/08/2018
16	S2B_MSIL1C_20180508T044659_N0206_R076_T45RVL_20180508T083014	05/08/2018
17	S2A_MSIL1C_20180513T044701_N0206_R076_T45RVM_20180513T075139	05/13/2018
18	S2A_MSIL1C_20180513T044701_N0206_R076_T45RVL_20180513T075139	05/13/2018

Figure 4.4 Emild Reach base (left side) and rover (right side) to measure the GCPs on the Ngozompa Glacier.

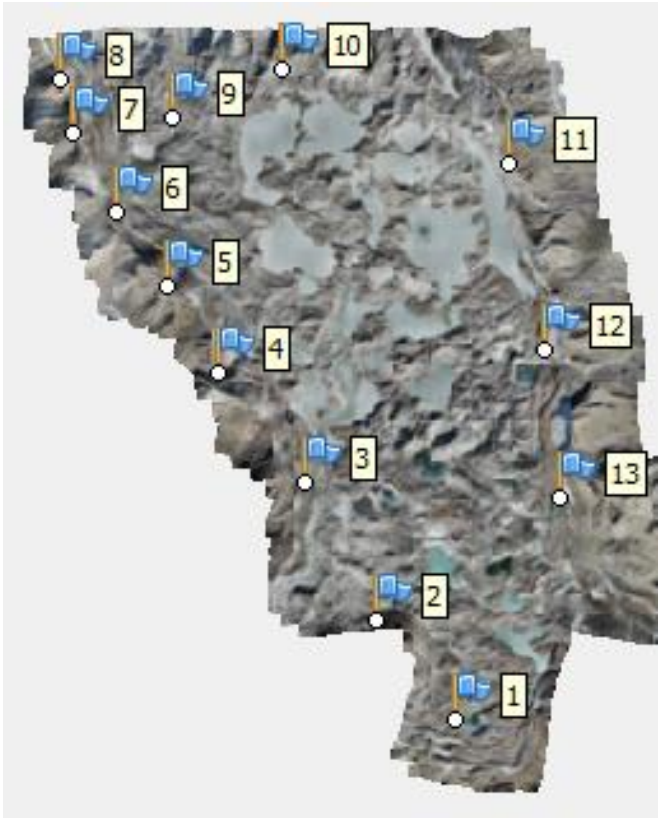

Figure 4.5 Distribution of ground control points over the survey area.

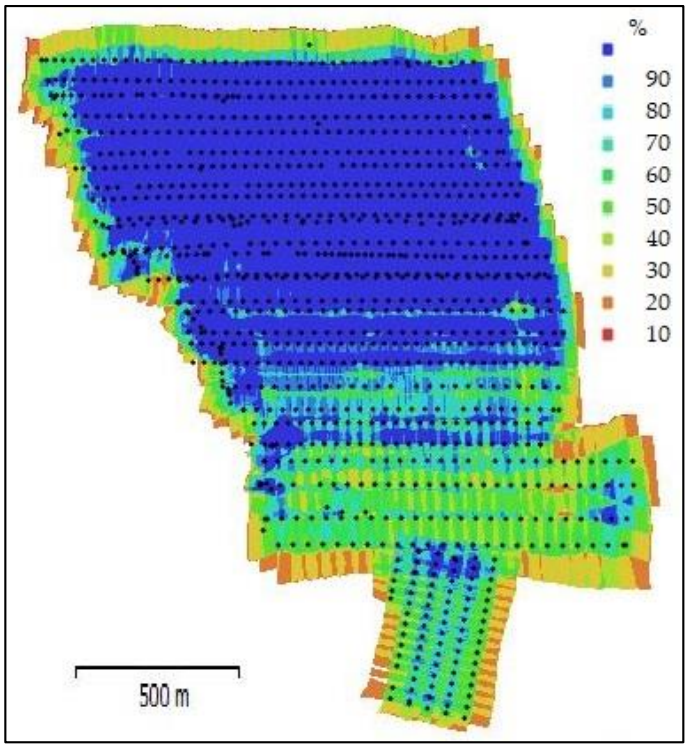

Figure 4.6 Overlapping of the photographs collected from UAV survey on the Ngozompa Glacier.

Table 4.4 Summary of UAV survey and generated models.

Images	1130
GCPs	13
GCPs error (m)	0.08
GCPs error (Pixel)	0.5
Check Points error (cm)	1.06
Check Points error (Pixel)	0.5
Sparse Cloud points	916412
Dense Cloud Points	338288277
Exported Orthomosaic Resolution (cm)	5
Exported DEM Resolution (cm)	10

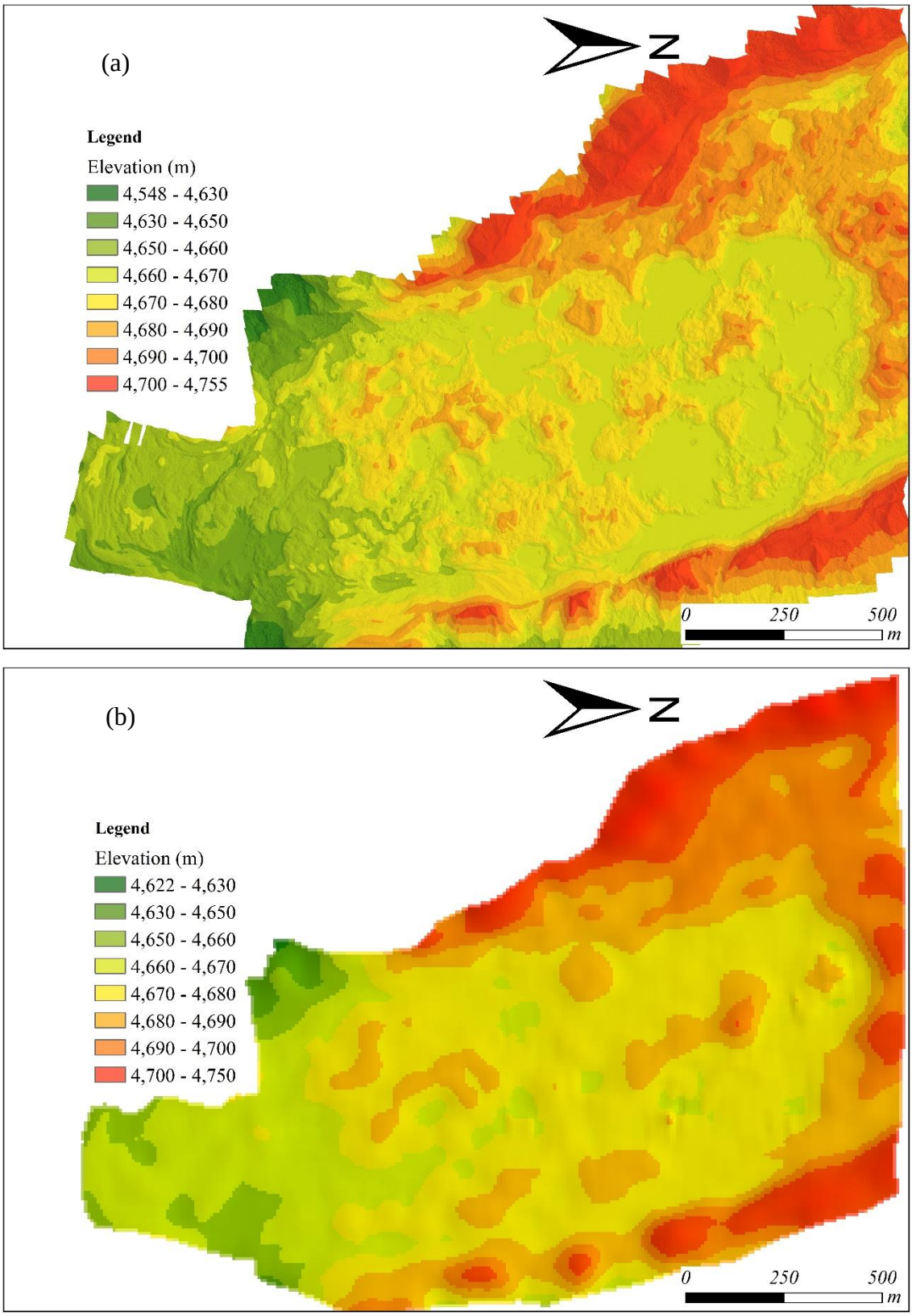

Figure 4.7 Digital Elevation Model (DEM) around the complex of spillway lakes on the Ngozompa Glacier in 2018 generated by UAV photographs (a), and High Mountain Asia DEM for 2010 (b). Elevation values were classified into eight classes in each image. Spillway lakes were distributed at elevation class of 4,660 – 4,670 m in 2018 image.

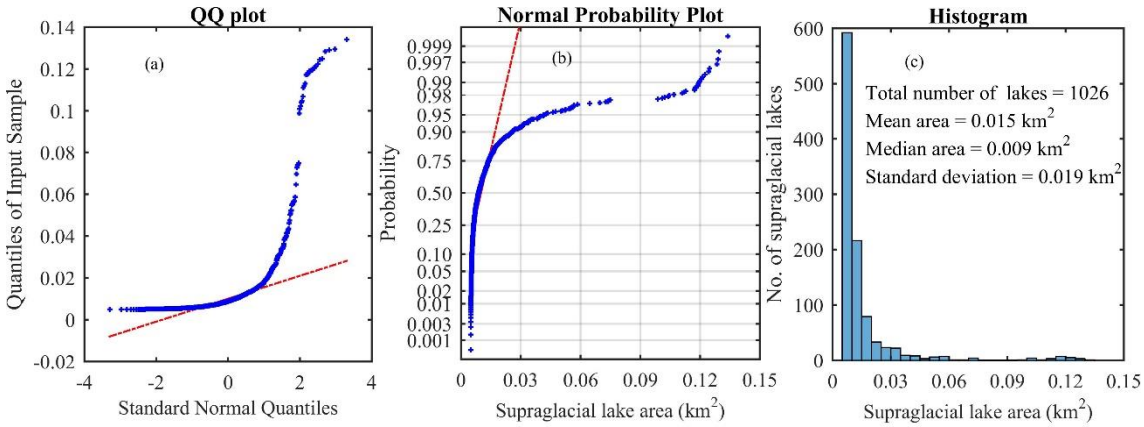

Figure 4.8 Distribution of lake areas (1989 – 2017) in the Everest region with (a) normal Q-Q plot of lake area, (b) normal probability plot of lake area, and (c) frequency distribution of lakes.

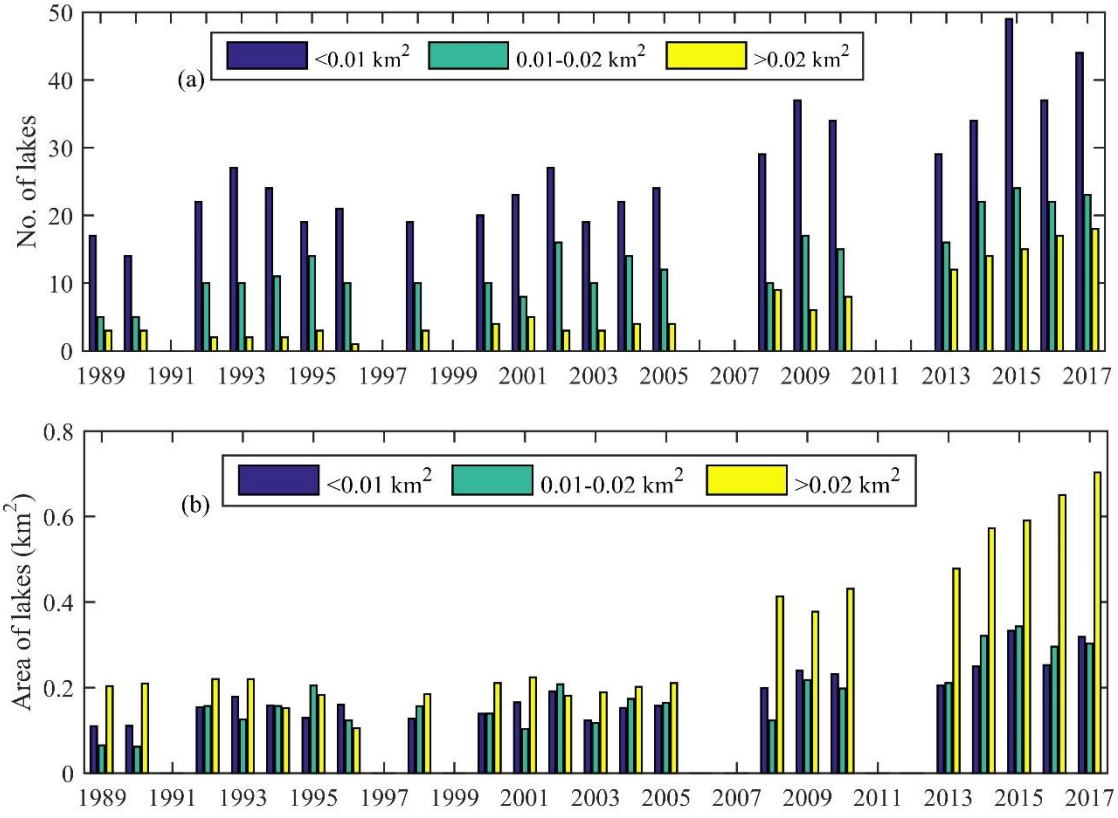

Figure 4.9 Long-term development of the supraglacial lakes in the Everest region from 1989 – 2017 with changes in number (a) and area (b) for three-dimensional classes.

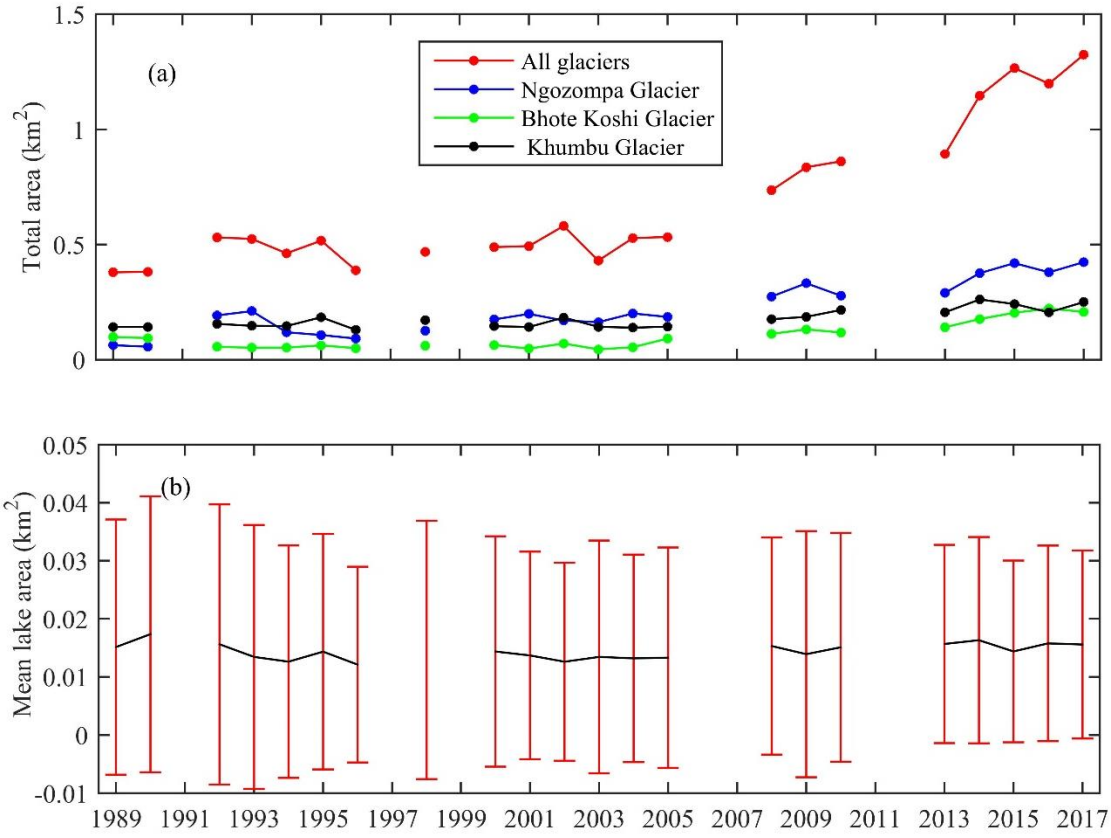

Figure 4.10 Long-term development of the supraglacial lakes in the Everest region from 1989 – 2017 with total lake area for all study glaciers and three selected glaciers, i.e., Ngozompa, Bhote Koshi, and Khumbu glaciers (a), and variation in the mean area of the lakes during the study period (b).

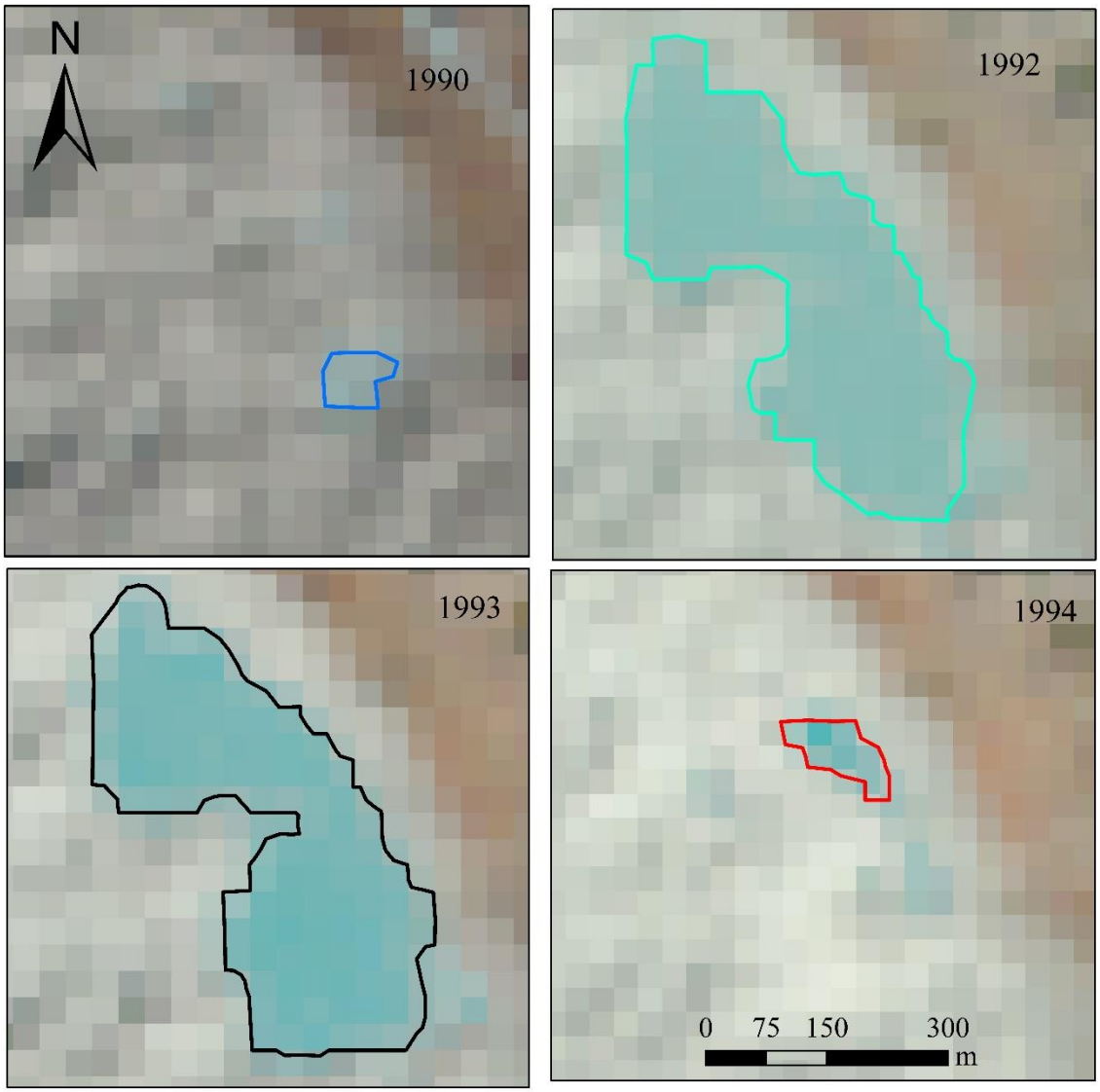

Figure 4.11 Example of the lake emergence, growth, persistence, and drain of the lake on the Ngozompa Glacier during the period between 1990 and 1994.

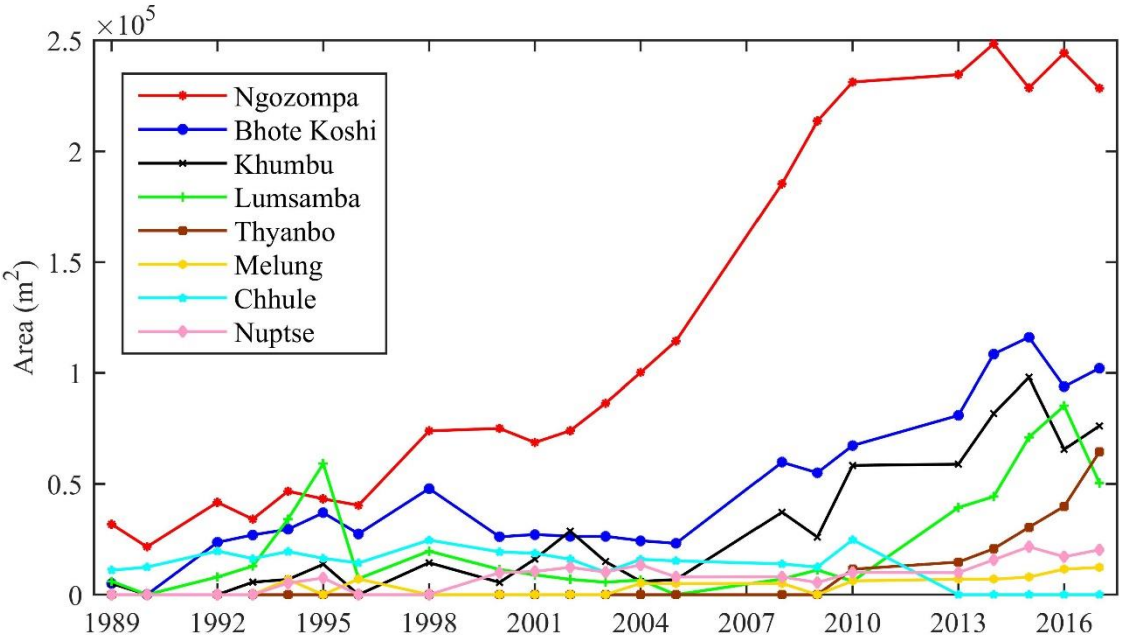

Figure 4.12 Spillway lake development in the Everest region from 1989 to 2017.

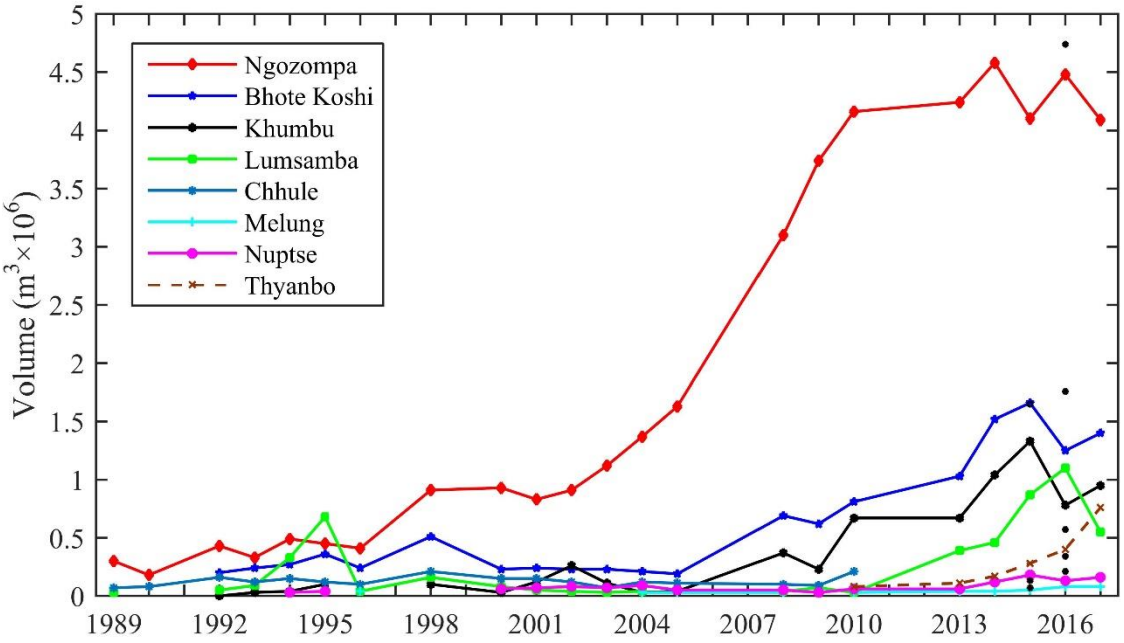

Figure 4.13 Volume change of the complex spillway lakes at the terminus of the eight glaciers from 1989 to 2017. The volume of the spillway lakes calculated based on the WorldView lake area of 2015 and 2016 is presented with black rounded shape.

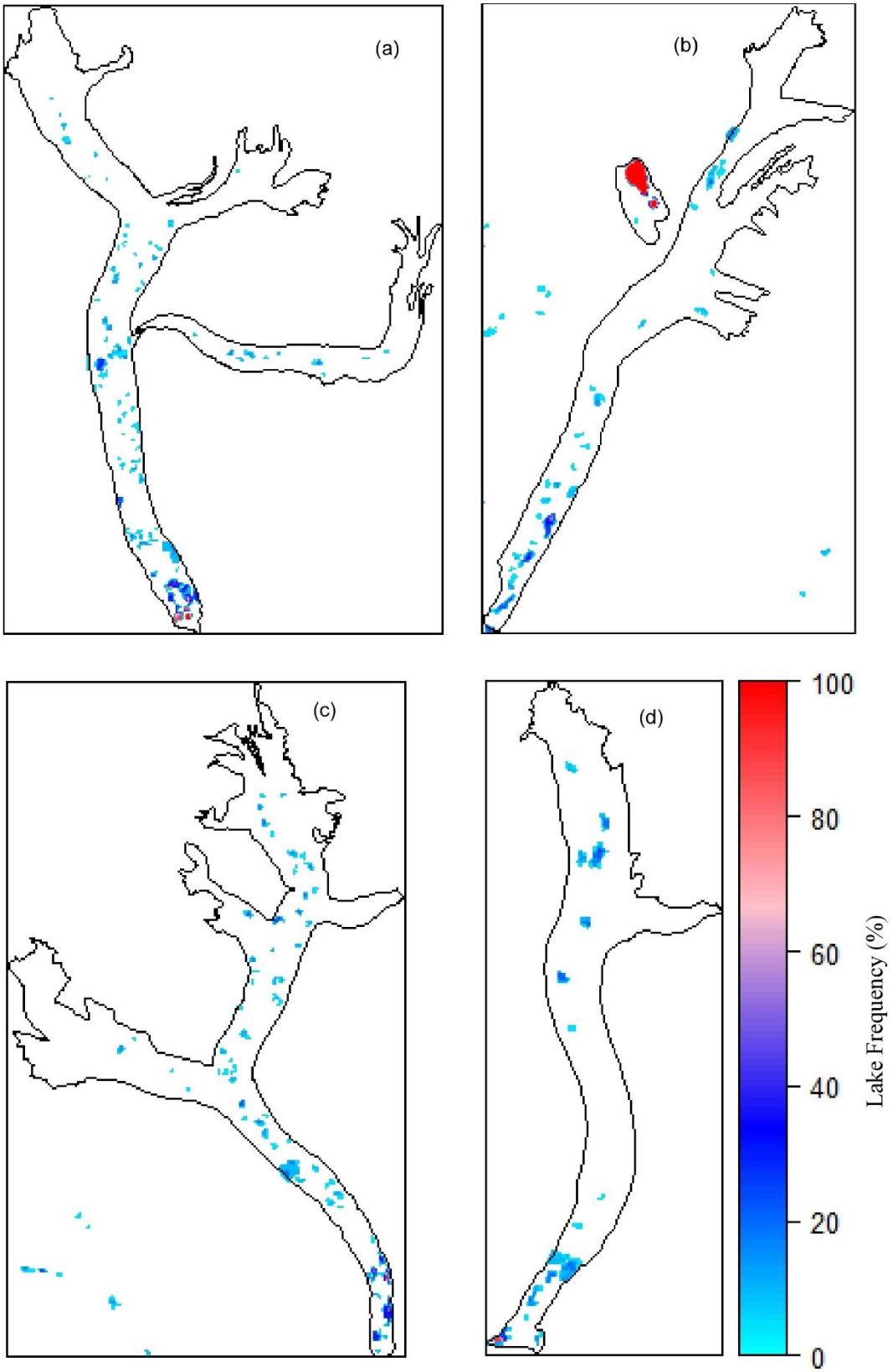

Figure 4.14 Distribution of supraglacial lakes and their frequency on the Ngozompa (a), Khumbu (b), Bhote Koshi (c), and Lumsamba (d) glaciers during the whole period from 1989 to 2017, highlighting the persistence of individual lakes.

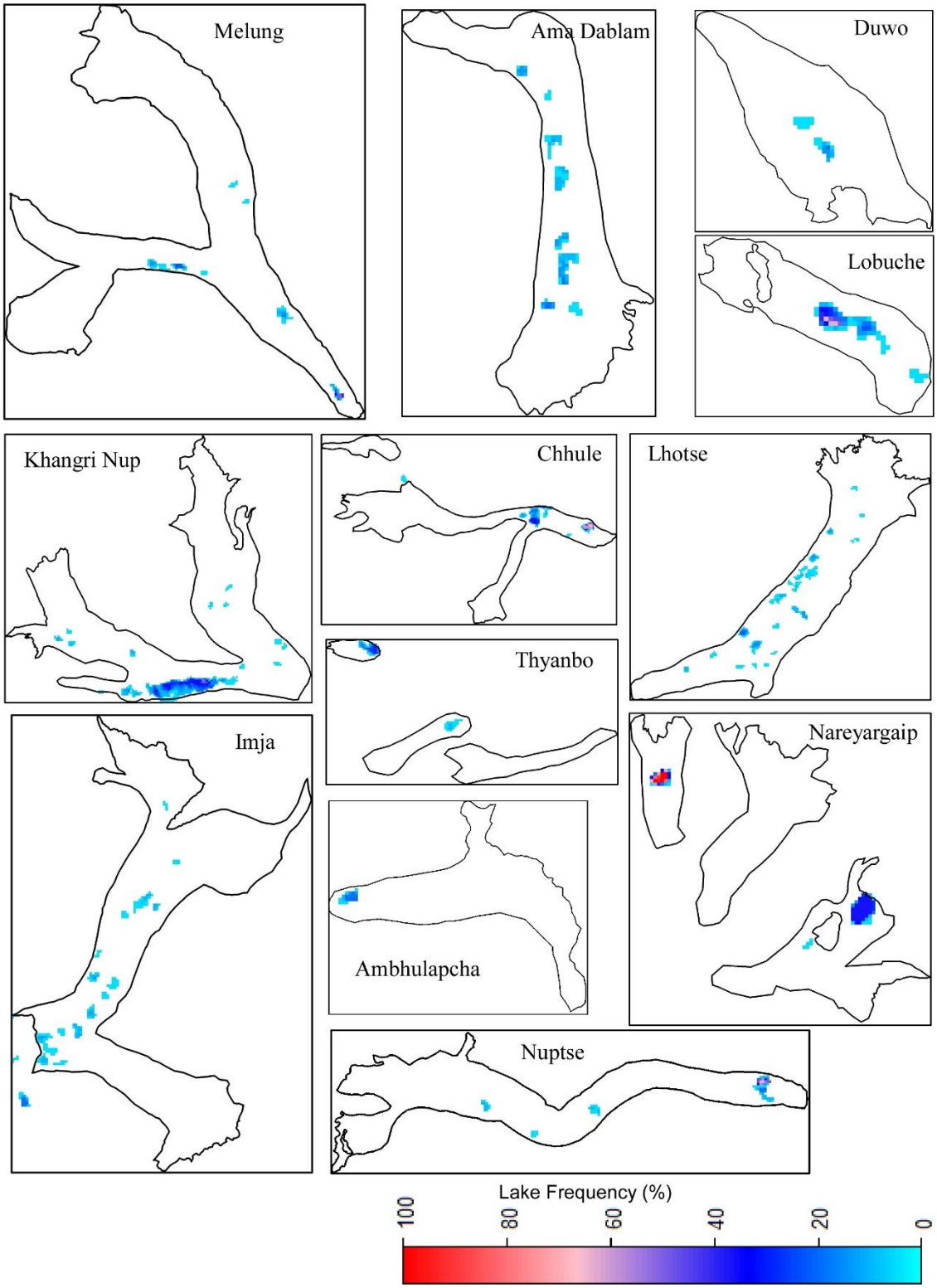

Figure 4.15 Distribution of supraglacial lakes and their frequency on the Melung, Ama Dablam, Duwo, Louche, Khangri Nup, Chhule, Thyanbo, Lhotse, Imja, Ambulapcha, Nareyargaip, and Nuptse glaciers during the period from 1989 to 2017, highlighting the persistency of individual lakes.

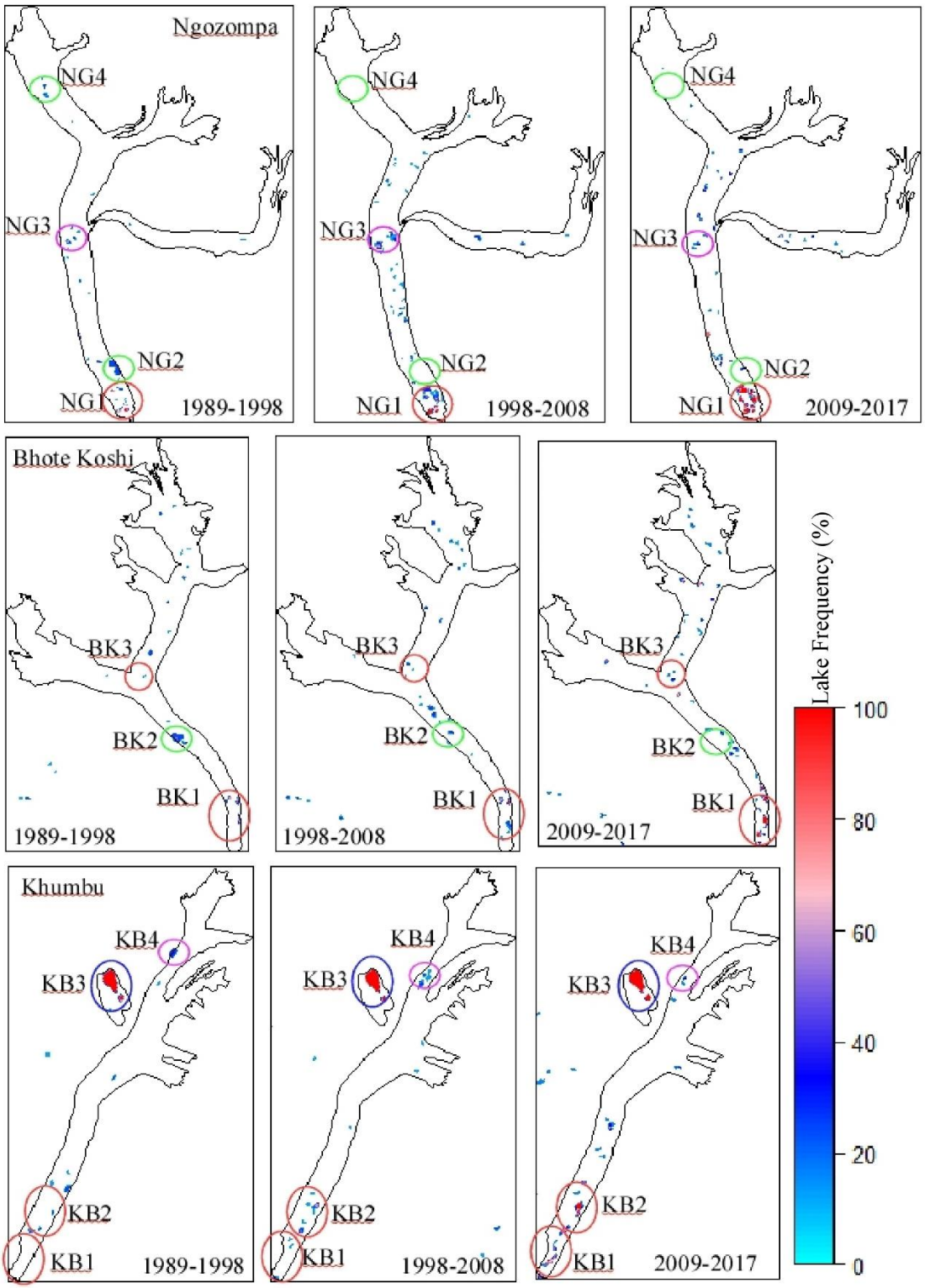

Figure 4.16 Distribution of supraglacial lakes and changes in their frequency in the three different periods, 1989 – 1998, 1999 – 2008, and 2009 – 2017 on the Ngozompa, Bhote Koshi, and Khumbu glaciers, highlighting the differences in persistency of lakes between two periods.

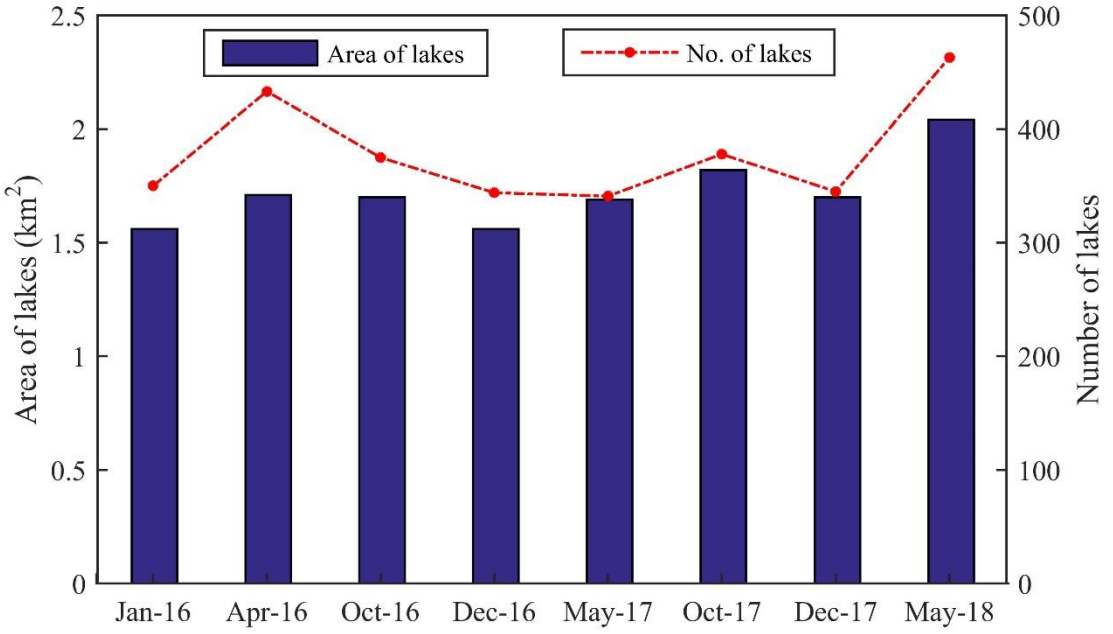

Figure 4.17 Seasonal change in the number and area of the supraglacial lakes (>500 m^2) between January 2016 and May 2018 obtained from Sentinel-2 images of 10-m resolution.

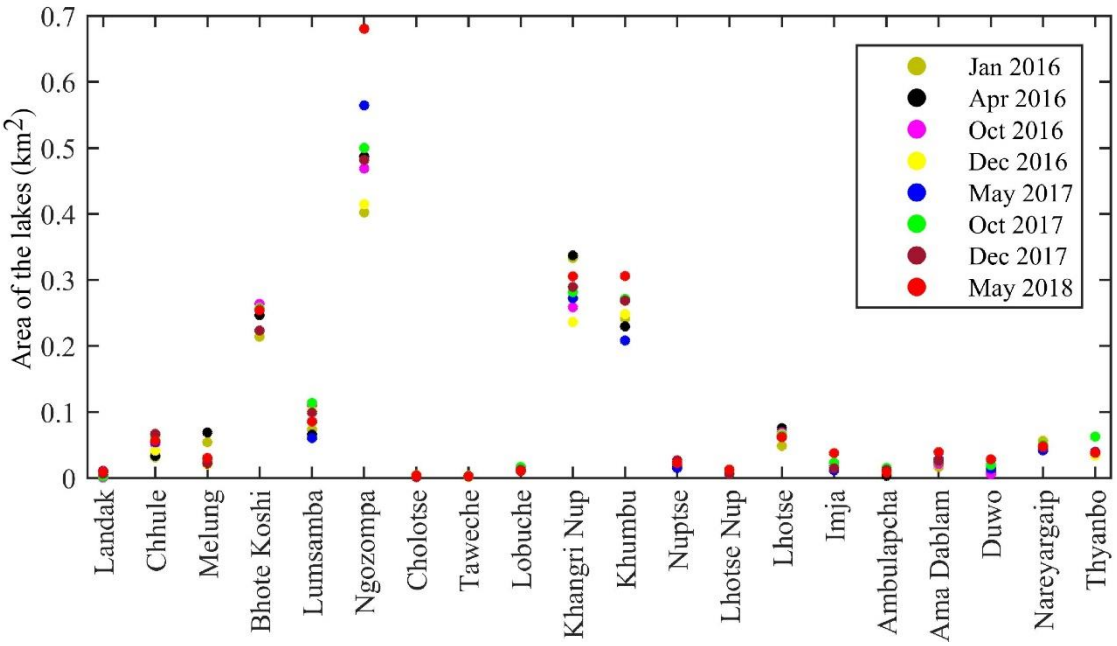

Figure 4.18 Seasonal variability of supraglacial lake area among 20 glaciers in the Everest region, where at least one lake was observed in one time.

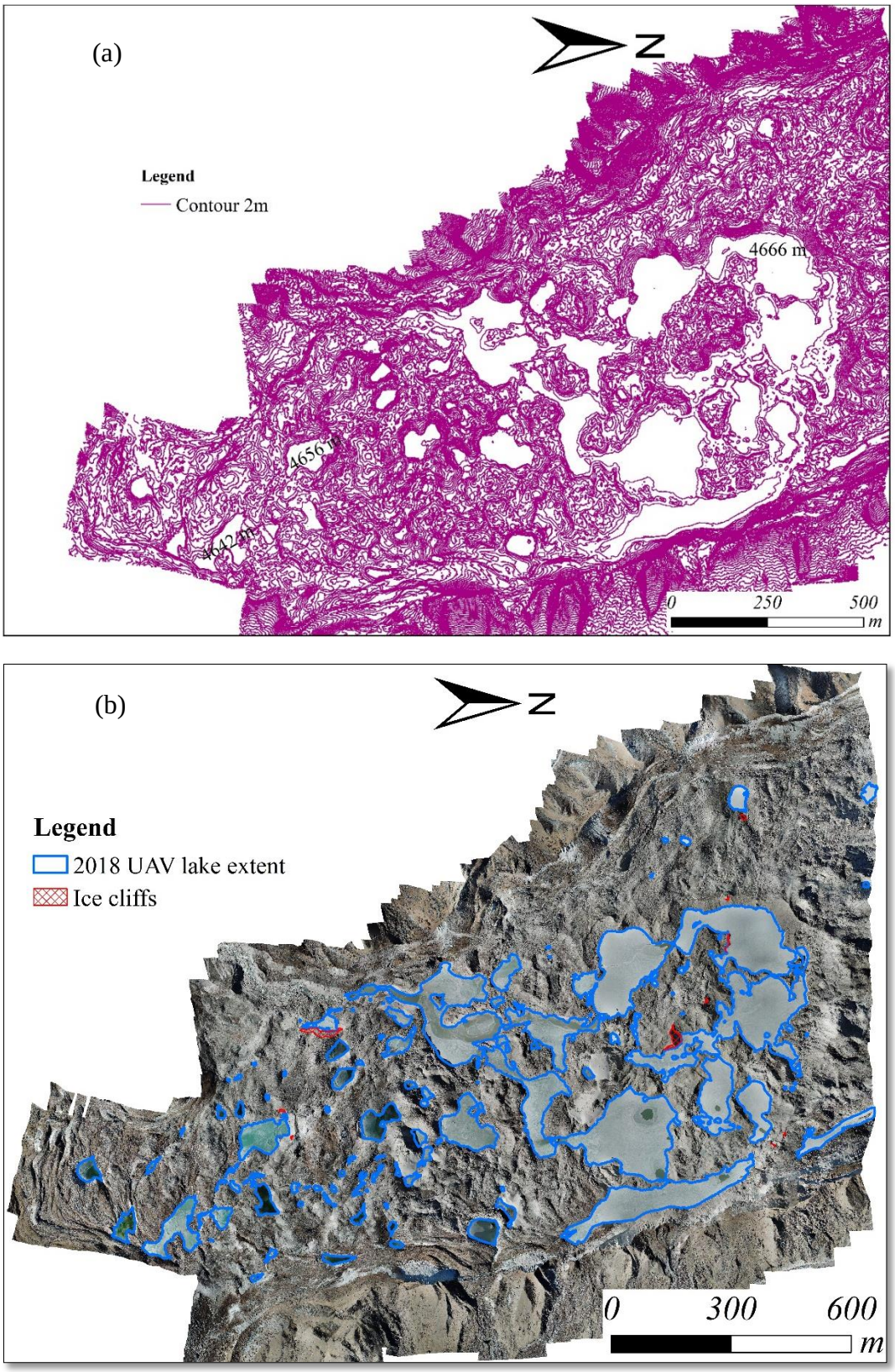

Figure 4.19 Topographic map around the complex of spillway lakes of the Ngozompa Glacier (a), and orthomosaic of the image showing the extent of the complex spillway lakes (b) generated by UAV photographs taken in December 2018.

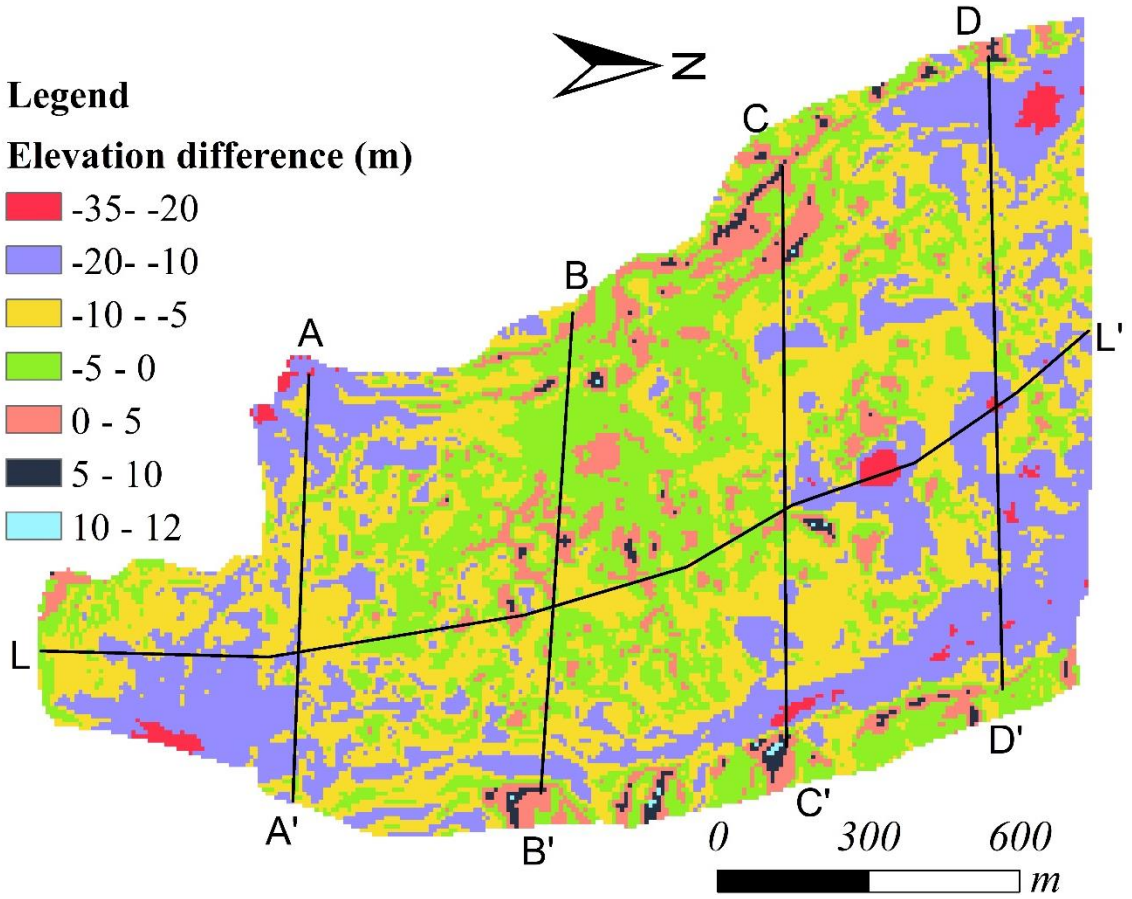

Figure 4.20 Elevation changes of the surface around the complex of spillway lakes on the Ngozompa Glacier between 2010 DEM and 2018 DEM. Cross sections (A–A′, B–B′, C–C′, D–D′, and L–L′) were used for comparing the elevation change between 2010 and 2018 DEM, which are shown in Figure 4.21.

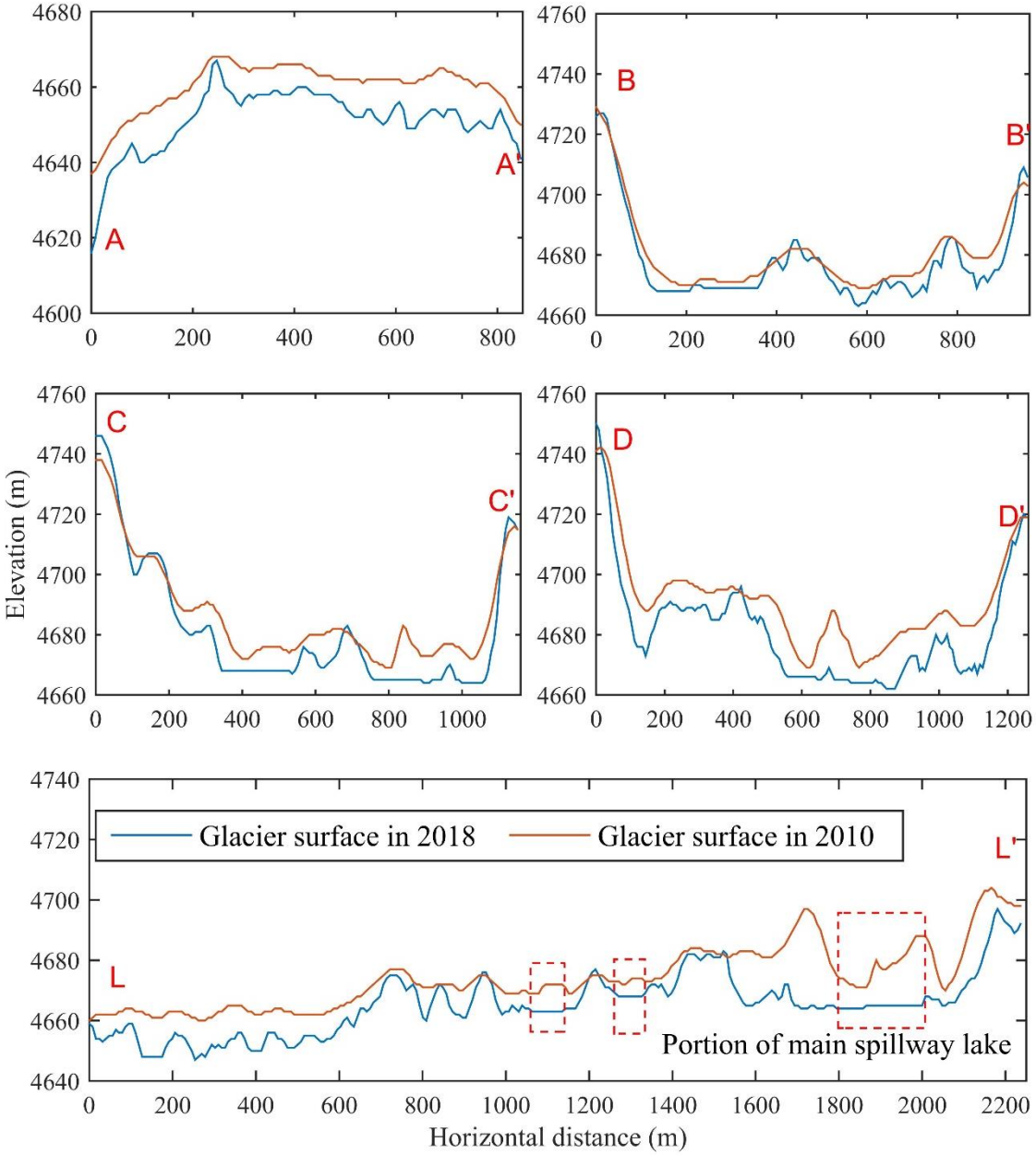

Figure 4.21 Cross sectional profiles (A–A′, B–B′, C–C′, and D–D′), and longitudinal profile (L–L′) showing glacier topographies in 2010 and 2018.

5. Development of glacial lakes in the Kangchenjunga region between 1964 and 2018

5.1 Introduction

5.1.1 Glacial lakes of the Kangchenjunga region

Past studies of glacial lakes were focused in the Everest region (Bajracharya et al., 2007; Bolch et al., 2008b; Salerno et al., 2012; Somos-Valenzuela et al., 2014b; Lamsal et al., 2016; Rounce et al., 2016a; Watanabe et al., 2016; Miles et al., 2018). Regional and nationwide studies have been documented (Gardelle et al., 2011; Nie et al., 2013, 2017; Khadka et al., 2018) to study the glacial lakes and their expansion. Similarly, study of glacial lake development for the Koshi river basin was also studied using 30-m spatial resolution Landsat images (Shrestha et al., 2017). However, a study specific to the Kangchenjunga region is missing, except a study carried out in the Nangama GLOF (Watanabe, 1998). In this chapter, the Kangchenjunga region of the Tamor River basin was chosen to study the decadal analysis of the glacial lakes from 1964 to 2018 based on multi-sensor satellite imageries. Glacial lakes were studied using CORONA, Landsat and Sentinel-2 images. These satellite images are of different spatial resolution from 2.74 m to 60 m. This chapter also aimed to trace and document past GLOFs before the 1980s using CORONA images, which have not reported before.

Shrestha et al. (2017) identified 269 glacial lakes covering an area of 8.73 km^2 in the Tamor River basin in 2010. They categorized the glacial lakes into bedrock-dammed (121), ice-dammed (38), moraine-dammed (108), and other types (2). Similarly, ICIMOD (2011) reported 209 glacial lakes in the region with an area of 6.57 km^2 by using the Landsat images of 2009. Their results showed the largest number of glacier erosion lakes (117). The number and area of the glacial lakes were decreased from 2001 to 2009. A more recent study in 2017 reported the 253 glacial lakes covering an area of 8.73 km^2 in the whole Tamor River basin (Khadka et al., 2018) (Figure 5.1). They plotted 169 lakes with the surface area of 6.05 km^2 in the Kangchenjunga region, UTR basin. Study of glacial lakes of the Tamor Khola and Yanma Khola sub-basins of UTR basin mapped total of 118 lakes using topographic map, which constituted the non-glacier-fed (62) and glacier-fed (56) lakes (Watanabe et al., 1998). The above statistics for the whole Tamor basin are contrasting to each other, and it is necessary to have an accurate datasets, which

can be achieved with manual method, considered as more precise than the automatic methods (Mergili et al., 2013; Shukla et al., 2018).

Yamada and Sharma (1993) reported the GLOF in Phucan Glacial Lake, which rose the water level of 20 m in the river with heavy debris of big rocks and damaged forest, river bed etc. The damages including deposited and eroded river was traced downstream as low as 3,040 m of elevation, where lake elevation was 4,950 m (Watanabe et al., 1998). The flood damaged the Lunthun, Siwa, and Dobhan settlements, where elevation of Dobhan was ~640 m, which was 71 km downstream from the glacial lake. Phucan Lake is known as Nangama Pokhari on the topographic map, and considered as potentially hazardous with medium priority lake (ICIMOD, 2011). Similarly, they categorized the lakes with GL code kotam_gl_0193 and kotam_gl_0111 as low priority potentially dangerous lakes in the Kangchenjunga region.

5.1.2 Glaciers of the Kangchenjunga region

Bajracharya et al. (2014) mapped the 262 glaciers that cover an area of 385.9 km^2 in the Tamor basin in 2010 (Figure 5.1). The inventory classified the 29 glaciers as debris-covered glaciers with an area of 71.2 km^2 in the basin, one of the basins with the greatest number of debris-covered glaciers. The UTR basin at Lelep, a study area for this chapter, comprised 253 glaciers covering an area of 383.7 km^2, 99% of total glacier area in the whole Tamor basin (Bajracharya et al., 2014). The number of glaciers with size <5 km^2 was 241, while 12 largest glaciers accounted for the 65% of the total glacier area. Similarly, glaciers with size >1 km^2 were 53, which account for the 86% of the total glacier area. The debris-covered part of the glaciers are with gentle slope (<15°) in comparison to clean type glaciers, which are mainly valley glaciers. The valley glaciers in the basin contributed about 68% of the total glacierized area. The mean minimum elevation of the debris-covered glaciers was ~500 m lower than the minimum elevation of clean type glaciers in the Tamor basin. The glaciers of the Tamor basin had the most concentrated altitudinal belt (8,400-8,500 m a.s.l.) among the glacierized sub-basins of the Nepal (Bajracharya et al., 2014; Ojha et al., 2016).

A high-resolution (<10 m) inventory using ALOS images from 2006 to 2010 revealed the 363 glaciers with the total area of 431.6 km^2 in the Tamor basin (Ojha et al., 2016). They categorized 80 glaciers as debris-covered glaciers in the region, and reported the disappearance of the glaciers since 1992. Glaciers of the Kangchenjunga region are retreating (Asahi and Watanabe, 2000; König, 2004; Bajracharya et al., 2014;

Racoviteanu et al., 2015; Ojha et al., 2016), which possess a negative mass balance of -0.18 ± 0.17 m w.e a^{-1} between 1975 and 2010 period in the Kangchenjunga Glacier of this region (Lamsal et al., 2017).

5.2 Datasets

In this study, declassified CORONA, Landsat, Sentinel-2A and 2B were used to map the glacial lakes and historical GLOFs in the Kangchenjunga region. Additionally, ALOS PALSAR DEM were also used as supplementary images to prepare the topographic map. The details of the images used for this purpose are described in the following sections.

5.2.1 Declassified CORONA

In this study, scanned photographs of CORONA were downloaded from the U.S. Geological Survey (USGS) (https://earthexplorer.usgs.gov). The CORONA systems were designated KH-1, KH-2, KH-3, KH-4, KH-4A, and KH-4B, and have spatial resolution from 2.74 m to 12.19 m. In this study, KH-4A images (Table 5.1) with 2.74 m of best ground resolution were used for mapping glacial lakes in 1964. Similarly, CORONA images (KH-4, KH-4A, KH-4B, and KH-9) were utlized for tracing and analyzing past GLOF events from 1962.

5.2.2 Landsat

Landsat images from 1975 to 2010 were used, which were acquired from the U.S. Geological Survey (USGS) (https://earthexplorer.usgs.gov) to map the glacial lakes in the study area (The details were provided in section 2.2.2.1): Landsat Multispectral Scanner (Landsat MSS or Landsat 2) for 1975, Landsat 5 for 1987/88, 2000, and 2009/10 (Table 2.5). The selection of years was based on the availability of cloud and snow free images. The Landsat MSS mission was started in 1972; however, good quality images were not available between 1972 and 1974. Therefore, image from 1975 year was selected to map the glacial lakes. Similarly, images were not available between 1980 and 1986, and image from 1987 was not enough to map all glacial lakes; therefore, glacial lakes were mapped using images from the 1988 to make the complete inventory for this period.

5.2.3 Sentinel-2 images

Sentinel-2 images of 10-m resolution were used to prepare the recent inventory of the glacier lakes. Images were acquired from October 2018 to map all the lakes existed in the Kangchenjunga region (Table 5.1).

5.3 Methods

5.3.1 Preprocessing of the CORONA images

The CORONA data for the period of 1962 – 1980 with the spatial resolution of 2.76 m to 10 m in the panchromatic band (Hamandawana et al., 2006) were used in this study. Part of this data archive was freely available to the global community, and utilized for historical glacial lake inventories and tracing the past GLOF events. The CORONA images are single band images without geographic referencing, and geometric correction was required for adequate mapping of the lakes. However, geometric correction is very difficult as CORONA calibration parameters (fiducial coordinates, lens distortion coefficients, and principal point coordinates) are not available (Altmaier and Kany, 2002; Casana and Cothren, 2008; Shahtahmassebi et al., 2017). Here, in this study, image-to-image registration was applied for the geometric corrections. CORONA imageries were registered to an orthorectified Sentinel-2 images of 10-m spatial resolution using clear and stable ground features as GCPs (Shahtahmassebi et al., 2017). Manually selected 10 to 20 points were used for georefrencing and geometric correction. Thereafter, CORONA images were projected to Universal Transverse Mercator (UTM) map coordinates (Zone 45, WGS 1984) of Sentinel-2 images, where second and third-order polynomial transformations were applied. The accuracy of the geometrically corrected images was within acceptable level with horizontal displacement of <10 m. In this study, this horizontal error was considered for mapping glacial lakes because the main purpose was to prepare the inventory of glacial lakes to compare in aggregate but not to work in methodological development. However, spatial adjustment of the images was applied to minimize the horizontal error for preparing growth history of the large sized lakes (>0.1 km^2).

5.3.2 Glacial lake inventory

In this chapter, satellite images from different sensors and different spatial resolution were used to prepare the long-term decadal inventory of the glacial lakes from

1964 to 2018. CORONA images used in this study were of single band, and automatic method using band metrics, i.e., *NDWI*, band ratios could not be applied. Automatic delineation of the glacial lakes caused the significant false classification of the lakes (Watson et al., 2016), and manual editing improve the results significantly (Mergili et al., 2013; Shukla et al., 2018). Therefore, manual delineation of the glacial lakes was carried out to prepare accurate mapping of the glacial lakes. The boundaries of lakes were checked visually within the study area, including all pure pixels of water body and about half of the pixels that surrounded the pure pixels.

All the glacial lakes were mapped with a threshold of 5,000 m^2 for making consistent decadal comparison, while a threshold of 500 m^2 was applied to prepare the newest inventory of glacial lakes for 2018. Separate analyses of all mapped lakes were also considered to discuss the quality of results from different spatial resolution images.

5.3.3 Tracing past GLOFs

Effort for tracing past GLOFs specifically before the 1980s was done to document the historical GLOF events, which were not documented in the past studies. CORONA images (KH-4, KH-4A, KH-4B, and KH-9) (Table 5.1) were exploited to identify the possible GLOFs. Landsat images were also used as supplementary data for the later period (after 1975). Dr. Alton Byers obtained hint of the past GLOFs in the region from social survey in 2019. Images were then manually inspected in each sub-basins of the Kangchenjunga region to identify the past GLOFs. Erosion and deposition caused by the possible GLOF events at the source (outlet channel) and along the river bed were identified by checking different satellite images. End moraines of the glaciers were focused during the visual interpretation. Finally, a list of possible past GLOF events before the 1980s were prepared for the Kangchenjunga region.

5.4 Results

5.4.1 Glacial lake inventory 2018

The analysis of hydrographic network in the basin led to identification of the five sub-basins in the study region. The naming convention of sub-basins was based on the name of the main tributary and named as: Tamor Khola (at Olanchungola) River, Yanma Khola (at Olanchungola) River, Tamor Khola (at Lelep) River, Ghunsa Khola (at Lelep), and Shimbuwa Khola (at Lelep) River basins. The Tamor and Yanma Khola basins were

delineated at the Olanchungola Village, confluence of the Tamor and Yanma Khola and each basins comprised an area of 206 km^2 and 416.9 km^2, respectively (Table 5.2). The Ghunsa Khola basin was the largest (742 km^2) basin, and the Tamor Khola basin (at Lelep) was the smallest basin (150.4 km^2) among the five sub-basins within the UTR basin. The Simbuwa Khola basin was located at left of the Ghunsa basin, and comprised an area of 267.7 km^2.

Glacial lakes within all the basins were mapped, and distribution of glacial lakes in each sub-basins was presented in Table 5.2 and Figures 5.2-5.5. The Tamor Khola (at Lelep) basin lacked glaciers; therefore, map is not shown here. Mapping of the lakes in the Kangchenjunga region delineated the 373 glacial lakes with the total area of 6.18 ± 0.75 km^2 in 2018. Average size of the mapped glacial lakes in the region was 0.016 km^2. The maximum glacial lake size was 0.69 ± 0.02 km^2 (Nangama Lake), which is considered as potentially dangerous lake of moderate priority by ICIMOD (2011). Similarly, lakes with GL codes kotam_gl_0193 and kotam_gl_0111 have an area of 0.18 km^2, and 0.27 km^2, respectively, are categorized as potentially dangerous glacial lakes with low priority (ICIMOD, 2011). Small glacial lakes of <0.01 km^2, predominantly supraglacial and unconnected lakes contributed 73% of the total number of lakes; however, they accounted only 14% of the total area of the lakes (Figure 5.6). Large sized lakes (>0.1 km^2) with total area of 3.45 km^2, contributed to 56% of the total lake area in the Kangchenjunga region.

Out of the total lakes in the Kangchenjunga region, this study identified 138 (0.57 ± 0.17 km^2) lakes as supraglacial lakes, 221 (3.27 ± 0.46 km^2) as unconnected lakes, and 14 (2.34 ± 0.12 km^2) as proglacial lakes (Table 5.2). Further, lakes were categorized based on their source of water, and 284 (4.46 ± 0.54 km^2) categorized as glacier-fed lakes and 89 (1.72 ± 0.21 km^2) as non-glacier-fed lakes. Unconnected glacial lakes comprised 126 glacier erosion lakes (1.52 km^2) and six lateral moraine-dammed lakes (0.03 km^2). Currently glaciers were not observed in the catchment of the non-glacier-fed lakes, and those lakes were fed by snowmelt and rainwater. These high-elevated lakes were spatially distributed over different sub-basins within the UTR basin (Table 5.2 and Figures 5.2-5.5). Overall, the number of the lakes in the Ghunsa basin was the largest (147), while the largest area (2.04 km^2) of the lakes was observed in the Tamor Khola basin (at Olanchungola), accounting for 39% and 33%, respectively of the total lake area. The largest number of lakes in the Ghunsa basin was contributed by the supraglacial lakes

(86), and largest area in the Tamor basin (at Olanchungola) was contributed from unconnected lakes (1.8 km^2).

The glacial lakes in the Kangchenjunga region of the Nepal Himalaya fall into the elevation range of 3,910–5,730 m, with a mean elevation of 4,897 m (Figure 5.7). About 89% of the lakes located above 4,500 m and 39% observed above 5,000 m. A single lake was observed below 4,000 m in the Tamor Khola basin (at Lelep), which was isolated from the glaciers. The mean elevations of lakes in the Tamor Khola River basin (at Lelep) was the lowest (4,441 m), where only non-glacier-fed lakes were observed, while the mean elevation of the lakes was the highest (5,012 m) in the Yanma Khola River basin. Lakes were observed as high as 5,730 m in the Ghunsa basin. The elevations of the glacial lakes corresponded to the distribution of the glaciers and their geometry within the sub-basins.

5.4.2 Decadal dynamics of glacial lakes

Decadal mapping of glacial lakes shows the increase in the number and area of lakes over time (Figure 5.8). The total number of the lakes was 31 in 1964, which was increased by 406% (n=157) in 2018 (Tables 5.3 and 5.4). Similarly, the total surface area of the lakes increased by 230% between 1964 and 2018. The number and area of glacial lakes were drastically increased by 167% and 68%, respectively during 1975 and 1987 because of the large number of emerged unconnected lakes (n=54) and supraglacial lakes (n=15) (Figure 5.9 and Table 5.5). This can be attributed to the use of different spatial resolution images in 1975 (60 m) and in 1987 (30 m). Similarly, the increased area between 1964 and 1975 was relatively high (55%), attributed to rapid expansion of the proglacial lakes during this period (Figure 5.9). The rapid expansion of Nangama Lake in the Yanma Khola basin was observed between 1964 and 1975, where the area increased by 0.49 km^2 and reached 0.74 km^2 in 2018 from 0.25 km^2 in 1964. This lake caused a GLOF in 1980 (Yamada and Sharma, 1993) and almost re-gained the similar size (0.70 km^2) by 1987. Lake with GL ID kotam_gl_0193 (ICIMOD, 2011) in the Shimbuwa Khola basin could not be observed in the CORONA image of 1964 and appeared in 1975 with the size of 0.12 km^2, which was doubled (0.25 km^2) in 1987 and remained almost similar size (0.27 km^2) till 2018. The number of non-glacier-fed lakes increased in the later period (2010 – 2018), where 18 new non-glacier-fed lakes were emerged, which was possibly due to the loss of glacier area in the individual lake basin.

5.4.3 Glacial lake change across different sub-basins

The glacial lakes in the Kangchenjunga region were spatially distributed over different sub-basins and they varied temporally. The number of glacial lakes in the Tamor (at Olanchungola), Yanma, Tamor (at Lelep), Ghunsa, and Shimbuwa Khola basins increased by 3.3, 2.6, 6, 8.3, 2.8, and 4.1 times, respectively (Table 5.4). The largest increase in the number (by 833%) was estimated for the Ghunsa Khola basin, which was highly glacierized and largest sub-basin within the Kangchenjunga region. The largest expansion in the surface area of lakes was observed in the Yanma Khola basin, where area was expanded by 1.6 km^2, accounted for 40% of the total surface area changes from 1964 to 2018. Similarly, the surface area changes in the Ghunsa basin contributed about 27% to the total area increased during 1964 and 2018. The largest increase of the surface area (by 0.63 km^2) occurred during 1964 and 1975 in the Tamor Khola basin, followed by the Yanma Khola basin, where the area expanded by 0.58 km^2 and 0.47 km^2 from 1964 to 1975, and 1975 to 1987, respectively.

5.4.4 Glacial lake changes by various size classes and topology

All mapped glacial lakes were categorized into four different size classes: <0.01 km^2, 0.01-0.02 km^2, 0.02 km^2, and >0.1 km^2. Overall, the number and area of lakes increased among all classes from 1964 to 2018 with variation between the different periods (Figure 5.10). Among different size classes of glacial lakes, small sized glacial lakes (<0.01 km^2) experienced the largest increase, where their number increased by more than 9.2 times in 2018 than in the 1964. For instance, 55 new lakes (<0.01 km^2) were added after 1964. The lakes of size <0.01 km^2 could not be mapped for the year 1975, where low-resolution (60 m) image was used for mapping. The area of small sized lakes found increased by 9.3 times from 1964 to 2018. However, the total increase in area of glacial lakes was largely contributed by the large sized lakes with size >0.1 km^2, accounting for 49% of the total increase in area, although the number of increase of lakes (>0.1 km^2) was the smallest (Figure 5.10). Large sized lakes were predominantly contributed by glacier-fed lakes (67%) and non-glacier-fed lakes accounted for only 33% of the total number of lakes (>0.1 km^2). Further, proglacial lakes (>0.1 km^2) accounted for 64% in the number and 65% in area, while no supraglacial lakes of this size were observed in 2018. The results of the decadal mapping revealed that the increase in glacier lake area was largely contributed by glacier-fed lakes (81%) of the total increased area,

while non-glacier-fed lakes contributed 19% of total increased area between 1964 and 2018. Similarly, increase in number of glacial lakes was contributed by glacier-fed lakes was large (68%) than the non-glacier-fed lakes (32%). These statistics revealed that the significant expansion of lakes was observed where glaciers were present in their catchments, and indicated the transform of glacier-fed lakes to non-glacier-fed lakes, caused by retreat of the glaciers.

5.4.5 Changes in proglacial lakes

Proglacial lakes were larger in size with the mean area of 0.17 km^2 in 2018, and showed the rapid expansion. Proglacial lakes, which were connected with the glacier showed the potential to expand continously. Eight glacial lakes found with size >0.1 km^2 and six proglacial lakes decribed below were compared based on their growth rate. Out of six selected lakes, three were categorized as potentially dangerous by ICIMOD (2011) and three lakes exhibited the most rapid expansion.

5.4.5.1 Nangama Lake

Nangama Lake had an area of 0.27 km^2 including three supraglacial lakes in 1964 and increased rapidly (three times) by 1975 with a surface area of 0.74 km^2 (Figure 5.11). The estimated lake area was about 0.93 km^2 in 1978 by Watanabe et al. (1998) before the GLOF occurred in 1980 and thereafter decreased its area (0.70 km^2) by 1987. The lake remained unchanged in its area after 1987, and currently not connected with the glacier. Current estimated elevation of the glacial lake was 4,883 m obtained from ALOS PALSAR DEM of 12.5-m resolution, while elevation estimated by Watanabe et al. (1998) was 4,950 in 1988. The difference in the elevation may be due to the lowering of the lake level with melt of the ice underneath the lake. The terminal dam of the lake was at distance of ~400 m from the lake shoreline. The triggering factors, i.e., avalanche, rockfalls must have been of large size to have displaced the large volume of water and to have cross the distance from the shoreline to the end moraine. This could be a possible reason for categorizing this lake with medium priority. However, the lake and its geomorphic setting need be continuously monitored to minimize the risk for the downstream villages. The downstream villages, i.e., Yanma, Chhija, and Nup are located very close to the river bed of the Yanma Khola and need to implement adaptation strategies including mitigation efforts.

5.4.5.2 Kotam_gl_0193 Lake (Khanlananma Lake)

Kotam_gl_0193 Lake is located in the Shinbuwa Khola basin of the UTR basin. This lake was at an elevation of 5,036 m, and name of this lake was adopted from ICIMOD (2011), which is categorized as potentially dangerous lake with low priority in their study. This lake also classified as very high hazard, very high risk with high impact lake because this GLOF may impact on 22 building, three bridges and agricultural area (Rounce et al., 2017).

Topographic map of 1992 has a glacier named Khanlananma Glacier and connected with the lake. Therefore, this lake renamed as Khanlananma Lake in this study. Khanlanama Lake was first observed in 1975 with size of 0.12 km^2 and doubled in size in 1987. However, this lake found stable in size with limited expansion after 1987, which attained the size of 0.27 km^2 in 2018 (Figure 5.11).

5.4.5.3 Kotam_gl_0111 Lake (Lahare Lake)

Kotam_gl_0111 Lake (ICIMOD, 2011) at elevation of 4,907 m is called Lahare Lake, which was found near the Tiptala Bhanjyang (pass) at border with the Tibet in the Google Map. Lahare Lake showed the limited expansion in its surface (Figure 5.11). This lake is classified as very high hazard, high risk with moderate impact lake in terms of GLOF (Rounce et al., 2017).

5.4.5.4 Tilpile Taal (Lake)

Tilpile Lake is located west of the Nangama Lake and northwest of the Cheche Pokhari (Lake) at the bottom of Nobuk peak (6,098 m). This lake was found with name Pabuktar in the topographic map of 1992 and trekking maps. Pabuktar Lake started to develop in 1975 with two small supraglacial lakes (0.05 km^2) and coalesced in 1987, but the size remained similar (Figure 5.11). However, the surface area rapidly expanded, and attained the size of 0.21 km^2 in 2000. It further increased to 0.38 km^2 by 2010, while it remained at the same size till 2018.

5.4.5.5 Pandra Lake

Pandra was named based on the nearest peak named Pandra with an elevation of 6,850 m. This lake was the newest emerging lake among above mentioned lakes and observed in 2000 for the first time with the surface area of 0.02 km^2 (Figure 5.11). Thereafter, the lake size has grown continuously and gained the size of 0.10 km^2 in 2018.

The Pandra Glacier connected with Pandra Lake (Figure 5.12) had size of 4.3 km^2 (RGI, 2017). This lake has also increasing potential to GLOF in the future based on the glacier slope, and need to monitor to minimize the risk for downstream villages.

5.4.5.6 Sisima Lake

Sisima Lake in the Ghunsa Khola basin was found one of the fast growing lakes (Figure 5.11) near Sisima. The Sisima Glacier linked with the lake originated near the Dongo peak in the Chulima Himal (Figure 5.12). The name of this lake based on the nearest spot Sisima that was pointed in the topographic map of 1992. The lake was first observed in 1975 with the surface area of 0.03 km^2 and doubled in 1987. The most significant increase in the area was observed between 1987 and 2000, and gained size of 0.15 km^2, while the area increase continuously till 2018 (0.24 km^2). The lake has elongated shape with a length of 1,200 m and width of 250 m in 2018. Comparison of all of the remote sensing data showed that the lake area had increased fourfold between 1987 and 2010. The lake area in 2018 was 8 times larger than that in 1975.

5.4.5.7 Other lakes

Besides the lakes described above, results of measurement also plotted eight additional proglacial lakes, which were found mostly stable conditions after 2000 and had size <0.15 km^2. Two proglacial lakes were located in the Yanma Khola basin and six in the Ghunsa Khola basin.

5.4.6 Glacier lake outburst floods (GLOFs)

This study identified six GLOFs in the Kangchenjunga region including Nangama GLOF in 1980. The details of the each possible GLOF described as follows.

5.4.6.1 Ghunsa GLOFs

Possible past GLOFs were inspected in the Ghunsa region of the Ghunsa Khola basin, and two possible GLOFs were identified. One GLOF was detected from north of the Kangchejungha Glacier probably either from Lhonak Glacier or Chhyantundunga Glacier (Figure 5.13). The second GLOF was identified close to the termini of the Ramdan and Kangchenjunga glaciers (Figure 5.14). Because, these two GLOFs were identified using CORONA image of 1962, there were no image available beore 1962, and occurrence date could not be possible. The damage caused by the GLOFs is not known.

However, small village, i.e., Lhonak is located very close to the sediment deposited area and assumed to be affected by the GLOF occurred from North of the Kangchenjunga Glacier. Similarly, Kangpachen and Lyakep villages were located downstream from both floods and were within distance of 10 km.

5.4.6.2 Olanchungola GLOFs

Traces of past GLOFs within the Tamor Khola sub-basin were examined using CORONA imageries of 1962 and 1964 (Figure 5.15a and b). A village located downstream of this area is Olanchungola. One possible GLOF was identified by the trace, so the GLOF named as Olanchungola GLOF. Olanchungola Village is at distance of 12 km down from the origin of the GLOF. The traces of the eroded river bed of the Tamor Khola River was clearly visible near and several km down from the Olanchungola Village (Figure 5.15c). No lakes at the upstream region was identified in the images of 1962 and 1964, which might be due to a poor visibility of the images. However, smooth flattened area of the lake was visible above of the red rectangle shown in the Figures 5.15a and b. The lake area was crosschecked and was clearly visible in CORONA image of the year 1967. This suggested that the lake of size 0.14 km^2, almost similar size of the lake in 1975 (0.17 km^2), existed in the source area where the breached moraine near the lake was clearly visible in the lakefront. The name of this lake is Lahare Lake in the Google imageries and categorized as potentially dangerous glacial lake with low priority by ICIMOD (2011). However, previous GLOF from this lake is not documented in any literature.

An occurrence of another GLOF is suggested in 1968 in the same area by interview survey (unpublished information obtained from Dr. Alton Byers), which might have possibly occurred from the same lake. This is because traces of breached end moraine, river erosion and glacial lakes were not identified in other glaciers of the corresponding Tamor Khola sub-basin (at Olanchungola). CORONA images of 1967 and 1970 were inspected, and no major changes in the river and lake morphology was detected. Therefore, it can be concluded that the GLOF that was identified by this study and that suggested by Dr. Alton Byers was the same GLOF that occurred in 1968.

5.4.6.3 Yanma Khola GLOFs

Nangama Lake is the largest proglacial lake in the Yanma Khola basin, and a GLOF in 1980 occurred from this lake was reported (Yamada and Sharma, 1993; Watanabe et

al., 1998). Landsat and CORONA images were checked, and changes in morphology surrounding the lake and downstream region was detected (Figure 5.16). The lake had an area of 0.74 km^2 in 1975 (Figure 5.16a), which increased by three times from 1964. GLOF from the Nangama Lake is considered as one of the most devastating floods. Area estimated for the lake in 1978 was 0.93 km^2 (Watanabe et al., 1998). The estimation suggested that the area of the lake was large enough to produce a catastrophic flood and to cause intensive deposition and erosion along the river (Figure 5.16b). The GLOF damaged the settlements of Lunthun, Siwa, and Dobhan. A bridge at an elevation of 640 m and at distance of 71 km downstream from the lake was reported to be damaged by the flood (Watanabe et al., 1998). Large amount of sediments transported from the lake blocked the river named as Chherchen Khola and created a Chhehe Pokhari (Lake) of size 0.35 km^2 (Figure 5.16c). Chheche Pokhari still exists with size of 0.34 km^2 that was estimated using the Sentinel-2 image of 2018. The Nangama Lake had an area of 0.70 km^2 in 1987 and similar size in 2018. However, the area immediately after the GLOF could not be estimated due to the image availability.

Similarly, breached end moraine of the Sharpu Glacier was detected in the CORONA image from 1962. Deposition and eroded materials were observed about 3 km downstream from the origin, which was close to the Jaritar Village. However, river erosion below the Jaritar Village could not be identified. Therefore, a small GLOF event originated from the Sharpu Glacier is suggested.

5.5 Summary

Open access satellite imageries including spy satellite images of the U. S. intelligence agencies, Landsat and Sentinel-2 were used to map and prepare inventories of the glacial lakes in the Kangchenjunga region, UTR basin of Nepal. These satellite images have spatial resolution from 2.76 m (CORONA in 1964) to 60 m (Landsat MSS in 1975). Sentinel-2 images of 10-m spatial resolution were used to prepare the latest inventory of the glacial lakes in the region and compared with other inventories. The inventory of 2018 mapped all glacial lakes with size >500 m^2, which plotted 373 glacial lakes with the total surface area of 6.18 ± 0.75 km^2 (Table 5.2). Out of 373 lakes, 284 lakes with area of 4.46 ± 0.54 km^2 were observed to be fed by the glaciers, and 89 lakes covering an area of 1.72 ± 0.21 km^2 were found non-glacier-fed lakes. Similarly, the inventory of 2018 identified 138 supraglacial lakes, 221 unconnected lakes, and 14

proglacial lakes. The largest number of the lakes (147) was identified in the Ghunsa Khola basin, a highly glacierized and largest sub-basin of the UTR basin.

Decadal inventories showed that the total number and area of glacial lakes in the Kangchenjunga region increased by 406% and 230%, respectively, between 1964 and 2018. The largest increase of the number of glacial lakes was estimated for the period 1975 – 1987. Similarly, the number of non-glacier-fed lakes increased significantly in later period (2010 – 2018), which indicated the emergence of new lakes and separation of the existing glacier-connected lakes from the galciers. The glacial lakes in different river sub-basins of the UTR basin exhibited the heterogeneous expansion during 1964 and 2018. The largest increase in the number of glacial lakes was estimated for the Ghunsa Khola basin, while the largest increase in the area was observed in the Yanma Khola basin between 1964 and 2018. The rapid expansion of the lakes between 1964 and 1975 was largely contributed by the Nangama Lake in the Yanma Khola basin, which accounted for 51% of total expansion during this period. Similarly, the largest increase in the number of glacial lakes was observed among small sized lakes (<0.01 km^2), while the largest increase in the area was observed among large sized lakes (>0.1 km^2), which accounted for 49% of the total increase in area between 1964 and 2018.

Five possible GLOF events were detected for the first time through an analysis of CORONA images from 1962 to 1980 in the Ghunsa, Tamor, and Yanma Khola sub-basins in this study. These GLOFs were validated from field study. Similarly, changes in morphology near the lake and downstream were analyzed for the possible GLOF affected area.

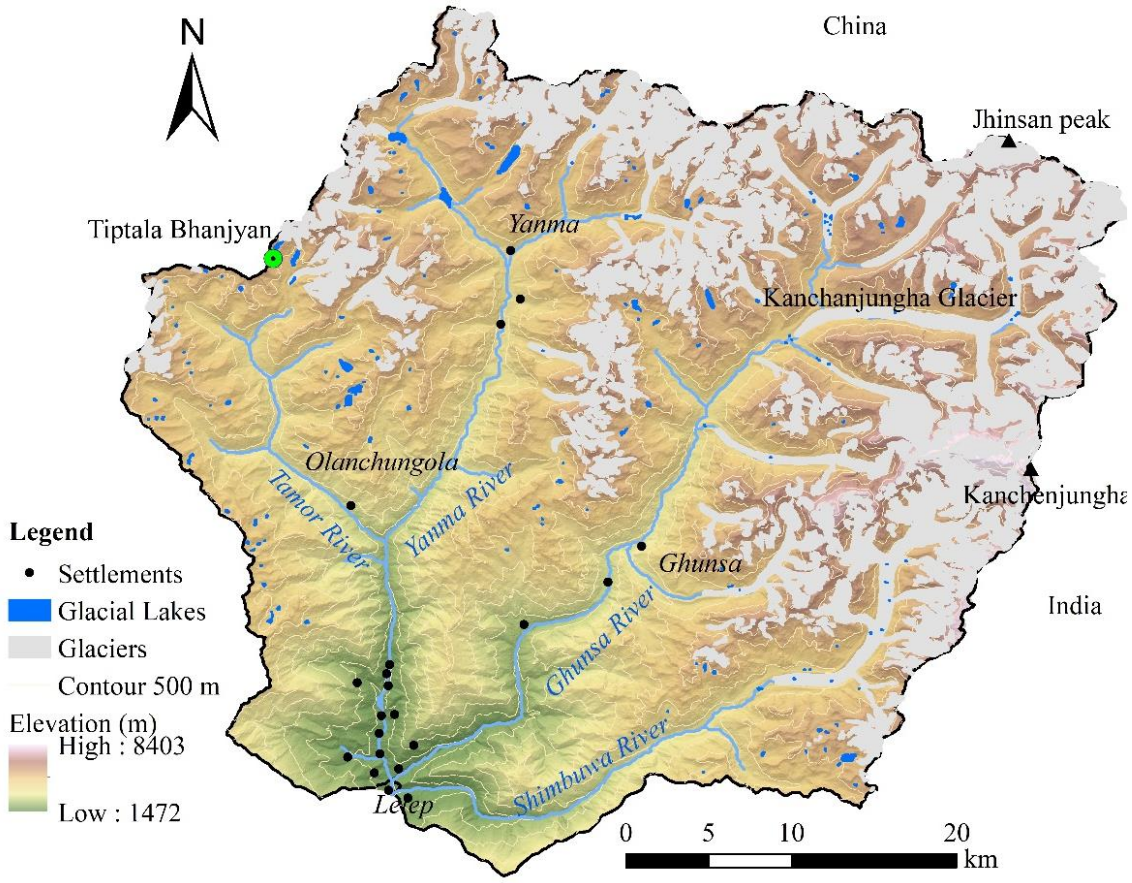

Figure 5.1 Glaciers and glacial lakes of the Kangchenjunga region, upper Tamor River basin.

Table 5.1 List of images used for mapping glacial lakes and tracing past GLOF events in the Kangchenjunga region from 1962 to 2018.

SN	Satellite Images	Image ID	Date	Resolution
1	CORONA (KH-4)	DS009048070DA242	10/25/1962	7.62 m
2	CORONA (KH-4A)	DS1014-2118DF194	11/26/1964	2.74 m
3	CORONA (KH-4A)	DS1014-2118DF195	11/26/1964	2.74 m
4	CORONA (KH-4A)	DS1014-2118DF196	11/26/1964	2.74 m
5	CORONA (KH-4A)	DS1044-1070DF098	11/07/1967	2.74 m
6	CORONA (KH-4B)	DS1112-1023DA165	10/20/1970	1.83 m
7	CORONA (KH-9)	DZB1216-500422L003001	09/27/1980	6.2-9.1 m
8	Landsat MSS	LM02_L1TP_150041_19751207_20180426_01_T2	12/7/1975	60 m
9	Landsat 5	LT05_L1TP_139041_19871231_20170210_01_T1	12/31/1987	30 m
10	Landsat 5	LT05_L1TP_139041_19881014_20170205_01_T1	10/14/1988	30 m
11	Landsat 5	LT05_L1TP_139041_20001031_20161213_01_T1	10/31/2000	30 m
12	Landsat 5	LT05_L1TP_139041_20091024_20161018_01_T1	10/24/2009	30 m
13	Landsat 5	LT05_L1TP_139041_20101214_20161011_01_T1	12/14/2010	30 m
14	Sentinel-2	S2A_MSIL1C_20181030T044921_N0206_R076_T45RXL_20181030T074553	10/30/2018	10 m
15	Sentinel-2	S2A_MSIL1C_20181030T044921_N0206_R076_T45RWL_20181030T074553	10/30/2018	10 m
16	Sentinel-2	S2B_MSIL1C_20181025T044849_N0206_R076_T45RWL_20181025T075235	10/25/2018	10 m

Table 5.2 Distribution of glacial lakes (>500 m^2) in the sub-basins of the upper Tamor River basin, using Sentinel-2 images of 10-m spatial resolution in 2018.

Sub-basins	Supraglacial lakes		Proglacial lakes		Unconnected lakes		All Lakes	
	Area (km^2)	No.	Area (km^2)	No.	Area (km^2)	No.	Area (km^2)	No.	Area (km^2)
Tamor (at Olanchungola)	206.0	4	0.06	1	0.18	71	1.80	76	2.04
Yanma	416.9	5	0.01	5	1.25	52	0.49	62	1.74
Tamor (at Lelep)	150.4					10	0.24	10	
Ghunsa	742.0	86	0.37	7	0.65	54	0.48	147	1.54
Shimbuwa	267.7	43	0.13	1	0.27	34	0.26	78	0.66
Total	1632.7	138	0.57	14	2.34	221	3.27	373	6.18

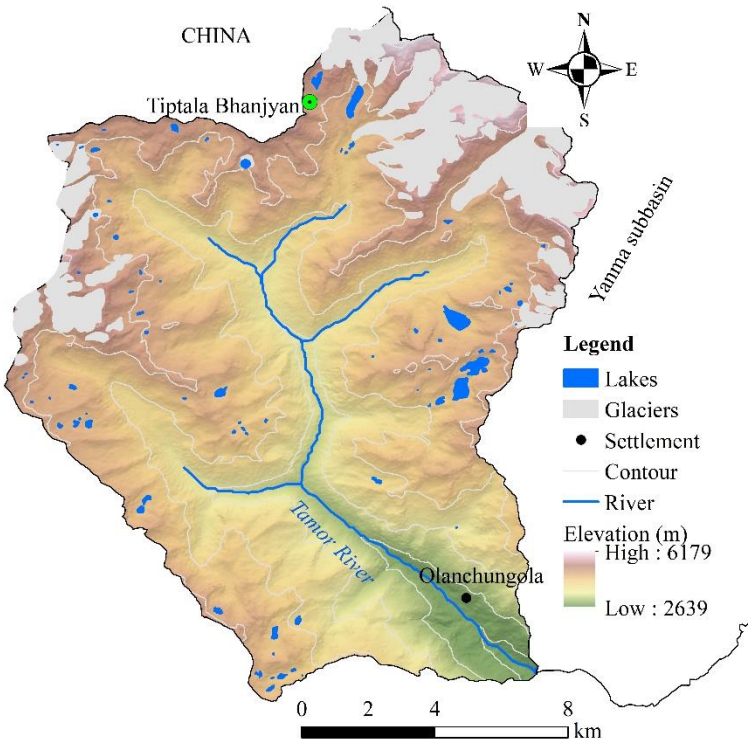

Figure 5.2 Map of the glacial lakes of the Tamor basin at Olanchungola obtained from Sentinel-2 images of 10-m spatial resolution in 2018. Glacier boundaries were taken from Bajracharya et al. (2014).

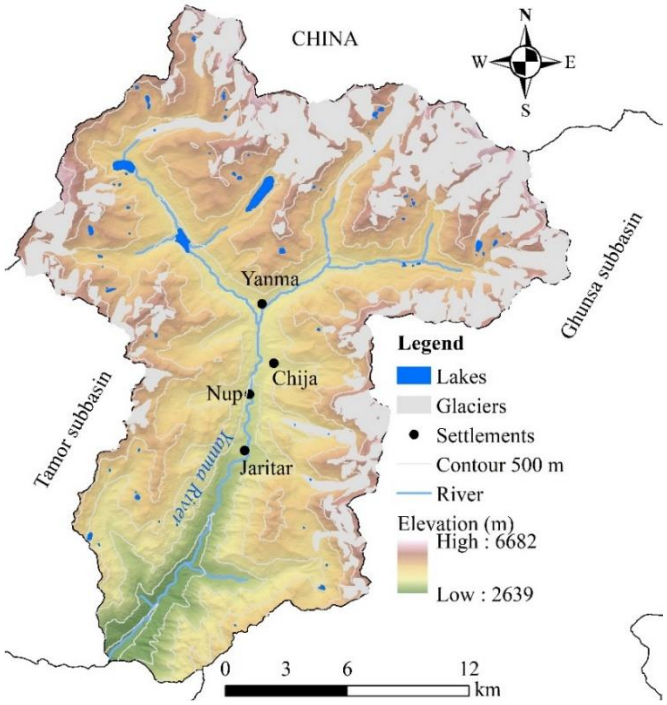

Figure 5.3 Map of the glacial lakes of the Yanma basin at Olanchungola obtained from Sentinel-2 images of 10-m spatial resolution in 2018. Glacier boundaries were taken from Bajracharya et al. (2014).

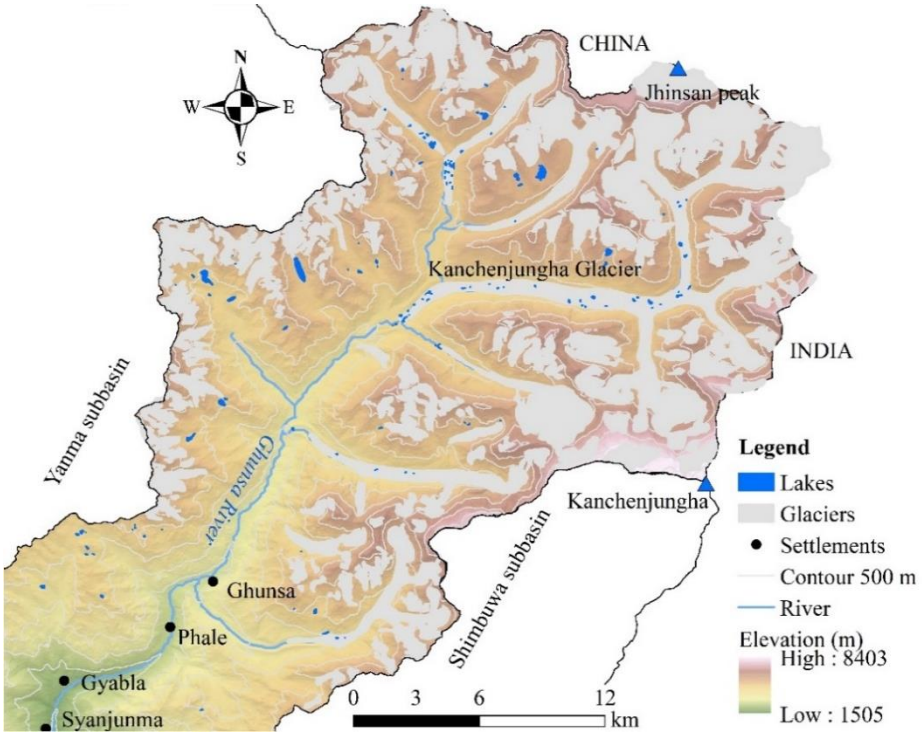

Figure 5.4 Map of the glacial lakes of the Ghunsa basin at Lelep obtained from Sentinel-2 images of 10-m spatial resolution in 2018. Area without glaciers and glacial lakes within the Ghunsa basin are not included for visualization. Glacier boundaries were taken from Bajracharya et al. (2014).

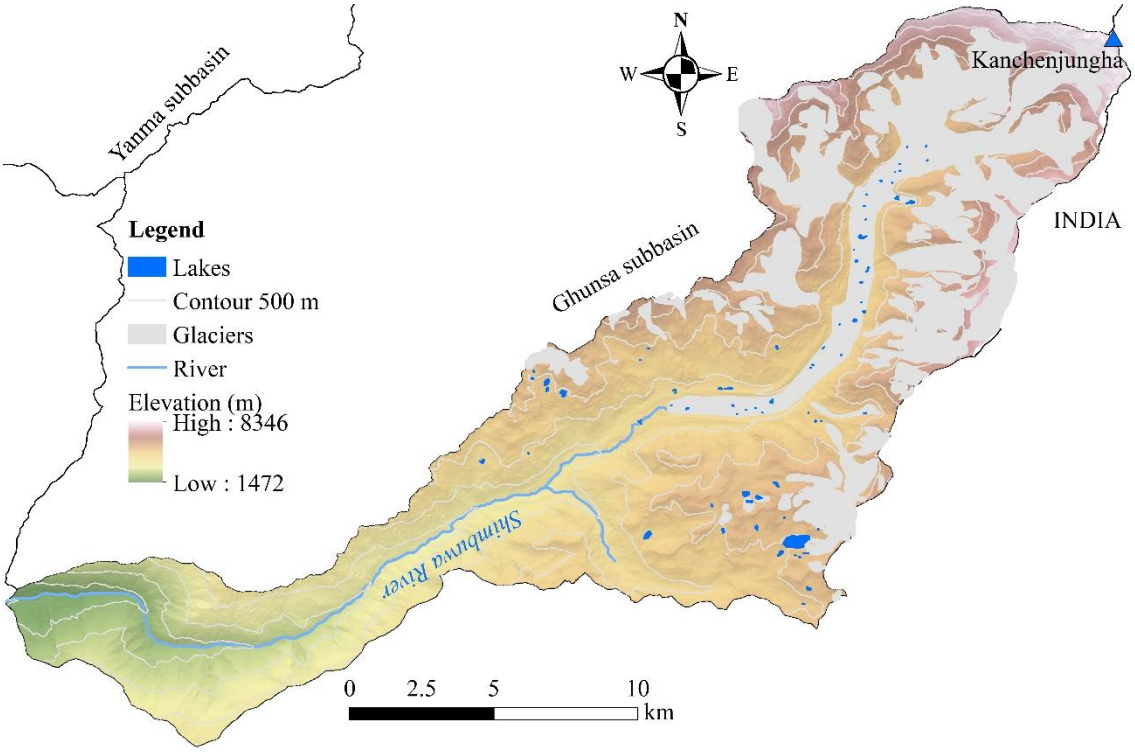

Figure 5.5 Map of the glacial lakes of the Shimbuwa basin at Lelep obtained from Sentinel-2 images of 10-m spatial resolution in 2018. Glacier boundaries were taken from Bajracharya et al. (2014).

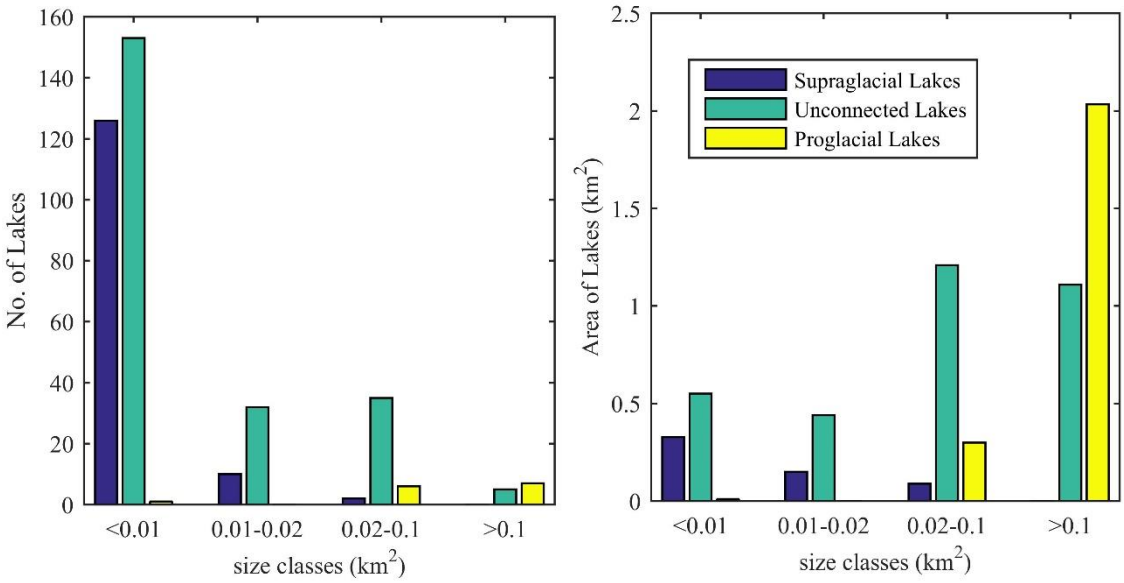

Figure 5.6 Distribution of the number (left hand side) and area (right hand side) of glacial lakes (>500 m^2) in the upper Tamor River basin according to their different size classes.

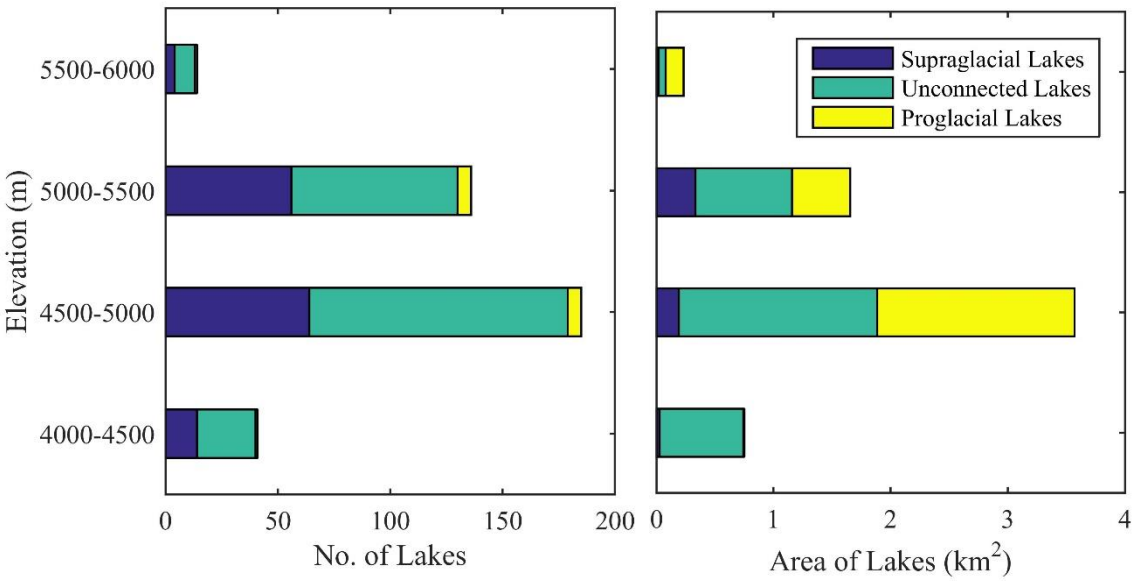

Figure 5.7 Total number (left hand side) and surface area (km^2) (right hand side) of the lakes (>500 m^2) by type in different elevation zones in the Kangchenjunga region except for one lake at the elevation of 3,910 m.

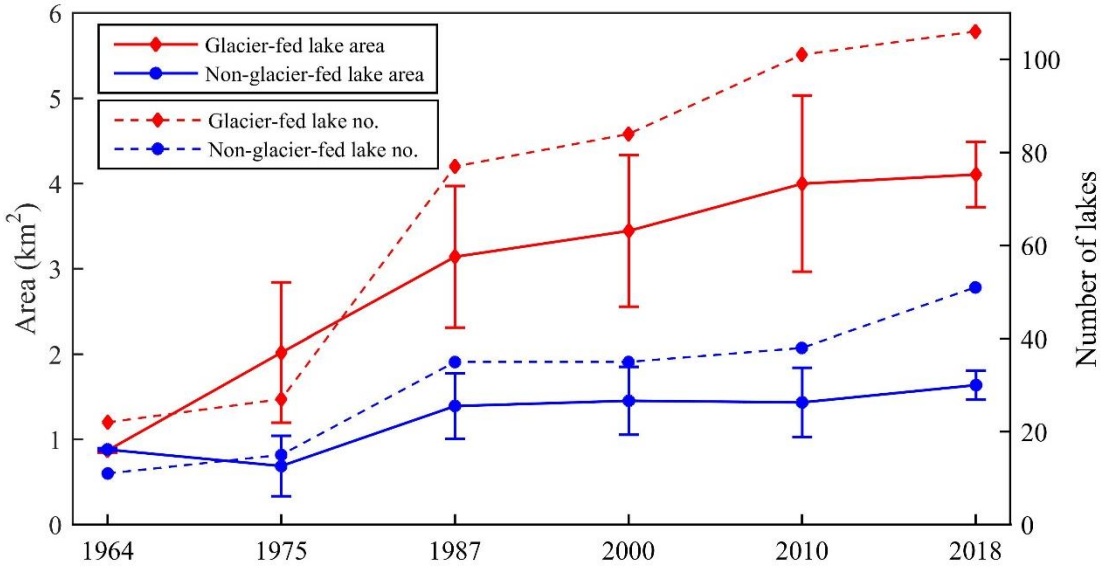

Figure 5.8 Changes in the total number and surface area of glacier-fed and non-glacier-fed lakes (>5,000 m^2) from 1964 to 2018 in the Kangchenjunga region.

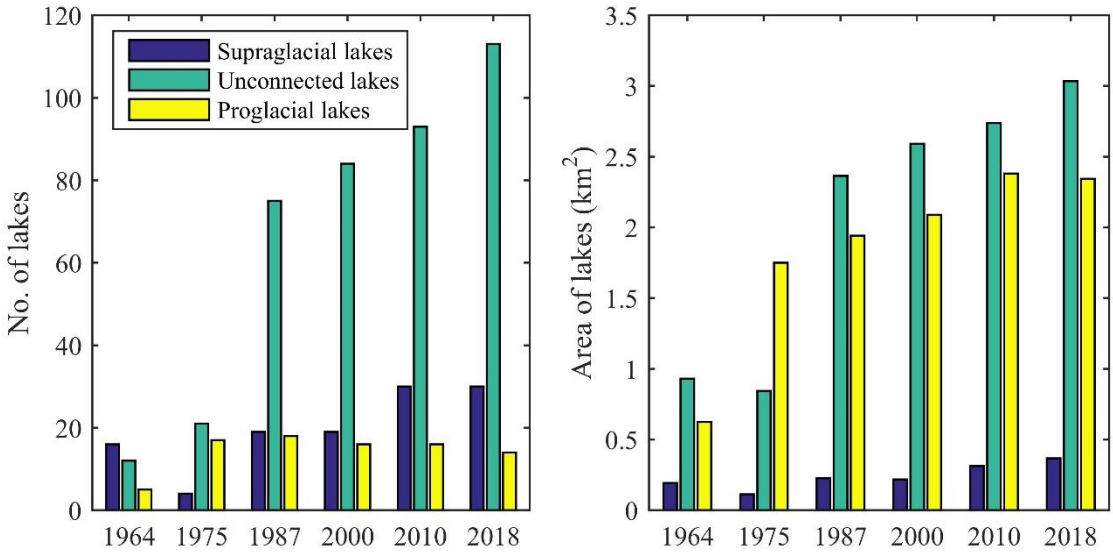

Figure 5.9 Changes in the total number (left hand side) and surface area (right hand side) of supraglacial, unconnected and proglacial lakes (>5,000 m^2) from 1964 to 2018 in the Kangchenjunga region.

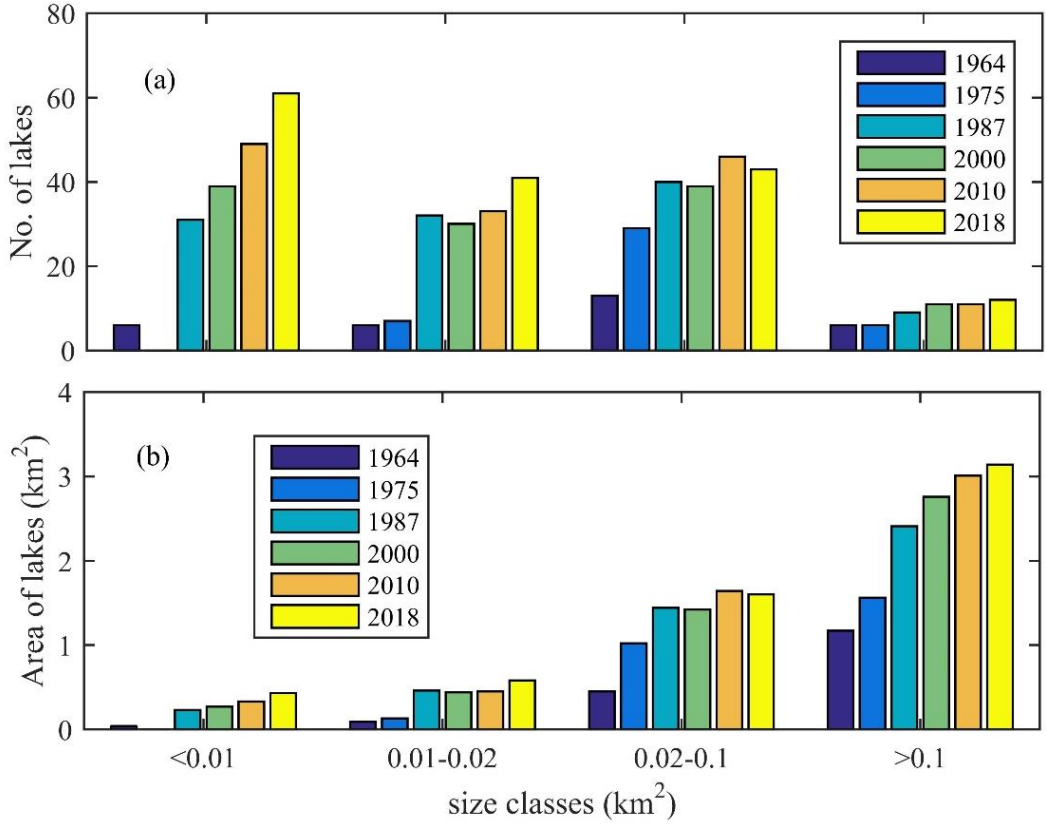

Figure 5.10 Total number (a) and surface area (b) of the glacial lakes (>5,000 m^2) of different size classes from 1964 to 2018.

Table 5.3 Total number and surface area (km^2) of the lakes (>5,000 m^2) between 1964 and 2018.

Year	1964		1975		1987		2000		2010		2018	
Basins	No.	Area	No.	Area	No.	Area	No.	Area	No.	Area	No.	Area
Tamor	9	0.92	10	0.72	27	1.35	28	1.40	29	1.44	39	1.56
Yanma	9	0.48	11	1.04	19	1.51	26	1.75	30	2.01	32	2.06
Tamor at Lelep	1	0.03	4	0.10	5	0.16	5	0.17	7	0.19	7	0.23
Ghunsa	6	0.25	13	0.63	39	0.97	39	1.08	47	1.25	56	1.32
Shimbuwa	6	0.07	4	0.21	22	0.53	21	0.50	26	0.54	23	0.56
Total	31	1.74	42	2.70	112	4.53	119	4.90	139	5.43	157	5.74

Table 5.4 Total number and surface area change (km^2) of lakes (>5,000 m^2) change during different period of study in sub-basins of the Kangchenjunga region.

Basins	1964-1975		1975-1987		1987-2000		2000-2010		2010-2018		1964-2018 (%)	
	No.	Area	No.	Area	No.	Area	No.	Area	No.	Area	No.	Area
Tamor	1	-0.20	17	0.63	1	0.05	1	0.04	10	0.12	333	69
Yanma	2	0.58	8	0.47	7	0.23	4	0.26	2	0.06	256	346
Tamor at Lelep	3	0.06	1	0.07	0	0.01	2	0.02	0	0.04	600	629
Ghunsa	7	0.37	26	0.34	0	0.11	8	0.17	9	0.07	833	422
Shimbuwa	-2	0.14	18	0.32	-1	-0.03	5	0.04	-3	0.02	283	710
Total	9	0.95	70	1.83	7	0.37	20	0.54	18	0.31	406	230

Table 5.5 Change in the number and area of supraglacial, unconnected and proglacial lakes (>5,000 m^2) during different periods of study in the Kangchenjunga region. The values in parenthesis are percentage of area increase.

Periods	Supraglacial lakes		Unconnected lakes		Proglacial lakes	
	Number	Area (km^2)	Number	Area (km^2)	Number	Area (km^2)
1964-1975	-10	-0.073	9	-0.087	12	1.123
1975-1987	15	0.114	54	1.520	1	0.192
1987-2000	0	-0.009	9	0.228	-2	0.148
2000-2010	11	0.096	9	0.147	0	0.292
2010-2018	0	0.054	20	0.294	-2	-0.037
1964-2018	16 (114)	0.18 (95)	101 (842)	2.10 (226)	9 (180)	1.72 (275)

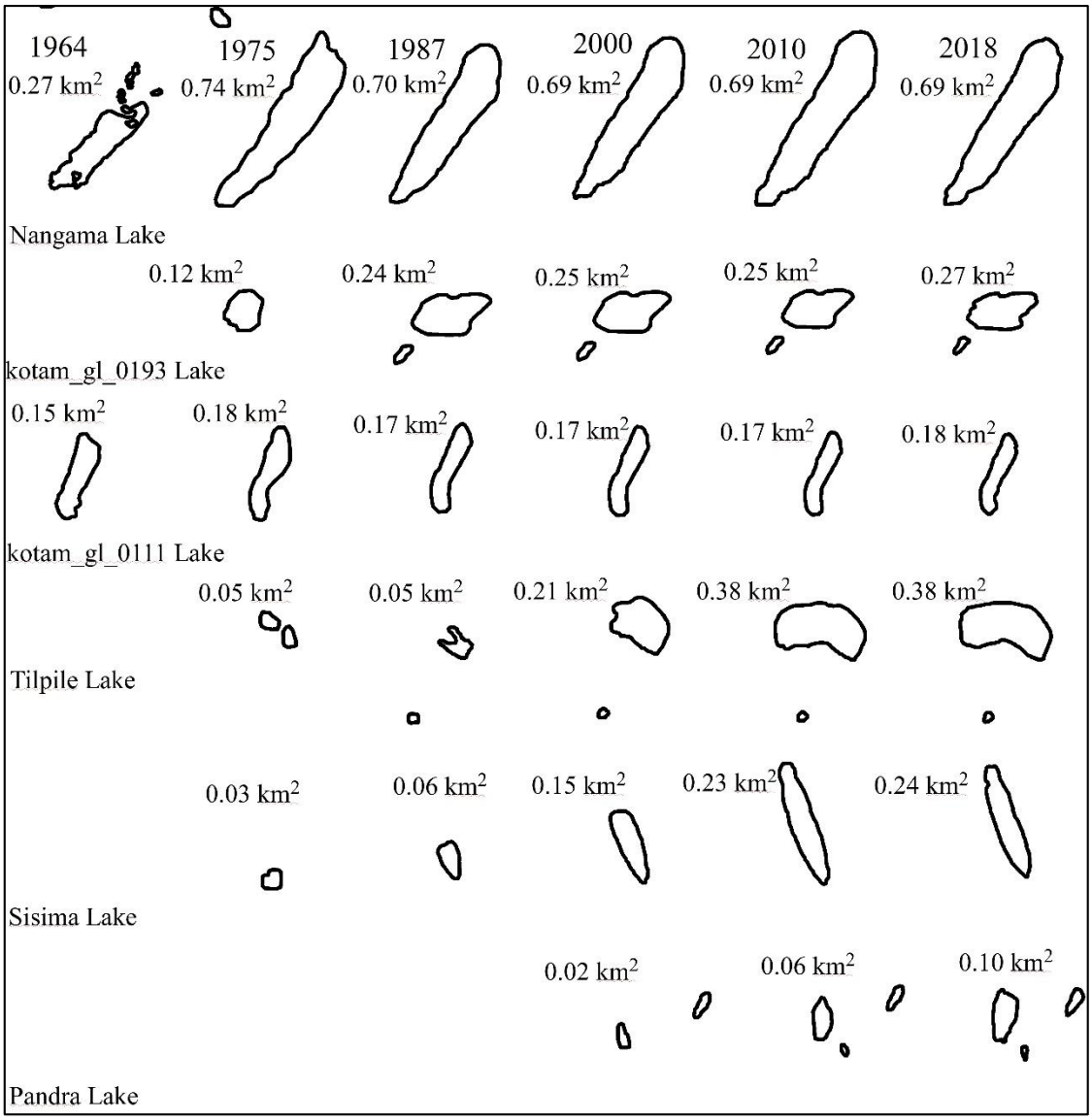

Figure 5.11 Growth pattern of six selected proglacial lakes in the Kangchenjunga region during 1964 and 2018.

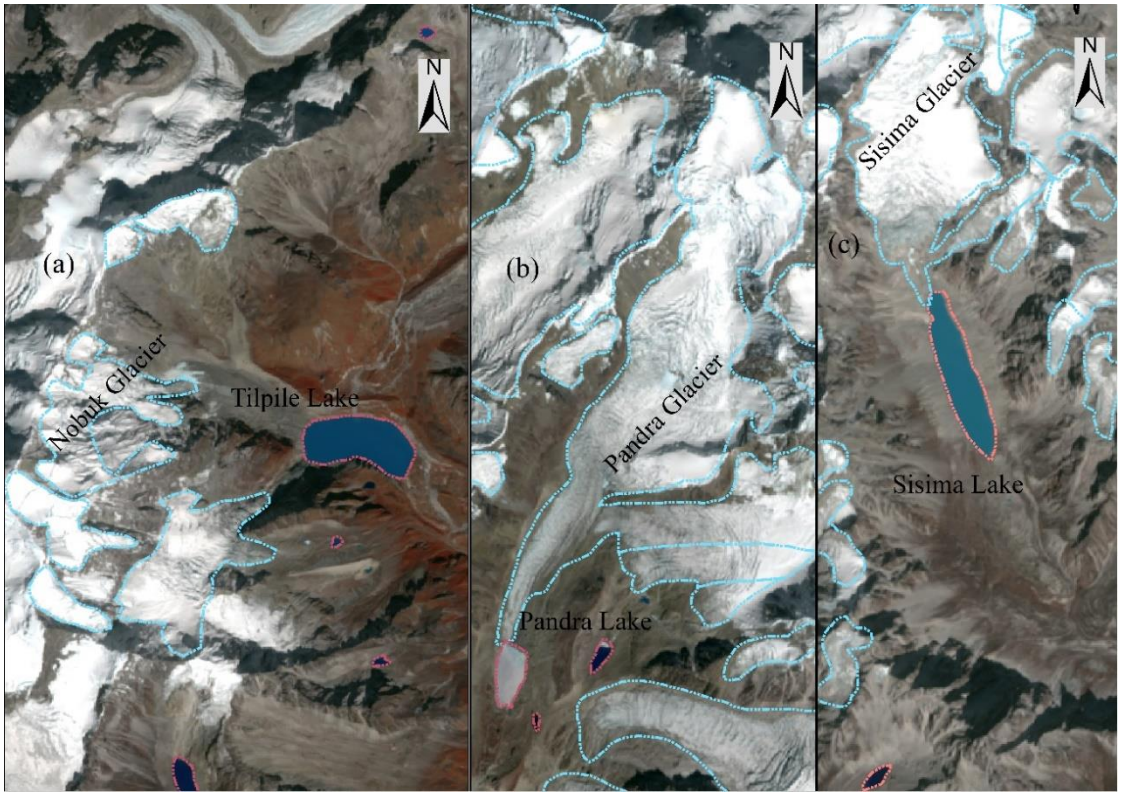

Figure 5.12 Areal extent of the Tilpile (a), Pandra (b), and Sisima (c) proglacial lakes, and present status of associate glaciers in the lake basin.

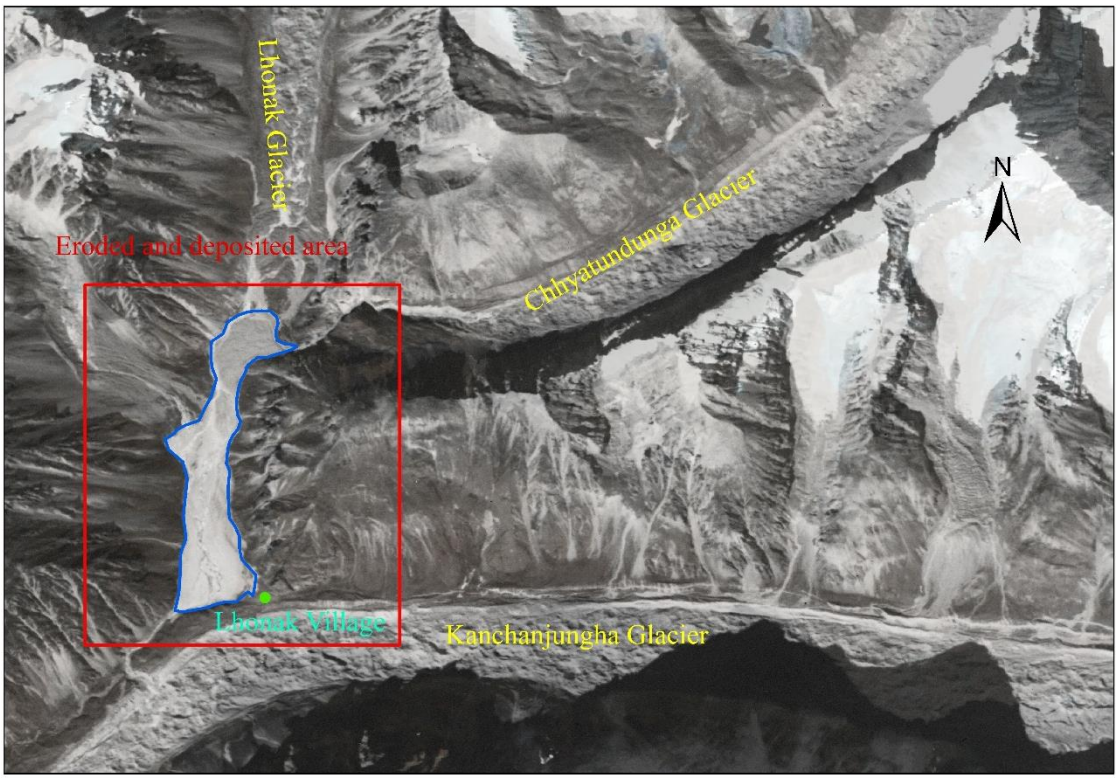

Figure 5.13 A CORONA image from November 1962 showing sediment deposition and eroded debris materials north of the Kangchenjunga Glacier and Lhonak Village.

Figure 5.14 A CORONA image from November 1962 showing a small lake on the Ramdan Glacier and eroded river channel in the downstream of the Kangchenjunga and Ramdan glaciers.

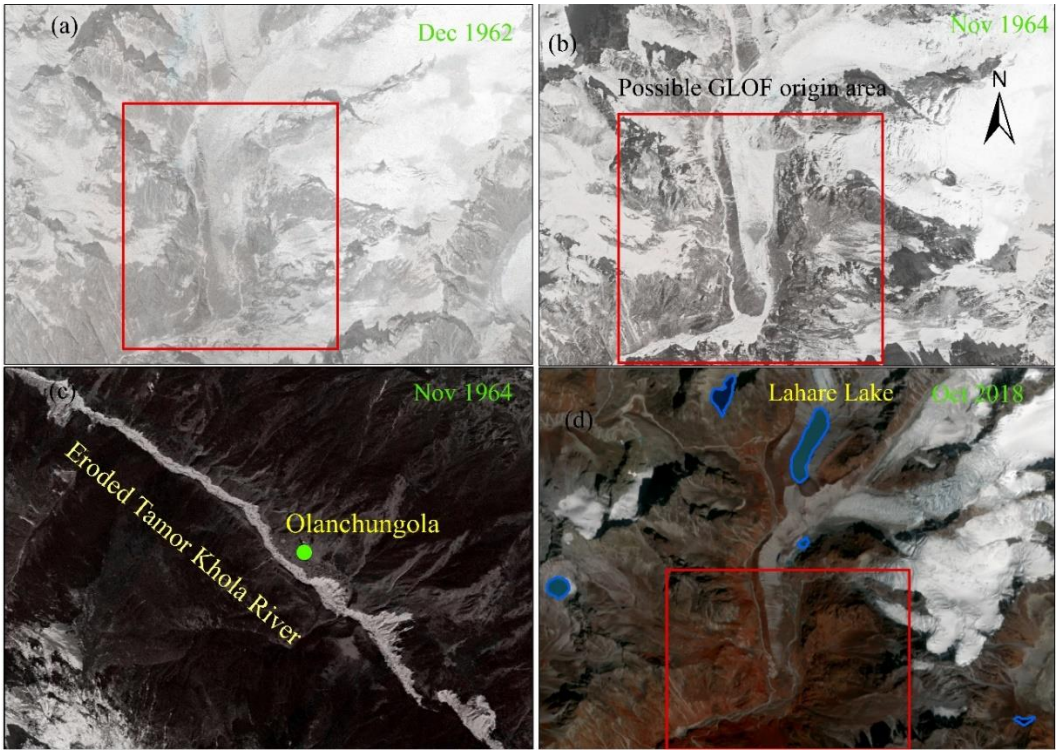

Figure 5.15 CORONA images of December 1962 (a), November 1964 (b and c), and Sentinel-2 image from October 2018 showing changes in morphology of the Lahare Lake in the Tamor Khola sub-basin.

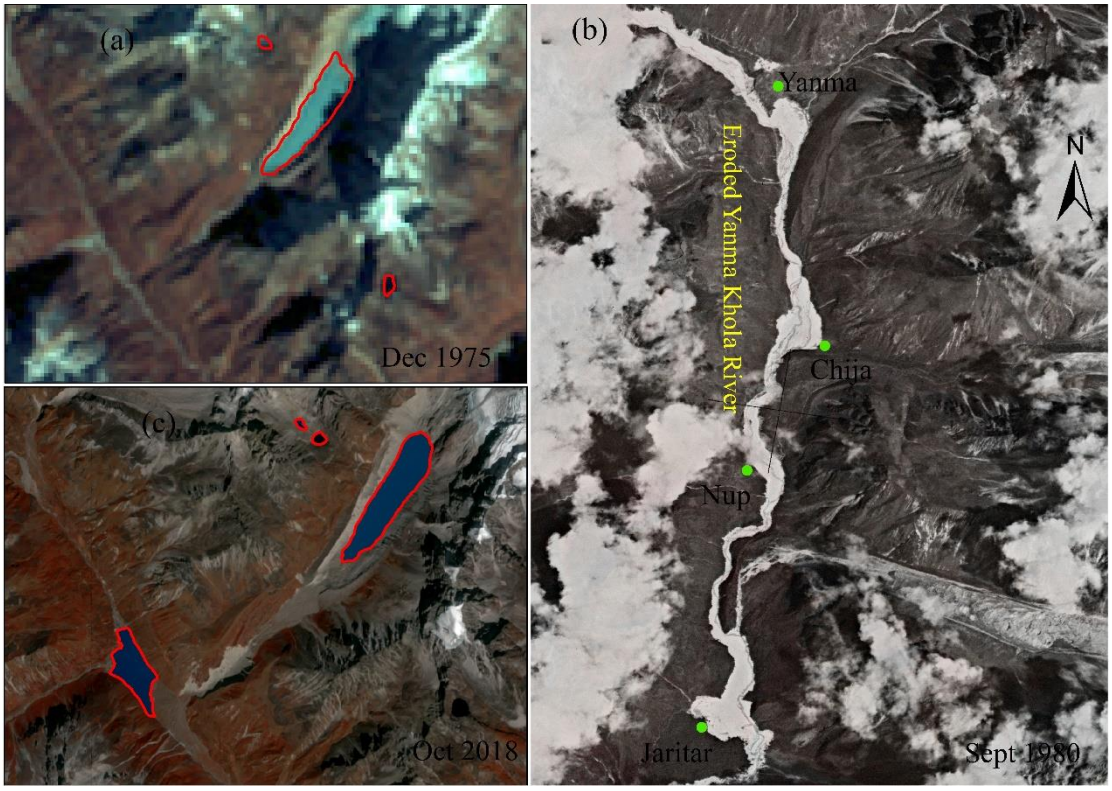

Figure 5.16 Landsat image from December 1975 (a), CORONA image from September 1980 (b), and Sentinel-2 image from October 2018 showing changes in morphology of the Nangama Lake and in the downstream river channel in the Yanma Khola sub-basin.

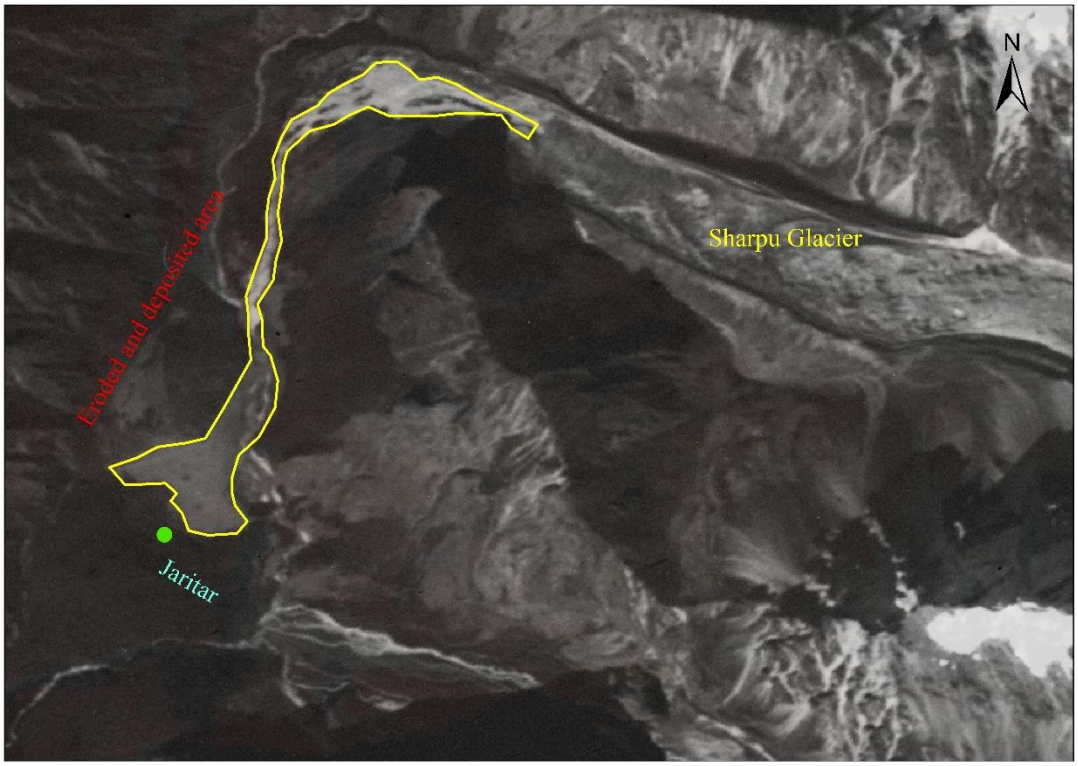

Figure 5.17 A CORONA image from November 1962 showing deposited materials near the Jaritar Village in the Yanma Khola sub-basin.

6. Discussion

6.1 Uncertainties of lake surface measurements

Uncertainty in measurement of lake surfaces can be attributed to sensor resolution and its perimeter. Error for larger shapes was proportionally smaller than that for smaller shapes and when sensors with high-resolution are used (Salerno et al., 2012). In this study, uncertainty of the surface area of glacial lakes was estimated by multiplying the perimeter of the feature with half the resolution of the sensors (Fujita et al., 2009; Jiang et al., 2018). The uncertainty associated with different size of the lakes obtained by using satellite images of 2-m, 10-m, and 30-m spatial resolution exhibited the reduction in percentage error with increase in size of the feature (Figure 6.1). Similarly, results also showed the decrease of percentage error with the increase in the spatial resolution. The uncertainty analysis suggested that high-resolution sensor (2 m) would be able to determine the lake surface with size up to 500 m^2, considering a generic error threshold of 15% that correspond to the differences observed by Tartari et al. (2008), and used by Salerno et al. (2012). Dimensional threshold would increase to 0.02 km^2 for a sensor with resolution of 10 m, and 0.1 km^2 for a sensor with the 30-m spatial resolution. Salerno et al. (2012) illustrated the relationship between the hypothetic surface of circular lakes and the respective uncertainty of measurement from sensors that is differentiated by the degree of resolution (Figure 6.2), and obtained the dimensional threshold of 0.05 km^2 for 10-m resolution and 0.5 km^2 for the sensor with 30-m resolution. The discrepancies with Salerno et al. (2012) was due to the use of hypothetical areas of lakes used in their study.

Medium-resolution satellite data (10-90 m) have been available for cryospheric studies since the 1970s (Salerno et al., 2012) specifically Landsat MSS, TM, ETM+, SPOT, the IRS LISS III, ALOS AVNIR-2, and Terra ASTER (Racoviteanu et al., 2008). Other optical satellite images with higher spatial resolution (up to sub-meter) such as Quickbird, WorldView, GeoEye and IKONOS have archive for the later period, which are suitbale for a detailed and accurate study of glaciers and glacial lakes. However, these images are commercial and used in limited studies. Sentinel-2A (S2A) on 23 June 2015 operating the new Multi Spectral Instrument (MSI) with the spatial resolution of 10 m (RGB bands). Sentinel-2 images are free to access, and became popular among scientific communities, and can provide more accurate results than Landsat images (Paul et al., 2016). High-resolution imageries of up to sub-meter spatial resolution for a cryospheric

study have been commercially available only after 2000; therefore, historical archive of Landsat is the only option for historical mapping and analysis.

Long-term archive of Landsat imageries with >30-m spatial resolution has been intensively used to map glacial lakes and glaciers in Nepal (Mool et al., 2001; ICIMOD, 2011; Bajracharya et al., 2014; Shrestha et al., 2017; Khadka et al., 2018). They have used different area thresholds for minimum area of the lake, i.e., 3,000 m^2 (Shrestha et al., 2017), 3,600 m^2 (Gardelle et al., 2011), 8,100 m^2 (Nie et al., 2013), and 0.1 km^2 (Rounce et al., 2016b) in regional and basin level studies. A threshold of less than four pixels may overestimate the lake area. A minimum of five pixels is considered as more realistic for mapping glacial lakes to avoid overestimation (Jiang et al., 2018) and minimize the uncertainty. Therefore, a threshold of five pixels was used for mapping glacial lakes for high- to moderate-resolution WorldView and Sentinel-2 imageries, while five and half pixels (5,000 m^2) was applied for the Landsat inventories. Use of minimum area threshold of 5,000 m^2 was helpful for measurement using different spatial resolution images (CORONA, Landsat, Sentinel-2) specifically in case of the Kangchenjunga region to prepare the consistent inventories.

The majority of glacial lakes were found with sizes <500 m^2, <0.02 km^2, <0.1 km^2 by using WorldView and GeoEye, Sentinel-2, and Landsat imageries, respectively by using the semi-automatic methods. Therefore, it cannot determine the surface of the majority of the lakes under an uncertainty threshold of 15% by using only automatic methods and high-resolution images (Watson et al., 2016). Manual corrections are recommended for short-term variability for glacier-scale lake dynamics. However, dynamics of the lakes with size of >0.02 km^2 can be understood using Sentinel-2 images of 10-m spatial resolution and temporal resolution of five days for the shorter period. Images with 30-m spatial resolution could not map the lakes that have size <0.1 km^2 with sufficient accuracy using only automatic method, rather than it could be utilized to understand the evolution of the only large sized lakes (>0.1 km^2) for the longer period. The larger uncertainty associated with 30-m Landsat was also attributed to the irregular shape (circularity index values >1) of the lakes, which can be improved using manual correction in case of the smaller study area. The size distribution of lakes does not lend to alignment with a 30-m pixel and has high chances for underestimation and overestimation (Figure 6.3). The 2-m mapping of glacial lakes in the Everest region exhibited the 369 lakes with an uncertainty of <15%, accounted for the 92% of the total lake area, while glaciers exhibited the lower order of uncertainty (Table 6.1). Similarly,

Sentinel-2 and Landsat mapped about 75%, and 39% of the total surface area of lakes, respectively with an uncertainty of <15%. These statistics proved that WorldView (2 m) and Sentinel-2 (10 m) could correctly characterize the water resource in the study region compared to the coarse-resolution images, i.e., Landsat.

In this study, intensive manual editing was conducted after automatic mapping and much higher accurate map of the glacial lakes was assumed, as manual editing significantly improve the accuracy (Mergili et al., 2013; Shukla et al., 2018). In this case, lower threshold than five pixels can be applied to identify the lakes, where uncertainty of the lake can be estimated by multiplying the perimeter of the lakes with the quarter of spatial resolution. The surface area of the lake that had <15% error was increased to 92% and 66% for Sentinel-2 and Landsat results, respectively, when uncertainty was estimated by multiplying perimeter with the quarter of spatial resolution.

The areal uncertainty of the delineated features obtained from the above mentioned method was larger, when compared with the results of much higher resolution imageries (0.5 m). Higher resolution of panchromatic images (0.5 m) were available for 25 October and 29 October 2016, which were almost the same time as that of the Sentinel-2 (30 October 2016) and Landsat (10 November 2016), and these images were used for the accuracy assessment for the surface area of lakes in the Everest region. These images covered the Khumbu, Nuptse, Lhotse Nup, and Lhotse glaciers. Lakes (>5,000 m^2) on these glaciers were manually digitized. The estimated mean uncertainty of lakes for the 0.5-m resolution images was 1.25%, which can be considered negligible. The aerial errors of the lakes were analyzed by comparing the surface area of the lakes obtained from 0.5-m resolution images with 2-m, 10-m, and 30-m images. In total, 12 supraglacial lakes with the total area of 0.3 km^2 were plotted and found the total areal difference of 5.7%, 9.2%, and 14.9% with the results obtained from 2-m, 10-m, and 30-m spatial resolution images, respectively. However, the maximum aerial error for individual lakes ranged from 20% to 85% for different resolution imageries. Larger error among the individual lakes was mainly caused by the inability of the semi-automatic method to detect narrow channels that connect the lakes, which can be manually mapped with high-resolution images (Figure 6.4). Nevertheless, the majority of the lakes (65-75%) had an aerial error of less than 7%, 14%, and 22% for the 2-m, 10-m, and 30-m resolution imageries, respectively. Therefore, high accurate mapping of the glacial lakes was achieved in this study.

Results of the 2-m inventory suggested that supraglacial lakes accounted for 91% of the total number of lakes in the Everest region, and Landsat and Sentinel-2 images were unable to map 45% and 13% of the total area of the lakes mapped by 2-m spatial resolution imageries, respectively. These statistics were 98% and 83% of the total number of lakes mapped by 2-m imagery for the Landsat and Sentinel-2 imagery, respectively. The inventory also revealed that lakes <1 pixel of Landsat (900 m^2) accounted for 19% of the total surface area of lake and those with size of <1 pixel of Sentinel-2 accounted for 4% of total area, are comparable with the findings of Watson et al. (2016).

Lakes (>0.1 km^2) were mapped with less than 15% uncertainty using Landsat images and manual correction may significantly improve the results, which can be used for understanding the long-term development of water bodies with size >5,000 m^2. Estimations also suggested that Sentinel-2 images have the potential to study seasonal variations with smaller size (>500 m^2), and WorldView images can be used for higher accuracy, detailed inventories of the lakes, and accuracy assessment for the coarser resolution results. The fluctuation of shallow and small size lakes can be large and require images with <10-m resolution (Cook and Quincey, 2015; Watson et al., 2016). The amount of sediments in the lakes and frozen state of the lakes also hindered the accurate mapping with coarse-resolution imagery (Wessels et al., 2002; Watson et al., 2016). The capability of 15-m ASTER images to detect and monitor the supraglacial lakes in comparison to much coarser resolution imageries has been highlighted (Wessels et al., 2002). Therefore, in this study, 10-m Sentinel-2 images were utilized to detect and monitor supraglacial lakes on seasonal basis. Sentinel-2 imageries with 10-m spatial resolution and 5-day temporal resolution can potentially be used for mapping the lakes of sizes >500 m^2 using in combination of automatic and manual methods, which may help to understand the short-term variations of the lakes with higher accuracy.

6.2 High-resolution inventory of the glaciers and glacial lakes

Latest inventory of the glaciers and glacial lakes in the Everest region was prepared using 2-m spatial resolution imageries. Imageries used for this inventory were obtained from the DigitalGlobe Foundation and mapping was conducted for the year 2016, where images of the year 2015 was also employed for the part of study area. Sentinel-2 images of 10-m spatial resolution was used for Thyanbo Glacier. The aim of the preparing high-resolution inventory of the glaciers and glacial lakes was to update and improve the past inventory for the Everest region with high accuracy.

This study revealed the 109 glaciers with the total surface area of 268.22 ± 1.46 km^2. Muller (1970) estimated the total number and area of the glaciers in 1970 for the Bhote Koshi, Ngozompa Glacier, and Imja Khola basins, which were 164 and 360 km^2, respectively. Similarly, Higuchi et al. (1980) documented 279 glaciers in the same region in the 1970s. Bajracharya et al. (2014) reported the 128 glaciers (343 km^2) in 1980 and 132 glaciers (262 km^2) in 2010. The discrepancy in the number of glaciers may be due to the methods applied, and retreat and fragmentation of the glaciers in the recent period. This was attributed to the disappearance of small sized glaciers over the period of the >30 years. Continuous retreat of the glaciers has been observed in past studies (Shiraiwa, 1993; Benn et al., 2012; Bajracharya et al., 2014; Thakuri et al., 2014; Bolch et al., 2019), and retreat of the glaciers in the Dudh Koshi region was observed since the 1970s (Fushimi and Ohata, 1980).

In this study, results of glacier mapping presented the 97% of glaciers with less than 2% uncertainty (Table 6.1), where uncertainty was larger in the past studies when they applied 30-m spatial resolution images. Similarly, in this study, isolated ice masses within the glacier basin also included as the part of the large glacier and considered as single glacier, which was another reason of larger surface area and less number of glaciers than the ICIMOD inventory of 2010.

The inventory of the glacial lakes in the Everest region exhibited the 349 lakes (7.4 km^2) in 2001 (Mool et al., 2001) and 148 glacial lakes (5.50 km^2) in 2009 (ICIMOD, 2011). These results presented the decrease in the number from 2001 to 2009 due to the use of different datasets and methodology (ICIMOD, 2011). Similarly, 143 glacial lakes of size 7.51 km^2 were mapped by Khadka et al. (2018) in 2017. They presented the greatest expansion of lakes in the Everest region. They used the Landsat images of 30-m spatial resolution and uncertainty of mapping increased with low-spatial resolution satellite images (Watson et al., 2016). Therefore, in this study, high-resolution inventory of the glacial lakes was prepared using semi-automatic method, where inventories improved by manual inspection and editing. Further, lake boundaries were crosschecked with the 0.5-m spatial resolution panchromatic WorldView imagery. Therefore, results of this inventory assumed as accurate mapping of the glacial lakes for the Everest region. All the glacial lakes were mapped with size of >20 m^2, and revealed the 3,290 glacial lakes with the total area of 8.11 ± 0.45 km^2. This inventory was first of its kind to map the water bodies in the Everest region to cover the whole area using the very high-resoution satellite imageris.

In this study, the total uncertainty of the lake mapping was 5.5%, whereas uncertainty were >18% in the previous inventories by Salerno et al. (2012) and Khadka et al. (2018). Therefore, results obtained from this research is more realistic than previous studies (ICIMOD, 2011; Salerno et al., 2012; Khadka et al., 2018), which have used the 30-m Landsat imageries. The surface area of the lakes increased by about 9% from 2008 corresponding the surface area of lakes plotted by Salerno et al. (2012).

Similarly, inventory of glacial lakes in the Kangchenjunga region using 10-m resolution Sentinel-2 imageries revealed the 373 glacial lakes with the total area of 6.18 ± 0.75 km^2 in 2018. Current results were comparable with ICIMOD (2011) and Khadka et al. (2018), which estimated the total surface area of lakes 6.57 km^2 and 6.05 km^2, respectively. The results by Shrestha et al. (2017) for the whole Tamor basin showed larger surface area of lakes (8.73 km^2) than the current study. Minor discrepancies was attributed to uncertainty associated with coarse-resolution images. The discussions of each type of lakes is presented in the following sections.

6.2.1 Supraglacial lakes

Supraglacial lakes were dominant features in the Everest region, and they contributed about 91% of the total number of lakes. These features were highly variable in space and time, and their lifetime is unpredictable (Benn et al., 2001). High-resolution inventory of supraglacial lakes at the surface of the 23 debris-covered glaciers in the Everest region accounted for 25% of total water surface and 0.18% of area of the upper DKR basin. In case of the Kangchenjunga region, supraglacial lakes accounted about 37% of total number of lakes and 9% of the total surface area of lake. Considering all the study glaciers, supraglacial lakes covered an average of 1.53% and 0.8% of the area of the debris-covered glaciers in the Everest and Kangchenjunga regions, respectively. Similarly, supraglacial water surface in the Everest and Kangchenjunga regions cover an average of 0.78% and 0.15% of the regions' total glacial area, respectively. Using Landsat data, Miles et al. (2017b) observed supraglacial lakes covering 1.4% of the Langtang basin's debris-covered area and 0.39% of the total glacial area. Gardelle et al. (2011) estimated the supraglacial lakes covering 3.4% and 0.85% of the debris-covered area of the Khumbu Glacier and Lhotse Glacier, respectively in the Everest region. The results of this study (Table 3.5) showed that percentage cover of supraglacial lakes were 3.89% and 1.54% for the Khumbu and Lhotse glacier, respectively, exhibiting the increase of percentage cover of the lake surface. Salerno et al. (2012) reported lakes covering from

0.29% to 2.07% of the total glacier surface in the Everest region using AVNIR-2 image (2008) of 10-m spatial resolution. A more recent study by Khadka et al. (2018) considered the >4 Landsat pixels (3,600 m^2) and showed the supraglacial lakes covering 0.76% and 0.49% of the total debris-covered area in the Everest and Kangchenjunga regions, respectively. Overall, increase in the surface area cover of lake was observed. The analysis presented the slightly higher density of the supraglacial lakes due to the use of higher resolution satellite images and threshold used in this study. Supraglacial lake surface area was 1.19% and 0.57% of the total debris-covered glacier area when the result was limited to threshold of 3,600 m^2 with the mean size of 0.015 km^2 and 0.010 km^2 in the Everest and Kangchenjunga region, respectively. This result has very close agreement with the results of Miles et al. (2017b) and Khadka et al. (2018).

Moderate resolution Sentinel-2 image could not map the lake size <500 m^2 with adequate accuracy; therefore, lakes with size <500 m^2 were considered for the inventory in the Kangchenjunga region. Use of Sentinel-2 in the Everest region estimated the 375 supraglacial lakes (1.70 km^2) and enabled to map 83% of the WorldView water surface area in 2016. The number of supraglacial lakes in the pre-monsoon season of 2018 was 463 with the surface area of 2.09 km^2 in the Everest region. Result showed the larger number and surface area of the supraglacial lakes in the Everest region than in the Kangchenjunga region using the same spatial resolution images in 2018. This can be attributed to the difference in area of debris-covered part of the glaciers. The Kangchenjunga region exhibited the larger area of the glaciers and basin than the Everest region. The Dudh Koshi basin has the largest proportion (28.1%) of the debris-covered glaciers and the majority of the glaciers oriented towards south and southeast in this region (Bajracharya et al., 2014).

The density of the supraglacial lakes is associated with the melt of the ice underneath of debris, which is determined by thickness of debris. A thin layer of debris enhances melt, while a thick layer of debris insulates the underlying ice and reduces melt (Östrem, 1959; Nicholson and Benn, 2006; Chand et al., 2015). Information and study related with the amount of debris at the surface of the glaciers in the Kangchenjunga region are not available and need future investigation to understand the relationship between the area of supraglacial lakes and debris thickness.

The smallest lakes mapped were the size of 20 m^2 and density of smaller lakes with size of >100 m^2 and >1,000 m^2 accounted about 90% and 54%, respectively to the total number of supraglacial lakes in the Everest region. These results suggested the typical

size of the supraglacial lakes on the surface of the Himalayan glaciers was dominated by the size <1,000 m^2. Lakes with size >0.03 km^2 were not evident at upstream of the spillway lakes. Exceptionally a supraglacial lake of size 0.21 km^2 was observed on the surface of the Khangri Nup Glacier (Figure 6.5a) and another lake of size 0.13 km^2 on the tributary of the Khumbu Glacier. Therefore, it can be said that supraglacial lakes of size between 20 m^2 and 0.03 km^2 existed throughout the surface of the glaciers with some exception in the Nepal Himalaya (Figure 6.5b and c).

The high-resolution inventory, annual, and seasonal study of the supraglacial lakes in the Everest region showed the presence of spillway lakes (Figure 3.19) at the termini of eight glaciers. These spillway lakes were relatively larger than the lakes in the upstream. Unlike, no typical spillway lakes were observed in the Kangchenjunga region, though a few lakes observed to be transformed into proglacial lakes. The discussion about development of spillway lakes and their trajectory is provided in section 6.4.

6.2.2 Unconnected lakes

Unconnected glacial lakes are either glacier-fed or non-glacier-fed, and are without direct connections with glaciers. The examples of glacier-fed and non-glacier fed-lake are shown in Figure 6.6. The unconnected lakes exhibited the largest surface area in both sites, where these lakes accounted for 45% (3.68 ± 0.1 km^2) and 53% (3.27 ± 0.46 km^2) of the total lake area with the mean size of 0.014 and 0.015 km^2, respectively for the Everest and Kangchenjunga regions. The majority of unconnected glacial lakes were located in the Ngozompa Glacier basin among 10 sub-basins within the Everest region, where 93 lakes with the surface area of 1.90 ± 0.04 km^2 (49%) were plotted. Similarly, unconnected lakes were most prevalent in the Tamor Khola basin (at Olanchungola) of the Kangchenjunga region, where 71 unconnected lakes were maped with the total surface of 1.80 ± 0.16 km^2, corresponding to 55% of unconnected glacial lakes. Salerno et al. (2012) reported the surface area of 2.41 km^2 for unconnected glacial lakes in the Ngozompa Glacier basin was slightly larger than this study. The difference was attributed to classification system of lakes and spatial resolution of the image used in the study. Some of the lakes at the termini of the glaciers were classified as unconnected lakes in their study, which were considered as supraglacial lakes in this study.

Unconnected lakes are being isolated from the glaciers and are supposed to be fed by runoff water preferably through snowmelt in the Kangchenjunga region. These lakes were mainly concentrated in western part of the region of less glacierized region. The

number of these lakes increased by 9.4 times from 1964 to 2018, while area increased by 3.3 times than in 1964 (Table 5.5). The increase in the number and area of the unconnected lakes was due to the loss of glacier area, which is evident from several past studies (Bolch et al., 2008a; Ojha et al., 2016; Lamsal et al., 2017; Maurer et al., 2019). The relationship between surface area of lakes and corresponding watershed area has been reported to be influenced by the amount of precipitation (Salerno et al., 2012). Therefore, monitoring of these lakes provides useful indications of the precipitation trend in climate change scenario.

6.2.3 Proglacial Lakes

Proglacial lakes were least frequent topology in both study regions; however, they contributed 30% and 38% in the total surface of the lakes in the Everest and Kangchenjunga regions, respectively. This topology featured the largest average size, i.e., 0.15 km^2 and 0.17 km^2 in both regions, respectively. Imja Glacial Lake re-accelerated its expansion of area from 1997 – 2007 and this has been repeatedly cited as one of the most dangerous glacial lakes in the Himalaya (Watanabe et al., 2009) (Figure 6.7). This lake is one of the most studied GLOF-risk lakes in the world (Mool et al., 2001; Fujita et al., 2009; Somos-Valenzuela et al., 2014b; Rounce et al., 2017). This study found the lake surface area of 1.43 ± 0.01 km^2, which was plotted using WorldView image of the year 2016. Khadka et al. (2018) assessed the same lake using Landsat image of the year 2017, and found the surface area of 1.44 ± 0.11 km^2. The lake had an area of 0.98 km^2 in 2008 measured by Salerno et al. (2012) with AVNIR image of 10-m resolution. These statistics presented the continuous expansion of the lakes since its formation in the 1960s (Lamsal et al., 2011). It has recently undergone channelized drainage, stabilizing its outlet (Haritashya et al., 2018); however, the lake is continuously growing by glacier calving even after the lake lowering works.

6.3 Spatial, temporal and seasonal variability of supraglacial lakes

Satellite imageries with different resolutions ranging from 2-m to 30-m were utilized to study the long-term development and short-term variation of the glacial lakes as well as to prepare the high-resolution inventory. Annual, seasonal and spatial variabilities of supraglacial lakes were focused to understand their dynamics over the different periods and different glaciers in the Everest region. Previous studies on supraglacial lakes in the Everest region were conducted by using single image or by using

imageries, which covered part of the region or by decadal timespan studies (Salerno et al., 2012; Watson et al., 2016; Shrestha et al., 2017). However, year-to-year variations of the lakes and their spatial hetereogeneity are required to understand their dynamics on studied glaciers. Here, the year-to-year, season-to-season, and glacier-to-glacier variations of the supraglacial lakes were presented for the SNP, Nepal.

The results from historical study revealed an increase in the number and area of the supraglacial lakes with the substantial temporal, spatial, and seasonal variations. However, seasonal variability between the pre-monsoon and post-monsoon was not clear. The detection of substantial increase in the area of supraglacial lakes suggested that ice melt is increasing at a higher rate in recent time periods (Sherpa et al., 2017; Acharya et al., 2018), and ice melt occurs more at ice cliffs with supraglacial lakes (Sakai et al., 1998; Reynolds, 2000). Lakes that occupy a closed basin with no perennial connections can undergo rapid growth (Benn et al., 2001). Similarly, development of new lakes increase the heat absorption, which increases ice melt through under- and side-cutting (Sakai et al., 2000). The development of new lakes also enhance the growth by the action of coalescing.

The increase in the area and number of lakes can be attributed to the increase in temperature in this region. Asian Precipitation–Highly-Resolved Observation Data Integration Towards Evaluation of the Water Resources (APHRODITE) datasets (APHRODITE, 2019) were used to understand the general trend of temperature for the region. Point data at an elevation of 5,000 m a.s.l. were extracted from the gridded dataset. Temperature showed a decreasing trend (-0.04 °C y^{-1}) from 1961 to 1988 (Figure 6.8a) and an increasing trend (0.02 °C y^{-1}) from 1989 to 2015 (Figure 6.8b). Significant surface-lowering of glaciers in many parts of the Himalayas has been observed (Bolch et al., 2012; Kääb et al., 2012; Acharya et al., 2018) with the increase in temperature.

Continous lowering of the glacier surface resulted in the lowering of the gradients and velocities (Quincey et al., 2009), which favors the development of supraglacial lakes (Benn et al., 2001; Shrestha et al., 2010; Li et al., 2015). Wastage of glaciers in the recent period provides the sufficient melt water to develop the supraglacial lakes and helps in expanding their size (Röhl, 2008; Benn et al., 2012; Thompson et al., 2012), which may likely grow monotonically if glaciers continue losing their mass (Benn et al., 2001). The expansion in lake area contributes substantially to ablation of the glacier due to undercutting, calving, and melting imposed by water surface.

The results of seasonal variation of the supraglacial lakes obtained from the 10-m imageries showed the intra-annual dynamics for three seasons; pre-monsoon, post-

monsoon and winter, corresponding to seasonal variability of ice melt (Chand et al., 2015; Chand and Kayastha, 2018). Here, monsoon season was excluded from the measurement because satellite observations during the monsoon periods were severely limited by sporadic cloud cover. Considering the three seasons for analysis, supraglacial lake cover in the Everest region showed the least area during the winter season, while it was comparable in the pre-monsoon and post-monsoon seasons. Seasonality of the lakes by previous studies due to the ablation processes of the glaciers in different seasons has been reported (Qiao et al., 2015; Miles et al., 2017b). The main reason for the less surface area of the lakes in the winter season is the unavailability of melt water. Further, presence of a frozen surface also hindered the accurate mapping. It was assumed that most dynamic activity of the supraglacial lakes occurred during the monsoon season due to large precipitation and high temperature. Because studies during the monsoon season are obscured by the clouds in optical images, and Radar satellite images might be potential to understand the short-term dynamics during the monsoon season.

6.4 Future trajectory of the spillway lakes

A significant increase in the area and number of supraglacial lakes in the study regions was clearly observed. The density and size of the supraglacial lakes were larger in the Everest region than those in the Kangchenjunga region. Therefore, spillway lakes near the termini of galciers in the Everest region were studied to understand their trajectory towards large glacial lakes.

The lakes which are located above the level of outlet channel of the glacier can grow until they are intercepted by an englacial conduit, and may fully or partially drain (Benn et al., 2000). However, nearly half of the total area was contributed to by the supraglacial lakes near the terminus (up to ~2 km) of the glaciers where the slope was 0–4°. The highest densities of the supraglacial lakes (Figure 6.9) and high persistent lakes with size >5,000 m^2 were observed at the termini of the four larger glaciers (Figure 4.12) suggested that these glaciers have the potential to form large lake. A series of lakes may evolve into a large glacial lake (Watanabe et al., 1994, 2009; Benn et al., 2000; Lamsal et al., 2016), corresponding to warming temperatures and a trend of negative glacier mass balance (Gardelle et al., 2013; Shea et al., 2015; Sherpa et al., 2017) if the level of outlet channel remains at the same elevation. An increasing temperature can reduce the snow extent, and reducing albedo also reduces glacier extent (Li et al., 2015), which provides more melt water to the glacial lakes. Furthermore, an increase in the area by 16% from

the 1990s to 2016 was estimated for the debris-covered portion of the glaciers in the Everest region, which increase the possibility to form and expand glacial lakes in the future. Lakes with sizes <0.1 km^2 have been considered as less hazardous (Aggarwal et al., 2016); however, drainage of supraglacial lakes with sizes <0.1 km^2 also has a potential for GLOFs (Rounce et al., 2016a; Miles et al., 2018) by coalescing several small lakes and contributing water from englacial storage. Therefore, an estimation of the volume of these features is required (Watson et al., 2016) to understand the potential flood volume. Area-volume relationships was used (Fujita et al., 2013; Cook and Quincey, 2015; Watson et al., 2016; Miles et al., 2018) for the volume estimation to make a first-order estimate of volume for the spillway lakes. Howvere, it is necessary to carryout field measurements for accurate estimation.

The spillway lakes on the Ngozompa, Bhote Koshi, Khumbu, and Lumsamba glaciers (Figures 6.10 and 6.12) appeared to have the greatest potential for developing into large glacial lakes. This corresponds to the dominance of very gentle slopes (<2°) (Reynolds, 2000; Quincey et al., 2007; Sakai and Fujita, 2010), stagnant glacier termini (Quincey et al., 2009), and higher mean DGM (>60 m) (Sakai and Fujita, 2010). Furthermore, most of these lakes were associated with islands of ice with cliffs, and well-built terminal moraines, which also favor a trajectory towards the large glacial lakes (Watson et al., 2016). Additionally, the lake-terminating glaciers which are rapidly retreating showed maximum thinning towards their termini (King et al., 2018). These glaciers also indicate the sign of lake expansion. It is possible that the lowering of the glacier's surface leads to a reduction in the gradients and may enhance the possibility of the development of glacial lakes (Sakai and Fujita, 2010).

Additionally, complex of lakes were observed at the termini of the Melung, Nuptse, Chhule and Thyanbo glaciers, which have relatively smaller size than the above described glaciers (Figure 6.12). However, growth pattern of these lakes showed continuous expansion with the minor variability from 1989 to 2018. Series of lakes connected through narrow channel were observed in the centerline of the Melung Glacier (Figure 6.12a), while scattered lakes of different sizes were mapped for the Chhule Glacier (Figure 6.12b). The Nuptse Glacier displayed the formation of lakes and their expansion in recent years (Figure 6.12c), while spillway lakes were observed only after 2010 in two tributaries of the Thyanbo Glacier, which presented the rapid expansion in last few years (Figure 6.12d). The estimated slope of these glaciers was also prevailed by <6° and

coalescing of the smaller lakes and formation of large glacial lake can be expected (Figure 6.13).

Unlike the situation in the Everest region, typical spillway lakes were not observed in the Kangchenjunga region. The spillway lakes at the termini existed before either already transformed into proglacial lakes through emergence of new lakes and their coalescence or not persisted for several years. The details of the proglacial lake development in the Kangchenjunga region is presented section 6.5.

6.5 Decadal changes in the surface area of proglacial lakes

In Chapter 5, historical growth from 1964 to 2018 (54 years) of the proglacial lakes was examined for the Kangchenjunga region, where studies were extremely limited. Result obtained from Sentinel-2 image of 2018 plotted the 14 proglacial lakes with the surface area of 2.34 ± 0.12 km^2 in the region. Decadal analysis of proglacial lakes presented the increase in the area at rate of 0.032 km^2y^{-1} from 1964 to 2018 in the region. Largest rate of increase (0.10 km^2y^{-1}) observed in the earliest period (1964 – 1975). There was a relatively slower increasing rate between 1975 and 1987 (0.02 km^2y^{-1}) and between 1987 and 2000 (0.01 km^2y^{-1}) than between 2000 and 2010 (0.03 km^2y^{-1}). Thereafter, lake area remained stable between 2010 and 2018.

Proglacial lakes are more susceptible to outburst, and can cause loss to downstream region than the supraglacial lakes due to their physical setting, size, and steep lakefront area. Although several supraglacial lakes are more close to an avalanche and rockfall prone area than the proglacial lakes, possible water displaced from the supraglacial lakes need to cross long distance through heterogeneous surface of the glacier. There are cases of flood flow through englacial channels once they find the connection (Rounce et al., 2016a), but hazards associated with these features will be less than the proglacial lakes of large size. Several proglacial lakes were developed to their full extent. There is a limited possibility of expansion as they are losing their connection with the glaciers, while several lakes were still growing in size that contains water volume up to 112.3×10^6 m^3 as observed in case of the Lower Barun Lake (Haritashya et al., 2018). Retreat of the glacier front due to calving has the significant contribution for their expansion (Pelto et al., 2013) along with meltwater received from the glacier. The significant calving in the Imja Glacier was observed, where several floating icebergs were observed in the Imja Lake during the melt season (Figure 6.14).

Further, new lakes were in their way to become a large glacial lake in the future, which was indicated by the increasing trend of temperature in the Everest region (Figure 6.8). However, many of them were positioned in the avalanche or rockfall prone area, and possess a high risk for the downstream region. The fragile ice-cored dam makes them more susceptible to breach once ice under the moraine melts. Physical setting of lake, lake area and volume, and GLOF triggering factors, e.g., avalanche, rockfall, condition of dam are dynamic in nature. Therefore, the existing categorization of the lakes into potentially dangerous category of different class must be regularly updated.

6.6 GLOFs

6.6.1 Past GLOFs

Nepal has experienced the greatest national-level economic consequences (22% of global total) due to the GLOFs (Carrivick and Tweed, 2016). The total number of GLOF events in Nepal documented from different sources by ICIMOD (2011) were 24, out of which 14 were originated in Nepal and 10 originated in Tibet, which caused floods in Nepal (Figure 6.15). Further, recent GLOFs in the upper Barun Valley in 2017 (Byers et al., 2019), Bhote Koshi/Sun Koshi River in 2016 (Cook et al., 2018) have caused geomorphic and infrastructure damages, and fatalities. Additionally, floods that originated from supraglacial lakes are also recorded on the Lhotse Glacier in 2015 and 2016 (Rounce et al., 2016a), and Khangri Shar Glacier in 2017 (Miles et al., 2018). The potential flood volume from the supraglacial lakes assumed to be smaller, and associated hazard could be minor due to their small size in comparison to the large glacial lakes.

Most GLOFs occurred in the remote and less inhabited regions. In such cases, no or less data availability on the past GLOFs can cause substantial misunderstanding, especially for the GLOF events that happened prior to the era of the satellite remote sensing (Nie et al., 2018). Several GLOFs that caused serious floods in Nepal have not been studied, although some of them appeared in the national newspapers. In, Chapter 5, historical GLOF events were traced for the Kangchenjunga region using CORONA satellite images from 1962 to 1980. In total, six GLOFs were identified including the Nangama GLOF of 1980, and are assumed to be of different size. Out of six GLOFs, two events were identified in each of the Ghunsa, Yanma, and Tamor Khola River sub-basins. Based on the changes in morphology around the source area and downstream region, Nangama GLOF in the Yanma Khola basin and Olanchungola GLOF in the Tamor Khola

basin assumed to be the largest GLOFs in the region. These GLOF caused the breach of the lake dams and significant erosion along the river bed and side with deposition of debris materials (Figures 5.15 and 5.16). The Nangama GLOF is documented in past studies (Yamada and Sharma, 1993; Watanabe et al., 1998; Mool et al., 2001; ICIMOD, 2011; Fujita et al., 2013); however, impact assessment was not carried out for this lake. The Nangama Lake developed a steep lakefront area in 1975, which had the significant potential flood volume (32.8×10^6 m^3) (Fujita et al., 2013).

The results obtained from this study can be used for 'first-pass' hazard assessment in the regions where field access is difficult (Quincey et al., 2007). Further detailed studies of the morphological characteristics of glaciers and the regular monitoring of lakes are required to understand the risk of GLOFs and glacier-related hazard management. More attention should be paid to rapidly expanding glacial lakes with high possibility of repetitive outbursts (Nie et al., 2018).

6.6.2. Future GLOFs

The main reason of the current expansion of the large glacial lakes including the Imja Lake can be attributed to the calving of the glacier, which is enhanced by the action of lake water. Imja Lake is believed to have probable change its status from moderate to high risk as its expansion will be susceptible cause surge waves by by avalanche (Rounce et al., 2017). Similarly, Dig Tsho Glacial Lake in the Bhote Koshi basin (at Thame) also one of the most studied glacial lakes in the Nepal Himalaya, as this lake experienced GLOF in 1985 (Vuichard and Zimmermann, 1987). However, this lake is still considered as one of the riskiest lakes since it will potentially impact the largest number of buildings (Rounce et al., 2017). However, Dig Tsho Lake was removed from category of "potentially dangerous" by the ICIMOD (2011), where they showed the complete breach of the end moraine and formation of low-level outlet channel. These outcomes are contradicting to each other and need further investigations. Not only the Imja and Dig Tsho lakes, but also all lakes need to be monitored continuously. The Everest and Kangchenjunga regions are most popular destinations for the tourists and have international attention. Any hazards occurred in the region may significantly affect the tourism industry of the region, where the majority of the people sustain their life from trekking tourism.

The Nangama Lake (Figure 6.16a) in the Yanma Khola basin of the Kangchenjunga region, upper Tamor River basin (at Lelep) was found the largest lake in the region with

size of 0.69 ± 0.02 km^2, which is one of the potentially dangerous glacial lakes in the Nepal Himalaya (ICIMOD, 2011). Similarly, Lahare Lake (Figure 6.16b) and Khanlananma Lake (Figure 6.16c) are also categorized as potentially dangerous glacial lakes with low priority (ICIMOD, 2011), which have the area of 0.18 km^2 and 0.27 km^2, respectively. Phuchan Glacier (Watanabe et al., 1988) with the size of 6.9 km^2 has its terminus hanging upside of the Nangama Lake (Figure 6.16a), and there is limited possibility of further expansion of the lake in future.

Yagmachhe Khola originates from the Khanlananma Lake that meets the Shimbuwa Khola River at Chheram. The clear end moraine of the lake was not visible in the Sentinel-2 image (Figure 6.16c) and water can be easily overtop the dam in case of avalanche or rockfall. Slope immediately after the lake found >20° and lake with steep lakefront area (SLA) have potential to suffer a GLOF (Fujita et al., 2013). This may attain its maximum possible speed and can have detrimental effect to lake's downstream. Similarly, geomorphology around the Lahare Lake revealed the breached end moraine (Figure 6.16b), and GLOF events assumed to be occurred in the past. Hanging glacier from the Chhochenpu Himal with slope >30° increase the possibility of avalanche and rockfall from the upstream region.

The growth of the Tilpile Lake was observed towards northwest side at calving front of the glacier. Glacier name associated with the lake is not mentioned in the topographic map, which is named here as Nobuk Glacier since it is originated from the Nobuk peak. The lake gained the size greater than two other lakes, i.e., Lahare and Khanlananma lakes in the region, which are categorized as potentially dangerous lakes by ICIMOD (2011). Further, Tilpile Lake has potential to grow in future as it has debris-covered glaciers with gentle slope towards the upstream side. Undercutting action of lake water has a significant role to retreat of the glacier and can cause rapid expansion.

The peak discharge in GLOF event that originated from supraglacial lakes on the Lhotse Glacier was estimated to be 210 ± 43 m^3s^{-1} and the total maximum flood volume of 2.65×10^6 m^3 (Rounce et al., 2016a). The stored water within englacial conduits through hydraulically efficient pathways, and/or catastrophic glacier buoyancy supplemented this event. Therefore, catastrophic GLOFs might occur where series of supraglacial lakes existed and interconnected with each other. Such events can cause as triggering factor for large proglacial or spillway lakes at the terminus of the glaciers. A database of the GLOF events obtained from this study will be helpful to reveal the process and mechanism of the GLOF for hazard assessment, mitigation, and consequently risk management.

Therefore, archive of the historical GLOFs is essential for risk management for the glacial lake downstream region.

Besides the lakes described above, remaining lakes were also found at different physical setting of slope, elevation, avalanche prone areas. Glacial lakes may burst out due to several natural factors, i.e., avalanche, rockfall, moraine failure, seismic activities, and need to monitor closely to assess the hazard and risk associated with possible GLOFs and impacts on downstream environment, settlements, and infrastructures. Therefore, geomorphological setting of the lakes need to be continuously monitored, and mitigation effort need to be implemented based on category the lake. Areal expansion, physical setting of the glacial lake are an important information to understand basic physical status of the glacial lakes, and further detailed investigation including field-work on hazards and risk assessment such as hydraulic and geotechnical properties of dam, topography, population, and infrastructures downstream are suggested for the future study.

6.7 Climatic trends over Nepal

Temperature trend at single point was analyzed using APHRODITE reanalysis dataset at an elevation of 5,000 m in the Everest region and discussed in section 6.3. A recent report on the climatic trends of Nepal showed the significant positive trends of annual and seasonal maximum temperature all over the country (DHM, 2017). The positive maximum temperature trend was highly significant in the all physiographic regions and seasons. The annual maximum temperature over Nepal is increasing at the rate of 0.056°C yr^{-1}, while the highest positive trend of the maximum temperature was 0.058°C yr^{-1} (Figure 6.17). The higher positive temperature trends were observed in the high mountain districts, and the Taplejung district in the Kangchenjunga region, which is the district with the largest temperature trend (0.091°C yr^{-1}) in the country. Similarly, Solukhumbu district, where the Everest region lies also displayed the high positive temperature trend (0.076°C yr^{-1}), larger than the mean trend over whole Nepal. The minimum temperature also showed the increasing trend but it was significant only in the monsoon season. These trends were larger than the world's average trend of 0.05°C $decade^{-1}$ (IPCC, 2014), and glaciers of the Nepal Himalayas are vulnerable to this warming. The higher trends in the high mountain regions imply that several new and large glacial lakes are potential to develop in the future. This condition also favored by the annual precipitation trend, which showed decreasing trend in the majority of the districts. Monsoon precipitation plays a significant role in accumulation of glaciers in the Nepal

Himalayas, which showed the negative trend in the high mountain regions. This negative trend of precipitation enhanced the loss of glacier mass and formation of glacial lakes.

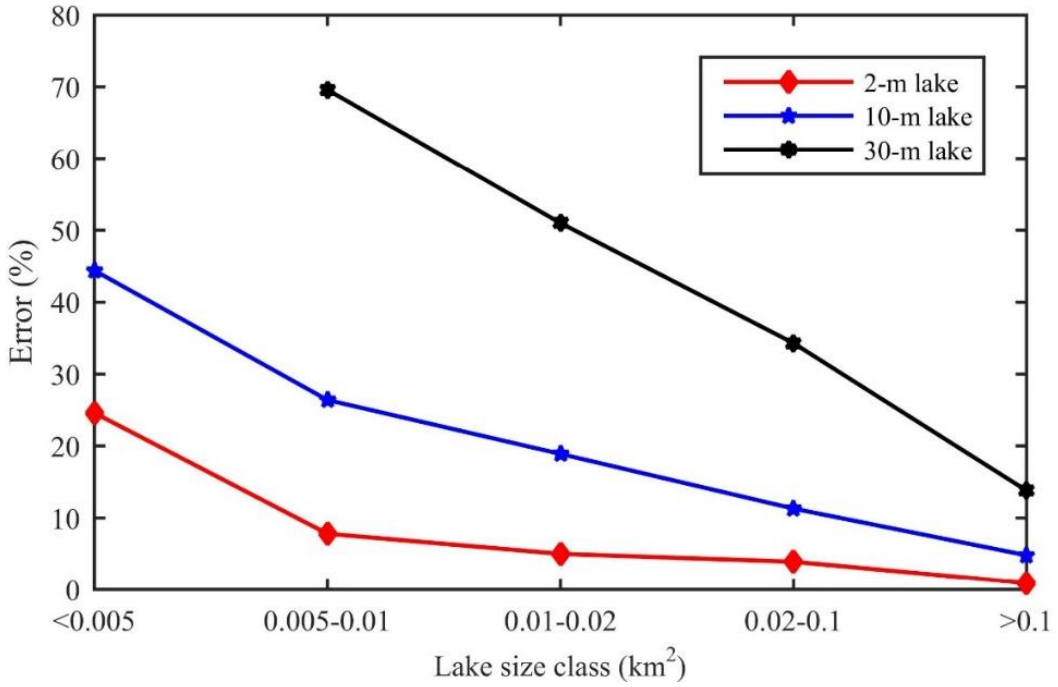

Figure 6.1 Uncertainty of surface area measurement among different spatial resolution images.

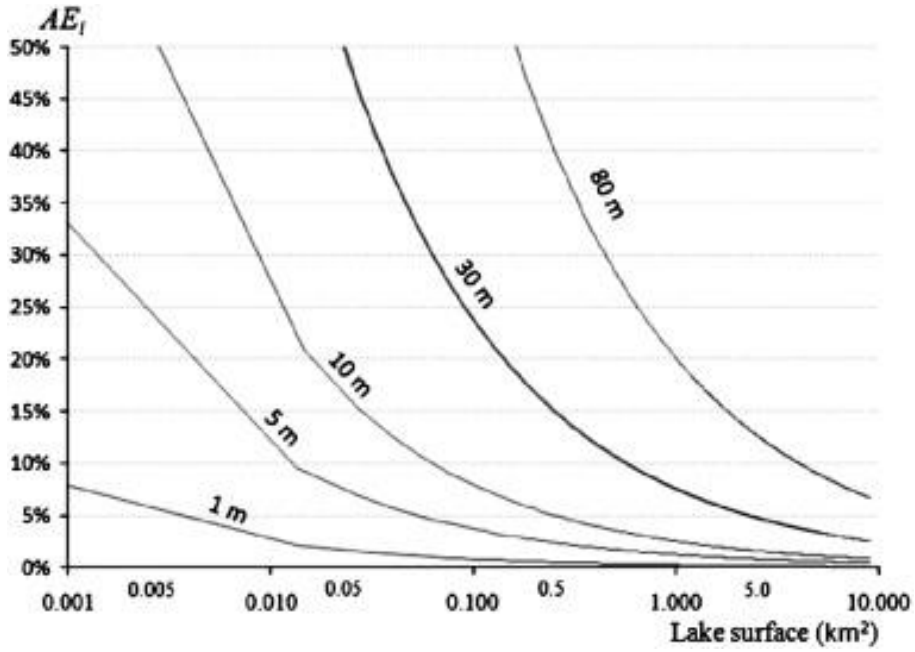

Figure 6.2 Relationship between the hypothetical surface of circular lakes and the respective uncertainty of measurement according to sensors that differ by degree of resolution (Salerno et al., 2012).

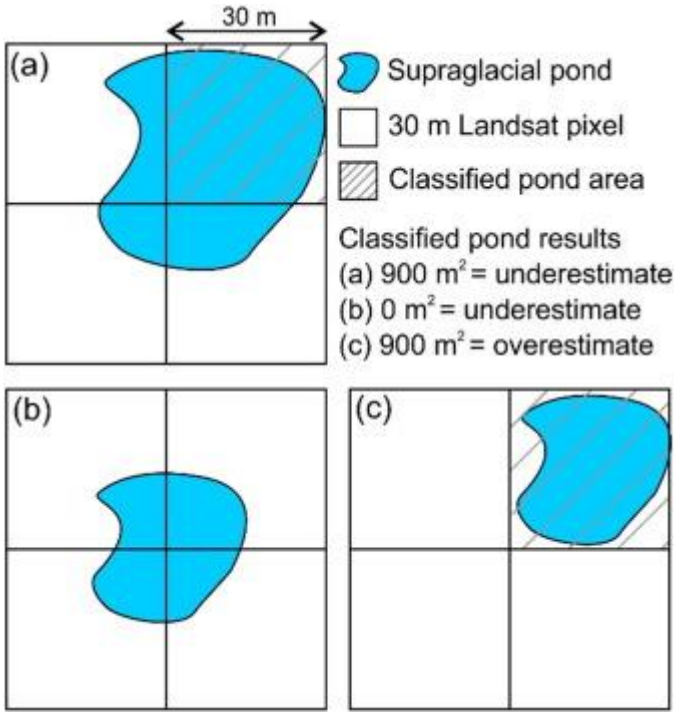

Figure 6.3 Hypothetical lake classification scenarios using Landsat imagery taken from Watson et al. (2016). The lake is larger than one pixel but covers a small proportion of three adjacent pixels (a), the lake is aligned at the center of four pixels but does not dominate any (b), and the lake is smaller than one pixel but dominates the spectral signature and classified as one pixel in size (c).

Table 6.1 Distribution of mapping uncertainty for glaciers and lakes plotted using satellite images of 2-m spatial resolution in the Everest region.

	Glaciers			Lake		
Uncertainty class	No	Area (km^2)	%	No	Area (km^2)	%
<1	36	249.05	92.9	5	3.22	39.7
1-2 %	44	11.11	4.1	9	1.00	12.3
2-5%	30	7.94	3.0	63	1.57	19.4
5-15%	1	0.12	0.0	262	1.65	20.4
>15%				2951	0.67	8.2
Total	109	268.22	100.0	3290	8.11	100.0

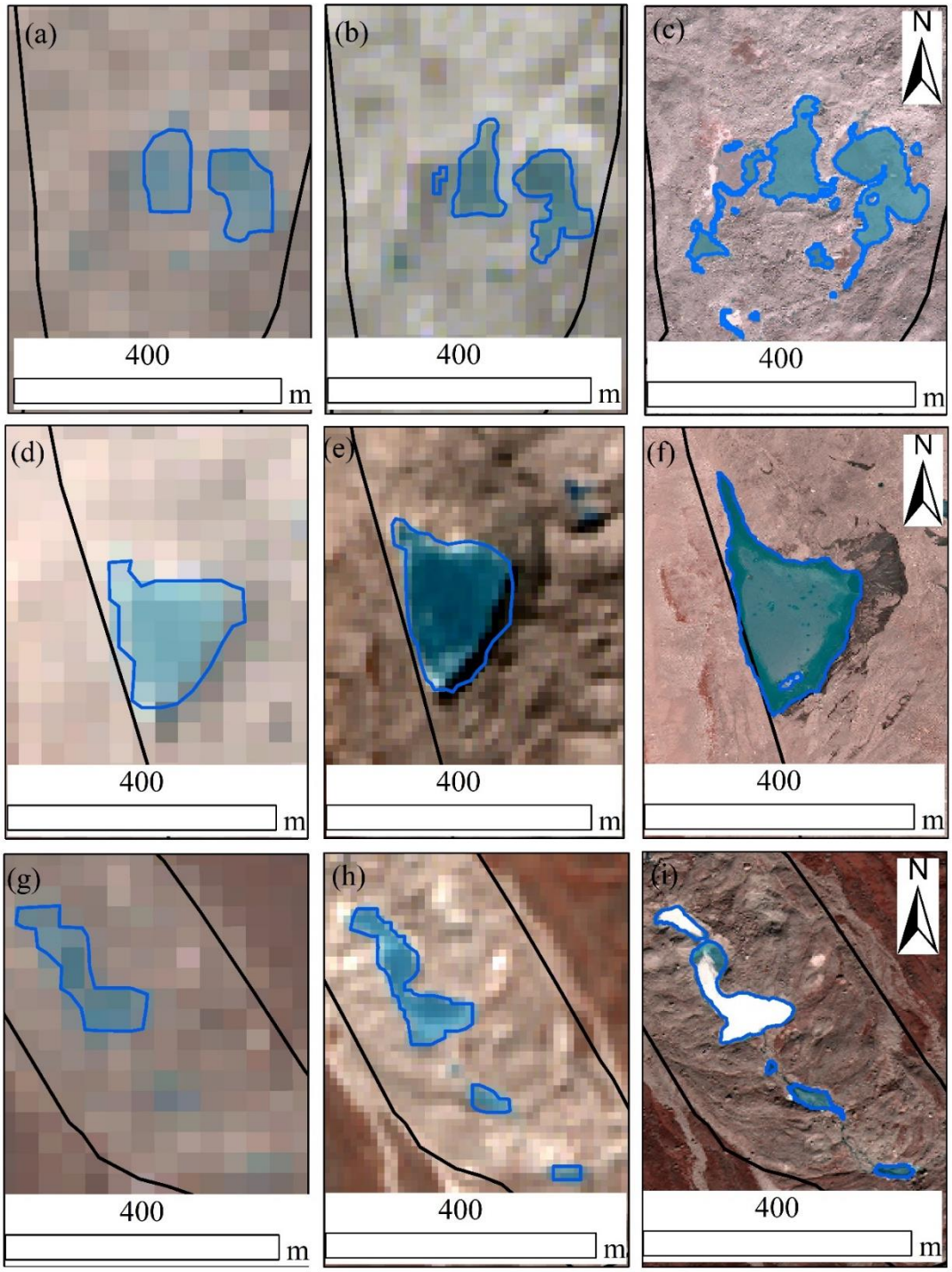

Figure 6.4 Examples of supraglacial lakes obtained with the Landsat (a, d, & g); Sentinel-2 (b, e, & h); WorldView-2 (c & i); and GeoEye-1 (f) on the surface of the selected glaciers, i.e., terminus of Nuptse Glacier (a, b, & c), near terminus of the Ngozompa Glacier (d, e, & & f), and terminus of the Melung Glacier (g, h, & i).

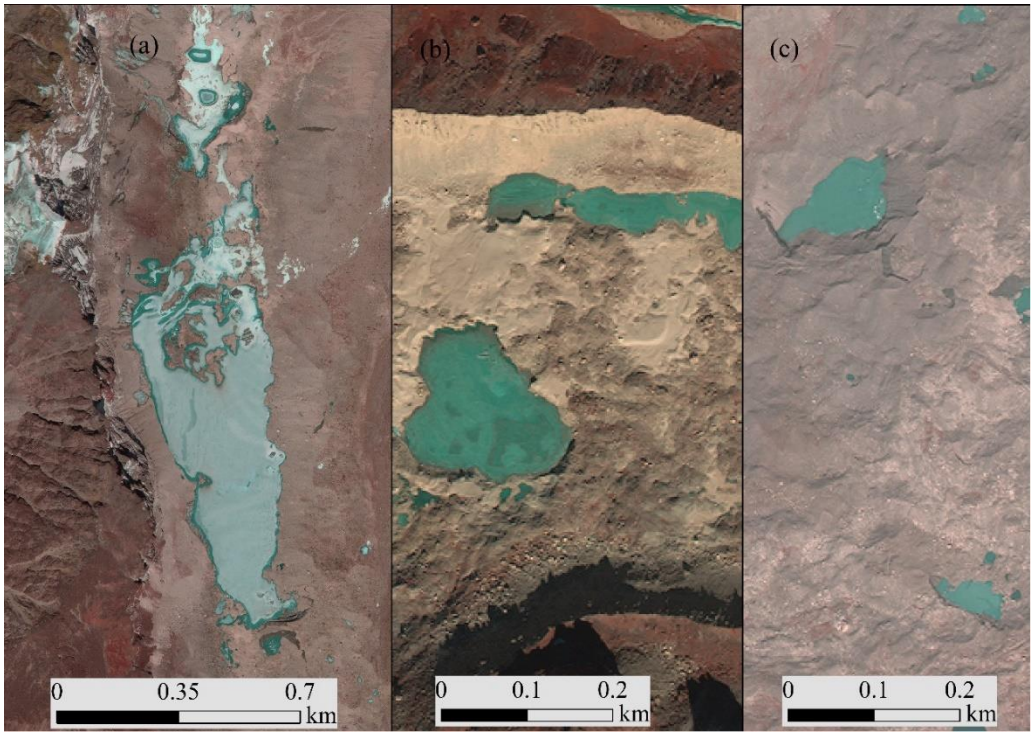

Figure 6.5 WorldView images showing supraglacial lakes in the Everest region. Largest supraglacial lake observed in the Khangri Nup Glacier (a); and typical size and shape of supraglacial lakes on the Chhule Glacier (b) and Lhotse Glacier (c).

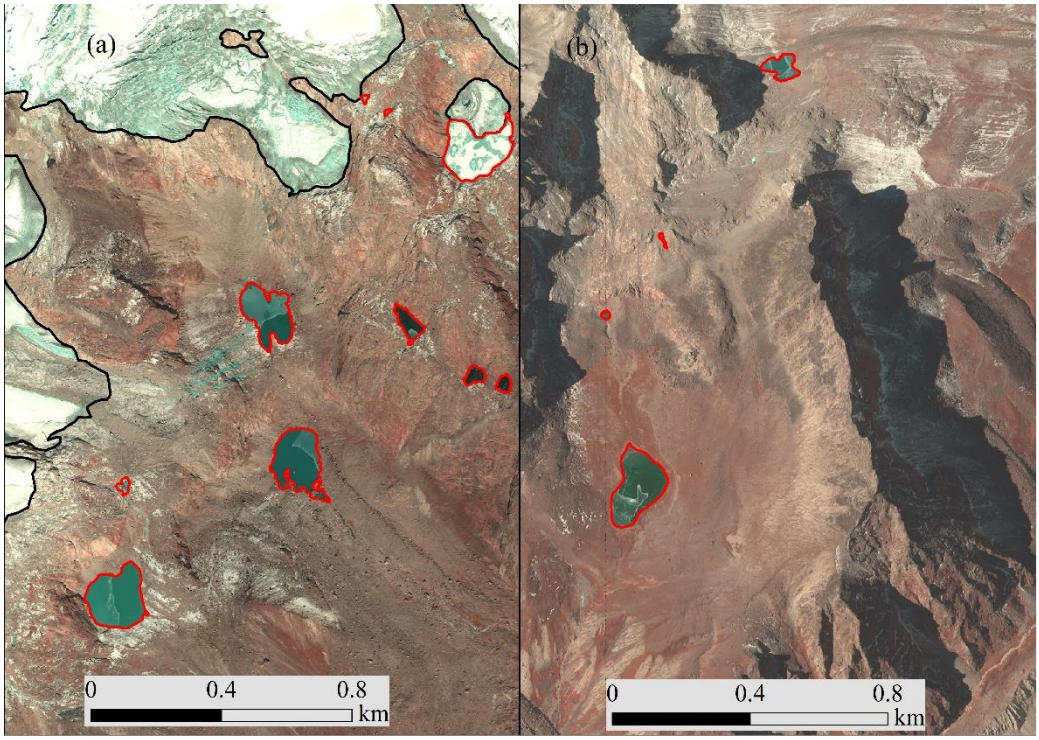

Figure 6.6 WorldView images showing the unconnected glacial lakes: glacier-fed lakes that have glaciers in their upstream (a); and non-glacier-fed lakes that do not have the glaciers in their upstream (b).

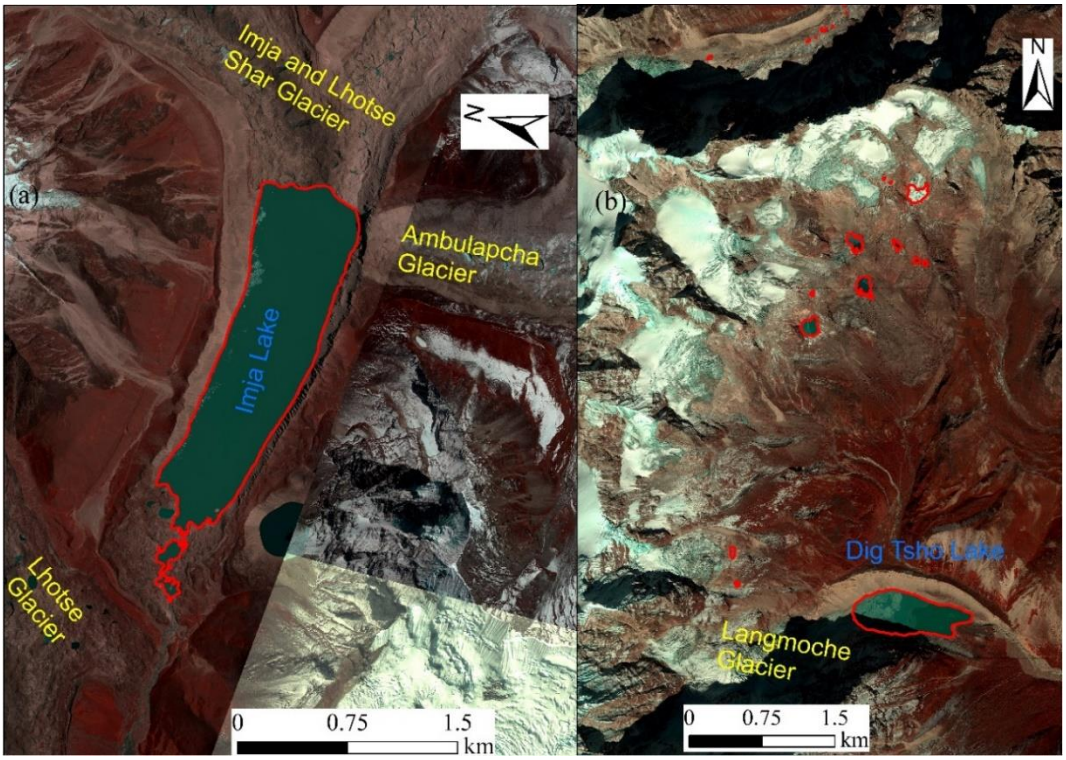

Figure 6.7 Geomorphic setting of the Imja Lake (a) and Dig Tsho Lake (b) in the Everest region. The background are WorldView images from 2016.

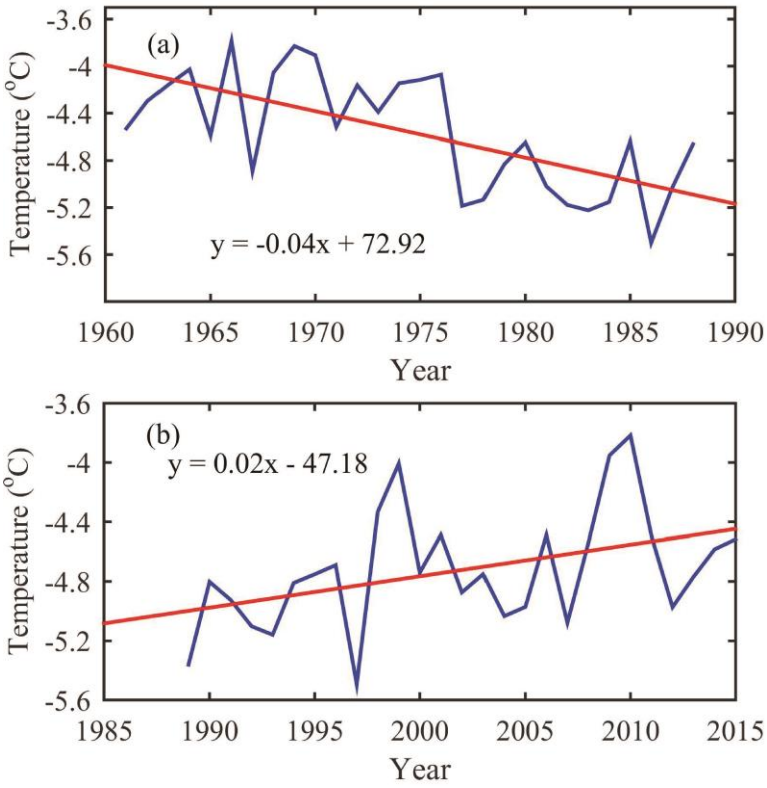

Figure 6.8 Temperature trend in the Everest region for the period (a) 1961 – 1988, and (b) 1989 – 2015.

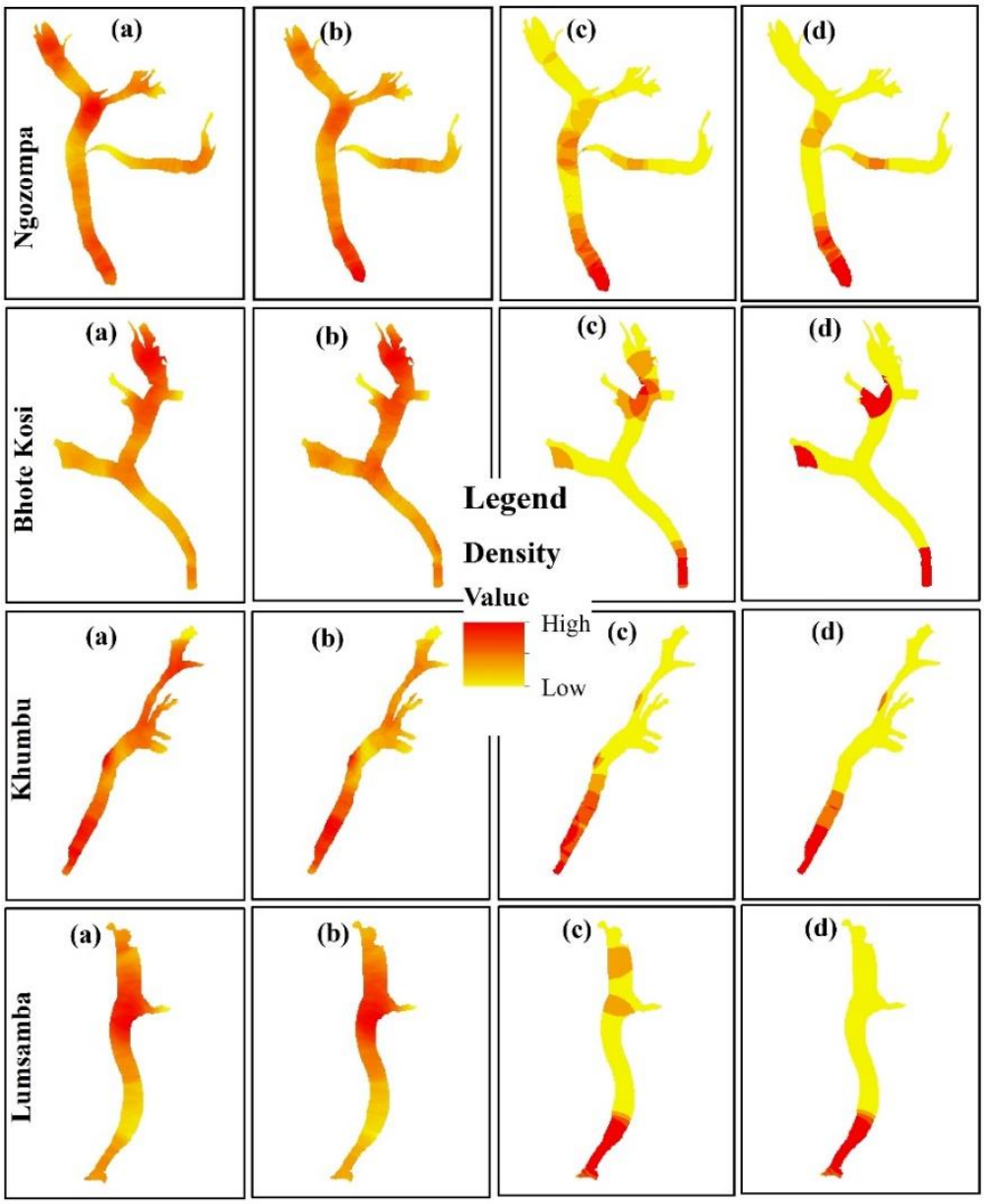

Figure 6.9 Density of the supraglacial lakes for the Ngozompa, Bhote Koshi, Khumbu, and Lumsamba glaciers with the size >20 m^2 (a), >100 m^2 (b), >3,600 m^2 (c), and >5,000 m^2 (d).

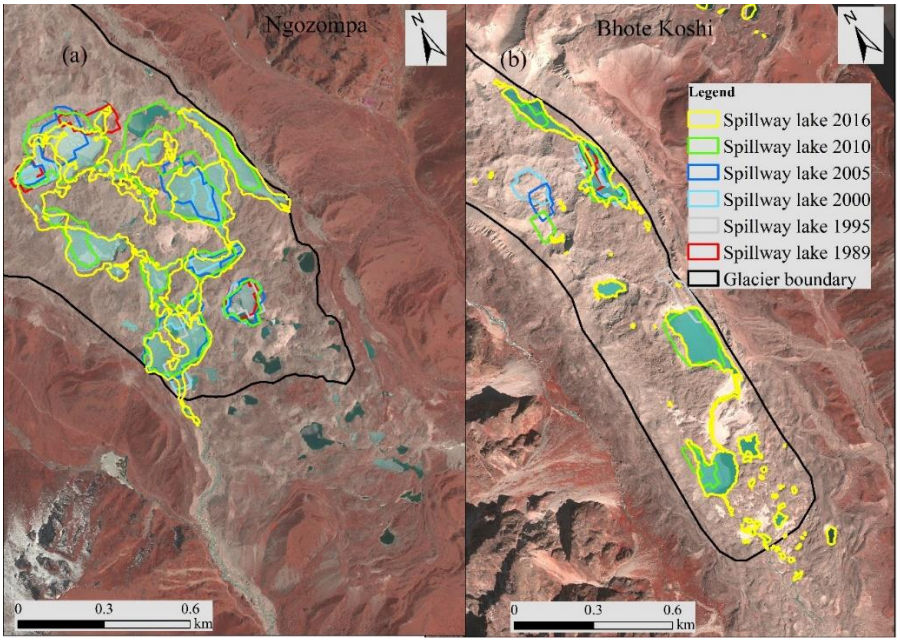

Figure 6.10 A comparison of the areal extent of the spillway lakes in 1989, 1995, 2000, 2005, 2010, and 2016 from remote sensing on the Ngozompa Glacier (a), and Bhote Koshi Glacier (b). Historical extent was based on the Landsat images, while UAV extent of 2018 for the Ngozompa Glacier and WorldView extent of 2016 for the Bhote Koshi Glacier are presented. The background are the WorldView images.

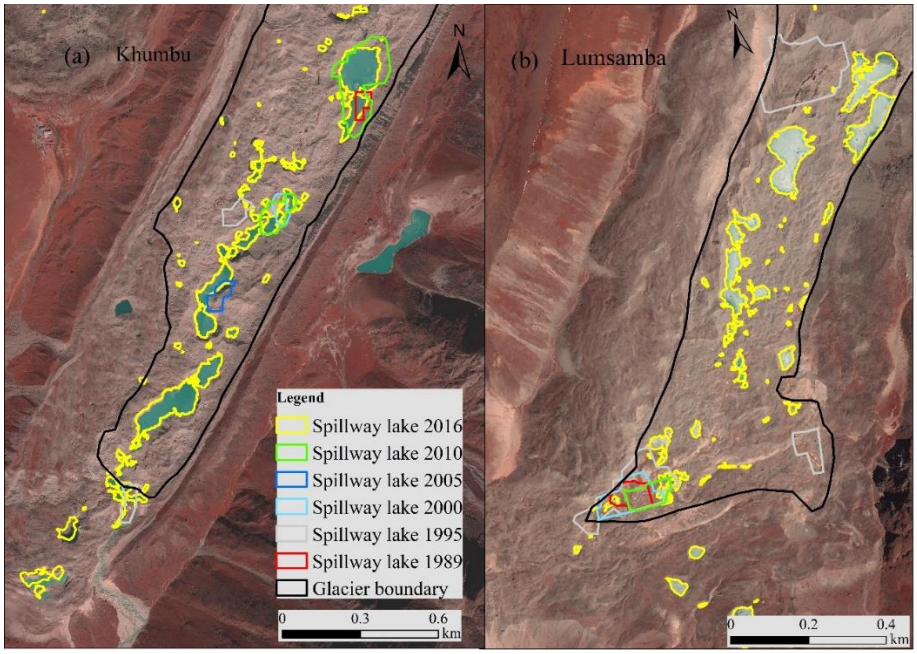

Figure 6.11 A comparison of the areal extent of the spillway lakes in 1989, 1995, 2000, 2005, 2010, and 2016 from remote sensing in Khumbu Glacier (a), and Lumsamba Glacier (b). Historical extent was based on the Landsat images, while WorldView extent was shown for the year 2016. The background are the WorldView images.

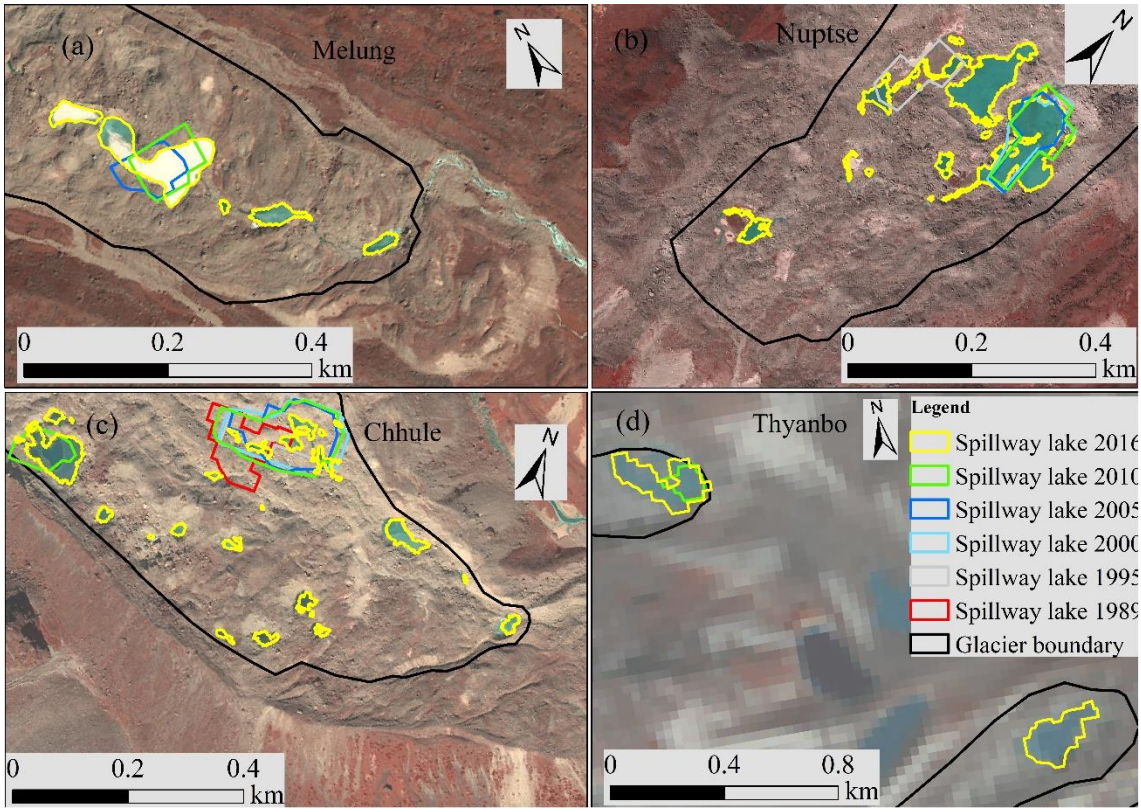

Figure 6.12 A comparison of the areal extent of spillway lakes in 1989, 1995, 2000, 2005, 2010, and 2016 from remote sensing on the Melung Glacier (a), Nuptse Glacier (b), Chhule Glacier (c), and Thyanbo Glacier (d). Historical extent was based on the Landsat images, while WorldView extent for the Melung, Nuptse, and Chhule was shown for the year 2016. The background are the WorldView images except for Thyanbo Glacier, where background is Sentinel-2 image.

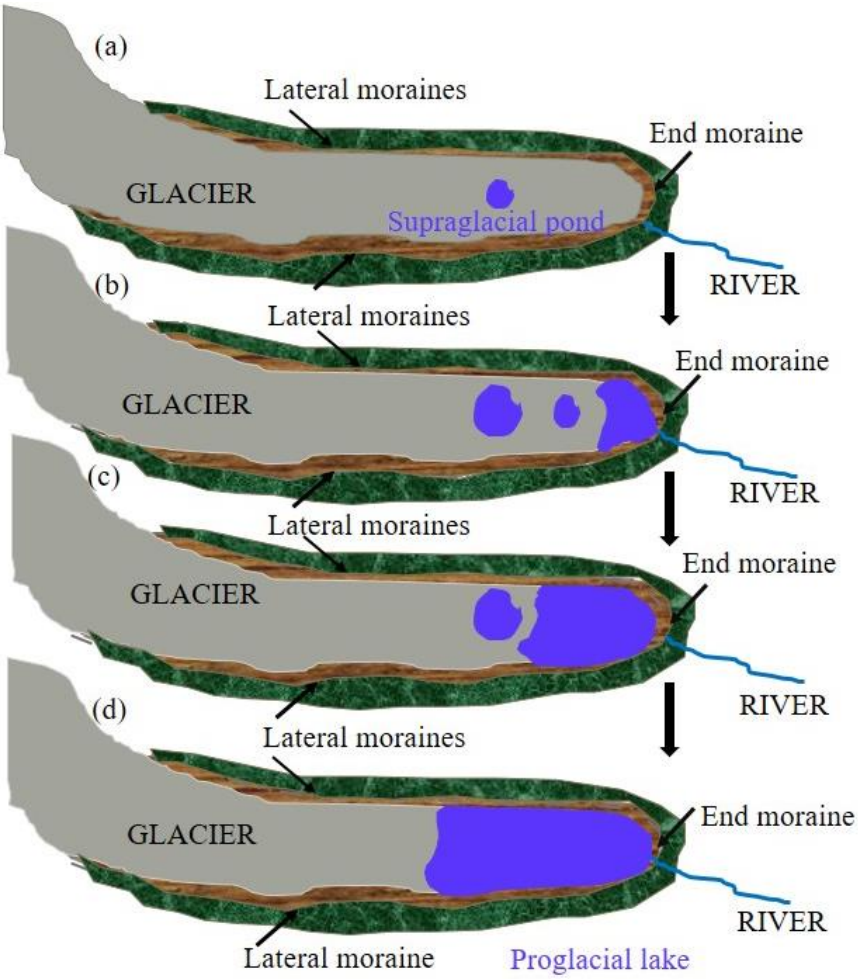

Figure 6.13 Schematic diagram showing development of a large proglacial lake from small lakes on the surface of a glacier.

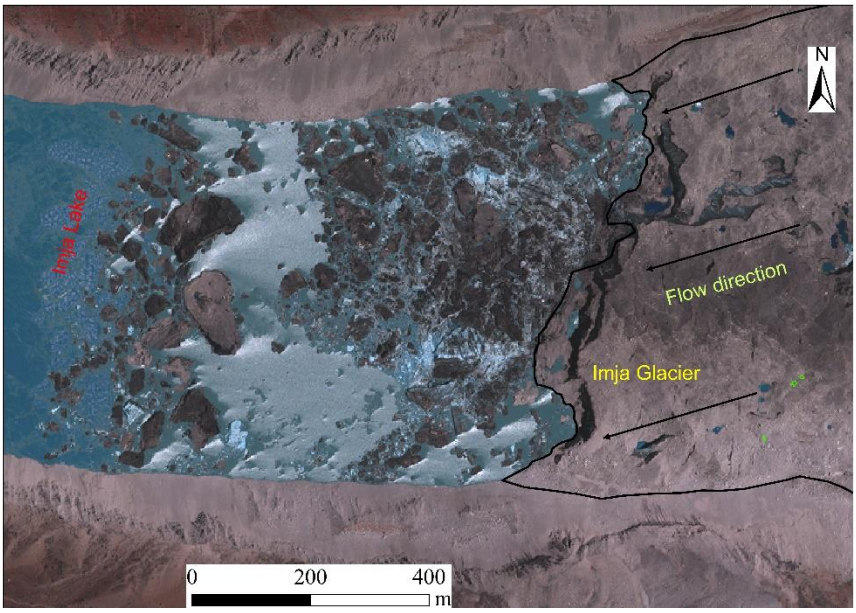

Figure 6.14 WorldView-2 image (May 2013) of the upper part of the Imja Lake showing calving front of the Imja Glacier and floating icebergs on the surface of the lake.

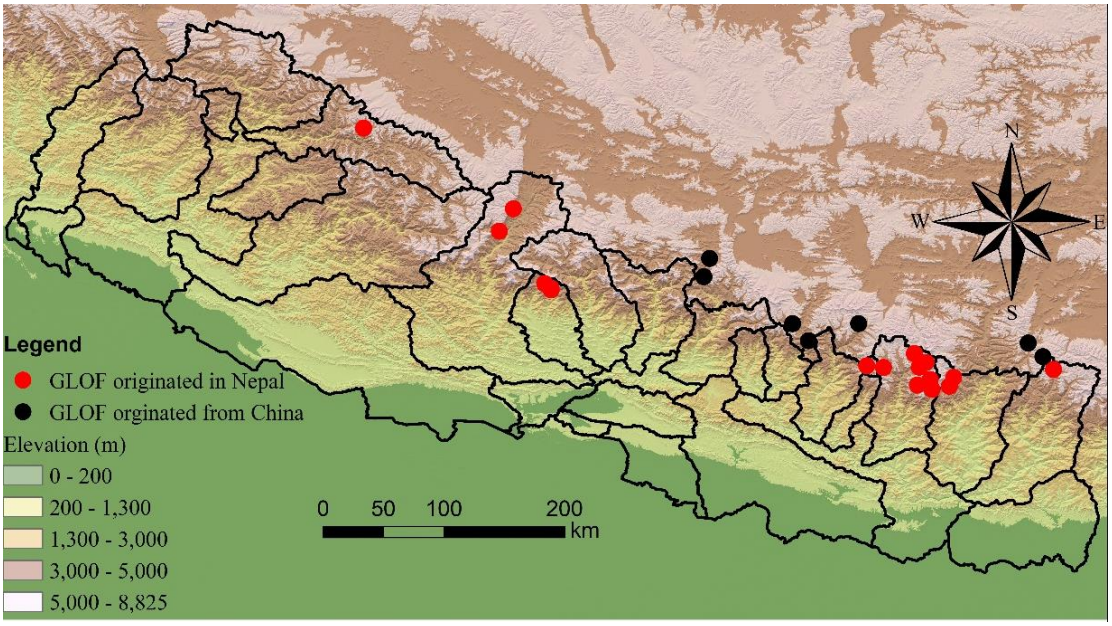

Figure 6.15 Record of the past GLOF events that caused damage in Nepal (After ICIMOD, 2011).

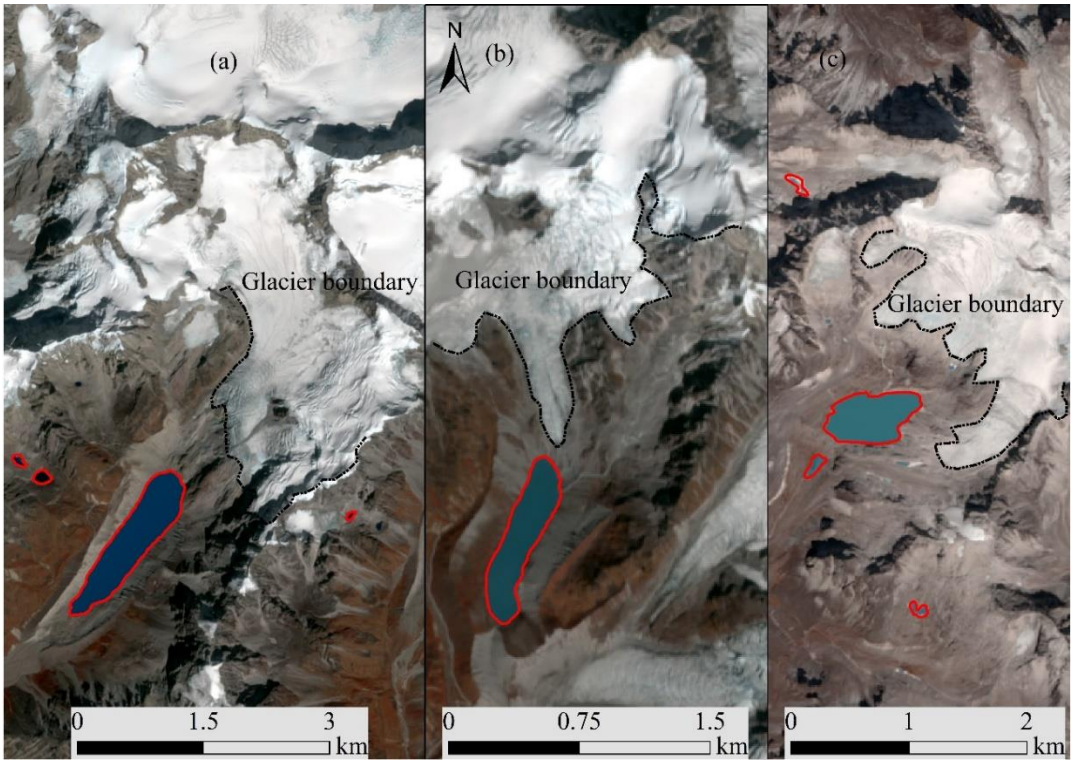

Figure 6.16 Geomorphic setting of the Nangama Lake (a), Lahare Lake (kotam_gl_0111) (b), and Khanlananma Lake (kotam_gl_0193) (c) in the Kangchenjunga region. The background are Sentinel-2 images.

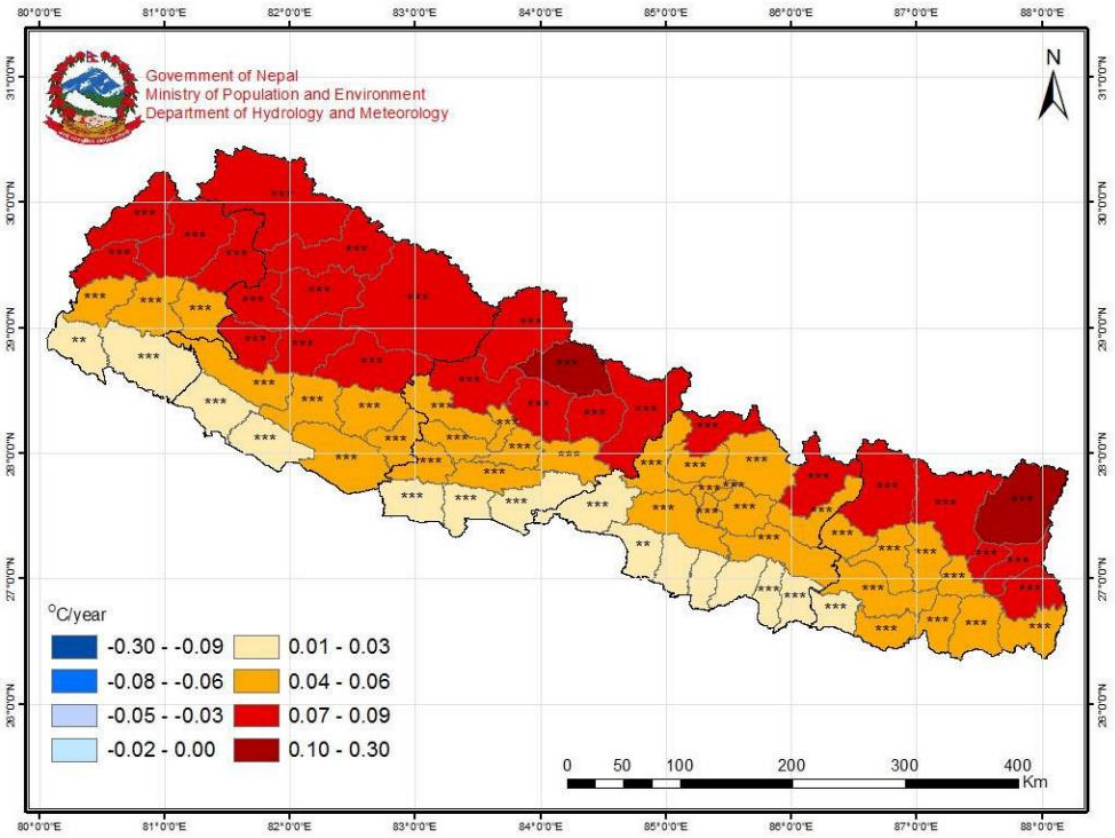

Figure 6.17 Annual maximum temperature trends for districts of Nepal (reference period: 1971 – 2014) (DHM, 2017).

7. Conclusions

This study aimed to understand the dynamics of glacial lakes and current extent of the glaciers in the Nepal Himalaya. For this purpose, glacial lakes were studied to understand the seasonal, annual, decadal, and spatial dynamics over time. Glacial lakes were plotted for the highly glacierized river basins of Nepal, i.e., upper Dudh Koshi (Everest region) and upper Tamor River (Kangchenjunga region) basins, tributaries of Koshi River basin based on satellite datasets of very high-resolution to moderate-resolution satellite images. Satellite imageries used in this study comprised the Worldview and GeoEye of 2-m, CORONA images of 2.74-m to 9.1-m, Sentinel-2 images of 10-m, and Landsat series of 30-m and 60-m spatial resolution. This study prepared the recent updated and highly accurate inventory of the glaciers for the Everest region by using very high-spatial resolution imageries.

Inventory of glacial lakes using 2-m satellite images of the year 2015 and 2016 displayed the 3,290 glacial lakes with the surface area of 8.11 ± 0.45 km^2 in the Everest region. Similarly, Sentinel-2 images of 2018 plotted the 373 glacial lakes with the total surface area of 6.18 ± 0.75 km^2 in the Kangchenjunga region. The size distribution of the glacial lakes showed the largest surface area of the glacial lakes that had size >0.1 km^2 in both study sites, while lakes that were not directly connected with glacier showed the largest surface area. Supraglacial lakes were most frequently occurred topology in the Everest region, which was obtained by using the minimum threshold of >20 m^2. Small sized-supraglacial lakes with size <500 m^2 were not mapped for the Kangchenjunga region, where 10-m images were utilized. The typical size of the supraglacial lakes was found <1,000 m^2, which accounted for 90% of the total number of supraglacial lakes. Correlation between geometric characteristics of the glaciers and the surface area of supraglacial lakes exhibited the very strong rank-order correlation with the total glacier area (r_s = 0.90) and debris-covered area (r_s = 0.90). Similarly, it showed the strong correlation with the mean slope (r_s = -0.75), mean elevation (r_s = 0.72), and glacier width (r_s = 0.70); and a moderate correlation with the AAR (r_s = 0.61), which was statistically significant at 99% confidence level. The rank-correlation indicated that supraglacial lakes have the potential to form at the surface of the glacier, which has large debris-covered area, width, and gentle slope. This was observed on the Ngozompa, Khumbu, and Bhote Koshi glaciers, where the largest number and area of the supraglacial lakes were observed. Similarly, these glaciers exhibited the presence of the large complex of spillway lakes at

their termini, which accounted for 41%, 28%, and 25% of the total area of supraglacial lakes on the Ngozompa, Khumbu, and Bhote Koshi glaciers, respectively.

Glacier inventory of the Everest region exhibited the 109 glaciers with the surface area of 268.22 ± 1.46 km^2. The Ngozompa Glacier was the largest glacier with an area of 80.15 ± 0.26 km^2. Out of 10 sub-basins in the upper Dudh Koshi basin, Ngozompa Glacier basin exhibited the largest area (86.22 ± 0.33 km^2) of the glaciers, while the largest number (27) of the glaciers were present in the Khumbu Glacier basin. Comparison with past studies showed the loss of glacier area by 92 km^2 since 1970 and by 75 km^2 from 1980.

The dynamics of supraglacial lakes in the Everest region was presented in Chapter 4, where historical development of the supraglacial lakes on the surface of 23 debris-covered glaciers was studied using the atmospherically corrected Landsat images from 1989 to 2017. Similarly, Sentinel-2 images with 10-m spatial resolution were utilized for understanding the seasonal variability of the water bodies. Use of long-term historical imageries to study the year-to-year variations for 28 years, and use of high-resolution imageries to know the seasonal variation of the supraglacial lakes are novel for this region. The results revealed that these features were widely distributed on the glaciers, and showed the rapid increase in their area and number from 1989 to 2017. The number of lakes was found increase by 3.4 times from 1989 to 2017, and a net increase in the area by 350% during the study period. High-persistent lakes were evident at the termini of the glaciers, and the persistency increased in the recent period (2009 – 2017) than in the earlier period (1989 – 1998). The highest densities of the lakes with sizes >5,000 m^2 were also evident around the terminus of the glaciers. Spillway lakes and associated lakes were observed at the tongues of the eight glaciers, while spillway lakes on the Ngozompa, Khumbu, Bhote Koshi, and Lumsamba glaciers were exponentially expanded during 1989 and 2017 relative to rest of the spillway lakes. This is suggestive of a large glacial lake developing in the future. The seasonal analysis showed the smallest supraglacial lake area to be in the winter season and comparable lake areas in the pre- and post-monsoon seasons.

The temperature trend showed that annual mean temperature increased at the rate of 0.02°C yr^{-1} from 1989 to 2015 in the region, which may enhance the ice melt rate and contribute to increasing in the lake area. However, a station-based study by DHM (2017) showed the temperature trend up to 0.092°C yr^{-1} indicated the high possibility of expansion of existing lakes and the development of new lakes in the Nepal Himalaya.

Additionally, the characteristics of the glaciers and roles of already developed supraglacial lakes have also had a significant influence on the increase in the area of the lakes.

Decadal variations and evolution of the glacial lakes were analyzed from 1964 to 2018 in the Kangchenjunga region, upper Tamor River basin. Glacier lakes were explored by using the minimum area threshold of 5,000 m^2, which indicated that the total surface area of glacial lakes expanded by 230% between 1964 and 2018. Similarly, the number of glacial lakes also increased by 406% during the study period. The largest increase in the area was contributed by lakes, which were not directly connected with glaciers, and followed by the proglacial lakes. These results were in line with the glacier retreat and loss of glacier area in the region. Loss of glacier area in the region is leading to the formation of unconnected glacial lakes, and it is expected that several connected lakes will be transformed into unconnected lakes with increased warming in the future. Proglacial lakes were found to expand by 275% from 1964 to 2018. The proglacial lakes which were expanded rapidly in the earlier period (before 1980) were found more or less static, while lakes which begin to develop in the later period were found expanding and need to be closely monitored.

The results from different resolution imageries showed the potentiality of Landsat, Sentinel, CORONA, and WorldView to study the glacial lakes for the different purpose. Landsat imagery (30 m) has the potential to map the glacial lakes (>5,000 m^2) to understand their historical evolution. However, theoretical uncertainty estimated by multiplying perimeter by half the resolution of the image was found >15% for the lake with the size <0.1 km^2. Therefore, Landsat images can be used with adequate accuracy for the lakes with size >0.1 km^2. Since manual correction methods were applied in this study, and therefore, the lower order of uncertainty is expected even for the lake with size >5,000 m^2. Sentinel-2 (10 m) with the high temporal resolution has high potential to map small features, and it will help to understand the seasonal dynamics of lakes with size >0.02 km^2 with less than 15% uncertainty. WorldView and GeoEye images with 2-m spatial resolution have the potential to map the features as small as of 20 m^2 size with higher accuracy, which can be used for accuracy assessment of the images with coarser resolution.

Five new GLOF events were discovered in the Kangchenjunga region, out of which three occurred before 1962, one in 1963, and one in 1968, using CORONA images for the first time. The eroded river bed and lake formed after GLOF from the Nangama Lake

in 1980 also discussed in this study. Existence of ice and earth masses, fragile dams, located in the seismically active zone and continuous expanding of the lakes with increased ice melt make glacial lakes more susceptible to GLOF. This study advances the understanding of the spatiotemporal distribution of lakes; their expansion including historical GLOFs and increasing capacity of a remote sensing observation system will play a crucial role in monitoring glacial lakes and will be helpful for minimizing the risk. A detailed study on glacial lakes including their physical setting, geomorphology, bathymetry, the existence of ice and earth mass surrounding the lakes and socioeconomic structure in the downstream region is required. The result of this study will be the baseline for future study in the region, which is essential for the implementation of GLOF risk management in the region.

References

Acharya, A., Kayastha, R.B., 2018. Mass and Energy Balance Estimation of Yala Glacier (2011–2017), Langtang Valley, Nepal. Water 11, 6. https://doi.org/10.3390/w11010006.

Ageta, Y., Higuchi, K., 1984. Estimation of Mass Balance Components of a Summer-Accumulation Type Glacier in the Nepal Himalaya. Geogr. Ann. Ser. A, Phys. Geogr. 66, 249. https://doi.org/10.2307/520698.

Ageta, Y., Iwata, S., Yabuki, H., Naito, N., Sakai, A., Narama, C., Karma, 2000. Expansion of glacier lakes in recent decades in the Bhutan Himalayas. IAHS-AISH Publ. 165–175.

Aggarwal, A., Jain, S.K., Lohani, A.K., Jain, N., 2016. Glacial lake outburst flood risk assessment using combined approaches of remote sensing, GIS and dam break modelling. Geomatics, Nat. Hazards Risk 7, 18–36. https://doi.org/10.1080/19475705.2013.862573.

Aguilar, M.A., Saldaña, M. del M., Aguilar, F.J., 2013. Assessing geometric accuracy of the orthorectification process from GeoEye-1 and WorldView-2 panchromatic images. Int. J. Appl. Earth Obs. Geoinf. 21, 427–435. https://doi.org/10.1016/J.JAG.2012.06.004.

Altmaier, A., Kany, C., 2002. Digital surface model generation from CORONA satellite images. ISPRS J. Photogramm. Remote Sens. 56, 221–235. https://doi.org/10.1016/S0924-2716(02)00046-1.

APHRODITE, 2019. APHRODITE's Water Resources [WWW Document]. URL http://aphrodite.st.hirosaki-u.ac.jp/ (accessed 2.25.19).

Asahi, K., Watanabe, T., 2000. Past and recent glacier fluctuations in Kanchenjunga Himal, Nepal. J. Nepal Geol. Soc. 22, 481–490.

Azam, M.F., Wagnon, P., Berthier, E., Vincent, C., Fujita, K., Kargel, J.S., 2018. Review of the status and mass changes of Himalayan-Karakoram glaciers. J. Glaciol. 64, 61–74. https://doi.org/10.1017/jog.2017.86.

Bajracharya, B., Shrestha, A.B., Rajbhandari, L., 2007. Glacial Lake Outburst Floods in the Sagarmatha Region. Mt. Res. Dev. 27, 336–344. https://doi.org/10.1659/mrd.0783.

Bajracharya, Maharjan, S., Shrestha, F., Bajracharya, O., Baidya, S., 2014. Glacier Status in Nepal and Decadal Change from 1980 to 2010 based on Landsat Data. Kathmandu,

ICIMOD.

Bajracharya, S.R., Maharjan, S.B., Shrestha, F., Guo, W., Liu, S., Immerzeel, W., Shrestha, B., 2015. The glaciers of the Hindu Kush Himalayas: current status and observed changes from the 1980s to 2010. Int. J. Water Resour. Dev. 31, 161–173. https://doi.org/10.1080/07900627.2015.1005731.

Bajracharya, S.R., Mool, P., 2009. Glaciers, glacial lakes and glacial lake outburst floods in the Mount Everest region, Nepal. Ann. Glaciol. 50, 81–86. https://doi.org /10. 3189/172756410790595895.

Basnett, S., Kulkarni, A. V., Bolch, T., 2013. The influence of debris cover and glacial lakes on the recession of glaciers in Sikkim Himalaya, India. J. Glaciol. 59, 1035–1046. https://doi.org/10.3189/2013JoG12J184.

Benn, D.I., Bolch, T., Hands, K., Gulley, J., Luckman, A., Nicholson, L.I., Quincey, D., Thompson, S., Toumi, R., Wiseman, S., 2012. Response of debris-covered glaciers in the Mount Everest region to recent warming, and implications for outburst flood hazards. Earth-Science Rev. 114, 156–174. https://doi.org/10.1016/j.earscirev.2012. 03.008.

Benn, D.I., Wiseman, S., Hands, K.A., 2001. Growth and drainage of supraglacial lakes on debris-mantled Ngozumpa Glacier, Khumbu Himal, Nepal. J. Glaciol. 47, 626–638. https://doi.org/10.3189/172756501781831729.

Benn, D.I., Wiseman, S., Warren, C.R., 2000. Rapid growth of a supraglacial lake, Ngozumpa Glacier, Khumbu Himal, Nepal. Int. Assoc. Hydrol. Sci. Publ. 264 (Symposium Seattle 2000 — Debris-Covered Glaciers) 177–185.

Bhandari, A.R., Rai, D.P., Wikranmanayake, E., Thapa, G.J., Koirala, S., Gyawali, T.P., Joshi, D., 2018. Kangchenjunga Conservation Area: A Retrospective Report. Baluwatar, Kathmandu, Nepal.

Bhatta, S., Kumar Dhamala, M., Chandra Aryal, P., Chauhan, R., Dawadi, B., 2018. Climate Variability and Associated Response of *Larix griffithii* in Kanchenjunga Conservation Area of Nepal. Appl. Ecol. Environ. Sci. 6, 23–30. https://doi.org /10.12691/aees-6-1-4.

Bhuju, U.R., Shakya, P.R., Basnet, T.B., Shrestha, S., 2007. Nepal Biodiversity Resource Book. International Centre for Integrated Mountain Development (ICIMOD), Kathmandu, Nepal.

Bolch, T., Buchroithner, M., Pieczonka, T., Kunert, A., 2008a. Planimetric and volumetric glacier changes in the Khumbu Himal, Nepal, since 1962 using Corona,

Landsat TM and ASTER data. J. Glaciol. 54, 592–600. https://doi.org/10.3189/002214308786570782.

Bolch, T., Buchroithner, M.F., Peters, J., Baessler, M., Bajracharya, S., 2008b. Identification of glacier motion and potentially dangerous glacial lakes in the Mt. Everest region/Nepal using spaceborne imagery. Nat. Hazards Earth Syst. Sci. 8, 1329–1340. https://doi.org/10.5194/nhess-8-1329-2008.

Bolch, T., Kulkarni, A., Kaab, A., Huggel, C., Paul, F., Cogley, J.G., Frey, H., Kargel, J.S., Fujita, K., Scheel, M., Bajracharya, S., Stoffel, M., 2012. The State and Fate of Himalayan Glaciers. Science. 336, 310–314. https://doi.org/10.1126/science.1215828.

Bolch, T., Peters, J., Yegorov, A., Pradhan, B., Buchroithner, M., Blagoveshchensky, V., 2011a. Identification of potentially dangerous glacial lakes in the northern Tien Shan. Nat. Hazards 59, 1691–1714. https://doi.org/10.1007/s11069-011-9860-2.

Bolch, T., Pieczonka, T., Benn, D.I., 2011b. Multi-decadal mass loss of glaciers in the Everest area (Nepal Himalaya) derived from stereo imagery. Cryosphere 5, 349–358. https://doi.org/10.5194/tc-5-349-2011.

Bolch, T., Shea, J.M., Liu, S., Azam, F.M., Gao, Y., Gruber, S., Immerzeel, W.W., Kulkarni, A., Li, H., Tahir, A.A., Zhang, G., Zhang, Y., 2019. Status and Change of the Cryosphere in the Extended Hindu Kush Himalaya Region, in: The Hindu Kush Himalaya Assessment. Springer International Publishing, Cham, pp. 209–255. https://doi.org/10.1007/978-3-319-92288-1_7.

Bonekamp, P.N.J., de Kok, R.J., Collier, E., Immerzeel, W.W., 2019. Contrasting Meteorological Drivers of the Glacier Mass Balance Between the Karakoram and Central Himalaya. Front. Earth Sci. 7, 107. https://doi.org/10.3389/feart.2019.00107.

Brun, F., Berthier, E., Wagnon, P., Kääb, A., Treichler, D., 2017. A spatially resolved estimate of High Mountain Asia glacier mass balances from 2000 to 2016. Nat. Geosci. 10, 668–673. https://doi.org/10.1038/ngeo2999.

Byers, A.C., McKinney, D.C., Somos-Valenzuela, M., Watanabe, T., Lamsal, D., 2013. Glacial lakes of the Hinku and Hongu valleys, Makalu Barun National Park and Buffer Zone, Nepal. Nat. Hazards 69, 115–139. https://doi.org/10.1007/s11069-013-0689-8.

Byers, A.C., Rounce, D.R., Shugar, D.H., Lala, J.M., Byers, E.A., Regmi, D., 2019. A rockfall-induced glacial lake outburst flood, Upper Barun Valley, Nepal. Landslides 16, 533–549. https://doi.org/10.1007/s10346-018-1079-9.

Carrivick, J.L., Tweed, F.S., 2016. A global assessment of the societal impacts of glacier outburst floods. Glob. Planet. Change 144, 1–16. https://doi.org/10.1016/J.GLOPLACHA.2016.07.001.

Casana, J., Cothren, J., 2008. Stereo analysis, DEM extraction and orthorectification of CORONA satellite imagery: archaeological applications from the Near East. Antiquity 82, 732–749. https://doi.org/10.1017/S0003598X00097349.

Chand, M.B., Kayastha, R.B., 2018. Study of thermal properties of supraglacial debris and degree-day factors on Lirung Glacier, Nepal. Sci. Cold Arid Reg. 10, 357–368. https://doi.org/10.3724/SP.J.1226.2018.00357.

Chand, M.B., Kayastha, R.B., Parajuli, A., Mool, P.K., 2015. Seasonal variation of ice melting on varying layers of debris of Lirung Glacier, Langtang Valley, Nepal. Proc. Int. Assoc. Hydrol. Sci. 368, 21–26. https://doi.org/10.5194/piahs-368-21-2015.

Cook, K.L., Andermann, C., Gimbert, F., Adhikari, B.R., Hovius, N., 2018. Glacial lake outburst floods as drivers of fluvial erosion in the Himalaya. Science 362, 53–57. https://doi.org/10.1126/science.aat4981.

Cook, S.J., Quincey, D.J., 2015. Estimating the volume of Alpine glacial lakes. Earth Surf. Dynam 3, 559–575. https://doi.org/10.5194/esurf-3-559-2015.

Dahal, R.K., 2006. Geology of Nepal [WWW Document]. URL http://www.ranjan.net.np/index.php/resources/geology-of-nepal (accessed 10.25. 19).

Dhital, M.R., 2015a. Geological Setting of Himalaya. pp. 13–21. https://doi.org/10.1007/978-3-319-02496-7_2.

Dhital, M.R., 2015b. Physiography of Nepal. pp. 23–33. https://doi.org/10.1007/978-3-319-02496-7_3.

DHM, 2017. Observed Climate Trend Analysis in the Districts and Physiographic Regions of Nepal (1971-2014).

DHM, 2015. Study of Climate and climatic variation over Nepal, Technical Report.

DNPWC, 2019a. Sagarmatha National Park | Department of National Parks and Wildlife Conservation [WWW Document]. URL https://www.dnpwc.gov.np/protected_areas/details/sagarmathanationalpark (accessed 10.24.19).

DNPWC, 2019b. Department of National Parks and Wildlife Conservation [WWW Document]. URL https://www.dnpwc.gov.np/protected_areas/details/kanchenjungaconservationarea (accessed 8.16.19).

DNPWC, 2016. Sagarmatha National Park and its buffer zone management plan 2016-2020. Namche Bazaar, Solukhumbu.

Farinotti, D., Huss, M., Fürst, J.J., Landmann, J., Machguth, H., Maussion, F., Pandit, A., 2019. A consensus estimate for the ice thickness distribution of all glaciers on Earth. Nat. Geosci. 12, 168–173. https://doi.org/10.1038/s41561-019-0300-3.

Ferrara, G., Tonarini, S., Lombardo, B., 1983. Rb/Sr geochronology of granites and gneisses from the Mount Everest region, Nepal Himalaya. Geol. Rundschau 72, 119–136. https://doi.org/10.1007/BF01765903.

Ferreira, E., Chandler, J., Wackrow, R., Shiono, K., 2017. Automated extraction of free surface topography using SfM-MVS photogrammetry. Flow Meas. Instrum. 54, 243–249. https://doi.org/10.1016/J.FLOWMEASINST.2017.02.001.

Fujita, K., Nakawo, M., Fujii, Y., Paudyal, P., 1997. Changes in glaciers in Hidden Valley, Mukut Himal, Nepal Himalayas, from 1974 to 1994. J. Glaciol. 43, 583–588. https://doi.org/10.3189/S002214300003519X.

Fujita, K., Nuimura, T., 2011. Spatially heterogeneous wastage of Himalayan glaciers. Proc. Natl. Acad. Sci. U. S. A. 108, 14011–4. https://doi.org/10.1073/pnas. 110624 2108.

Fujita, K., Sakai, A., Nuimura, T., Yamaguchi, S., Sharma, R.R., 2009. Recent changes in Imja Glacial Lake and its damming moraine in the Nepal Himalaya revealed by *in situ* surveys and multi-temporal ASTER imagery. Environ. Res. Lett. 4, 045205. https://doi.org/10.1088/1748-9326/4/4/045205.

Fujita, K., Sakai, A., Takenaka, S., Nuimura, T., Surazakov, A.B., Sawagaki, T., Yamanokuchi, T., 2013. Potential flood volume of Himalayan glacial lakes 13, 1827–1839. https://doi.org/10.5194/nhess-13-1827-2013.

Fushimi, H., Ohata, T., 1980. Fluctuations of Glaciers from 1970 to 1978 in the Khumbu Himal, East Nepal. Seppyo.

Fyffe, C.L., Brock, B.W., Kirkbride, M.P., Mair, D.W.F., Arnold, N.S., Smiraglia, C., Diolaiuti, G., Diotri, F., 2019. Do debris-covered glaciers demonstrate distinctive hydrological behaviour compared to clean glaciers? J. Hydrol. 570, 584–597. https://doi.org/10.1016/J.JHYDROL.2018.12.069.

Fyffe, C.L., Reid, T.D., Brock, B.W., Kirkbride, M.P., Diolaiuti, G., Smiraglia, C., Diotri, F., 2014. A distributed energy-balance melt model of an alpine debris-covered glacier. J. Glaciol. 60, 587–602. https://doi.org/10.3189/2014JoG13J148.

Gardelle, J., Arnaud, Y., Berthier, E., 2011. Contrasted evolution of glacial lakes along the Hindu Kush Himalaya mountain range between 1990 and 2009. Glob. Planet. Change 75, 47–55. https://doi.org/10.1016/j.gloplacha.2010.10.003.

Gardelle, J., Berthier, E., Arnaud, Y., Kääb, A., 2013. Region-wide glacier mass balances over the Pamir-Karakoram-Himalaya during 1999–2011. Cryosph. 7, 1263–1286. https://doi.org/10.5194/tc-7-1263-2013.

Garrard, R., Kohler, T., Price, M.F., Byers, A.C., Sherpa, A.R., Maharjan, G.R., 2016. Land Use and Land Cover Change in Sagarmatha National Park, a World Heritage Site in the Himalayas of Eastern Nepal. Mt. Res. Dev. 36, 299. https://doi.org/10.1659/mrd-journal-d-15-00005.1.

Gautam, C.M., Watanabe, T., 2004. Reliability of Land Use/Land Cover Assessment in Montane Nepal. Mt. Res. Dev. 24, 35–43. https://doi.org/10.1659/0276-4741(2004)024[0035:roluca]2.0.co;2.

Gurung, G., 2006. Reconciling biodiversity conservation priorities with livelihood needs in Kangchenjunga Conservation Area, Nepal. University of Zurich. https://doi.org/https://www.zora.uzh.ch/id/eprint/76917/.

Hall, D.K., Riggs, G.A., Salomonson, V. V., 1995. Development of methods for mapping global snow cover using moderate resolution imaging spectroradiometer data. Remote Sens. Environ. 54, 127–140. https://doi.org/10.1016/0034-4257(95)00137-P.

Hamandawana, H., Eckardt, F., Ringrose, S., 2006. The use of step-wise density slicing in classifying high-resolution panchromatic photographs. Int. J. Remote Sens. 27, 4923–4942. https://doi.org/10.1080/01431160600857436.

Haritashya, U., Kargel, J., Shugar, D., Leonard, G., Strattman, K., Watson, C., Shean, D., Harrison, S., Mandli, K., Regmi, D., Haritashya, U.K., Kargel, J.S., Shugar, D.H., Leonard, G.J., Strattman, K., Watson, C.S., Shean, D., Harrison, S., Mandli, K.T., Regmi, D., 2018. Evolution and Controls of Large Glacial Lakes in the Nepal Himalaya. Remote Sens. 10, 798. https://doi.org/10.3390/rs10050798.

Harrison, S., Kargel, J.S., Huggel, C., Reynolds, J., Shugar, D.H., Betts, R.A., Emmer, A., Glasser, N., Haritashya, U.K., Klimeš, J., Reinhardt, L., Schaub, Y., Wiltshire, A., Regmi, D., Vilímek, V., 2018. Climate change and the global pattern of moraine-dammed glacial lake outburst floods. Cryosph. 12, 1195–1209. https://doi.org/10.5194/tc-12-1195-2018.

He, J., Wang, N., Chen, A., Yang, X., Hua, T., 2019. Glacier Changes in the Qilian Mountains, Northwest China, between the 1960s and 2015. Water 11, 623. https://doi.org/10.3390/w11030623.

Hexagon Geospatial, 2019. Rapid Atmospsheric Correction [WWW Document]. URL

https://hexagongeospatial.fluidtopics.net/reader/XWswM6TZr3V__hu3iKjbGA/eWxe5pKM97cbVthy4wiX5w (accessed 9.2.19).

Higaki, D., Sato, G., 2012. Erosion and Sedimentation Caused by Glacial Lake Outburst Floods in the Nepal and Bhutan Himalayas. Glob. Environ. Res. 16, 71–76.

Higuchi, K., Fushimi, H., Ohata, T., Takenaka, S., Iwata, S., Yokoyama, K., Higuchi, H., Nagoshi, A., Iozawa, T., 1980. Glacier inventory in the Dudh Kosi region, East Nepal. Proc. Riederalp Work. Sept. 1978 IAHS-AISH.

Huggel, C., Kääb, A., Haeberli, W., Teysseire, P., Paul, F., 2002. Remote sensing based assessment of hazards from glacier lake outbursts: a case study in the Swiss Alps. Can. Geotech. J. 39, 316–330. https://doi.org/10.1139/t01-099.

ICIMOD, 2011. Glacial lakes and glacial lake outburst floods in Nepal. International Centre for Integrated Mountain Development, Kathmandu.

Immerzeel, W.W., van Beek, L.P.H., Bierkens, M.F.P., 2010. Climate change will affect the Asian water towers. Science 328, 1382–5. https://doi.org/10.1126/science.1183188.

IPCC, 2014. Climate Change 2014: Synthesis Report. Contribution of working Groups I, II and III to the fifth assessment report of the Intergovernmental Panel of Climate Change. Geneva, Switzerland.

IPCC, 2013. Climate Change 2013 The Physical Science Basis Working Group I Contribution to the Fifth Assessment Report of the Intergovernmental Panel on Climate Change. Cambridge University Press, Cambridge, United kingdom and New York, NY, USA.

Irvine-Fynn, T.D.L., Porter, P.R., Rowan, A. V., Quincey, D.J., Gibson, M.J., Bridge, J.W., Watson, C.S., Hubbard, A., Glasser, N.F., 2017. Supraglacial Ponds Regulate Runoff From Himalayan Debris-Covered Glaciers. Geophys. Res. Lett. 44, 11,894-11,904. https://doi.org/10.1002/2017GL075398.

Iturrizaga, L., 2011. Glacier Lake Outburst Floods. In. Singh V. P., Singh P., Haritashya U. K. (eds) Encyclopedia of Snow, Ice and Glaciers. Encyclopedia of Earth Sciences Series. Springer, Dordrecht, pp. 381–399. https://doi.org/10.1007/978-90-481-2642-2_196.

Iwata, S., Aoki, T., Kadota, T., Seko, K., Yamaguchi, S., 2000. Morphological evolution of the debris cover on Khumbu Glacier, Nepal, between 1978 and 1995. IAHS-AISH Publ. 3–11.

Jean-Philippe, A., John E., G., Ratna Mani, G., Lok Bijay, A., 2015. Nepal GPS netwrok-

JIR2-JIR2., UNAVCO, Inc., GPS/GNSS observations dataset [WWW Document]. https://doi.org/https://doi.org/10.7283/T5348HQS.

Jha, L.K., Khare, D., 2017. Detection and delineation of glacial lakes and identification of potentially dangerous lakes of Dhauliganga basin in the Himalaya by remote sensing techniques. Nat. Hazards 85, 301–327. https://doi.org/10.1007/s11069-016-2565-9.

Ji, L., Zhang, L., Wylie, B., 2009. Analysis of Dynamic Thresholds for the Normalized Difference Water Index. Photogramm. Eng. Remote Sens. 75, 1307–1317. https://doi.org/10.14358/PERS.75.11.1307.

Jiang, S., Nie, Y., Liu, Q., Wang, J., Liu, L., Hassan, J., Liu, X., Xu, X., 2018. Glacier Change, Supraglacial Debris Expansion and Glacial Lake Evolution in the Gyirong River Basin, Central Himalayas, between 1988 and 2015. Remote Sens. 10, 986. https://doi.org/10.3390/rs10070986.

Kääb, A., Berthier, E., Nuth, C., Gardelle, J., Arnaud, Y., 2012. Contrasting patterns of early twenty-first-century glacier mass change in the Himalayas. Nature. https://doi.org/10.1038/nature11324.

Kaser, G., Grosshauser, M., Marzeion, B., 2010. Contribution potential of glaciers to water availability in different climate regimes. Proc. Natl. Acad. Sci. U. S. A. 107, 20223–7. https://doi.org/10.1073/pnas.1008162107.

Kattel, D.B., Yao, T., 2013. Recent temperature trends at mountain stations on the southern slope of the central Himalayas. J. Earth Syst. Sci. 122, 215–227.

Kellenberger, T.W., Schubiger, W.A., Itten, K.I., 2006. Object oriented land cover mapping of the Kanchenjunga Conservation Area (KCA) in Nepal, for sustainable development and use of natural resources, in: International Geoscience and Remote Sensing Symposium (IGARSS). pp. 2365–2368. https://doi.org/10.1109/IGARSS.2006.612.

Khadka, N., Zhang, G., Chen, W., 2019. The state of six dangerous glacial lakes in the Nepalese Himalaya. Terr. Atmos. Ocean. Sci. 30, 63–72. https://doi.org/10.3319/TAO.2018.09.28.03.

Khadka, N., Zhang, G., Thakuri, S., 2018. Glacial Lakes in the Nepal Himalaya: Inventory and Decadal Dynamics (1977–2017). Remote Sens. 10, 1913. https:// doi.org/10.3390/rs10121913.

King, O., Dehecq, A., Quincey, D., Carrivick, J., 2018. Contrasting geometric and dynamic evolution of lake and land-terminating glaciers in the central Himalaya.

Glob. Planet. Change 167, 46–60. https://doi.org/10.1016/J.GLOPLACHA. 2018.05. 006.

King, O., Quincey, D.J., Carrivick, J.L., Rowan, A. V., 2017. Spatial variability in mass loss of glaciers in the Everest region, central Himalayas, between 2000 and 2015. Cryosph. 11, 407–426. https://doi.org/10.5194/tc-11-407-2017.

Kirkbride, M.P., 2011. Debris-Covered Glaciers. In: Singh V.P., Singh P., Haritashya U.K. (eds) Encyclopedia of Snow, Ice and Glaciers. Encyclopedia of Earth Sciences Series. Springer, Dordrecht, pp. 180–182. https://doi.org/10.1007/978-90-481-2642-2_622.

Kirkbride, M.P., 2000. Debris-Covered Glaciers. IAHS Publ.

Kirkbride, M.P., 1993. The temporal significance of transitions from melting to calving termini at glaciers in the central Southern Alps of New Zealand. The Holocene 3, 232–240. https://doi.org/10.1177/095968369300300305.

König, O., 2004. The glaciation of the Rolwaling Himal and the Kangchenjunga Himal during the Last Glacial Maximum (Nepal, E-Himalaya). Dev. Quat. Sci. 2, 279–284. https://doi.org/10.1016/S1571-0866(04)80133-7.

Lamsal, D., Fujita, K., Sakai, A., 2017. Surface lowering of the debris-covered area of Kanchenjunga Glacier in the eastern Nepal Himalaya since 1975, as revealed by Hexagon KH-9 and ALOS satellite observations. Cryosph. 11, 2815–2827. https://doi.org/10.5194/tc-11-2815-2017.

Lamsal, D., Sawagaki, T., Watanabe, T., 2011. Digital terrain modelling using Corona and ALOS PRISM data to investigate the distal part of Imja Glacier, Khumbu Himal, Nepal. J. Mt. Sci. 8, 390–402. https://doi.org/10.1007/s11629-011-2064-0.

Lamsal, D., Sawagaki, T., Watanabe, T., Byers, A.C., 2016. Assessment of glacial lake development and prospects of outburst susceptibility: Chamlang South Glacier, eastern Nepal Himalaya. Geomatics, Nat. Hazards Risk 7, 403–423. https://doi.org/ 10.1080/19475705.2014.931306.

Li, Z., Fan, K., Tian, L., Shi, B., Zhang, S., Zhang, J., 2015. Response of Glacier and Lake Dynamics in Four Inland Basins to Climate Change at the Transition Zone between the Karakorum And Himalayas. PLoS One 10, e0144696. https://doi.org/ 10.1371/journal.pone.0144696.

Liu, L., Jiang, L., Sun, Y., Wang, H., Yi, C., Hsu, H., Liu, L., Jiang, L., Sun, Y., Wang, H., Yi, C., Hsu, H., 2016. Morphometric Controls on Glacier Mass Balance of the Puruogangri Ice Field, Central Tibetan Plateau. Water 8, 496. https://doi.org/

10.3390/w8110496.

Lutz, A., 2016. Impact of climate change on the hydrology of High Mountain Asia. Universiteit Utrecht, Netherlands. https://doi.org/ISSN 2211-4335.

Lutz, A.F., Immerzeel, W.W., Shrestha, A.B., Bierkens, M.F.P., 2014. Consistent increase in High Asia's runoff due to increasing glacier melt and precipitation. Nat. Clim. Chang. 4, 587–592. https://doi.org/10.1038/nclimate2237.

Maurer, J.M., Schaefer, J.M., Rupper, S., Corley, A., 2019. Acceleration of ice loss across the Himalayas over the past 40 years. Sci. Adv. 5, eaav7266. https://doi.org/ 10.1126 /sciadv.aav7266.

Mayr, E., Hagg, W., 2019. Debris-Covered Glaciers. Springer, Cham, pp. 59–71. https:// doi.org/10.1007/978-3-319-94184-4_4.

McFEETERS, S.K., 1996. The use of the Normalized Difference Water Index (NDWI) in the delineation of open water features. Int. J. Remote Sens. 17, 1425–1432. https:// doi.org/10.1080/01431169608948714.

Mergili, M., Müller, J.P., Schneider, J.F., 2013. Spatio-temporal development of high-mountain lakes in the headwaters of the Amu Darya River (Central Asia). Glob. Planet. Change 107, 13–24. https://doi.org/10.1016/J.GLOPLACHA.2013.04.001.

Mertes, J.R., Gulley, J.D., Benn, D.I., Thompson, S.S., Nicholson, L.I., 2017. Using structure-from-motion to create glacier DEMs and orthoimagery from historical terrestrial and oblique aerial imagery. Earth Surf. Process. Landforms 42, 2350–2364. https://doi.org/10.1002/esp.4188.

Miles, E.S., Pellicciotti, F., Willis, I.C., Steiner, J.F., Buri, P., Arnold, N.S., 2016. Refined energy-balance modelling of a supraglacial pond, Langtang Khola, Nepal. Ann. Glaciol. 57, 29–40. https://doi.org/10.3189/2016AoG71A421.

Miles, E.S., Steiner, J., Willis, I., Buri, P., Immerzeel, W.W., Chesnokova, A., Pellicciotti, F., 2017a. Pond Dynamics and Supraglacial-Englacial Connectivity on Debris-Covered Lirung Glacier, Nepal, Frontiers in Earth Science. Frontiers. https://doi.org /10.3389/feart.2017.00069.

Miles, E.S., Watson, C.S., Brun, F., Berthier, E., Esteves, M., Quincey, D.J., Miles, K.E., Hubbard, B., Wagnon, P., 2018. Glacial and geomorphic effects of a supraglacial lake drainage and outburst event, Everest region, Nepal Himalaya. Cryosph. 12, 3891–3905. https://doi.org/10.5194/tc-12-3891-2018.

Miles, E.S., Willis, I.C., Arnold, N.S., Steiner, J., Pellicciotti, F., 2017b. Spatial, seasonal and interannual variability of supraglacial ponds in the Langtang Valley of Nepal,

1999-2013. J. Glaciol. 63, 88–105. https://doi.org/10.1017/jog.2016.120.

Mool, P.K., Bajracharya, S.R., Joshi, S.P., 2001. Inventory of glaciers, glacial lakes and glacial lake outburst floods. International Centre for Integrated Mountain Development (ICIMOD), Kathmandu, Nepal.

Muller, F.M., 1970. Inventory of glaciers in the Mount Everest region, in: Perennial Ice and Snow Masses. UNESCO/IAHS, pp. 47–59.

Nicholson, L., Benn, D.I., 2013. Properties of natural supraglacial debris in relation to modelling sub-debris ice ablation. Earth Surf. Process. Landforms 38, 490–501. https://doi.org/10.1002/esp.3299.

Nicholson, L., Benn, D.I., 2006. Calculating ice melt beneath a debris layer using meteorological data. J. Glaciol. 52, 463–470. https://doi.org/10.3189/172756506781828584.

Nicholson, L.I., McCarthy, M., Pritchard, H.D., Willis, I., 2018. Supraglacial debris thickness variability: impact on ablation and relation to terrain properties. Cryosph. 12, 3719–3734. https://doi.org/10.5194/tc-12-3719-2018.

Nie, Y., Liu, Q., Liu, S., 2013. Glacial Lake Expansion in the Central Himalayas by Landsat Images, 1990–2010. PLoS One 8, e83973. https://doi.org/10.1371/journal.pone.0083973.

Nie, Y., Liu, Q., Wang, J., Zhang, Y., Sheng, Y., Liu, S., 2018. An inventory of historical glacial lake outburst floods in the Himalayas based on remote sensing observations and geomorphological analysis. Geomorphology 308, 91–106. https://doi.org/10.1016/J.GEOMORPH.2018.02.002.

Nie, Y., Sheng, Y., Liu, Q., Liu, L., Liu, S., Zhang, Y., Song, C., 2017. A regional-scale assessment of Himalayan glacial lake changes using satellite observations from 1990 to 2015. Remote Sens. Environ. 189, 1–13. https://doi.org/10.1016/J.RSE.2016.11.008.

Nuimura, T., Fujita, K., Yamaguchi, S., Sharma, R.R., 2012. Elevation changes of glaciers revealed by multitemporal digital elevation models calibrated by GPS survey in the Khumbu region, Nepal Himalaya, 1992-2008. J. Glaciol. 58, 648–656. https://doi.org/10.3189/2012JoG11J061.

Ojha, S., Fujita, K., Asahi, K., Sakai, A., Lamsal, D., Nuimura, T., Nagai, H., 2016. Glacier area shrinkage in eastern Nepal Himalaya since 1992 using high-resolution inventories from aerial photographs and ALOS satellite images. J. Glaciol. 62, 512–524. https://doi.org/10.1017/jog.2016.61.

Östrem, G., 1959. Ice Melting under a Thin Layer of Moraine, and the Existence of Ice Cores in Moraine Ridges. Geogr. Ann. 41, 228–230. https://doi.org/10.1080/20014422.1959.11907953.

Parkes, D., Marzeion, B., 2018. Twentieth-century contribution to sea-level rise from uncharted glaciers. Nature 563, 551–554. https://doi.org/10.1038/s41586-018-0687-9.

Paul, F., Barry, R.G., Cogley, J.G., Frey, H., Haeberli, W., Ohmura, A., Ommanney, C.S.L., Raup, B., Rivera, A., Zemp, M., 2009. Recommendations for the compilation of glacier inventory data from digital sources. Ann. Glaciol. 50, 119–126. https://doi.org/10.3189/172756410790595778.

Paul, F., Winsvold, S., Kääb, A., Nagler, T., Schwaizer, G., 2016. Glacier Remote Sensing Using Sentinel-2. Part II: Mapping Glacier Extents and Surface Facies, and Comparison to Landsat 8. Remote Sens. 8, 575. https://doi.org/10.3390/rs8070575.

Pelto, M., Capps, D., Clague, J.J., Pelto, B., 2013. Rising ELA and expanding proglacial lakes indicate impending rapid retreat of Brady Glacier, Alaska. Hydrol. Process. 27, 3075–3082. https://doi.org/10.1002/hyp.9913.

Pratap, B., Dobhal, D.P., Mehta, M., Bhambri, R., 2015. Influence of debris cover and altitude on glacier surface melting: a case study on Dokriani Glacier, central Himalaya, India. Ann. Glaciol. 56, 9–16. https://doi.org/10.3189/2015AoG70A971.

Pritchard, H.D., 2017. Asia's glaciers are a regionally important buffer against drought. Nature 545, 169–174. https://doi.org/10.1038/nature22062.

Qiao, B., Zhu, L., 2019. Difference and cause analysis of water storage changes for glacier-fed and non-glacier-fed lakes on the Tibetan Plateau. Sci. Total Environ. 693, 133399. https://doi.org/10.1016/j.scitotenv.2019.07.205.

Qiao, L., Mayer, C., Liu, S., 2015. Distribution and interannual variability of supraglacial lakes on debris-covered glaciers in the Khan Tengri-Tumor Mountains, Central Asia. Environ. Res. Lett. 10. https://doi.org/10.1088/1748-9326/10/1/014014.

Quincey, D.J., Luckman, A., Benn, D., 2009. Quantification of Everest region glacier velocities between 1992 and 2002, using satellite radar interferometry and feature tracking. J. Glaciol. 55, 596–606. https://doi.org/10.3189/002214309789470987.

Quincey, D.J., Richardson, S.D., Luckman, A., Lucas, R.M., Reynolds, J.M., Hambrey, M.J., Glasser, N.F., 2007. Early recognition of glacial lake hazards in the Himalaya using remote sensing datasets. Glob. Planet. Change 56, 137–152. https://doi.org/10.1016/j.gloplacha.2006.07.013.

Racoviteanu, A., Williams, M., Barry, R., 2008. Optical Remote Sensing of Glacier Characteristics: A Review with Focus on the Himalaya. Sensors 8, 3355–3383. https://doi.org/10.3390/s8053355.

Racoviteanu, A.E., Arnaud, Y., Williams, M.W., Manley, W.F., 2015. Spatial patterns in glacier characteristics and area changes from 1962 to 2006 in the Kanchenjunga–Sikkim area, eastern Himalaya. Cryosph. 9, 505–523. https://doi.org/10.5194/tc-9-505-2015.

Raj, K.B.G., Kumar, K.V., 2016. Inventory of Glacial Lakes and its Evolution in Uttarakhand Himalaya Using Time Series Satellite Data. J. Indian Soc. Remote Sens. 44, 959–976. https://doi.org/10.1007/s12524-016-0560-y.

Reynolds, J.M., 2000. On the formation of supraglacial lakes on debris-covered glaciers. Debris-covered glaciers 264, 153–161.

RGI, 2017. Randolp Glacier Inventory - A Dataset of Global Glacier Outlines: version 6.0. Colorado, USA. https://doi.org/https://doi.org/10.7265/N5-RGI-60.

Richardson, S.D., Reynolds, J.M., 2000. An overview of glacial hazards in the Himalayas. Quat. Int. 65–66, 31–47. https://doi.org/10.1016/S1040-6182(99)00035-X.

Rodell, M., Famiglietti, J.S., Wiese, D.N., Reager, J.T., Beaudoing, H.K., Landerer, F.W., Lo, M.-H., 2018. Emerging trends in global freshwater availability. Nature 557, 651–659. https://doi.org/10.1038/s41586-018-0123-1.

Röhl, K., 2008. Characteristics and evolution of supraglacial ponds on debris-covered Tasman Glacier, New Zealand. J. Glaciol. 54, 867–880. https://doi.org/10.3189/002214308787779861.

Rokni, K., Ahmad, A., Selamat, A., Hazini, S., 2014. Water Feature Extraction and Change Detection Using Multitemporal Landsat Imagery. Remote Sens. 6, 4173–4189. https://doi.org/10.3390/rs6054173.

Rounce, D., Watson, C., McKinney, D., 2017. Identification of Hazard and Risk for Glacial Lakes in the Nepal Himalaya Using Satellite Imagery from 2000–2015. Remote Sens. 9, 654. https://doi.org/10.3390/rs9070654.

Rounce, D.R., Byers, A.C., Byers, E.A., Mckinney, D.C., 2016a. Brief Communications : Observations of a Glacier Outburst Flood from Lhotse Glacier , Everest Area , Nepal 1–10. https://doi.org/10.5194/tc-2016-239.

Rounce, D.R., King, O., McCarthy, M., Shean, D.E., Salerno, F., 2018. Quantifying Debris Thickness of Debris-Covered Glaciers in the Everest Region of Nepal Through Inversion of a Subdebris Melt Model. J. Geophys. Res. Earth Surf. 123,

1094–1115. https://doi.org/10.1029/2017JF004395.

Rounce, D.R., McKinney, D.C., Lala, J.M., Byers, A.C., Watson, C.S., 2016b. A new remote hazard and risk assessment framework for glacial lakes in the Nepal Himalaya. Hydrol. Earth Syst. Sci. 20, 3455–3475. https://doi.org/10.5194/hess-20-3455-2016.

Sakai, A., 2019. Brief communication: Updated GAMDAM glacier inventory over high-mountain Asia. Cryosphere 13, 2043–2049. https://doi.org/10.5194/tc-13-2043-2019.

Sakai, A., 2012. Glacial Lakes in the Himalayas: A Review on Formation and Expansion Processes. Glob. Environ. Res. 16, 23–30.

Sakai, A., Fujita, K., 2010. Formation conditions of supraglacial lakes on debris-covered glaciers in the Himalaya. J. Glaciol. 56, 177–181. https://doi.org/10.3189/002214310791190785.

Sakai, A., Nakawo, M., Fujita, K., 1998. Melt rate of ice cliffs on the Lirung Glacier, Nepal Himalayas, 1996. Bull. Glacier Res. 16, 57–66.

Sakai, A., Nishimura, K., Kadota, T., Takeuchi, N., 2009. Onset of calving at supraglacial lakes on debris-covered glaciers of the Nepal Himalaya. J. Glaciol. 55, 909–917. https://doi.org/10.3189/002214309790152555.

Sakai, A., Takeuchi, N., Fujita, K., Nakawo, M., 2000. Role of supraglacial ponds in the ablation process of a debris-covered glacier in the Nepal Himalayas. Debris-Covered Glaciers 119–130.

Salerno, F., Guyennon, N., Thakuri, S., Viviano, G., Romano, E., Vuillermoz, E., Cristofanelli, P., Stocchi, P., Agrillo, G., Ma, Y., Tartari, G., 2015. Weak precipitation, warm winters and springs impact glaciers of south slopes of Mt. Everest (central Himalaya) in the last 2 decades (1994-2013). Cryosph. 9, 1229–1247. https://doi.org/10.5194/tc-9-1229-2015.

Salerno, F., Thakuri, S., D'Agata, C., Smiraglia, C., Manfredi, E.C., Viviano, G., Tartari, G., 2012. Glacial lake distribution in the Mount Everest region: Uncertainty of measurement and conditions of formation. Glob. Planet. Change 92–93, 30–39. https://doi.org/10.1016/j.gloplacha.2012.04.001.

Salerno, F., Thakuri, S., Guyennon, N., Viviano, G., Tartari, G., 2016. Glacier melting and precipitation trends detected by surface area changes in Himalayan ponds. Cryosph. 10, 1433–1448. https://doi.org/10.5194/tc-10-1433-2016.

Sawagaki, T., Lamsal, D., Byers, a. C., Watanabe, T., 2012. Changes in Surface

Morphology and Glacial Lake Development of Chamlang South Glacier in the Eastern Nepal Himalaya since 1964. Glob. Environ. Res. 14, 83–94.

Scherler, D., Bookhagen, B., Strecker, M.R., 2011. Spatially variable response of Himalayan glaciers to climate change affected by debris cover. Nat. Geosci. 4, 156–159. https://doi.org/10.1038/ngeo1068.

Scherler, D., Wulf, H., Gorelick, N., 2018. Global Assessment of Supraglacial Debris-Cover Extents. Geophys. Res. Lett. 45, 11,798-11,805. https://doi.org/10.1029/2018GL080158.

Schomacker, A., Benediktsson, Í.Ö., 2018. Supraglacial Environments. Past Glacial Environ. 159–179. https://doi.org/10.1016/B978-0-08-100524-8.00005-1.

Shahtahmassebi, A.R., Lin, Y., Lin, L., Atkinson, P.M., Moore, N., Wang, K., He, S., Huang, L., Wu, J., Shen, Z., Gan, M., Zheng, X., Su, Y., Teng, H., Li, X., Deng, J., Sun, Y., Zhao, M., 2017. Reconstructing Historical Land Cover Type and Complexity by Synergistic Use of Landsat Multispectral Scanner and CORONA. Remote Sens. 9, 682. https://doi.org/10.3390/rs9070682.

Shea, J.M., Immerzeel, W.W., Wagnon, P., Vincent, C., Bajracharya, S., 2015. Modelling glacier change in the Everest region, Nepal Himalaya. Cryosph. 9, 1105–1128. https://doi.org/10.5194/tc-9-1105-2015.

Shean, D., 2017. High Mountain Asia 8-meter DEMs derived from along-track optical imagery, version 1. Boulder, Colorado USA. NASA National Snow and Ice Data Center Distributed Active Archive Center. [WWW Document]. https://doi.org/10.5067/GSACB044M4PK.

Sherpa, S.F., Wagnon, P., Brun, F., Berthier, E., Vincent, C., Lejeune, Y., Arnaud, Y., Kayastha, R.B., Sinisalo, A., 2017. Contrasted surface mass balances of debris-free glaciers observed between the southern and the inner parts of the Everest region (2007–15). J. Glaciol. 63, 637–651. https://doi.org/10.1017/jog.2017.30.

Shiraiwa, T., 1993. Glacial fluctuations and cryogenci environments in the Langtang Valley, Nepal Himalaya. Hokkaido University.

Shiraiwa, T., Ueno, K., Yamada, T., 1992. Distribution of mass input on glaciers in the Langtang Valley, Nepal Himalayas. Bull. Glacier Res. 10, 21–30.

Shrestha, A.B., Eriksson, M., Mool, P., Ghimire, P., Mishra, B., Khanal, N.R., 2010. Glacial lake outburst flood risk assessment of Sun Koshi basin, Nepal. Geomatics, Nat. Hazards Risk 1, 157–169. https://doi.org/10.1080/19475701003668968.

Shrestha, F., Gao, X., Khanal, N.R., Maharjan, S.B., Shrestha, R.B., Wu, L., Mool, P.K.,

Bajracharya, S.R., 2017. Decadal glacial lake changes in the Koshi basin, central Himalaya, from 1977 to 2010, derived from Landsat satellite images. J. Mt. Sci. 14, 1969–1984. https://doi.org/10.1007/s11629-016-4230-x.

Shrestha, M.L., 2000. Interannual variation of summer monsoon rainfall over Nepal and its relation to Southern Oscillation Index. Meteorol. Atmos. Phys. 75, 21–28. https://doi.org/10.1007/s007030070012.

Shukla, A., Garg, P.K., Srivastava, S., 2018. Evolution of Glacial and High-Altitude Lakes in the Sikkim, Eastern Himalaya Over the Past Four Decades (1975–2017). Front. Environ. Sci. 6, 81. https://doi.org/10.3389/fenvs.2018.00081.

Singh, R.B., Schickhoff, U., Mal, S., 2016. Climate change, glacier response, and vegetation dynamics in the Himalaya: Contributions toward future earth initiatives. Clim. Chang. Glacier Response, Veg. Dyn. Himalaya Contrib. Towar. Futur. Earth Initiat. 1–399. https://doi.org/10.1007/978-3-319-28977-9.

Smith, M.W., Carrivick, J.L., Quincey, D.J., 2016. Structure from motion photogrammetry in physical geography. Prog. Phys. Geogr. Earth Environ. 40, 247–275. https://doi.org/10.1177/0309133315615805.

SNP, 2019. Biodiversity [WWW Document]. Sagarmatha Natl. Park. URL http://www.sagarmathanationalpark.gov.np/index.php/biodiversity (accessed 10.24.19).

Somos-Valenzuela, M.A., McKinney, D.C., Byers, A.C., Rounce, D.R., Portocarrero, C., Lamsal, D., 2014a. Assessing downstream flood impacts due to a potential GLOF from Imja Lake in Nepal. Hydrol. Earth Syst. Sci. Discuss. 11, 13019–13053. https://doi.org/10.5194/hessd-11-13019-2014.

Somos-Valenzuela, M.A., McKinney, D.C., Rounce, D.R., Byers, A.C., 2014b. Changes in Imja Tsho in the Mount Everest region of Nepal. Cryosph. 8, 1661–1671. https://doi.org/10.5194/tc-8-1661-2014.

Song, C., Sheng, Y., 2016. Contrasting evolution patterns between glacier-fed and non-glacier-fed lakes in the Tanggula Mountains and climate cause analysis. Clim. Change 135, 493–507. https://doi.org/10.1007/s10584-015-1578-9.

Stevens, S., 2003. Tourism and Deforestation in the Mt Everest Region of Nepal. Geogr. J. https://doi.org/10.2307/3451451.

Tartari, G., Salerno, F., Buraschi, E., Bruccoleri, G., Smiraglia, C., 2008. Lake surface area variations in the North-Eastern sector of Sagarmatha National Park (Nepal) at the end of the 20th Century by comparison of historical maps. J. Limnol. 67, 139.

https://doi.org/10.4081/jlimnol.2008.139.

Tartari, G., Verza, G., Bertolami, L., 1998. Meteorological data at the Pyramid Observatory Laboratory (Khumbu Valley, Sagarmatha National Park, Nepal). J. Limnol. 57, 23–40.

Thakuri, S., Salerno, F., Smiraglia, C., Bolch, T., D'Agata, C., Viviano, G., Tartari, G., 2014. Tracing glacier changes since the 1960s on the south slope of Mt. Everest (central Southern Himalaya) using optical satellite imagery. Cryosphere 8, 1297–1315. https://doi.org/10.5194/tc-8-1297-2014.

Thompson, S.S., Benn, D.I., Dennis, K., Luckman, A., 2012. A rapidly growing moraine-dammed glacial lake on Ngozumpa Glacier, Nepal. Geomorphology 145–146, 1–11. https://doi.org/10.1016/J.GEOMORPH.2011.08.015.

Veh, G., Korup, O., Roessner, S., Walz, A., 2018. Detecting Himalayan glacial lake outburst floods from Landsat time series. Remote Sens. Environ. 207, 84–97. https://doi.org/10.1016/J.RSE.2017.12.025.

Vincent, C., Wagnon, P., Shea, J.M., Immerzeel, W.W., Kraaijenbrink, P., Shrestha, D., Soruco, A., Arnaud, Y., Brun, F., Berthier, E., Sherpa, S.F., 2016. Reduced melt on debris-covered glaciers: investigations from Changri Nup Glacier, Nepal. Cryosph. 10, 1845–1858. https://doi.org/10.5194/tc-10-1845-2016.

Vuichard, D., Zimmermann, M., 1987. The 1985 Catastrophic Drainage of a Moraine-Dammed Lake, Khumbu Himal, Nepal: Cause and Consequences. Mt. Res. Dev. 7, 91. https://doi.org/10.2307/3673305.

Wang, W., Xiang, Y., Gao, Y., Lu, A., Yao, T., 2015. Rapid expansion of glacial lakes caused by climate and glacier retreat in the Central Himalayas. Hydrol. Process. 29, 859–874. https://doi.org/10.1002/hyp.10199.

Watanabe, T., 2006. Geoecological Studies in the Kangchenjunga Conservation Area, Eastern Nepal Himalaya. Glob. Environ. Res. 10, 87–98.

Watanabe, T., Byers, A.C., Somos-Valenzuela, M.A., McKinney, D.C., 2016. The Need for Community Involvement in Glacial Lake Field Research: The Case of Imja Glacial Lake, Khumbu, Nepal Himalaya, in: Climate Change, Glacier Response, and Vegetation Dynamics in the Himalaya. Springer International Publishing, Cham, pp. 235–250. https://doi.org/10.1007/978-3-319-28977-9_13.

Watanabe, T., Ives, J.D., Hammond, J.E., 1994. Rapid Growth of a Glacial Lake in Khumbu Himal, Himalaya: Prospects for a Catastrophic Flood. Mt. Res. Dev. 14, 329. https://doi.org/10.2307/3673729.

Watanabe, T., Kameyama, S., Sato, T., 1995. Imja Glacier Dead-Ice Melt Rates and Changes in a Supra-Glacial Lake, 1989-1994, Khumbu Himal, Nepal: Danger of Lake Drainage. Mt. Res. Dev. 15, 293. https://doi.org/10.2307/3673805.

Watanabe, T., Khanal, N.R., Gautam, M.P., 1998. The Nangama glacial lake outburst flood occured on 23 June 1980 in the Kanchanjungha Area, eastern Nepal. Ann. Hokkaido Geogr. Soc. 13–19.

Watanabe, T., Lamsal, D., Ives, J.D., 2009. Evaluating the growth characteristics of a glacial lake and its degree of danger of outburst flooding: Imja Glacier, Khumbu Himal, Nepal. Nor. Geogr. Tidsskr. 63, 255–267. https://doi.org/10.1080/00291950903368367.

Watson, C., Kargel, J., Tiruwa, B., 2019. UAV-Derived Himalayan Topography: Hazard Assessments and Comparison with Global DEM Products. Drones 3, 18. https://doi.org/10.3390/drones3010018.

Watson, C.S., King, O., Miles, E.S., Quincey, D.J., 2018b. Optimising NDWI supraglacial pond classification on Himalayan debris-covered glaciers. Remote Sens. Environ. 217, 414–425. https://doi.org/10.1016/J.RSE.2018.08.020.

Watson, C.S., Quincey, D.J., Carrivick, J.L., Smith, M.W., 2016. The dynamics of supraglacial ponds in the Everest region, central Himalaya. Glob. Planet. Change 142, 14–27. https://doi.org/10.1016/J.GLOPLACHA.2016.04.008.

Watson, C.S., Quincey, D.J., Carrivick, J.L., Smith, M.W., Rowan, A. V., Richardson, R., 2018a. Heterogeneous water storage and thermal regime of supraglacial ponds on debris-covered glaciers. Earth Surf. Process. Landforms 43, 229–241. https://doi.org/10.1002/esp.4236.

Watson, S., Quincey, D.J., Carrivick, J.L., Smith, M.W., 2017. Ice cliff dynamics in the Everest region of the Central Himalaya. Geomorphology 278, 238–251. https://doi.org/10.1016/j.geomorph.2016.11.017.

WECS, 2011. Water resources of Nepal in the context of climate change. Water and Energy Commission Secretariat (WECS), Government of Nepal, Kathmandu.

Wessels, R.L., Kargel, J.S., Kieffer, H.H., 2002. ASTER measurement of supraglacial lakes in the Mount Everest region of the Himalaya. Ann. Glaciol. 34, 399–408. https://doi.org/10.3189/172756402781817545.

Westoby, M.J., Brasington, J., Glasser, N.F., Hambrey, M.J., Reynolds, J.M., 2012. 'Structure-from-Motion' photogrammetry: A low-cost, effective tool for geoscience applications. Geomorphology 179, 300–314. https://doi.org/10.1016/ J.GEOMORP

H.2012.08.021.

Xu, H., 2006. Modification of normalised difference water index (NDWI) to enhance open water features in remotely sensed imagery. Int. J. Remote Sens. 27, 3025–3033. https://doi.org/10.1080/01431160600589179.

Yamada, T., 1998. Glacier lake and its outburst flood in the Nepal Himalaya. Japanese Society of Snow and Ice, Tokyo.

Yamada, T., Sharma, C.K., 1993. Glacier Lakes and Outburst Floods in the Nepal Himalaya.

Yan, D., Wang, X., Zhu, X., Huang, C., Li, W., 2017. Analysis of the use of NDWI $_{green}$ and NDWI $_{red}$ for inland water mapping in the Yellow River Basin using Landsat-8 OLI imagery. Remote Sens. Lett. 8, 996–1005. https://doi.org/10.1080/2150704X.2017.1341664.

Yao, X., Liu, S., Han, L., Sun, M., Zhao, L., 2018. Definition and classification system of glacial lake for inventory and hazards study. J. Geogr. Sci. 28, 193–205. https://doi.org/10.1007/s11442-018-1467-z.

Yi, S., Sun, W., 2014. Evaluation of glacier changes in high-mountain Asia based on 10 year GRACE RL05 models. J. Geophys. Res. Solid Earth 119, 2504–2517. https://doi.org/10.1002/2013JB010860.

Zemp, M., Frey, H., Gärtner-Roer, I., Nussbaumer, S.U., Hoelzle, M., Paul, F., Haeberli, W., Denzinger, F., Ahlstrøm, A.P., Anderson, B., Bajracharya, S., Baroni, C., Braun, L.N., Cáceres, B.E., Casassa, G., Cobos, G., Dávila, L.R., Delgado Granados, H., Demuth, M.N., Espizua, L., Fischer, A., Fujita, K., Gadek, B., Ghazanfar, A., Ove Hagen, J., Holmlund, P., Karimi, N., Li, Z., Pelto, M., Pitte, P., Popovnin, V. V., Portocarrero, C.A., Prinz, R., Sangewar, C. V., Severskiy, I., Sigurđsson, O., Soruco, A., Usubaliev, R., Vincent, C., 2015. Historically unprecedented global glacier decline in the early 21st century. J. Glaciol. 61, 745–762. https://doi.org/10.3189/2015JoG15J017.

Zemp, M., Huss, M., Thibert, E., Eckert, N., McNabb, R., Huber, J., Barandun, M., Machguth, H., Nussbaumer, S.U., Gärtner-Roer, I., Thomson, L., Paul, F., Maussion, F., Kutuzov, S., Cogley, J.G., 2019. Global glacier mass changes and their contributions to sea-level rise from 1961 to 2016. Nature 568, 382–386. https://doi.org/10.1038/s41586-019-1071-0.

Zhang, G., Yao, T., Xie, H., Wang, W., Yang, W., 2015. An inventory of glacial lakes in the Third Pole region and their changes in response to global warming. Glob. Planet.

Change 131, 148–157. https://doi.org/10.1016/J.GLOPLACHA. 2015.05. 013.

Zhang, Y., Fujita, K., Liu, S., Liu, Q., Nuimura, T., 2011. Distribution of debris thickness and its effect on ice melt at Hailuogou glacier, southeastern Tibetan Plateau, using in situ surveys and ASTER imagery. J. Glaciol. 57, 1147–1157. https://doi.org/10.3189/002214311798843331.

Annex I. Glaciers of the Everest region obtained from 2-m spatial resolution WorldView imageries of 2015 and 2016 and 10 m Sentinel-2 images of 2016.

Sub-basins	Year	GLIMSID	Glacier Name	Area (km^2)	Perimeter (km^2)	Uncertainty (%)	Elevation (m)		Mean aspect (°)	Mean Slope (°)
							Minimum	Maximum		
BhoteKoshi at Namche	2015	G086679E27865N		0.03	0.656	2.5	5078	5267	102.4	14.2
BhoteKoshi at Namche	2015	G086676E27898N		0.73	5.731	0.8	5261	5623	111.5	28.3
BhoteKoshi at Namche	2015	G086677E27874N		0.02	0.565	2.9	5375	5424	119.3	21.1
BhoteKoshi at Namche	2015	G086680E27860N		0.02	0.846	4.0	5255	5452	141.6	47.4
BhoteKoshi at Namche	2015	G086671E27887N		0.55	5.650	1.0	5267	5696	148.2	39.9
Thame Khola	2015	G086561E27846N		0.96	4.726	2.5	5242	5834	164.3	25.1
Thame Khola	2015	G086551E27844N		0.26	2.270	4.4	5499	5994	83.0	34.1
Thame Khola	2015	G086548E27834N		0.13	1.670	6.5	5661	6142	118.0	39.0
Thame Khola	2015	G086553E27829N		1.35	7.442	2.8	4881	6105	107.5	29.1
Thame Khola	2015	G086553E27820N		0.71	5.086	3.6	5019	5715	87.0	24.1
Thame Khola	2015	G086568E27819N		0.82	5.435	3.3	4620	5341	94.7	22.7
Thame Khola	2015	G086586E27818N		0.77	5.827	3.8	4350	4795	90.9	13.7
Thame Khola	2015	G086571E27844N		0.42	2.750	3.3	5078	5594	204.9	30.2
Thame Khola	2015	G086581E27840N		0.45	2.772	3.1	5162	5781	174.2	40.8
BhoteKoshi at Thame	2015	G086581E27856N		0.24	2.175	4.6	4912	5473	68.9	34.8
BhoteKoshi at Thame	2015	G086587E27852N		0.86	3.821	2.2	4779	5755	60.0	32.1
BhoteKoshi at Thame	2015	G086593E27849N		0.27	1.996	3.7	4874	5373	39.6	33.6
BhoteKoshi at Thame	2015	G086568E27864N		2.38	9.369	0.4	4677	6582	111.0	40.6
BhoteKoshi at Thame	2015	G086560E27878N		0.53	5.736	1.1	5079	6207	80.5	36.3
BhoteKoshi at Thame	2015	G086558E27890N		0.37	4.466	1.2	5331	6088	120.2	32.9
BhoteKoshi at Thame	2015	G086561E27899N		1.04	10.226	1.0	5219	6111	125.7	26.3
BhoteKoshi at Thame	2015	G086568E27908N		1.19	7.655	0.6	5242	5741	119.9	17.1

Sub-basins	Year	GLIMSID	Glacier Name	Area (km^2)	Perimeter (km^2)	Uncertainty (%)	Elevation (m)		Mean aspect (°)	Mean Slope (°)
							Minimum	Maximum		
BhoteKoshi at Thame	2015	G086582E27918N		1.49	13.104	0.9	5193	5889	146.7	19.4
BhoteKoshi at Thame	2015	G086666E27925N		0.10	1.677	1.7	5451	5701	203.4	35.6
BhoteKoshi at Thame	2015	G086667E27913N		0.13	2.110	1.7	5305	5684	271.6	37.5
BhoteKoshi at Thame	2015	G086668E27905N		0.11	1.722	1.5	5469	5728	193.1	29.2
BhoteKoshi at Thame	2015	G086670E27882N		0.06	1.246	1.9	5322	5534	235.6	30.6
Chule Glacier	2015	G086566E27926N	Landak	1.61	9.677	0.6	4869	5844	119.5	17.1
Chule Glacier	2015	G086542E27954N	Chhule	5.00	31.574	0.6	4799	6508	107.1	15.5
Chule Glacier	2015	G086539E27996N	Melung	7.15	31.559	0.4	4970	6554	136.5	13.9
Chule Glacier	2015	G086543E27942N		0.67	5.371	0.8	5138	6068	85.3	24.2
Chule Glacier	2015	G086534E27973N		0.34	3.133	0.9	5303	5710	116.6	19.3
BhoteKoshi Glacier	2015	G086579E28055N	Bhote Koshi	30.77	123.208	0.4	4756	7025	172.0	16.7
BhoteKoshi Glacier	2015	G086632E28043N	Lumsamba	10.89	50.234	0.5	4905	6988	189.7	17.3
BhoteKoshi Glacier	2015	G086644E28002N		0.37	4.244	1.2	5224	5577	201.1	23.4
BhoteKoshi Glacier	2015	G086638E27997N		0.12	2.232	1.8	5571	5846	124.7	37.9
BhoteKoshi Glacier	2015	G086640E27985N		0.54	6.412	1.2	5168	5640	192.5	26.5
BhoteKoshi Glacier	2015	G086603E28030N		0.15	1.492	1.0	5419	5674	121.6	28.2
BhoteKoshi Glacier	2015	G086600E28035N		0.02	0.644	2.9	5591	5667	176.9	32.4
Ngozompa Glacier	2016	G086755E27906N	Cholotse	1.17	9.099	0.8	4861	6242	244.5	19.1
Ngozompa Glacier	2016	G086769E27889N	Taweche	0.31	2.635	0.8	4969	5159	237.9	16.8
Ngozompa Glacier	2016	G086714E28046N	Ngozompa	80.15	262.996	0.3	4668	8065	180.8	18.8
Ngozompa Glacier	2016	G086643E27994N		0.35	4.262	1.2	5289	5750	119.4	23.5
Ngozompa Glacier	2016	G086650E27998N		0.31	3.987	1.3	5381	5664	142.2	19.4
Ngozompa Glacier	2016	G086643E27980N		0.05	0.973	2.0	5406	5560	53.7	35.8

Sub-basins	Year	GLIMSID	Glacier Name	Area (km^2)	Perimeter (km^2)	Uncertainty (%)	Elevation (m)		Mean aspect (°)	Mean Slope (°)
							Minimum	Maximum		
Ngozompa Glacier	2016	G086654E27957N		0.21	3.222	1.6	5248	5534	107.0	25.1
Ngozompa Glacier	2016	G086670E27940N		0.41	5.044	1.2	5158	5807	210.2	25.0
Ngozompa Glacier	2016	G086674E27928N		0.78	7.797	1.0	5216	5998	177.3	21.7
Ngozompa Glacier	2016	G086679E27906N		0.19	2.031	1.0	5101	5551	147.0	31.1
Ngozompa Glacier	2016	G086675E27911N		0.11	2.007	1.9	5203	5754	84.0	50.4
Ngozompa Glacier	2016	G086695E27892N		0.14	2.564	1.8	5059	5391	83.6	31.0
Ngozompa Glacier	2016	G086723E27982N		0.10	2.288	2.4	5637	5993	184.1	42.2
Ngozompa Glacier	2016	G086733E27983N		0.15	2.629	1.8	5426	5856	210.4	32.5
Ngozompa Glacier	2016	G086749E27980N		0.56	4.140	0.7	5336	5719	251.2	17.6
Ngozompa Glacier	2016	G086757E27930N		0.38	3.278	0.9	5039	5623	236.6	30.3
Ngozompa Glacier	2016	G086756E27921N		0.07	1.176	1.7	5129	5347	283.5	33.3
Ngozompa Glacier	2016	G086763E27917N		0.31	4.615	1.5	5359	6176	215.2	51.8
Ngozompa Glacier	2016	G086755E27916N		0.33	3.719	1.1	5056	5798	274.8	35.3
Ngozompa Glacier	2016	G086756E27900N		0.14	1.893	1.4	5274	5645	220.7	38.9
Khumbu Glacier	2016	G086800E27995N	Khangri Nup	14.37	53.952	0.4	5099	6669	157.4	20.0
Khumbu Glacier	2016	G086799E27961N	Loboche	1.35	9.829	0.7	4949	5795	132.3	19.5
Khumbu Glacier	2016	G086786E27908N	Cholo	1.25	12.835	1.0	4447	6412	115.5	28.2
Khumbu Glacier	2016	G086873E27983N	Khumbu	27.17	106.658	0.4	4883	8069	211.9	25.8
Khumbu Glacier	2016	G086757E27972N		0.80	5.310	0.7	5336	5670	154.8	15.4
Khumbu Glacier	2016	G086762E27976N		0.16	2.699	1.7	5658	6104	196.5	49.9
Khumbu Glacier	2016	G086755E27961N		0.27	3.302	1.2	5245	5452	117.3	16.8
Khumbu Glacier	2016	G086756E27966N		0.03	0.957	3.0	5374	5488	185.8	21.1
Khumbu Glacier	2016	G086752E27969N		0.04	1.182	2.7	5586	5706	112.7	31.0

Sub-basins	Year	GLIMSID	Glacier Name	Area (km^2)	Perimeter (km^2)	Uncertainty (%)	Elevation (m)		Mean aspect (°)	Mean Slope (°)
							Minimum	Maximum		
Khumbu Glacier	2016	G086754E27954N		0.08	1.228	1.5	5204	5414	58.4	30.4
Khumbu Glacier	2016	G086754E27945N		0.09	1.496	1.7	5285	5566	62.5	33.4
Khumbu Glacier	2016	G086766E27919N		0.06	1.636	2.6	5865	6236	163.1	45.7
Khumbu Glacier	2016	G086792E27954N		0.36	5.709	1.6	5318	5958	191.9	40.4
Khumbu Glacier	2016	G086787E27959N		0.03	0.984	3.5	5322	5764	279.0	54.3
Khumbu Glacier	2016	G086783E27967N		0.05	1.272	2.7	5623	5901	174.5	41.0
Khumbu Glacier	2016	G086774E27971N		0.08	1.838	2.4	5450	5931	184.6	49.8
Khumbu Glacier	2016	G086776E27969N		0.04	0.837	1.9	5355	5539	196.8	33.0
Khumbu Glacier	2016	G086777E27967N		0.02	0.693	2.9	5331	5539	249.2	42.9
Khumbu Glacier	2016	G086823E28002N		0.22	2.622	1.2	5497	5996	186.6	35.3
Khumbu Glacier	2016	G086841E28012N		1.10	8.565	0.8	5345	6308	141.6	39.5
Khumbu Glacier	2016	G086850E27966N		0.44	3.231	0.7	5294	5900	273.9	31.3
Khumbu Glacier	2016	G086850E27961N		0.02	0.613	2.5	5575	5690	214.0	30.5
Khumbu Glacier	2016	G086848E27951N		0.10	1.695	1.7	5378	5808	259.1	35.6
Khumbu Glacier	2016	G086839E27944N		0.02	0.699	3.2	5676	5743	142.4	27.0
Khumbu Glacier	2016	G086832E27926N		0.10	1.425	1.5	5419	5689	290.6	29.0
Khumbu Glacier	2016	G086790E27898N		0.24	2.302	1.0	5088	5483	83.8	33.3
Khumbu Glacier	2016	G086773E27905N		0.07	1.546	2.1	5376	5992	45.1	47.4
Upper Imja Khola	2016	G086869E27947N	Nuptse	5.25	29.327	0.6	4940	7152	206.8	18.6
Upper Imja Khola	2016	G086891E27936N	Lhotse Nup	2.29	16.873	0.7	4931	6862	197.9	18.3
Upper Imja Khola	2016	G086918E27931N	Lhotse	10.54	48.819	0.5	4825	7260	203.6	21.8
Upper Imja Khola	2016	G086936E27878N	Ambulapcha	2.17	9.845	0.5	5034	5569	217.0	20.0

Sub-basins	Year	GLIMSID	Glacier Name	Area (km^2)	Perimeter (km^2)	Uncertainty (%)	Elevation (m)		Mean aspect (°)	Mean Slope (°)
							Minimum	Maximum		
Upper Imja Khola	2016	G086960E27923N	Imja	16.38	65.569	0.4	4995	8048	207.9	27.6
Upper Imja Khola	2016	G086856E27878N	Duwo	1.58	7.522	0.5	4714	6221	208.6	21.5
Upper Imja Khola	2016	G086891E27873N	Ama Dablam	8.45	35.381	0.4	4756	6283	238.2	26.0
Upper Imja Khola	2016	G086840E27938N		0.07	1.552	2.3	5543	5685	190.5	18.4
Upper Imja Khola	2016	G086934E27920N		0.43	6.443	1.5	5532	6067	197.6	36.1
Lower Imja Khola	2016	G086875E27838N	Nareyargaip	5.80	36.694	0.6	5044	6323	237.0	21.8
Lower Imja Khola	2016	G086872E27818N	Nare	2.51	16.418	0.7	4981	6447	229.3	30.6
Lower Imja Khola	2016	G086846E27859N	Tingbo	0.89	8.086	0.9	4853	5780	245.2	26.4
Lower Imja Khola	2016	G086844E27871N		0.07	1.153	1.6	4988	5313	284.2	36.3
Lower Imja Khola	2016	G086873E27855N		0.25	3.173	1.2	5535	6030	220.0	45.1
Lower Imja Khola	2016	G086860E27857N		0.06	1.025	1.7	5725	6082	158.7	49.7
Lower Imja Khola	2016	G086806E27806N		0.46	7.030	1.5	4908	6096	134.3	46.8
Lower Imja Khola	2016	G086811E27808N		0.09	1.270	1.4	4971	5271	117.0	36.2
Lower Imja Khola	2016	G086817E27809N		0.36	5.527	1.6	4765	5815	240.0	37.5
Lower Imja Khola	2016	G086825E27813N		0.08	1.800	2.4	4966	5463	293.1	42.5
Lower Imja Khola	2016	G086783E27893N		0.18	2.045	1.1	5520	6085	152.7	46.8
Lower Imja Khola	2016	G086788E27891N		0.03	0.812	2.9	5375	5533	130.6	35.7
Phungi Khola	2016	G086771E27798N		0.27	2.354	0.9	4966	5473	303.2	34.9
Phungi Khola	2016	G086791E27798N		1.61	12.776	0.8	4592	6531	199.0	42.7

Annex II Area (km^2) of supraglacial lakes in 16 glaciers in different years from 1989 – 2017 mapped using Landsat images.

Year	Thyanbo	Chule	Melung	Bhote Koshi	Lumsamba	Ngozompa	Lobuche	Khangri Nup	Khumbu	Nuptse	Lhotse	Imja	Ambulapcha	Ama Dablam	Duwo	Nareyargaip	Total Area
1989		0.011	0.007	0.099	0.011	0.063	0.024		0.142		0.016					0.005	0.378
1990		0.022	0.018	0.094	0.007	0.057	0.015		0.143		0.018					0.008	0.382
1992		0.020		0.057	0.014	0.193	0.026	0.016	0.156		0.008	0.018		0.015		0.009	0.531
1993		0.016		0.053	0.037	0.211			0.147		0.034			0.015		0.010	0.524
1994		0.025	0.017	0.053	0.055	0.119			0.146	0.007	0.011	0.007		0.008		0.013	0.462
1995		0.016		0.062	0.091	0.108		0.005	0.184	0.008	0.014	0.013				0.015	0.516
1996		0.037	0.007	0.051	0.032	0.092		0.010	0.130	0.000	0.010	0.006				0.013	0.388
1998		0.030		0.061	0.031	0.126		0.005	0.172	0.000	0.014	0.013				0.017	0.469
2000		0.019		0.064	0.020	0.175	0.026		0.146	0.010	0.012	0.000				0.018	0.489
2001		0.019	0.006	0.049	0.009	0.199	0.021	0.006	0.142	0.010	0.013	0.005				0.013	0.493
2002		0.023	0.020	0.071	0.007	0.170	0.006	0.006	0.183	0.012	0.027	0.029		0.012		0.013	0.580
2003		0.010	0.010	0.045	0.006	0.163		0.006	0.143	0.017		0.012		0.006		0.012	0.430
2004		0.038	0.005	0.055	0.007	0.201	0.008	0.006	0.140	0.024		0.019		0.016		0.011	0.528
2005		0.031	0.005	0.092		0.186	0.026	0.005	0.144	0.015		0.008		0.007		0.014	0.532
2008		0.044	0.019	0.113	0.015	0.275	0.007		0.176	0.008	0.011	0.012		0.009		0.048	0.735
2009		0.029	0.013	0.132	0.029	0.332			0.186	0.011	0.012	0.030		0.012		0.049	0.835
2010	0.011	0.049	0.030	0.119	0.024	0.278		0.020	0.216	0.010	0.020	0.023		0.016		0.045	0.860
2013	0.015	0.034	0.015	0.141	0.054	0.290	0.009		0.206	0.016	0.020	0.026		0.005	0.006	0.055	0.893
2014	0.021	0.029	0.007	0.177	0.057	0.376	0.011	0.014	0.262	0.025	0.049	0.023	0.016	0.020	0.008	0.053	1.146
2015	0.030	0.036	0.008	0.204	0.110	0.419	0.020	0.024	0.242	0.022	0.034	0.006	0.013	0.024	0.008	0.067	1.266
2016	0.040	0.043	0.012	0.222	0.108	0.379	0.011	0.023	0.206	0.017	0.052	0.007	0.009	0.015	0.000	0.054	1.198
2017	0.065	0.051	0.012	0.208	0.087	0.423	0.012	0.039	0.250	0.020	0.047		0.009	0.023	0.018	0.059	1.324

Annex III. Number of supraglacial lakes in 16 glaciers in different years from 1989 – 2017 mapped using Landsat images.

Year	Thyanbo	Chule	Melung	Bhote Koshi	Lumsamba	Ngozompa	Lobuche	Khangri Nup	Khumbu	Nuptse	Lhotse	Imja	Ambulapcha	Ama Dablam	Duwo	Nareyargaip	Total
1989		1	1	4	2	8	2	0	4		2					1	25
1990		2	2	3	1	7	1		3		2					1	22
1992			1	7	2	11	2	2	4		1	1		2		1	34
1993		1		8	6	13			5		3	0		2		1	39
1994		2	3	7	5	12			3	1	1	1		1		1	37
1995		1		7	6	9		1	7	1	1	2				1	36
1996		4	1	6	4	10		1	3		1	1				1	32
1998		2		5	4	11		1	5		2	1				1	32
2000		1		7	2	15	1		4	1	2	0				1	34
2001		1	1	6	1	14	2	1	5	1	2	1				1	36
2002		2	3	7	1	15	1	1	6	1	3	3		2		1	46
2003		1	1	4	1	14		1	4	2		2		1		1	32
2004		2	1	6	1	17	1	1	4	2		2		2		1	40
2005		2	1	12		13	3	1	3	2		1		1		1	40
2008		4	2	10	2	14	1	0	8	1	1	2		1		2	48
2009		2	1	13	3	19		0	10	2	2	4		2		2	60
2010	1	3	4	10	3	15		3	6	1	3	4		2		2	57
2013	1	2	2	12	5	14	1	0	10	2	2	2		1	1	2	57
2014	1	2	1	13	4	18	1	2	12	3	5	2	1	2	1	2	70
2015	1	2	1	18	9	28	2	2	9	2	5	1	1	3	1	3	88
2016	2	2	1	17	7	21	1	2	8	2	7	1	1	2		2	76
2017	2	1	1	17	6	27	1	4	11	2	5	0	1	3	2	2	85
Total	8	40	28	199	75	325	20	23	134	26	50	31	4	27	5	31	1026

Annex IV. Lake cover percentage with the debris-covered area in 16 glaciers in respect to the area of debris portion of the glacier from 1989 – 2017.

Year	Thyanbo	Chule	Melung	Bhote Koshi	Lumsamba	Ngozompa	Lobuche	Khangri Nup	Khumbu	Nuptse	Lhotse	Imja	Ambulapcha	Ama Dablam	Duwo	Nareyargaip
1989		0.3	0.1	0.7	0.2	0.3	5.3		2.0		0.3					0.3
1990		0.6	0.4	0.7	0.2	0.2	3.3		2.0		0.3					0.4
1992		0.6		0.4	0.3	0.8	5.8	0.2	2.1		0.1	0.3		0.6		0.5
1993		0.5		0.4	0.8	0.9			2.0		0.6			0.7		0.6
1994		0.7	0.4	0.4	1.1	0.5			2.0	0.3	0.2	0.1		0.3		0.7
1995		0.5		0.5	1.9	0.5		0.1	2.5	0.4	0.3	0.2				0.8
1996		1.1	0.2	0.4	0.7	0.4		0.1	1.8	0.0	0.2	0.1				0.7
1998		0.9		0.5	0.6	0.5		0.1	2.4	0.0	0.3	0.2				0.9
2000		0.6		0.5	0.4	0.8	5.7		2.0	0.5	0.2					0.9
2001		0.6	0.1	0.4	0.2	0.9	4.6	0.1	2.0	0.5	0.3	0.1				0.7
2002		0.7	0.5	0.5	0.1	0.7	1.4	0.1	2.5	0.6	0.5	0.5		0.5		0.7
2003		0.3	0.2	0.3	0.1	0.7		0.1	2.0	0.8		0.2		0.2		0.6
2004		1.1	0.1	0.4	0.1	0.9	1.7	0.1	1.9	1.1		0.3		0.7		0.6
2005		0.9	0.1	0.7		0.8	5.8	0.1	2.0	0.7		0.1		0.3		0.8
2008		1.3	0.4	0.8	0.3	1.2	1.5		2.4	0.4	0.2	0.2		0.4		2.5
2009		0.9	0.3	1.0	0.6	1.4			2.6	0.5	0.2	0.5		0.5		2.6
2010	0.8	1.4	0.7	0.9	0.5	1.2		0.3	3.0	0.5	0.4	0.4		0.7		2.4
2013	1.1	1.0	0.3	1.1	1.1	1.3	2.0		2.8	0.8	0.4	0.5		0.2	0.5	2.9
2014	1.5	0.9	0.2	1.3	1.2	1.6	2.5	0.2	3.6	1.2	0.9	0.4	1.6	0.8	0.6	2.8
2015	2.2	1.1	0.2	1.5	2.3	1.8	4.5	0.4	3.3	1.0	0.6	0.1	1.3	1.0	0.6	3.6
2016	2.8	1.3	0.3	1.7	2.3	1.6	2.4	0.3	2.8	0.8	1.0	0.1	0.9	0.6		2.9
2017	4.6	1.5	0.3	1.5	1.8	1.8	2.7	0.6	3.4	0.9	0.9		0.9	1.0	1.4	3.1
Avg.	2.2	0.9	0.3	0.8	0.8	1.0	3.5	0.2	2.4	0.6	0.4	0.3	1.2	0.6	0.8	1.5